THE BIOTRANSFORMATIONS AND BIOMOBILITY OF MONOMETHYLARSONATE AND DIMETHYLARSINATE IN THE MARINE ENVIRONMENT

by

JOHN CHRISTIAN NELSON

B. Sc., University of British Columbia, Canada, 1989

A THESIS SUBMITTED IN PARTIAL FULFILLMENT
OF THE REQUIREMENTS FOR THE DEGREE OF
DOCTOR OF PHILOSOPHY

in

THE FACULTY OF GRADUATE STUDIES
DEPARTMENT OF CHEMISTRY

We accept this thesis as conforming
to the required standard

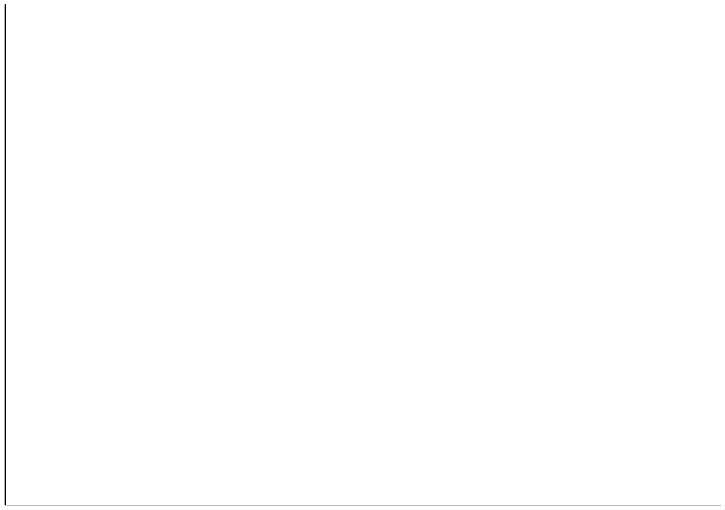

THE UNIVERSITY OF BRITISH COLUMBIA

1993

In presenting this thesis in partial fulfilment of the requirements for an advanced degree at the University of British Columbia, I agree that the Library shall make it freely available for reference and study. I further agree that permission for extensive copying of this thesis for scholarly purposes may be granted by the head of my department or by his or her representatives. It is understood that copying or publication of this thesis for financial gain shall not be allowed without my written permission.

(Signature) _____

Department of Chemistry

The University of British Columbia
Vancouver, Canada

Date Dec. 4/93

ABSTRACT

The biotransformations and the biomobility of monomethylarsonate (MMA) and dimethylarsinate (DMA) in the marine environment were investigated.

The biotransformations were studied by exposing blue mussels (*Mytilus edulis*) to either [^{3}H]-MMA or [^{3}H]-DMA in seawater tanks. Metabolic products including arsenobetaine ($(CH_3)_3As^+CH_2COO^-$) were identified in both the seawater and the mussels by using chromatographic techniques. The HPLC columns were coupled to a scintillation counter which acted as the detector. Arsenobetaine was also produced in seawater tanks which did not contain mussels which indicates that arsenobetaine is biosynthesized by microscopic organisms which are naturally occurring in seawater. It is likely that the arsenobetaine found in mussels is not a metabolic product of the mussels.

The biomobility of DMA and MMA was studied by measuring the rate at which these arsenicals diffused through liposomes as models for biological membranes. (Previously studies have shown that both DMA and MMA enter cells via slow passive diffusion.) Traditional techniques employing both radiolabelled permeants and liposomal membranes showed that DMA was much more permeable to the membranes than MMA. A ^{1}H-NMR spectroscopic technique employing shift agents to differentiate the spectroscopic signals of the permeant on either side of the liposomal membrane, was developed to measure the rate of diffusion of molecules across membranes. This technique was applied to DMA and MMA. Permeability coefficients of $(5.8 \pm 1.0) \times 10^{-8}$ cm s^{-1} and $(7.8 \pm 2.7) \times 10^{-9}$ cm s^{-1} at 24°C were measured for the neutral forms of DMA and MMA, respectively. In addition, the effects of pH, temperature, and membrane composition on the diffusion coefficients for DMA and MMA through the liposomal membrane were investigated. It was determined that only the neutral form of these weak acids permeates across the membrane and that cholesterol decreases the rate of permeation of DMA.

TABLE OF CONTENTS

Abstract ii

List of Tables x

List of Figures xii

List of Abbreviations xviii

Acknowledgements xx

Chapter 1

General Introduction 1

1.1 Speciation and Concentration of Arsenic in the Marine Environment 2

1.1.1 Seawater 2

1.1.2 Marine Plants and Algae 3

1.1.3 Marine Animals 6

1.2 MMA and DMA in the Aquatic Environment 8

1.2.1 Freshwater 8

1.2.2 Seawater 8

1.3 Overview of Thesis 11

Chapter 2

Exposure of Mussels to [^{3}H]-MMA 12

2.1 Introduction 12

2.1.1 Origins of Organoarsenicals in Marine Animals 12

2.1.2 Biomethylation of Arsenic 14

2.1.3 Proposed mechanism for the biosynthesis of arsenosugars 16

2.1.4 Proposed conversion of arsenosugars to arsenobetaine 18

2.1.5 Scope of Work 19

2.2 Experimental 21

2.2.1 Scintillation Counting 21

2.2.2 Atomic Absorption Spectrometry 21

2.2.3 HPLC system 22

2.24 TLC plates 24

2.2.5 Chemicals and reagents 25

2.2.6 The uptake of [^{3}H]-compounds by mussels from seawater which initially contained [^{3}H]-MMA 25

2.2.7 Isolation of the [^{3}H]-labeled arsenicals in the mussel flesh 26

2.2.8 Identification of the [^{3}H]-labeled compounds in the mussel flesh which eluted from the Dowex column in the NH_4OH raction 30

2.2.9 Analysis of the [^{3}H]-labeled compounds in the mussel flesh which eluted from the Dowex column in the HCl fraction 30

2.2.10 Determination of the total arsenic concentration in the mussel flesh, byssal threads and shells 30

2.3 Results and Discussion 33

2.3.1 The uptake of [^{3}H]-labeled arsenicals from the seawater 33

2.3.2 Purification of the [^{3}H]-labeled arsenicals from the mussel flesh. 33

2.3.3 Identification of the [^{3}H]-labeled arsenicals in the NH_4OH fraction. 36

2.3.4 Attempted identification of the [^{3}H]-labeled arsenicals in the HCl fraction. 39

2.3.5 Total arsenic concentration in the mussel flesh, byssal threads and shells. 40

2.3.6 Summary 42

Chapter 3

The biotransformation of MMA and DMA into arsenobetaine in seawater and mussels 43

3.1 Introduction 43

3.1.1 The origins of arsenobetaine in seawater and marine animals 43

3.1.2 Scope of work 44

3.2 Experimental 45

3.2.1 Instrumentation 45

3.2.2 Chemicals and reagents 45

3.2.3 The uptake and conversion of [^{3}H]-MMA and [^{3}H]-DMA to [^{3}H]-arsenobetaine in seawater and mussels. 45

3.2.4 Isolation and identification of the [^{3}H]-labeled arsenicals in the seawater and the mussel flesh. 46

3.2.5 The diversity of [^{3}H]-labeled compounds in the seawater 47

3.2.6 Examination of the [^{3}H]-labeled compounds in the seawater from the experiment described in section 3.2.5 47

3.3 Results and Discussion 48

3.3.1 Experimental seawater after exposure to [^{3}H]-MMA and [^{3}H]-DMA 48

3.3.2 Control seawater after exposure to [^{3}H]-MMA and [^{3}H]-DMA 57

3.3.3 Mussel flesh after exposure to [^{3}H]-MMA and [^{3}H]-DMA 62

3.3.4 The extraction efficiency of the [^{3}H]-labeled compounds which were extracted from the seawater and mussel samples 67

3.3.5 Examination of the [^{3}H]-labeled compounds in the seawater

after the experiment described in section 3.2.5 68

3.6 Summary 72

Chapter 4

The use of liposomes in predicting the biomobility and bioaccumulation of MMAand DMA 73

4.1 Introduction 73

4.1.1 How do molecules get across membranes? 73

4.1.2 Structures of the main phospholipids found in cell membranes 76

4.1.3 Structures of hydrated phospholipids 77

4.1.4 The mobility of the lipid components within the bilayer 79

4.1.5 Liposomes as models for biological membranes 81

4.1.6 Types of liposomes 81

4.1.7 Large Unilamellar Vesicles (LUVs) 82

4.1.8 How is the biomobility of environmentally sensitive compounds traditionally modelled? 85

4.1.9 Difficulties in using partition coefficients to predict the biomobility of weak acids 85

4.1.10 The bioaccumulation of arsenicals by *Candida humicola* 86

4.1.11 The bioaccumulation of DMA and MMA by unicellular organisms 87

4.1.12 Scope of work and proposed use of diffusion coefficients across liposomal membranes as a model for the prediction of biomobility and bioaccumulation 88

4.2 Theory 89

4.2.1 The rate constant, permeability coefficient and activation energy 89

4.3 Experimental 91

4.3.1 Scintillation counting 91

4.3.2 Chemicals and Reagents 91

4.3.3 Preparation of LUVs and Sampling Technique 91

4.3.4 Determination of Octanol/Water partition Coefficients 93

4.4 Results and Discussion 94

4.4.1 Rate constants and permeabilities for the diffusion of MMA and DMA across liposomal membranes (100 nm LUVs at pH 7.4) 94

4.4.2 Activation energy for the diffusion of MMA and DMA across liposomal membranes (100 nm LUVs at pH 7.4) 96

4.4.3 Octanol/Water partition coefficients 98

4.4.4 Summary 99

Chapter 5

The Development of an NMR technique to measure the rate of diffusion through LUVs and its applications to MMA and DMA 100

5.1 Introduction 100

5.1.1 Traditional techniques used to measure the diffusion coefficients through LUVs 100

5.1.2 Spectroscopic techniques used to measure the diffusion coefficients through LUVs 101

5.1.3 Advantages of using spectroscopy over traditional techniques to measure the diffusion of molecules across membranes 102

5.1.4 Difficulties in using NMR spectroscopy to measure the diffusion of molecules across membranes 102

5.1.5 Scope of work 103

5.2 Theory 104

5.2.1 What causes molecules to diffuse across membranes? 104

5.2.2 Diffusion from a spherical vesicle 106

5.2.3 The permeability coefficient and activation energy 109

5.2.4 Derivation of the equations used to describe the number of particles on either side of the membrane 110

5.2.5 Permeation of a weak acid 113

5.2.6 Comment on D, P, k', k, $\underline{k}$, k_{AH}, $\underline{k}_{AH}$, and P_{AH} (to avoid confusion later) 115

5.3 Experimental 117

5.3.1 Instrumentation 117

5.3.2 Chemicals and reagents 119

5.3.3 Determination of the pK's for DMA and MMA 119

5.3.4 Preparation of LUVs and Sampling technique 120

5.3.5 Concepts to consider when designing these experiments 121

5.3.6 Bligh-Dyer Extraction 122

5.3.7 Phosphorus assay 123

5.3.8 Processing the spectra 123

5.3.9 Permeability coefficient determination 134

5.4 Results and Discussion 135

5.4.1 pK determinations for MMA and DMA 135

5.4.2 The diffusion of DMA through LUVs of various sizes 140

5.4.3 DMA pH study 141

5.4.4 MMA pH and temperature study 145

5.4.5 DMA temperature study 150

5.4.6 DMA temperature study with cholesterol in the membrane 153

5.4.7 Comments on how the results obtained in this chapter apply to biological samples and possible uses for the technique in the future 157

5.5 Summary 158

Chapter 6

The synthesis of organoarsenicals relevant to this thesis 159

6.1 Introduction 159

6.2 Experimental and Results 159

6.2.1 Synthesis of [^{3}H]-MMA from arsenite 159

6.2.2 Synthesis of [^{3}H]-DMA from [^{3}H]-MMA 161

6.2.3 Synthesis of trimethylarsine from arsenic trichloride 162

6.2.4 Synthesis of tetramethylarsonium iodide from trimethylarsine 163

6.2.5 Synthesis of trimethylarsine oxide from trimethylarsine 165

6.2.6 Synthesis of arsenobetaine from trimethylarsine 168

Bibliography 170

LIST OF TABLES

TABLES		PAGE
2.1	Graphite Furnace Operating Parameters.	22
2.2	Operating conditions for the continuous Hydride Generation Atomic Absorption assembly.	24
2.3	Rf values for the unknown from the "NH_4OH fraction".	36
2.4	The [^{3}H]-containing compound(s) in the "HCl fraction".	40
2.5	Arsenic concentrations in the mussel flesh, byssal threads and shells.	40
2.6	The radioactivity in the shells.	41
3.1	Percentage of [^{3}H]-labeled compounds which were extracted from the seawater and mussel samples.	67
4.1	Mean diameter of LUVs produced via the extrusion technique.	84
4.2	Rate constants and permeability coefficients for MMA and DMA at pH 7.4 across the liposomal membrane (100 nm filter size).	94
4.3	The activation energy for the diffusion of across liposomal membranes.	96
4.4	The octanol/water parition coefficients for MMA and DMA.	98
5.1	Raw data from a diffusion experiment.	125
5.2	Integral ratios and time for a diffusion experiment.	126
5.3	Calculated integral ratios for the diffusion experiment in Table 5.2.	132
5.4	pK's for MMA and DMA	135
5.5	The ^{1}H-NMR methyl resonance positions for MMA and DMA with variations in pH.	138
5.6	The ^{1}H-NMR methyl resonance positions for DMA during a diffusion experiment.	138
5.7	DMA diffusion through different sized LUVs (Temp = 24°C and pH = 7.4).	140
5.8	DMA pH Study (Temp = 24°C with NaCl outside).	142

5.9	DMA pH Study (Temp = 24°C with glucose outside).	142
5.10	MMA Diffusion Coefficients (pH = 6.98) through 200 nm LUVs.	146
5.11	MMA Diffusion Coefficients (pH = 7.40) through 200 nm LUVs.	146
5.12	MMAH Diffusion Coefficients through 200 nm LUVs (from Table 5.10)	147
5.13	MMAH Diffusion Coefficients through 200 nm LUVs (from Table 5.11)	147
5.14	The activation energy for the permeation of MMAH through the phospholipid bilayer of LUVs.	149
5.15	Permeability coefficient determination for the anion of MMA.	149
5.16	Rate constant determination for the anion of MMA.	150
5.17	DMA Diffusion Coefficients (pH 7.4) through 200 nm LUVs.	151
5.18	DMAH Diffusion Coefficients through 200 nm LUVs.	151
5.19	The activation energy for the permeation of DMAH through the phopholipid bilayers of LUVs.	152
5.20	DMA Diffusion Coefficients (pH 7.0) through 200 nm LUVs (55:45, EPC:Cholesterol).	154
5.21	DMAH Diffusion Coefficients through 200 nm LUVs (55:45, EPC:Cholesterol).	154
5.22	The activation energy for the permeation of DMAH through a phospholipid bilayer which contains cholesterol.	156

LIST OF FIGURES

FIGURES		PAGE
1.1	Formulas and pKs of arsenic containing compounds found in seawater.	2
1.2	Structures of arsenic containing ribosides found in marine algae.	4
1.3	Stuctures for arsenic containing phospholipids found in marine algae.	5
1.4	Some arsenic containing compounds found in marine animals.	6
1.5	Water column profiles of arsenate (As V), arsenite (As III), MMA, DMA, phosphate (HPO_4^{-2}), and chlorophyll (CHL) concentrations during a bloom in Alice Arm B.C.	9
2.1	Challenger's Mechanism for the biomethylation of arsenic. The arsenic (III) intermediates in braces are unknown.	15
2.2	Structure of S-adenosylmethionine (SAM).	15
2.3	Proposed mechanism for the biosynthesis of arsenosugars by marine algae.	17
2.4	Proposed biosynthetic pathway from arsenosugars to arsenobetaine.	19
2.5	Schematic diagram of the continuous Hydride Generation Atomic Absorption assembly.	23
2.6	A) 200 liter seawater tank with continually circulating seawater; B) 15 liter experimental tank containing [^{3}H]-MMA; C) "control group" of mussels; D) wire cage containing "experimental group" of mussels; E) aeration stones and tubing.	27
2.7	Schematic representation of the proceedures used for the extraction of arsenic compounds from the mussels and for the purification of the extract.	29
2.8	Wet ashing apparatus; (A) Teflon cylindrical plugs; (B) Teflon diffusion funnels; (C) Teflon stopper with capillary; (D) 250 ml round bottom flask. All joints are 14.5/23. All dimensions are mm.	32
2.9	The elution profile from a Sephadex LH-20 column for the water soluble	

[^{3}H]-labeled compouds which were MeOH extracted from the mussels. 34

2.10 The elution profile from the Dowex column for the [^{3}H]-labeled compounds which eluted in fraction 8 to 21 from the Sephadex column. 35

2.11 HPLC chromatograms from the anion exchange column at pH 6.67; (A) arsenobetaine and dimethylarsinate on the anion exchange column at pH 6.67, (B) the compound eluting in fractions 11 to 17 from the Dowex column. 38

3.1 The cation exchange chromatograme for the standards of MMA, DMA, and arsenobetaine. 49

3.2 The cation exchange chromatograms for the phenol extract from the "experimental seawater" on days 4 (A) and 7 (B) after [^{3}H]-MMA exposure. 50

3.3 HPLC chromatograms; (A) arsenobetaine, MMA, and DMA on the anion exchange column at pH 4, (B) the compound eluting in fraction 3 (Figure 3.2 (B)) on the anion exchange column at pH 4. 51

3.4 HPLC chromatograms; (A) MMA on the size exclusion column and (B) of the compound eluting in fraction 3 (Figure 3.2 (B)) on the size exclusion column. 52

3.5 HPLC chromatograms; (A) arsenobetaine and DMA on the anion exchange column at pH 6.67, (B) the compound eluting in fraction 7 (Figure 3.2 (B)) on the anion exchange column at pH 6.67. 53

3.6 HPLC chromatograms; (A) arsenobetaine on the size exclusion column, and (B) of the compound eluting in fraction 7 (Figure 3.2 (B)) on the size exclusion column. 54

3.7 The cation exchange chromatograms for the experimental seawater on days 4 (A) and 7 (B) after [^{3}H]-DMA exposure. 56

3.8 The HPLC chromatogram for the compound eluting in fraction 7 (Figure

	3.7 (A)) on the anion exchange column at pH 6.67.	57
3.9	The cation exchange chromatograms for the phenol extract from the "Control seawater" on days 4 (A) and 7 (B) after [^{3}H]-MMA exposure.	58
3.10	The HPLC chromatogram for the compound eluting in fraction 7 (Figure 3.9 (B)) on the anion exchange column at pH 6.67.	59
3.11	The cation exchange chromatograms for the phenol extract from the "Control seawater" on days 4 (A) and 7 (B) after [^{3}H]-DMA exposure.	61
3.12	The HPLC chromatogram for the compound eluting in fraction 7 (Figure 3.11 (B)) on the anion exchange column at pH 6.67.	62
3.13	The cation exchange chromatograms for the phenol extracted compounds from the mussel flesh on days 4 (A) and 7 (B) after [^{3}H]-MMA exposure.	63
3.14	The HPLC chromatograms for the compound eluting in fractions 2 and 3 (Figure 3.13 (B)) on the anion exchange column at pH 4.	64
3.15	The cation exchange chromatograms for the phenol extracted compounds from the mussel flesh on days 4 (A) and 7 (B) after [^{3}H]-DMA exposure.	66
3.16	The size exclusion HPLC chromatogram for the "experimental seawater" on days 4 (A), 7 (B), and 10 (C).	71
3.17	The size exclusion HPLC chromatograms for the DMA standard.	71
4.1	The Fluid Mosaic model of the cell membrane. The arrows represent the directions of the lateral diffusion of the proteins.	74
4.2	Mechanisms of permeation through the bilayer without entry into the hydrophobic region.	75
4.3	Structures of the major phospholipids found in cell membranes; PA, phosphatidic acid; PS, phosphatidyl serine; PC, phosphatidyl choline; PE phosphatidylethanolamine; PI, phosphatidyliniositol; DPG, diphosphatidylglycerol. R is the side chain (Figure 4.4)	76

4.4 The structures of the side chains of egg phosphatidyl choline and palmitic acid (a), stearic acid (b), oleic acid (c), and linoleic acid (d). 77

4.5 Structures of phospholipids which are formed upon hydration; A) a monolayer formed at an air-liquid interface; B) a micelle; C) an example of a liposome; D) a black membrane, a planar bilayer, that separates two aqueous phases. 78

4.6 Modes of mobility of the lipid components of the bilayer. 79

4.7 Insertion of cholesterol into a phospholipid bilayer. A schematic representation of the alignment of a cholesterol molecule with a phospholipid in a lipid bilayer. 80

4.8 The Extruder. 82

4.9 Electron micrographs of vesicles prepared by extrusion through; A) 400; B) 200; C) 100; D) 50; E) 30 nm pore size polycarbonate filters. 83

4.10 Test of the unilamellarity of vesicles extruded the indicated number of times through 400 (•), 200 (■), and 100 (□) nm pore size filters. 84

4.11 Radiolabeled sampling proceedure. 92

4.12 Efflux measurements of MMA and DMA. Data is plotted according to equation 4.6. 95

4.13 Activation energy determinations for MMA and DMA. Data is plotted according to equation 4.8. 97

5.1 Flux across a membrane in response to a difference in chemical potential. 105

5.2 Schematic depiction of V^{aq}_{in}, V^{aq}_{out}, V^{m}_{in}, V^{m}_{out}, D, K, k', k, $[HA]^{m}_{out}$, $[HA]^{m}_{in}$, $[HA]^{aq}_{out}$, $[HA]^{aq}_{in}$. 107

5.3 Schematic depiction of C^{m}_{in}, C^{m}_{out}, r_{in}, and r_{out}. 108

5.4 The two chemical species of DMA in aqueous solution. 113

5.5 The pulse sequence used for water suppression. 117

5.6 The microprogram designed to operate the spectrometer. 118

5.7 The ^{1}H-NMR spectrum of DMA and LUVs. 124

5.8 An example of a plot of the inside (■) and outside (+) integral ratios versus time for the diffusion of DMA through a liposomal membrane. 127

5.9 An example of a plot of $\ln(n^t_{in}-n^{eq}_{in})$ (■) and $\ln(n^{eq}_{out}-n^t_{out})$ (+) versus time for the diffusion of DMA through a liposomal membrane. 130

5.10 An example of the inside (■) and outside (+) integral ratios versus time for the diffusion of DMA through liposomal membranes. The solid lines are the experimental fits for the data which were generated by using equations [5.47] and [5.48]. 133

5.11 A plot of the ^{1}H-NMR methyl resonance positions for MMA versus pH. 136

5.12 A plot of the ^{1}H-NMR methyl resonance positions for DMA versus pH. 137

5.13 A plot of the ^{1}H-NMR methyl resonance positions for DMA versus time for a diffusion experiment. 139

5.14 A plot of the pH dependant rate constants (k in ml s^{-1}) vs the $[H^+]$ for the efflux of DMA at 24°C. Either glucose (▲) or NaCl (■) was added to the outside of the 200 nm LUVs to balance the osmotic pressure. 143

5.15 A plot of the pH dependant rate constants ($\underline{k}$ in s^{-1}) vs the $[H^+]$ for the efflux of DMA at 24°C. Either glucose (▲) or NaCl (■) was added to the outside of the 200 nm LUVs to balance the osmotic pressure. 144

5.16 A plot of the $\ln(P_{AH})$ from the MMAH difffusion experiments at pHs 6.98 (✱) and 7.4 (□) versus 1/T. 148

5.17 A plot of the $\ln(P_{AH})$ versus 1/T for the activation energy determination for DMAH diffusion through a phospholipid bilayer. 152

5.18 A plot of the $\ln(P_{AH})$ versus 1/T for the activation energy determination for DMAH diffusion through a phospholipid bilayer which contains cholesterol. 155

6.1 ^{1}H-NMR (200MHz in D_2O) spectrum of [^{3}H]-MMA. 160

6.2	^{1}H-NMR (200MHz in D_2O) spectrum of [^{3}H]-DMA.	162
6.3	^{1}H-NMR (200MHz in D_2O) spectrum of tetramethylarsonium iodide.	164
6.4	DCI mass spectrum of tetramethylarsonium iodide.	165
6.5	^{1}H-NMR (200MHz in D_2O) spectrum of trimethylarsine oxide.	166
6.6	DCI mass spectrum of trimethylarsine oxide.	167
6.7	^{1}H-NMR (200MHz in D_2O) spectrum of arsenobetaine.	168
6.8	DCI mass spectrum of arsenobetaine.	169

LIST OF ABBREVIATIONS

ACS	American Chemical Society
cm	centimeter
DCI-MS	desorption chemical ionization-mass spectrometry
DMA	dimethylarsinate and/or dimethylarsinic acid
DMA^-	dimethylarsinate
DMAH	dimethylarsinic acid
g	gram
HPLC	high performance liquid chromatography
kg	kilogram
L	liter
LUVs	large unilamellar vesicles
M	molar (mol L^{-1})
mA	milliampere
mCi	millicurie
mg	milligram
ml	milliliter
mm	millimeter
mM	millimolar
MMA	monomethylarsonate and/or monomethylarsonic acid
MMA^-	monomethylarsonate
MMAH	monomethylarsonic acid
nm	nanometer
ppb	parts per billion
ppm	parts per million
psi	pounds per square inch

rpm	revolutions per minute
s	second
TSP	3-(Trimethylsilyl) proprionic-2,2,3,3-d_4 sodium salt
µCi	microcurie
µg	microgram
vs	versus
v/v	volume-to-volume ratio
w/v	weight-to-volume ratio

ACKNOWLEDGEMENTS

I would like to extend my sincere gratitude to my research supervisors, Dr. W.R. Cullen and Dr. F.G. Herring, for their guidance, patience, encouragement, and financial support throughout the course of this project.

I would also like to thank Dr. P.R. Cullis and K. Wong for allowing me to perform the experiments described in Chapter 4 in their lab.

In addition, Iwould also like to thank Dr. P.S. Philips for helping me with the mathematics behind the diffusion equations and Dr. O. Chan for helping me with the NMR spectrometer.

I would also like to acknowledge the members of my research group, both past and present, for many helpful discussions.

CHAPTER 1

GENERAL INTRODUCTION

Arsenic is the 20th most abundant element in the earth's crust.[1] Its average concentration is often quoted as 3 ppm (parts per million), but this may vary widely depending upon geographical location.[2,3] Arsenic is generally associated with igneous and sedimentary rocks[4] and in particular, with the sulfidic ores of realgar (As_4S_4), orpiment (As_2S_3) and arsenopyrite (FeAsS). Arsenic is released into the environment by natural processes such as weathering, volcanic and biological activity, and by anthropogenic activities such as the smelting of ore and the burning of fossil fuels.[5,6]

Arsenic is present in virtually all types of soils, sediments, aquatic environments and organisms.[5] In particular, it is present in high concentrations (up to 100 mg/kg) in marine algae and animals.[7] Since marine organisms are a major source of arsenic in human beings, [7] information about its chemical forms is important from toxicological and nutritional points of view.

The literature on arsenic in the sea dates back to the beginning of the century.[8-10] By the 1920's it was firmly established that marine organisms contained high levels of arsenic.[11,12] In spite of much effort, however, the chemical form of arsenic in marine organisms remained unknown until 1977, when arsenobetaine **1** was isolated and identified in the tail of the Western rock lobster.[13] Arsenobetaine has since been identified in various marine animals and the ubiquitous nature of this arsenical in marine animals has been well established.[5] In addition to arsenobetaine, numerous other arsenic containing compounds have been isolated and identified in marine organisms.

Each of the individual arsenic containing compounds has different physical and chemical properties, toxicities, mobilities and biotransformations. In order to fully understand the arsenic biogeochemical cycle in marine organisms, the different characteristics of each of these compounds must be throughly investigated.[5]

1.1 SPECIATION AND CONCENTRATION OF ARSENIC CONTAINING COMPOUNDS IN THE MARINE ENVIRONMENT

1.1.1 Seawater

In seawater the total arsenic concentration is typically 1 to 8 ppb (parts per billion).[14-17] Arsenate **2** and arsenite **3** are the predominant arsenic species in seawater and their concentrations depend upon the nature and degree of biological activity at the time of sampling and the redox potential of the seawater.[18] The ratio of arsenate to arsenite in seawater is typically about 10:1. Both phytoplankton and bacteria can reduce arsenate to arsenite.[19] In addition to the inorganic arsenic species, two methylated arsenicals, monomethylarsonate (MMA) **4** and dimethylarsinate (DMA) **5** are also present as a small percentage of the total arsenic concentration in seawater.[20-22] Arsenobetaine is identified in seawater as part of this thesis. Arsenate, MMA, DMA and arsenobetaine all contain arsenic in an oxidation state of (V), whereas in arsenite and trimethylarsine the oxidation state is (III).[5]

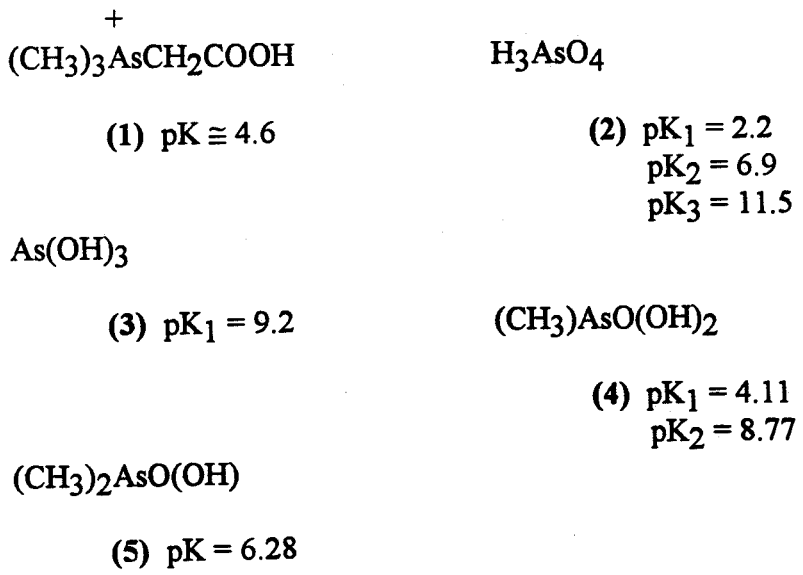

Figure 1.1 Formulas and pKs of arsenic containing compounds found in seawater.

1.1.2 Marine Plants and Algae

Arsenate is typically found in marine plants and algae,[23] however, the details of the uptake mechanism are poorly understood. Arsenate is either accumulated by algae due to its similarity with phosphate[22,24,25] or absorbed by a non-competitive mechanism.[26] Regardless of the mechanism of arsenate uptake, however, the primary producers such as the phytoplankton and algae must adapt for the accumulation of cellular arsenate. The marine phytoplankton (diatoms, coccolithophorids, dinoflagellates, and green algae) have adapted to cellular arsenate by converting it to arsenite, MMA and DMA which are then excreted from the cells.[22] The metabolism of arsenic species depends upon the type of marine phytoplankton, but in general 30 to 50% of the arsenic which is not excreted is converted to lipid soluble arsenic compounds.

The three main classes of macroalgae contain arsenic concentrations between 0.4 - 32 ppm.[27] The classes and percentages of arsenic in the organic form are as follows: Phaeophyceae, 78%; Rhodophyceae, 57%, and Chlorophyceae, 53%. The organoarsenicals in macroalgae were first isolated and identified by Francesconi and Edmonds.[28,29] They extracted these organoarsenicals from the seaweed *Ecklonia radiata*, and used chromatographic and spectroscopic techniques to show that the algal arsenic was incorporated into both water soluble and lipid soluble compounds. The water soluble compounds were found to be the arsenic containing ribosides **6a** and **6b** and accounted for 81% of the total arsenic which was present in the seaweed. The arsenic containing ribosides **6c** and **6d** were subsequently isolated from the kidney of the giant clam *Tridacna maxima*,[30] these organoarsenicals were attributed to the symbiotic, unicellular, green algae which lives in the clam tissue.[30,31] These arsenic containing ribosides along with **6e** have since been shown to be present in many other marine seaweeds.[28-30,32-36] Recent studies on the macroalgae *Sargassum thurbergii* have shown the presence of **6f** the trimethylarsonium analogue of **6e**, as a minor arsenical.[37]

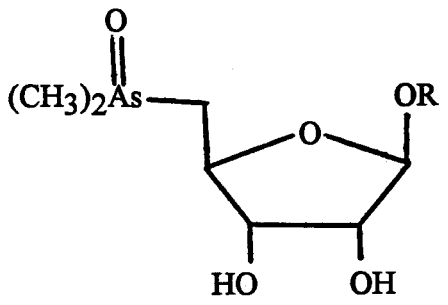

(6)

a R = $CH_2CHOHCH_2OH$

b R = $CH_2CHOHCH_2SO_3H$

c R = $CH_2CHOHCH_2OPO(OH)OCH_2CHOHCH_2OH$

d R = $CH_2CHOHCH_2OSO_3H$

e R = $CH_2CHNH_2CH_2SO_3H$

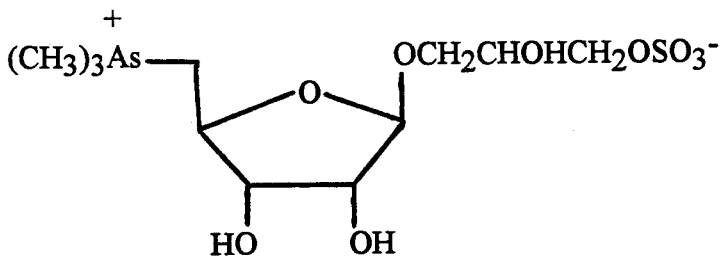

(6f)

Figure 1.2 Structures of arsenic containing ribosides found in marine algae.

Two of the structures[34] for the arsenic containing phospholipids are **7a** and **7b**. The phosphorus containing arsenical **7c** has been identified in *E. radiata*[28] and *Hizikia fusiforme*.[39] It has been speculated that arsenic containing phospholipids may be biosynthesized by the algae to facilitate the incorporation of arsenic into the membrane lipid bilayers which will ultimately result in its excretion from the algae.[31]

The ability of algae to tolerate high levels of arsenic is exemplified by the the green flagellate, *Tetraselmis chuii*, which survives in arsenic concentrations as high as 1000 ppm arsenate.[40] (The average concentration of arsenic containing compounds in marine algae is about 10 ppm.[5])

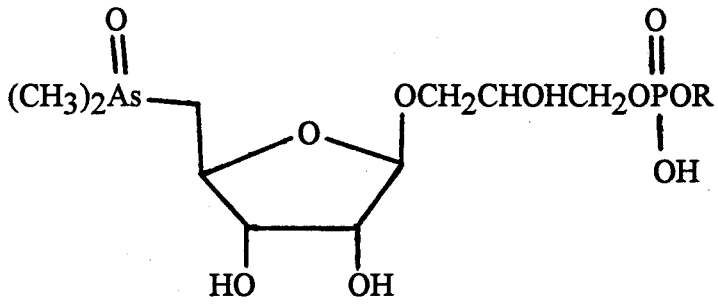

(7)

a R = $CH_2CH(OOCX)CH_2OOCX'$

b R = $CH_2CH(OH)CH_2OOCX'$

c R = $CH_2CH(OH)CH_2OH$

Figure 1.3 Structures for arsenic containing phospholipids found in marine algae.

1.1.3 Marine Animals

The arsenic concentration in marine animals varies widely between 0.31 ppm found in the flesh of a typical salmon to about 340 ppm found in the midgut of the carnivorous gastropod *Charonia sauliae.*[5] The arsenic containing compounds in marine animals are relatively non-toxic. Crustaceans and other benthic organisms have higher arsenic concentrations than fish. Since its identification from the tail of the Western rock lobster,[13] arsenobetaine has been shown to be the predominant arsenical in most marine animals.[5,28,32,41] When arsenobetaine was injected into mice at concentrations of up to 500 mg kg^{-1}, it was rapidly excreted without being altered metabolically.[42] The mice in these experiments showed no symptoms of poisoning. Arsenobetaine has also been isolated from the urine of human subjects who had eaten cooked lobster tails and place.[43,44] Additional feeding experiments with arsenobetaine and humans showed that 69-85% of the ingested arsenic was excreted within 5 days.[44]

In addition to arsenobetaine, other methylated arsenicals have been identified in marine animals. The tetramethyl arsonium ion **8** has been found in the clam *Meretrix lusoria*[45] and in several gastropods.[46,47] There have been claims of the presence of arsenocholine **9** in shrimp,[48-50] however, its presence could not be confirmed by others.[50,51] Arsenocholine **9** is generally believed to be a probable precursor to arsenobetaine.[52] Trimethylarsine oxide **10** has been found as a minor component of fish and some molluscs.[47,53-55]

Shibata and Morita have recently shown the presence of the arsenic containing ribosides **6a** and **6c** in a wide variety of bivalves,[56] by using high performance liquid chromatography coupled to an inductively coupled argon plasma atomic emission spectrometer as the detector. They speculate that these arsenic containing ribosides enter the bivalves via their food, i.e., the phytoplanktons are the origin of these sugars. The quantity of the arsenic containing ribosides varies widely even within the same species.

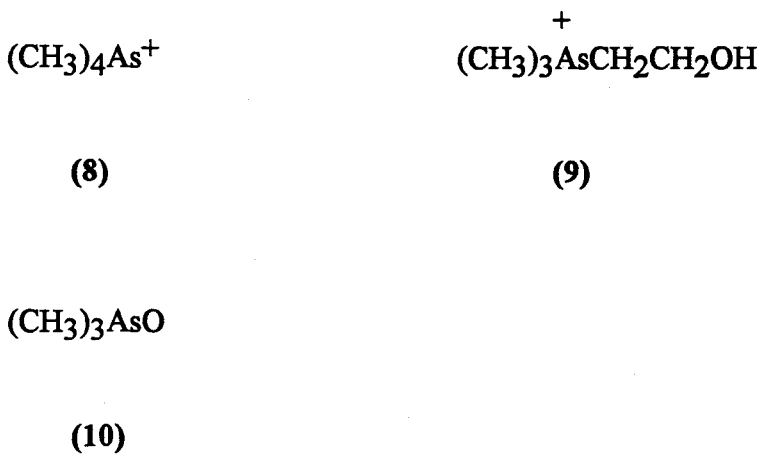

Figure 1.4 Some arsenic containing compounds found in marine animals.

An interesting feature of the arsenic compounds in marine animals is that, with the exception of the arsenic containing ribosides found in marine animals, all of the nitrogen analogues of the arsenic compounds are abundant in these organisms. For example, glycinebetaine, tetramethylammonium ion, and trimethylamine oxide are the nitrogen analogues of arsenobetaine, tetramethylarsonium ion, and trimethylarsine oxide, respectively.[7] These nitrogen containing compounds are thought to be the end products of the nitrogen metabolism, and are probably retained in the body as osmo-regulators.[57] The nitrogen containing compounds are present in much greater quantities than their arsenic analogues.[7]

1.2 MMA AND DMA IN THE AQUATIC ENVIRONMENT

1.2.1 Freshwater

The arsenic concentration in fresh water environments is typically 1-10 ppb,[2] although values as high as 3500 ppb have been reported.[58] Braman and Foreback[59] first detected MMA and DMA in aquatic systems in 1973. They reported on the arsenic speciation in both freshwater and saline samples. The freshwater samples contained arsenicals, arsenate and usually arsenite. MMA and DMA were also usually present, typically between 10 and 15% of the total arsenic, but values up to 70% were reported. In all cases the dominant organoarsenic compound was DMA. A similiar study by Andreae on the distribution of the organoarsenicals in fresh water suggested that there is a correlation between the sites with the highest density of planktonic algae and the highest concentration of methylarsenicals.[60]

Arsenite is methylated by various freshwater species of green algae, including *Ankistrodesmus sp.*, *Chlorella sp.*, and *Selenastrum sp.* Each of these organisms transformed arsenite at a concentration of 5000 ppb to MMA, DMA and trimethylarsine oxide.[61]

MMA[62-66] and DMA[67] are used as herbicides and, therefore, it may be expected that MMA and DMA would find their way into the surrounding lakes and rivers. Fortunately, both MMA and DMA are highly retained by the soils and hence leaching into fresh water does not readily occur.[65]

1.2.2 Seawater

Andreae has also reported detailed concentration versus depth profiles for MMA and DMA in northeast Pacific and Californian coastal waters.[60,68] The general trend in these profiles seems to be a depletion of arsenate concentration in the photosynthetically active surface waters (eutropic zone) with a corresponding increase in arsenite, MMA, and

DMA concentrations. The DMA to MMA concentration ratios in these profiles was typically about 10:1. The concentration of DMA decreased towards the base of the photic zone while the concentration of MMA remained fairly constant. In deeper water the methylarsenicals were either below the detection limits or barely detectable. This observation suggests that DMA and MMA were produced by phytoplankton or closely related heterotrophs. This idea is further supported by correlations which were found between typical indicators of primary productivity, i.e., chlorophyll concentrations[60] and/or ^{14}C uptake.[68] It was concluded from these studies that arsenate was taken up by phytoplankton in the eutrophic surface waters and subsequently converted to arsenite, MMA and DMA which were then released back into the water column. The above trends are prevelant in the concentration versus depth profiles in Figure 1.5. The sharp decrease in DMA concentration with depths below 20 m (Figure 1.5) would suggest release of DMA from live algal cells rather than bacterial decomposition of organoarsenical, as the later process would be expected to distribute these compounds to a greater depth.

Other studies have shown how the type of algal species[17] and temperature[69,70] affects the appearance, concentration and relative proportions of these two methylarsenicals.

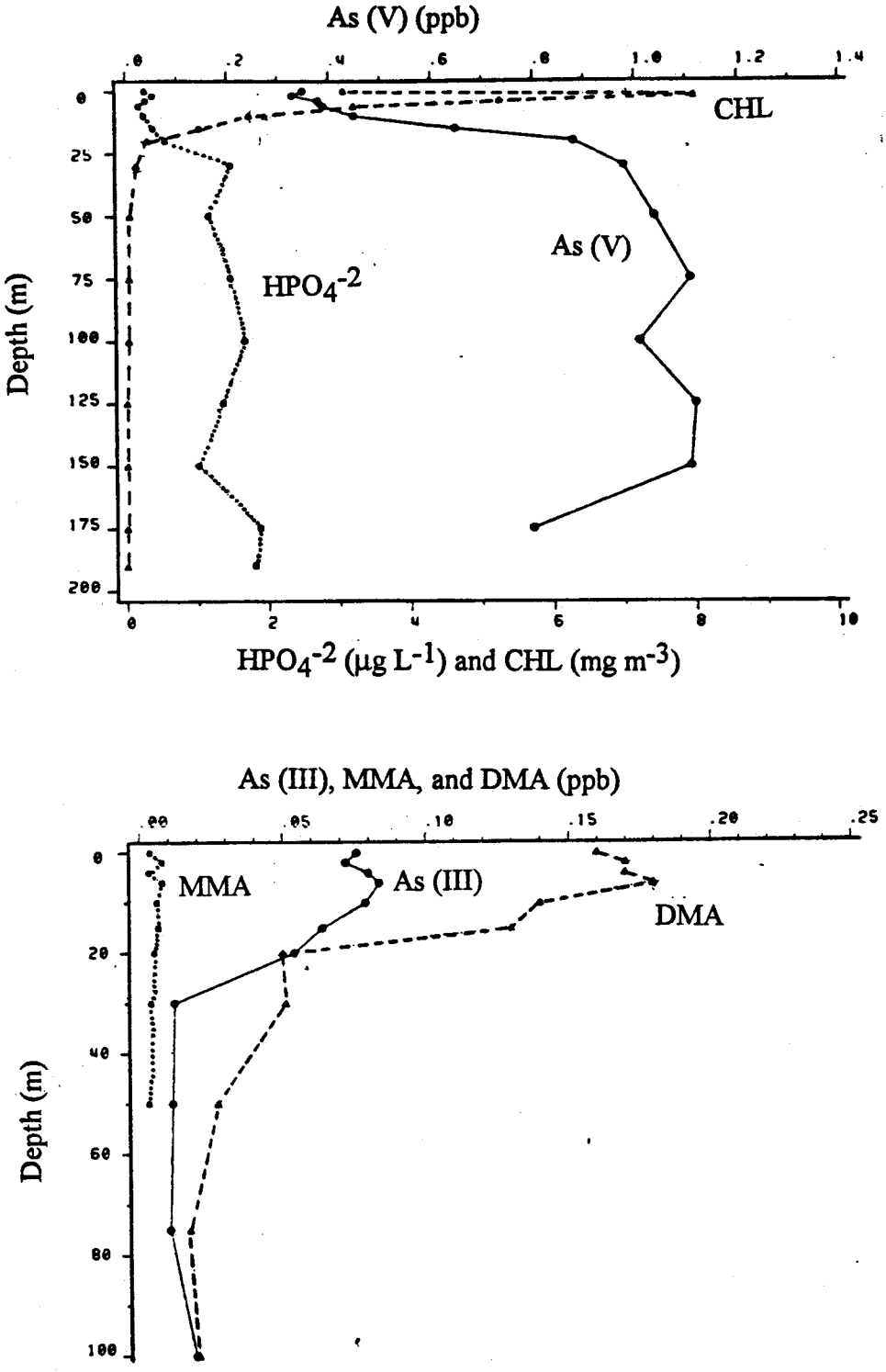

Figure 1.5 Water column profiles of arsenate (As V), arsenite (As III), MMA, DMA, phosphate (HPO_4^{-2}), and chlorophyll (CHL) concentrations during a bloom in Alice Arm B.C.[5]

1.3 OVERVIEW OF THESIS

The work described in this thesis was initiated so that the role of MMA and DMA in the marine biogeochemical cycle of arsenic could be better understood. These two methylarsenicals are the simplest organoarsenicals found in the aquatic environment and, therefore, MMA and DMA may be likely precursors to many of the more complex organoarsenicals. Thus, the results from this work should provide information about the metabolic pathways of arsenic in the marine environment. In addition, different amounts of these two very similiar compounds are bioaccumulated by marine organisms and are found in seawater. This is quite possibly the result of differences in the ability of MMA and DMA to pass through biological membranes.

The biotransformations of MMA and DMA were investigated by adding either [^{3}H]-MMA or [^{3}H]-DMA to a seawater tank. This seawater tank also contained mussels and at the end of the exposure period the [^{3}H]-labeled arsenic compounds in the mussels and seawater were identified or an attempt was made to identify them. In addition, the total arsenic concentrations in the mussel flesh, byssal threads and shells were determined.

The diffusion coefficients of MMA and DMA across phospholipid membranes were determined by using a radiolabeled permeant and by using a NMR technique which was developed as part of this thesis. These coefficients are suggested as a way to predict biomobility and the disadvantages of using partition coefficients for such predictions is discussed. The effects of temperature, membrane composition, and pH on the diffusion coefficients of MMA and DMA across membranes were investigated.

The synthesis of many of the organoarsenicals which were used in this thesis is also described, including the synthesis of radiolabeled [^{3}H]-MMA and [^{3}H]-DMA.

CHAPTER 2

EXPOSURE OF MUSSELS TO [^{3}H]-MMA

2.1 INTRODUCTION

2.1.1 Origins of the Organoarsenicals in Marine Animals

It is generally assumed that the organoarsenicals which are found in marine organisms are partially synthesized from arsenate by organisms at lower trophic levels.[5] This hypothesis is based upon the observation that species at the higher trophic levels (fish, crustaceans, and gastropods) do not seem to be able to synthesize compounds such as arsenobetaine from arsenate.

The accumulation hypothesis is supported by Unlu and co-workers[71-73] who showed that [^{74}As]-algal organoarsenicals (presumably compounds **6a-f**) were readily taken up by crabs, whereas inorganic [^{74}As]-arsenate, fed via arsenate injected mussels was not readily taken up, and the [^{74}As]-arsenate that was taken up was readily eliminated from the crab without being converted to any [^{74}As]-organoarsenicals. Francesconi and Edmonds injected earthworms with arsenate which were hand-fed to catfish and school whiting. Very little of the ingested arsenate was retained by the fish and the amount of arsenobetaine in the fish did not increase over the controls.[53] However, trimethylarsine oxide was detected in the dosed whiting and the catfish showed an increase in this arsenical relative to the control. It was argued that arsenate was not converted to trimethylarsine by the fish, but that the biotransformation was the result of bacterial action in the gut tract of the fish.[53]

The direct transfer of organoarsenicals along the food chain is not a universal phenomenom. The organoarsenicals found in algae are clearly not the same compounds

found in the animals which feed on them as shown by the following example. The algae *Dunaliella tertiolecta* was cultured in the presence of [^{74}As]-arsenate and fed to the lobster *Homarus americanus*. The results of a chromatographic study showed that no [^{74}As]-arsenobetaine was produced during the time scale of the experiment (2 days). In addition, the arsenic containing phospholipids **7a,b,c** were degraded to the simple arsenic containing ribosides, such as **6a**.[74] Thus, the lobster appears to be unable to convert the arsenic containing ribosides into arsenobetaine, its natural organoarsenical. When [^{74}As]-arsenate is fed directly to the lobster, no organoarsenicals seem to be produced. Subsequent experiments yielding similiar results have been tried with gastropods.[75]

However, Klumpp and Peterson[75-77] have obtained experimental results which seem to contradict the generality of the accumulation hypothesis. In the marine food chain, *Fucus spiralis→Littorina littoralis→Nucella lapillus*, algae are being consumed by a herbivorous snail which is in turn being consumed by a carnovorious snail. *L. littoralis* incorporates [^{74}As]-arsenate from the water or the [^{74}As]-labeled *F. spiralis*, whereas, *N. lapillus* incorporates much less [^{74}As]-arsenate from water. Both snails are equally efficient of accumulating arsenic from their food and this is their main source of the element. The majority of the [^{74}As] in the snails, regardless of the feeding mechanism, seems to be a single water-soluble compound which is not present at the first trophic level. Some of the lipid-soluble arsenical found in *F. spiralis* is present in both snails at about 10% of the label. These results indicate that the principal water soluble arsenical in the snails does not come from the algae and that the snails can synthesize it directly from arsenate. Furthermore, the lipid soluble arsenic compound is passed along the food chain. In general, the arsenic concentration in herbivorous species is lower than in carnivores.[78-80]

Also, the arsenic concentration in a marine animal is not necessarily the same as the arsenic concentration in the surrounding environment. For example, the arsenic

content in clams is certainly not dependent upon the arsenic content of the sediments in which they are living. This was shown by the chalky Macoma (*Malcoma calcarea*) which when living in the mine-polluted sediment (46.5 ppm As wet weight) was observed to contains 3.2 ppm As and when living in cleaner sediment (9.4 ppm As) contains 3.9 ppm As.[5]

2.1.2 Biomethylation of Arsenic

The products of the biomethylation of inorganic arsenic have been observed in microorganisms, plants, mice, monkeys and humans.[81] It has been suggested that organisms biomethylate arsenic as a method to detoxify it.[82]

The biomethylation of arsenic was first described in detail by Challenger after he correctly identified the volatile compound produced by the mould *Scopulariopsis brevicaulis* as trimethylarsine.[83] Trimethylarsine had a garlic like odor and had been linked to several cases of arsenic poisoning.[82,84] Challenger proposed a mechanism for the biotransformation of arsenate to trimethylarsine[82] (Figure 2.1). This scheme involves alternating reduction and oxidative steps with the transfer of a methyl group to the arsenic occuring during the oxidation step. Support for this sequence comes from the observation that arsenite, arsenate, MMA, and DMA are all substrates for the production of trimethylarsine by *S. brevicaulis.*

Challenger suggested that the methyl donor was probably a methylated compound such as betaine, methionine or a choline derivative. Of these three suggestions he found that only [$^{14}CH_3$]-methionine transferred its label to arsenite to any significant extent.[85,86] The active form of methionine has subsequently been identified as S-adenosylmethionine (SAM)[87,88] (Figure 2.2). This has been supported by Cullen *et al.*[89-91] who showed that the CD_3 group from labeled L-methionine-methyl-d_3

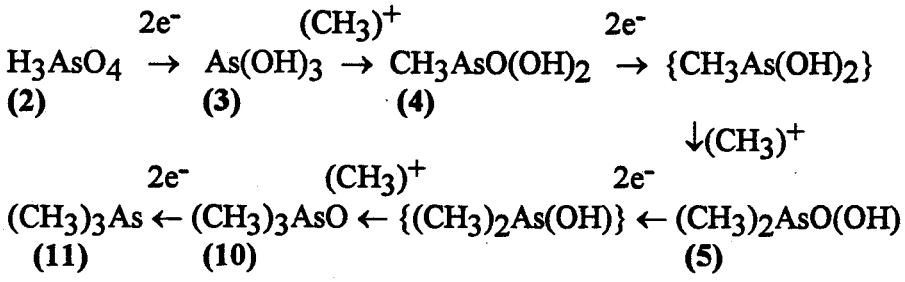

Figure 2.1 Challenger's Mechanism for the biomethylation of arsenic. The arsenic (III) intermediates in braces are unknown.

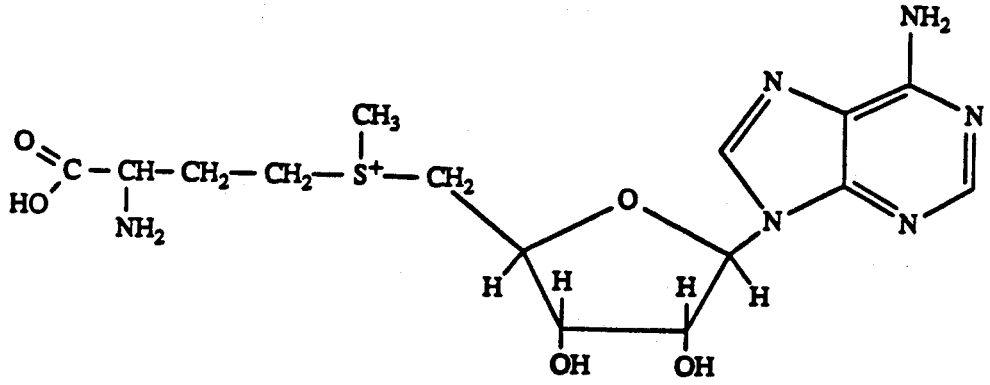

Figure 2.2 Structure of S-adenosylmethionine (SAM)

was tranferred intact to a wide variety of arsenicals by *Scopulariopsis* and *Candida* cultures.

Investigations into the identity of the reducing agent in the scheme have been carried out[92] and a range of thiols and dithiols including: cysteine, glutathione, dithiothreitol, and lipoic acid were found to be capable of carrying out the reductions via a two electron transfer process.[92,93]

The first well documented report of an arsine being produced by bacteria was not made until 1971, when an anaerobic strain of *Methanobacterium* produced a volatile gas with a garlic odor from arsenate.[94] This volatile gas was probably dimethylarsine. Carbon dioxide was necessary for its production. Both dimethylarsine and trimethylarsine were produced by cell extracts of *Methanobacterium thermoautotrophicum.*[95]

Since 1971, a number of nonmethanogenic bacteria have been identified by Anderson and co-workers as methylarsine producers.[96-98] The bacteria that were used in their studies were isolated from the environment and cultured in media containing arsenate (≤100 ppm). Under aerobic conditions arsenate and MMA were methylated by the bacteria to dimethyl and trimethyl species. In addition, the bacteria also reduced MMA to methylarsine and demethylated MMA to arsenate.

The occurence of MMA, DMA, and trimethylarsine oxide in the sediments, seawater, and selected marine organisms and plants seems to support Challenger's mechanism (Figure 2.1) of biomethylation.

2.1.3 Proposed mechanism for the biosynthesis of arsenosugars

Francesconi and Edmonds have proposed the following scheme, Figure 2.3, to account for the biosynthesis of arsenosugars by marine algae.[99,100] The scheme begins with the incorporation of arsenate by the algae, which may be accumulated because of its similarity to phosphate. The arsenate is then presumably metabolized by the

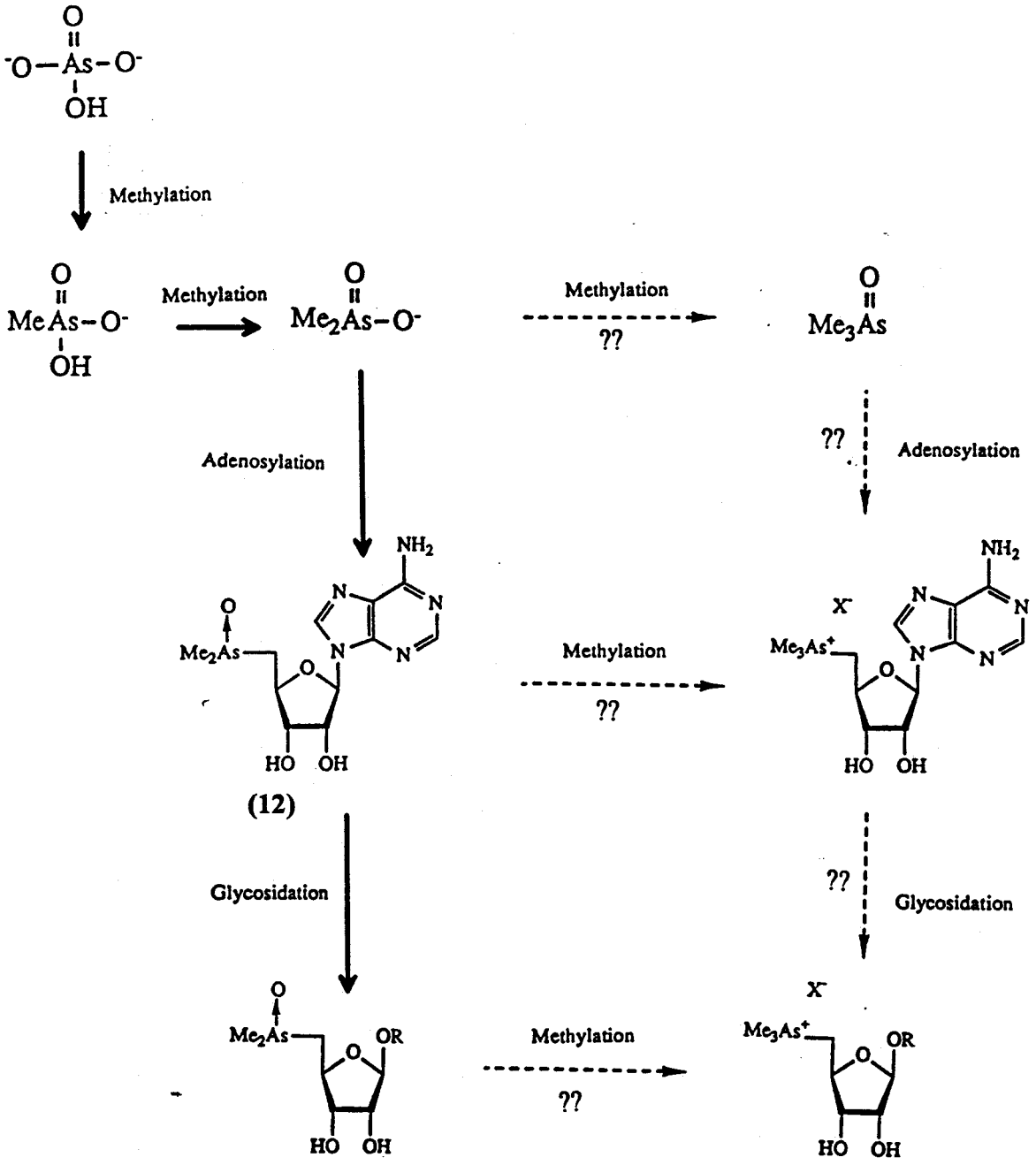

Figure 2.3 Proposed mechanism for the biosynthesis of arsenosugars by marine algae.[99]

mechanisms outlined by Challenger (Figure 2.1), to initially produce MMA and then DMA. It would also seem plausible to start the scheme with either DMA or MMA, both of which are present in seawater in varying amounts.[5] The arsenic containing nucleoside **12** is produced if S-adenosylmethionine (Figure 2.2) donates an adenosyl group to DMA instead of a CH_3 group. The nucleoside **12** has recently been isolated by Edmonds *et al.* from the kidney of the giant clam, *Tridacna maxima.*[101] This nucleoside (upon enzymatic hydrolysis) could yield the range of dimethylarsinoribosides which have been identified from algae sources. A possible biosynthetic pathway to the formation of the trimethylarsinoriboside is also shown in Figure 2.3 and the incorporation of a third methyl group attached to the arsenic may occur at three possible steps.

2.1.4 Proposed conversion of arsenosugars to arsenobetaine

Francesconi and Edmonds have suggested that the arsenic containing ribosides which are found in algae are the likely precursors of arsenobetaine.[99,100] The proposed routes are shown in Figure 2.4. Anaerobic decomposition experiments on the naturally occuring arsenic containing ribosides which are found in the kelp *E. radiata* provide evidence to support this hypothesis. Anaerobic conditions occur in marine sediments and the reactions may be microbially mediated. Clevage of the C3-C4 bond in the ribose ring of the dimethylarsenoribosides yields dimethyloxarsylethanol, and cleavage of the same bond in the trimethylarsenoriboside yields arsenocholine. Both dimethylarsenoylethanol **13** and arsenocholine were produced from the appropriate precursors in the experiments. The trimethylarsenoriboside is only a minor constituent (≈5%) of the total organoarsenicals in algae, therefore, both possible pathways to the formation of

arsenobetaine will be considered. Dimethyloxarsylethanol would require a methylation of the arsenic and the oxidation of the primary alcohol through intermediates such as dimethylarsinylacetic acid **14** or arsenocholine. Arsenocholine is the more likely immediate precursor to arsenobetaine as its presence has been reported in shrimps[49,50,102] and it is readily converted to arsenobetaine when administered to the juvenile yelloweye mullet.[103]

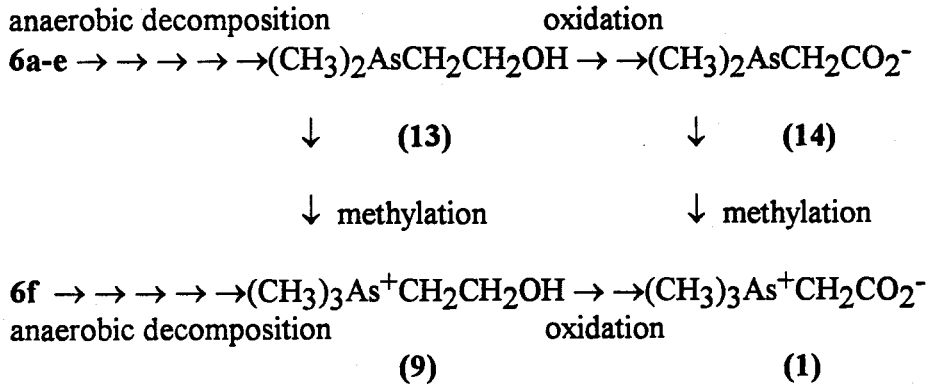

Figure 2.4 Proposed biosynthetic pathway from arsenosugars to arsenobetaine.

2.1.5 Scope of work

The objective of the present study is to investigate the uptake of [^{3}H]-labeled arsenicals by mussels after they had been exposed to seawater which initially contained [^{3}H]-MMA. After exposure, the [^{3}H]-labeled arsenicals in the mussel flesh were identified or an attempt was made to identify them. The total arsenic concentration in the

mussel flesh, byssal threads and shells were determined before and after exposure to [^{3}H]-MMA.

Mussels were chosen for this study because they are readily available, easily maintained and globally distributed. They are known to contain arsenobetaine, arsenosugars, and tetramethylarsonium ion. Mussels are filter feeders and phytoplankton and diatoms form the bulk of their diet.[104]

2.2 EXPERIMENTAL

2.2.1 Scintillation counting

A Packard Tricarb 1900 TR liquid scintillation counter was used to measure the [^{3}H]-activity of chromatographic fractions, extracts, and wipe tests. Packard software was used to run the counter which was standardized daily by using Packard standard #22 which contained $\cong$ 0.2 μCi of [^{3}H]. The scintillation counter was coupled to an Epson LX-810 printer.

Typically, between 100 to 300 μl of sample or a strip of TLC sheeting (1cm × 3 cm) was added to a 7 ml glass scintillation vial which contained 5 ml of scintillation cocktail. The samples were counted for three minutes each and then recounted. The results for each sample were averaged and tabulated.

2.2.2 Atomic Absorption Spectroscopy

A Varian Techtron Model AA 1275 single beam atomic absorption spectrometer was used to determine the arsenic concentrations in the samples. The spectrometer was fitted with a Varian Spectra AA hollow cathode lamp which operated at 7 mA. The atomic absorption signal was monitored at a wavelength of 193.7 nm for all arsenic determinations. The spectrometer was equipped with a deuterium background corrector and a GTA-95 accessory for graphite furnace atomic absorption (GFAA) spectroscopy. GFAA spectroscopy was used as the detection method for standards which were run on the various types of chromatographic systems employed in this work. The sample was injected into a pyrolytically coated graphite tube in the furnace by using the automatic delivery system of the accessory. It was mixed with 20 μl of palladium nitrate (100 ppm in 2% w/v citric acid) modifier prior to injection. The optimized furnace operating

Table 2.1 Graphite Furnace Operating Parameters.

Step No.	Temp. (°C)	Time (s)	Gas flow ($L\ min^{-1}$)	Read Command	Comment
1	85	5	3.0	No	dry
2	95	40	3.0	No	dry
3	120	10	3.0	No	dry
4	1400	6	3.0	No	ash
5	1400	2	0	No	ash
6	2400	0.7	0	Yes	atomize
7	2400	2	0	Yes	atomize
8	2400	2	3.0	No	clean

parameters are given in Table 2.1. The graphite furnace could be removed and replaced by a hydride generation apparatus for hydride generation atomic absorption (HGAA) spectroscopy. HGAA spectroscopy was used for the determination of the total arsenic concentrations in the seawater and in the acid digested mussel flesh, byssal threads, and shells. The continuous flow hydride generation assembly is illustrated in Figure 2.5. It consisted of a Gilson Miniplus 2 four channel peristaltic pump which was used to withdraw the sample and mix it with hydrochloric acid or buffer solution. This solution was then reacted with sodium borohydride solution (2% w/v) and introduced into the gas-

liquid separator via a 20 turn mixing coil. The gases were led into an open-ended T-shaped quartz curvette (8.5 cm × 1 cm (o.d.)) mounted in the air/acetylene flame of a standard Varian burner. The operating conditions which were previously established by Cullen and Dodd[46] are shown in Table 2.2.

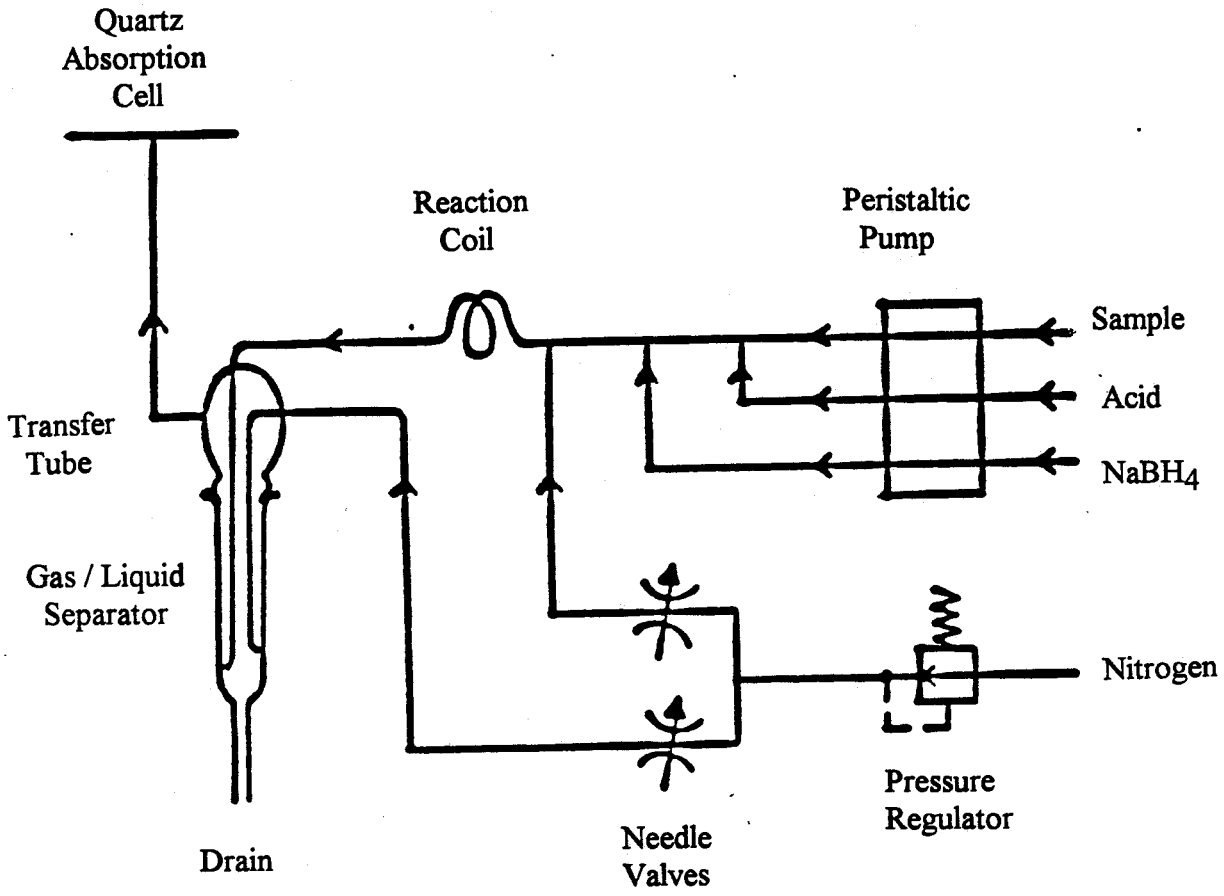

Figure 2.5 Schematic diagram of the continuous Hydride Generation Atomic Absorption assembly.

Table 2.2 Operating conditions for the continuous Hydride Generation Atomic Absorption assembly.

Uptake flow	Sample	7.5 ml min^{-1}
	HCl	2.0 ml min^{-1}
	$NaBH_4$	4.0 ml min^{-1}
Carrier gas flow	Nitrogen	0.6 L min^{-1}
HCl concentration		4 M
$NaBH_4$ concentration		2% (w/v) in 0.1% (w/v) NaOH solution

2.2.3 HPLC system

The HPLC system consisted of a Waters M45 pump, a Waters U6K injector, a Waters column (either a Protein Pak DEAE column 7.5 mm (ID) × 7.5 cm or a Protein Pak 300SW column 7.5 mm (ID) × 30 cm) and a Gilson Micro Fractionator automated collector. The eluants were degassed and filtered through 0.5 μm pore size filters from Millipore. Prior to injection the samples were filtered through 0.5 μm pore size cartriage filters from Millipore. The collected fractions were manually transferred to either the scintillation counter or the atomic absorption spectrometer for detection.

2.2.4 TLC plates

The TLC plates were aluminum backed, precoated with 0.2mm of silica gel, and had dimensions of 20 × 20cm.

2.2.5 Chemicals and reagents

All chemicals used from BDH and Fisher Scientific were classified as analytical grade and meet ACS specifications, respectively. The solvents which were used were obtained from Fisher Scientific and were classified as HPLC grade. A standard arsenic solution (1000 $\mu g\ ml^{-1}$) was prepared by dissolving 1.3203 g of arsenic trioxide (As_2O_3, Fisher Scientific) and 2 g of NaOH in 20 ml of deionized water. The solution was diluted to 200 ml, neutralized with HCl (12 M) and made up to 1000 ml. This solution was diluted as necessary to prepare working solutions for GFAA and HGAA spectroscopy.

Deionized water (Aquanetics Aqua Media System) was used for solution preparation and in all of the liquid chromatography. All glassware and plasticware that were not used with the [^{3}H]-labeled compounds were cleaned by soaking overnight in 2% (v/v) Extran solution, rinsing with water and soaking in HCl (1 M) overnight. All of the glassware and plasticware that were used with the [^{3}H]-labeled compounds were rinsed with water, soaked overnight in a 5% (v/v) solution of Count-Off. After the overnight soakings the utensils were first thoroughly rinsed using tap-water and then deioinized water.

The synthesis of the [^{3}H]-MMA, [^{3}H]-DMA, arsenobetaine, trimethylarsine oxide and tetramethylarsonium ion used in this chapter is described in Chapter 6.

2.2.6 The uptake of [^{3}H]-compounds by mussels from seawater which initially contained [^{3}H]-MMA

Approximately 150 mussels (*Mytilus edulis*), ranging in shell length from 2.5 to 5.0 cm, were collected from the beach surrounding Point Grey in Vancouver B.C. These were divided into two groups of about 75 mussels each. The first group was designated

the "control group". These mussels were placed in a 200 liter seawater tank (Figure 2.6a) where they remained for the duration of the experiment. The water in this tank was continually replenished with fresh seawater which was pumped in from the ocean. The second group, the "experimental group", was placed in a wire cage and submersed in a 15 liter seawater tank (Figure 2.6b). The water in this tank was not replenished and initially contained 45 μCi [^{3}H]-MMA. Compressed air was bubbled through both of the tanks. The sea water in the smaller tank originated from the same source as used for the control tank. The mussels from the "experimental group" were left in the static tank for 3 days before being transferred into the larger tank which also contained the "control group". After 4 additional days, the "experimental group" was transferred back into the smaller tank. This cycle of exposure followed by washing was continued for a total of 5 weeks. The water in the static tank was changed after 3 weeks and replaced with fresh sea water which also contained 45 μCi [^{3}H]-MMA. The water was replenished so that the waste products of the mussels would not accumulate to unhealthy levels for the mussels. At the end of the experiment, the mussels were left in the large tank for one day in order to wash away any radiolabeled compounds that were loosely attached to the surfaces of the mussel shells and flesh.

2.2.7 Isolation of the [^{3}H]-labeled arsenicals in the mussel flesh

The mussels from the "experimental group" (≈75) were shucked and the byssal threads, shells and flesh were isolated and pooled. Each pool was washed with deionized water and then was set aside for subsequent total arsenic determinations. This process was repeated for the "control group".

The following procedure for isolating arsenicals in the mussel flesh was

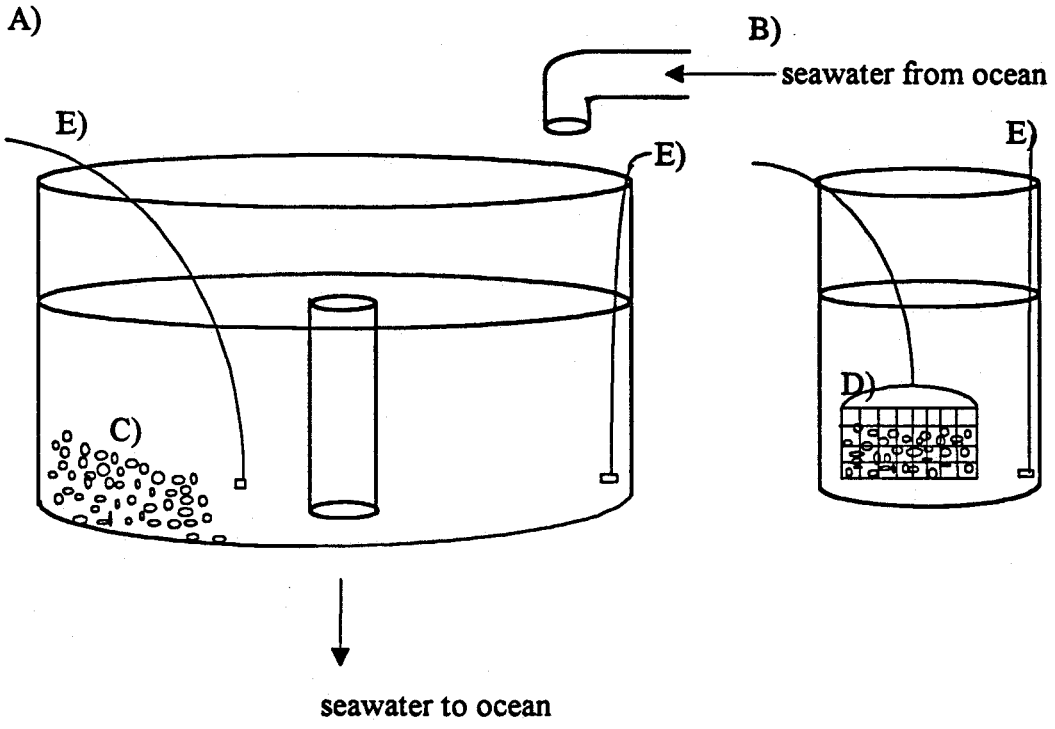

Figure 2.6 A) 200 liter seawater tank with continually circulating seawater; B) 15 liter experimental tank containing [^{3}H]-MMA; C) "control group" of mussels; D) wire cage containing "experimental group" of mussels; E) aeration stones and tubing.

developed by M. Dodd[46] and is summarized in Figure 2.7. Some flesh (5 g) from the "experimental group" was set aside for total arsenic determinations and the remaining flesh (65 g) was homogenized and extracted with MeOH (2.5 ml MeOH per gram of flesh). The resulting slurry was mechanically shaken for 2 days and then filtered to separate the soft brown residue from the extract. Another MeOH extraction was performed on the residue and both of the MeOH extracts were combined. The MeOH was evaporated (rotary), and the black-gummy residue was redissolved in a minimum amount of water (25 ml). A small amount of this solution (200 µl) was set aside and counted. The remaining solution was repeatedly extracted with 25 ml portions of diethyl ether until the ether extracts were colourless. The pooled ether extracts were also counted. The ether extracts were not further examined. The water fraction was evaporated (rotary) to dryness and the resulting residue was redissolved in about 10 ml of MeOH. This solution was applied to a Sephadex LH-20 column (1.5 × 2.5 cm) and eluted with MeOH (450 ml). Fractions (10 ml) were collected and counted by using the scintillation counter (100 µl samples). The [^{3}H] containing compounds eluted within one band and the appropriate fractions were combined and evaporated (rotary) to dryness. The residue was redissolved in 10 ml of water and applied to a Dowex 50W×8 cation exchange column (1.5 × 20 cm). (The resin in the [H^+] form was prepared as follows: wash with 2 M NaOH (3 times), wash with deionized water until neutral, wash with 2 M HCl (3 times) and then with deionized water until neutral.) The [^{3}H]-labeled compounds were eluted from the Dowex column by using 100 ml H_20 (fractions 1-9), 200 ml of 5% NH_4OH (fractions 10-30), 50 ml H_2O (fractions 31-35), and 150 ml 2 M HCl(fractions 36-50). Fractions (10 ml) were collected and counted (100 µl samples). The fractions containing [^{3}H]-labeled compounds which eluted in the NH_4OH fraction were combined and concentrated on the rotary-evaporator.

The fractions containing [^{3}H]-labeled compounds which eluted in the HCl fraction were treated in a similiar fashion. The fractions containing [^{3}H]-labeled compounds which eluted with H_2O were not further analysed because these fractions were not expected to contain either arsenobetaine or tetramethylarsonium ion.

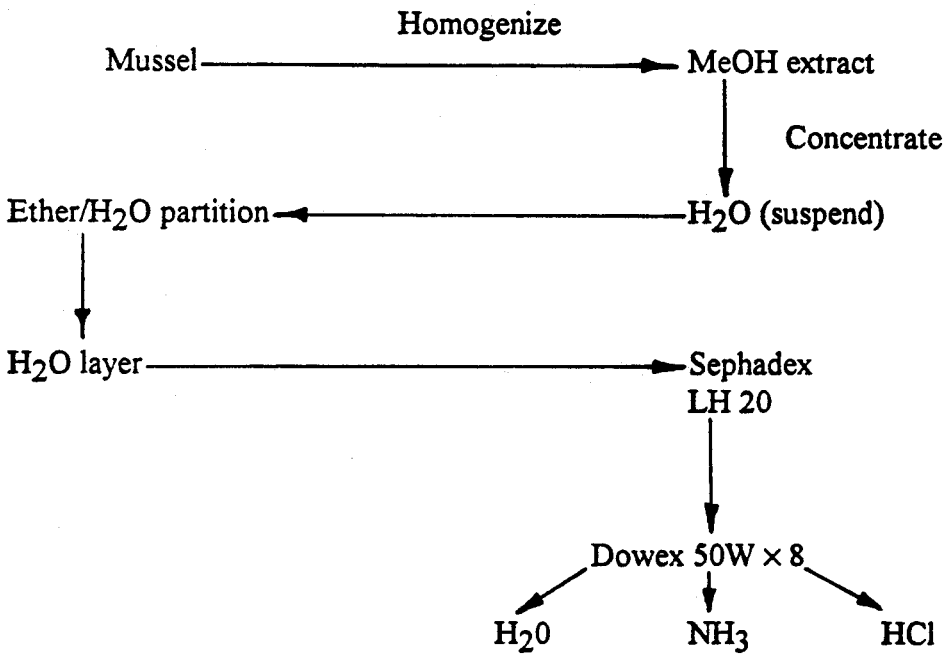

Figure 2.7 Schematic representation of the procedures used for the extraction of arsenic compounds from mussels and for the purification of the extract.

2.2.8 Identification of the [^{3}H]-labeled compound in the mussel flesh which eluted from the Dowex column in the NH_4OH fraction

The residue in the NH_4OH fraction was redissolved in a minimum amount of H_2O (2 ml). A small aliquot was then applied via a drawn out capillary tube to a TLC plate (3 × 20 cm strip of silica gel). Two different solvent systems were used as eluents. Solvent system #1 was composed of ethanol-acetic acid-water (65:1:34) and solvent system #2 was composed of acetonitrile-acetic acid-water (65:1:34). When the solvent had risen about 16 cm the plates were removed from the solvent chamber and dried. The dried plates were cut into 16 segments (1 × 3cm) which were placed into 7 ml scintillation vials containing 5 ml of scintillation fluid. The vials were counted to determine which fraction contained the radiolabeled compound(s).

The [^{3}H]-labeled compound(s) in the NH_4OH fraction were also examined by using HPLC. A Waters Protein Pak DEAE anion exchange column was used and the sample was eluted by using 5mM sodium acetate (pH = 6.67) as the eluent at a flow rate of 1 ml per minute. Fractions were collected every minute and counted (100 µl samples).

2.2.9 Analysis of the [^{3}H]-labeled compounds in the mussel flesh which eluted from the Dowex column in the HCl fraction

The compound(s) in the HCl fraction were examined by TLC, using solvent system #1, as described in Section 2.2.8.

2.2.10 Determination of the total arsenic concentration in the mussel flesh, byssal threads and shells

The determinations of the total arsenic levels followed the procedures developed

by Dodd.[46] The flesh and the byssal threads for both the "experimental group" and the "control group" were decomposed by using a solution of 69% nitric acid (3 ml), 98% sulphuric acid (1 ml) and 30% hydrogen peroxide (3 ml). This mixture was added to approximately 1gm of accurately weighed sample in a 250 ml round bottom flask. The flask was fitted with a specially designed stopper and air condensor containing a diffusion funnel as shown in Figure 2.8. The reaction mixture was heated to a gentle reflux for 3 hours and then allowed to cool. The digested sample was transferred into a 100 ml volumetric flask and made up to the mark with deionized water.

The shells were washed with deionized water and ground to a fine powder by using a mortar and pestle. Hydrochloric acid (2M) was added to the powder. For every gram of shell 15 ml of acid was used. After an hour the resulting suspension was filtered and the filtrate was transferred to a 100 ml volumetric flask and made up to the mark with deionized water. The total arsenic was determined in the samples by using HGAA spectroscopy. The digestate for both the "control group" and the "experimental group" was also counted. All digestions described above were performed in duplicate.

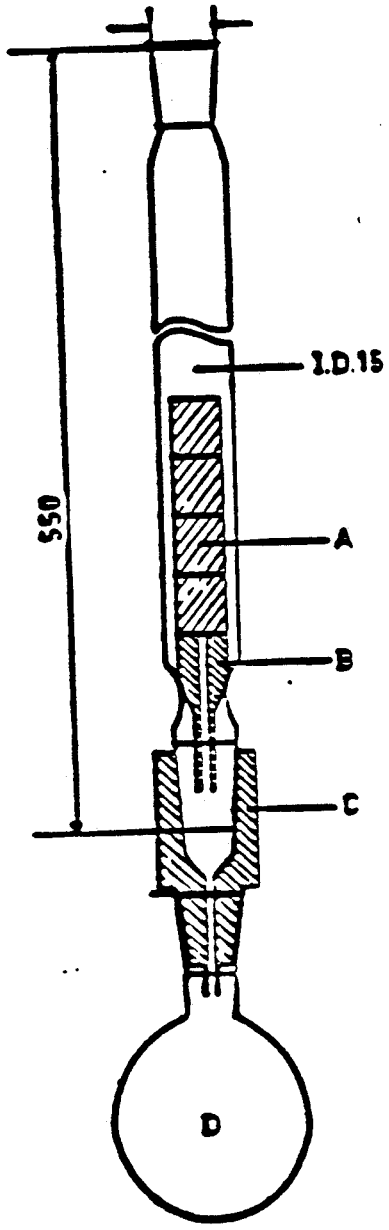

Figure 2.8 Wet ashing apparatus; (A) Teflon cylindrical plugs; (B) Teflon diffusion funnels; (C) Teflon stopper with capillary; (D) 250 ml round bottom flask. All joints are 14.5/23. All dimensions are mm.

2.3 RESULTS AND DISCUSSION

2.3.1 The uptake of [^{3}H]-labeled arsenicals from the seawater

The mussels in the "experimental group" were exposed to seawater which initially contained [^{3}H]-MMA for a five week cycle of exposure/washing. The mussels in the "control group" were not exposed to any [^{3}H]-labeled compounds. At the end of the experiment the mussels in the "experimental group" appeared to be as healthy as the mussels in the "control group", despite exposure to arsenic concentrations well in excess of the normal environmental levels. This statement is made after observing that the two groups were not visually different and the effort needed to pry open the shells was about the same. If a mussel is unhealthy the shell will open very easily and the flesh will not adhere to the inside of the shell very well. There were no casualties in either group during the five weeks.

2.3.2 Purification of the [^{3}H]-labeled arsenicals in the mussel flesh of the experimental group

The [^{3}H]-labeled compounds were extracted with MeOH from the homogenized mussel flesh of the "experimental group" as outlined in Section 2.2.6. The diethyl ether extraction withdrew approximately 10% of the [^{3}H]-labeled compounds from the MeOH flesh extracts. This indicates that some of the [^{3}H]-labeled MMA has been biotransformed into more complex arsenicals which may include the arsenic containing lipids **7a** and **7b**. The water soluble [^{3}H]-labeled compounds were added to a Sephadex column, eluted by using water, and the fractions were counted to yield the chromatogram in Figure 2.9. The [^{3}H]-labeled compounds eluted from the column in one band and

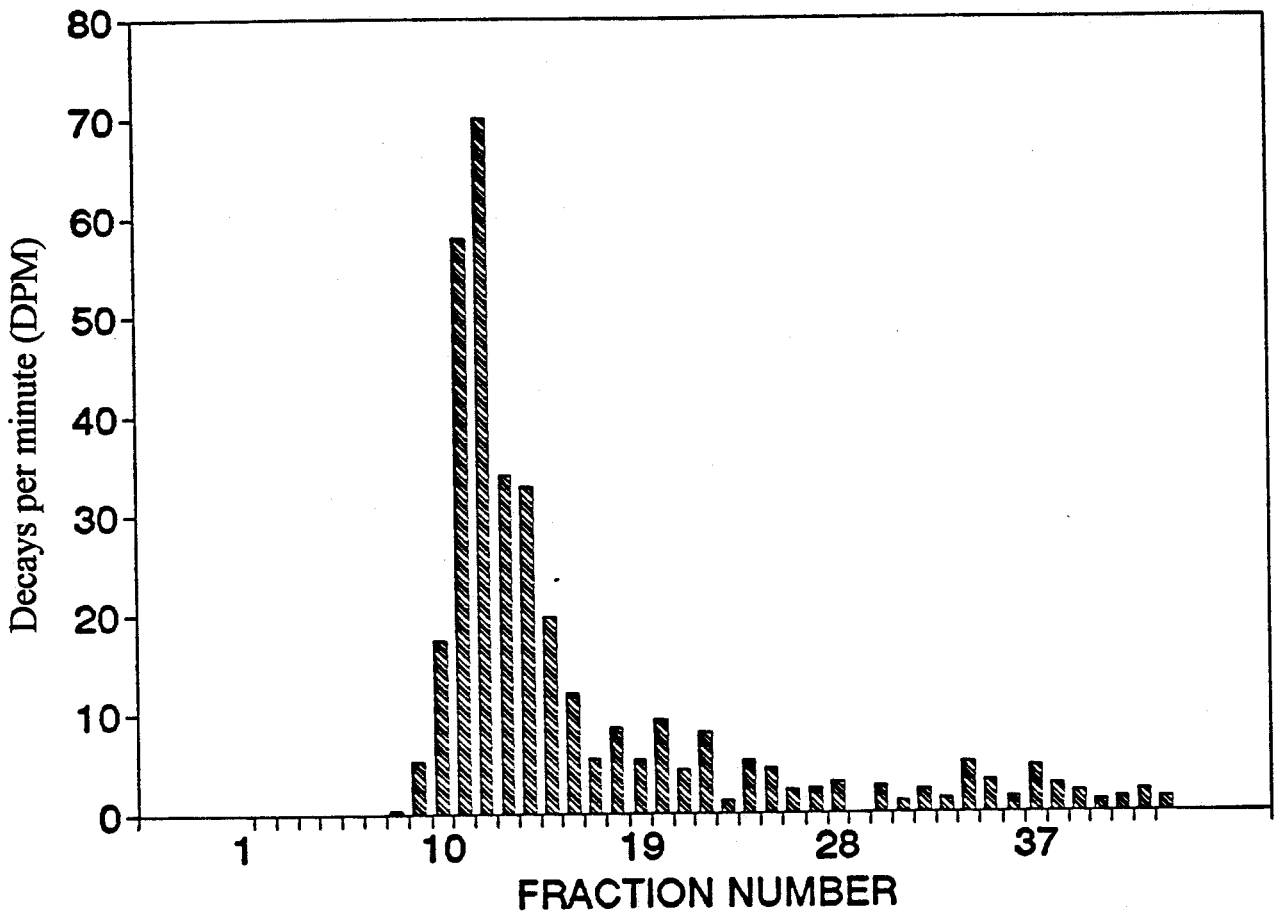

Figure 2.9 The elution profile from a Sephadex LH-20 column for the water soluble [^{3}H]-labeled compounds which were MeOH extracted from the mussels.

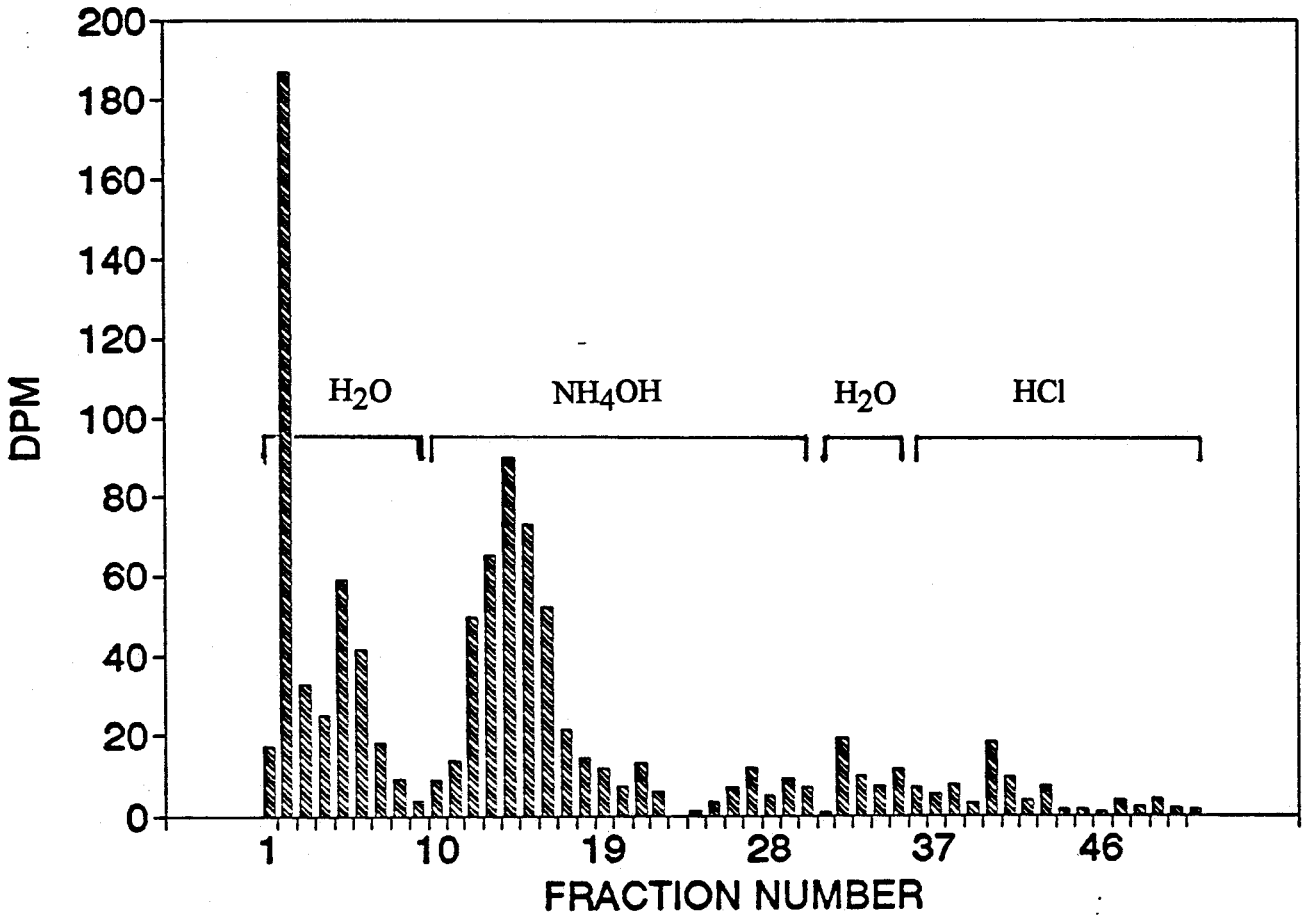

Figure 2.10 The elution profile from the Dowex column for the [^{3}H]-labeled compounds which eluted in fraction 8 to 21 from the Sephadex column.

fractions 8 to 21 were combined. The combined fractions were concentrated, applied to a Dowex column, and eluted by using H_2O, 5% NH_4OH and 2M HCl to yield the chromatogram in Figure 2.10. A number of different [^{3}H]-labeled compounds seem to be present with the bulk of the radioactivity being eluted in both the H_2O and the NH_4OH fractions. There also seems to be a small amount of [^{3}H]-labeled compounds in the HCl fraction. Little is known about the arsenic containing compounds which elute off of this type of column in the water fraction and there are no standards for Rf comparison, so the [^{3}H]-labeled compounds in the water fraction were not further investigated. Fraction numbers 11 to 17 eluting with a retention volume of between 110 ml and 180 ml were concentrated and designated the "NH_4OH fraction" for future reference. Fraction numbers 39 and 40 eluting with a retention volume between 390 ml and 410 ml were concentrated and designated "the HCl fraction" for future reference.

2.3.3 Identification of [^{3}H]-arsenobetaine in the NH_4OH fraction

The compound(s) which eluted from the Dowex column in fractions 11 to 17 (the NH_4OH fraction) were further examined by using TLC with two different solvent systems. The results of comparing the Rf's of arsenobetaine standard and the unknown are displayed in Table 2.3.

Table 2.3 Rf values for the unknown from the "NH_4OH fraction."

Solvent System	Rf: Arsenobetaine	Rf: Unknown
#1	0.52 ± 0.05	0.55 ± 0.05
#2	0.43 ± 0.05	0.43 ± 0.05

These results show that the [^{3}H]-labeled compound eluting in the "NH_4OH fraction" has the same Rf values as does arsenobetaine. The arsenobetaine standard was chosen because it is the major arsenical found in most marine organisms and its elution in the "NH_4OH fraction" is well documented.[100] Additional evidence for this identification is provided by anion exchange HPLC. The arsenobetaine and DMA standards were eluted through the anion exchange column, Figure 2.11a, by using 5 mM sodium acetate. The unknown compound was eluted through the anion exchange column, Figure 2.11b, by using 5 mM sodium acetate. The unknown and the arsenobetaine have the same retention time under these conditions. This result confirms the identification of the unknown compound in the "NH_4OH fraction" as arsenobetaine and eliminates DMA (the other known arsenical which elutes off of the Dowex column in the "NH_4OH fraction") as a possibility.

The exposure of mussels to [^{3}H]-MMA and the subsequent identification of [^{3}H]-arsenobetaine in the mussels confirms that MMA is a possible precursor to arsenobetaine. This is suggested by a combination of the schemes in Sections 2.1.3 and 2.1.4. This result is significant because it is the first time that radiolabeled arsenobetaine has been isolated from a marine organism after the organism had been exposed to a simple radiolabeled arsenic compound. This is unlike the experiments described in Section 2.1.1 with crabs, fish and gastropods where [^{74}As]-arsenate was investigated as the precursor to arsenobetaine. The success of the experiment described in this chapter may be due to the fact that [^{3}H]-MMA was added directly to natural seawater which contained all different types of algae, bacteria, phytoplankton, diatoms and nutrients. Thus, the natural conditions were duplicated as closely as possible, except for the exclusion of the sediments. The experiments which attempted to use [^{74}As]-arsenate as the precursor either fed the precursor to the marine organism directly or cultured one specific strain of

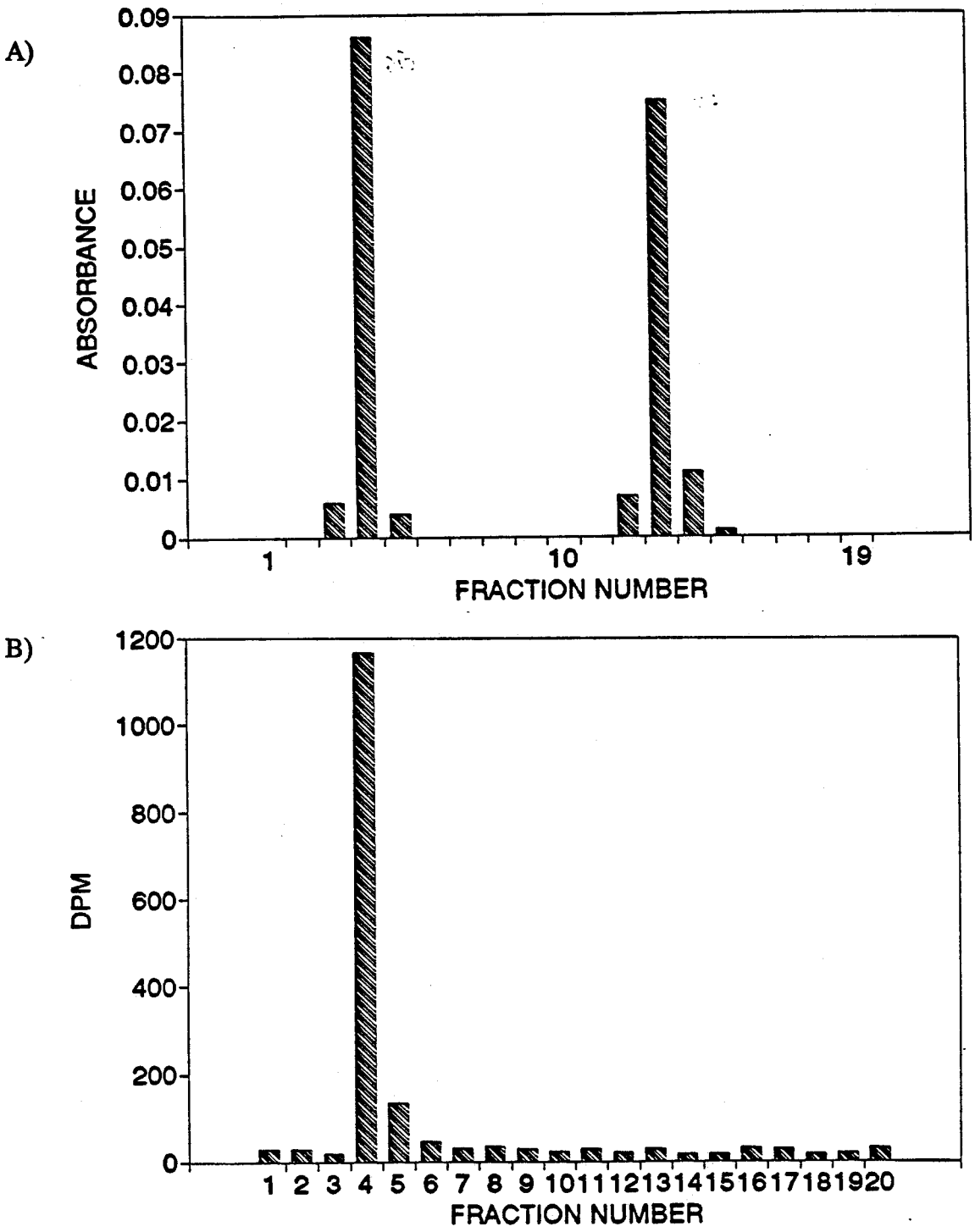

Figure 2.11 HPLC chromatograms from the anion exchange column at pH 6.67; (A) arsenobetaine and dimethylarsinate on the anion exchange column at pH 6.67, (B) the compound eluting in fractions 11 to 17 from the Dowex column.

algae with the precursor. Thus, any complex interactions between various marine organisms which may be necessary for this biotransformation to occur would not be possible under these conditions. The experiment described in this chapter also had a much longer duration than the previous experiments and it is possible that this biotransformation is a relatively slow process. In the proposed scheme, Section 2.1.4, it is suggested that in order for the C3-C4 bond in the arsenic containing riboside to be cleaved, anaerobic conditions are necessary. It was suggested that this cleavage may occur in the sediments, however, the experiment described in this chapter demonstrates that arsenobetaine can be formed in the absence of any sediments.

2.3.4 Attempted identification of the [^{3}H]-containing arsenicals in the HCl fraction

Identification of the [^{3}H]-labeled compound(s) in the "HCl fraction" was hampered because of the relatively low level of radioactivity in this fraction. The two major arsenicals known to elute off of the Dowex in the "HCl fraction" are the cationic tetramethylarsonium ion and arsenocholine. TLC analysis of the sample was inconclusive as shown in Table 2.4. Lack of additional sample made further analysis impossible. From the results it would be quite reasonable to suggest that the unknown [^{3}H]-labeled compound(s) eluting off of the Dowex column in the "HCl fraction" could have been either arsenocholine or tetramethylarsonium ion. Arsenocholine is postulated to be the immediate precursor to arsenobetaine, (see Section 2.1.4) however, it has not been found to occur naturally in mussels. Tetramethylarsonium ion is present in most types of mussels.[56]

Table 2.4 The [^{3}H]-containing compound(s) in the "HCl Fraction."

Solvent System	Rf: tetramethyl-arsonium ion	Rf: arsenocholine	Rf: Unknown
#1	0.38 ± 0.05	0.32 ± 0.05	0.35 ± 0.05

2.3.5 Total arsenic concentrations in the mussel flesh, byssal threads and shells.

The mussels were sacrificed after five weeks of intermittent exposure to the [^{3}H]-labeled MMA and any other [^{3}H]-labeled compounds that may have been produced by the micro-organisms present in the seawater. The "control group" and "experimental group" of mussels were shucked and the flesh, byssal threads and shells for each group were pooled. These three components were acid digested as outlined in Section 2.2.10. The initial arsenic concentration of [^{3}H]-MMA that the mussels were exposed to was 2 ppm. The total arsenic concentrations in the mussel flesh, byssal threads, and shells of both the "experimental group" and the "control group" are summarized and displayed in Table 2.5. The natural arsenic concentration in the seawater that was being pumped into the tanks was determined by using HGAA spectroscopy to be 0.0054 ppm.

Table 2.5 Arsenic concentration in the mussel flesh, byssal threads, and shells.

	As concentration (ppm) "Control group"	As concentration (ppm) "Experimental group"
Flesh	0.45 ± 0.04	0.87 ± 0.07
Shells	0.24 ± 0.03	0.32 ± 0.04
Byssal threads	4.20 ± 0.20	6.30 ± 0.30

The total arsenic concentration in each of the three compartments increased significantly during the course of the exposure experiment. This result is expected as the mussels were intermittently exposed to an arsenic concentration that was approximately 400 times the natural level. The arsenic concentration in the byssal threads is much greater (≈10 times) than the concentration in the flesh or the shells. The excretion of heavy metals into the byssal threads by the mussels is thought to be part of the detoxification mechanism of the organism.[105] The digestion procedure for both the flesh and the byssal threads would have decomposed any organoarsenicals which may have been present, thus counting techniques were not employed. The procedure used to dissolve the shells would not have led to the complete degradation of the organoarsenical, in particular the bond between the As and [^{3}H]-methyl may not been cleaved, so this digestate was counted to yield the results displayed in Table 2.6.

Table 2.6 The radioactivity in the shells.

	"Control group"	"Experimental group"
Shells	22.15, 22.95 DPM	32.43, 31.26 DPM

Compounds may be either adsorbed onto the shell from the surrounding media or incorporated into the shell by the mussel. The percentage increase in the arsenic concentration in the shells corresponds almost exactly with the increase in radioactivity. This result suggests that the arsenicals which were incorporated into the shells during the experiment were methylated. This finding is consistent with the finding of low levels of

methyl- and dimethyl- arsenicals in the shells of some costal bivalves of British Columbia.[106]

2.3.6 Summary

The results described in this chapter show that feeding-type experiments can yield valuable infomation about the biotransformations of arsenic in the marine environment, in particular that MMA is a precursor to arsenobetaine. As a cautionary note, the biotransformation was observed in a situation where the arsenic levels were elevated to about 400 times the natural concentration. This biotransformation occurs in the absence of the strongly anaerobic conditions which are found in the sediments. These conditions were thought to be necessary for the decomposition of the arsenosugars which have been postulated to be key intermediates in the scheme for arsenobetaine formation. Other [^{3}H]-labeled compounds were present in the mussels, but were not positively identified. The overall arsenic concentration increased in the mussel flesh, byssal threads and shells during the course of the experiment. Data were also collected which suggests that the arsenicals present in the shells were methylated.

The results from this chapter do not, however, establish the source of the arsenobetaine. The biotransformation either is performed by the microscopic organisms (for the purposes of this thesis, the term microscopic organisms will refer to any organism which is not normally seen by the human eye) in the seawater, or by the mussels themselves. Another possible scenario is a combination of the two possibilities. Clearly, these experiments should be modified in order to answer these questions (see Chapter 3).

CHAPTER 3

THE BIOTRANSFORMATION OF MMA AND DMA INTO ARSENOBETAINE IN SEAWATER AND MUSSELS

3.1 INTRODUCTION

3.1.1 The origin of arsenobetaine in seawater and marine animals

Arsenobetaine is the major form of arsenic in most marine animals. There are two possible ways for marine animals to acquire arsenobetaine. Either it is accumulated directly from food and/or seawater or it is synthesized from other arsenicals within the animal. Studies in this area have not been fruitful, partly because the analytical techniques available for determining arsenic speciation in seawater are generally not suitable for the detection of arsenobetaine. There have been no previous reports of the presence of arsenobetaine in seawater, although it was estimated by Francesconi[99] that if it was present, its concentration would be less than 0.5 $\mu g\ As\ L^{-1}$.

Francesconi has also examined the ability of marine animals to bioaccumulate arsenobetaine, arsenocholine, dimethylarsinylethanol, and dimethylarsinylacetic acid. He showed that both arsenobetaine and arsenocholine were readily taken up by the yelloweye mullet from raw beef which was fed to the fish.[103] The raw beef had been injected with both arsenobetaine and arsenocholine. When the same experiments were carried out with dimethylarsinylethanol and dimethylarsinylacetic acid in the raw beef there were no increases in the arsenic concentration in the yelloweye mullet. Similar experiments involving adding arsenobetaine directly to a tank of seawater which contained mussels (*M. edulis*) showed that the mussels were unable to regulate their uptake of arsenobetaine from the seawater. The amount of arsenobetaine in the mussels at the end of the

experiments was simply dependent upon the amount of arsenobetaine in the seawater and the amount of time that the mussels were exposed to it.[99] When trimethylarsine oxide was added directly to a tank of seawater which contained mussels (*M. edulis*), the trimethylarsine oxide was not appreciably accumulated. In the experiments which involved arsenobetaine accumulation, the marine animals did not metabolize arsenobetaine.

The results from experiments which investigated the ability of marine animals to synthesize arsenobetaine from algal arsenic are outlined in Chapter 2, Section 2.11.

3.1.2 Scope of work

The objective of the experiments described in this chapter was to modify the feeding-type experiments described in the previous chapter to answer the major questions which arose in the interpretation of the results. What is the source of the arsenobetaine in the mussels? Is the biotransformation of MMA into arsenobetaine performed by the microscopic organisms in the seawater, by the mussels, or by some combination of the two possibilities? These questions were answered by investigating the quantities and speciation of the [^{3}H]-labeled arsenicals during the course of the modified feeding-type experiments.

In this experiment either [^{3}H]-MMA or [^{3}H]-DMA was added to seawater both with and without the presence of mussels. After exposure the [^{3}H]-labeled arsenicals in the mussel flesh and the seawater were identified or an attempt was made to identify them.

3.2 EXPERIMENTAL

3.2.1 Instrumentation

The instrumentation and techniques for scintillation counting, atomic absorption spectrometry, and HPLC were identical with those described in Sections 2.2.1, 2.2.2, and 2.2.3.

3.2.2 Chemicals and reagents

The chemicals and reagents used in this chapter are identical to those described in Section 2.2.5.

3.2.3 The uptake and conversion of [^{3}H]-MMA and [^{3}H]-DMA to [^{3}H]-arsenobetaine in seawater and mussels

Approximately 75 mussels (*M. edulis*), ranging in shell length from 2.5 to 5.0 cm, were collected from the beach surrounding Point Grey in Vancouver B.C. They were placed in a wire cage which was submerged in a 15 liter seawater tank. Another 15 liter tank was set up as the control. The seawater sampled from the tank containing mussels will be referred to as the "experimental seawater" and the seawater sampled from the other tank will be referred to as the "control seawater". The water in these tanks was not replenished and initially contained either [^{3}H]-MMA or [^{3}H]-DMA at an activity level of 45 μCi. The mussels were left in the 15 liter tank for 4 days before being transferred into a third tank which contained 200 liters of seawater. The water in this tank was continually replenished with fresh seawater which was pumped in from the ocean. The seawater in all three tanks originated from the same source and aeration was achieved by the use of compressed air. The same tanks shown in Figure 2.6 were used with the addition of a

second static tank which held only the control seawater. On days 4 and 7 the "experimental seawater", "control seawater", and mussels were sampled. This sampling procedure involved the collection of 200 ml of both the experimental and control seawater along with 10 medium sized mussels.

3.2.4 Isolation and identification of the [^{3}H]-labeled arsenicals in the seawater and the mussel flesh

The "experimental seawater" samples (200 ml) were filtered through a hydrophilic membrane filter (0.45 μm pore size). The pH of the filtrate was adjusted to 4 by adding a few drops of concentrated HCl. This solution was counted (200 μl) and extracted with phenol (2 × 50 ml). The combined phenol extracts were diluted with diethyl ether (400 ml) and the water soluble compounds were extracted with deionized water (2 × 50 ml). The aqueous extracts were combined, counted (200 μl), evaporated (rotary) to dryness and redissolved in deionized water (10 ml). This solution was applied to a cation exchange column (Dowex 50W×8, 1.5cm × 20cm in the [H^+] form). The [^{3}H]-labeled compounds eluted from the column by using deionized water (70 ml) and 5% ammonium hydroxide (200 ml). These conditions were sufficient to elute all of the [^{3}H]-activity. Fractions were collected (20 ml) and counted (600 μl samples). The [^{3}H]-containing fractions were bulked, evaporated (rotary) to dryness, and redissolved in a minimum amount of deionized water (1 ml). Aliquots (100 μl) of these solutions were examined by using two different types of HPLC columns. The first, a Protein Pak DEAE column was run by using 5 mM sodium acetate at pH 4.0 and pH 6.67 as the eluant. The second, a Protein Pak 300SW column was run by using 5 mM sodium acetate at pH 6.67 as the eluant. The flow rate was set at 1 ml per minute and fractions were collected every minute

and counted (100 µl samples). Standard solutions of MMA, DMA and arsenobetaine in deionized water were chromatographed on both the cation exchange and HPLC columns, fractions were detected by using GFAA spectroscopy. The "control seawater" was treated in an identical fashion.

The mussels were washed with deionized water and the shells were removed from the flesh which was then homogenized. The resulting slurry was made up to 200 ml by using deionized water. This slurry was treated in an identical fashion to the 200 ml seawater filtrate.

3.2.5 The diversity of [^{3}H]-labeled compounds in the seawater

The experimental conditions in this section were virtually identical with those described in Section 3.2.3, except for the following: only [^{3}H]-MMA was used as the starting substrate, the duration of this experiment was 10 days and the mussels were transferred from the large tank where the seawater was circulating to the smaller tank where the seawater was not circulated on day 7. Seawater samples were collected on days 4, 7 and 10 from the smaller tank which contained the [^{3}H]-labeled compounds.

3.2.6 Examination of the [^{3}H]-labeled compounds in the seawater from the experiment described in Section 3.2.5

The seawater was subjected to the set of extractions which were described in Section 3.2.4 and the extracted compounds were applied directly to a size exclusion HPLC (HPLC Protein Pak 300SW) column. The [^{3}H]-labeled compounds were eluted by using 5mM sodium acetate at a flow rate of 1ml per minute. Fractions were collected every minute and counted (100 µl samples).

3.3 RESULTS AND DISCUSSION

3.3.1 Experimental seawater after exposure to [^{3}H]-MMA and [^{3}H]-DMA

[^{3}H]-MMA or [^{3}H]-DMA was added to seawater which contained mussels (*M.edulis*). After four days the mussels were transferred into another tank. The seawater from the tank which contained the mussels was examined on days 4 and 7. The seawater was filtered, counted, extracted with phenol, back extracted with deionized water, and then counted again. The chromatographic results and identification of the [^{3}H]-labeled compounds phenol extracted from the seawater are described below.

It is important to note that there is no possibility of proton exchange in situ for the compounds which are being investigated. Any casual exchange of the label between compounds would require a cleavage of the methyl-arsenic bond. Also, the various [^{3}H]-labeled compounds in the seawater will all have different extraction efficiencies into phenol, therefore, the ratio of compounds in the extracts will be different from the actual ratio of compounds in the seawater. Both MMA and DMA have extraction efficiencies of about 10%, whereas the extraction efficiency for arsenobetaine is closer to 100%.

a) [^{3}H]-MMA:

The cation and anion exchange chromatograms of the standards and of the [^{3}H]-containing compounds extracted from the experimental seawater on days 4 and 7 are displayed in Figures 3.1, 3.2, 3.3, and 3.4.

The compound eluting in fraction 3 from the cation exchange column (Figure 3.2) was identified as MMA, on the basis of its retention time which was identical with that of the standard (Figure 3.1). This identification was confirmed by the chromatograms in Figures 3.3 and 3.4 for the elution profiles from the anion exchange (pH 4.0) and size exclusion HPLC columns, respectively.

The compound eluting in fraction 7 from the cation exchange column (Figure 3.2) was identified as arsenobetaine on the basis of its chromatographic coordinates which were identical with that of the standard. This identification was confirmed by the chromatograms in Figures 3.5 and 3.6 for the elution profiles from the anion exchange (pH 6.67) and size exclusion HPLC columns, respectively.

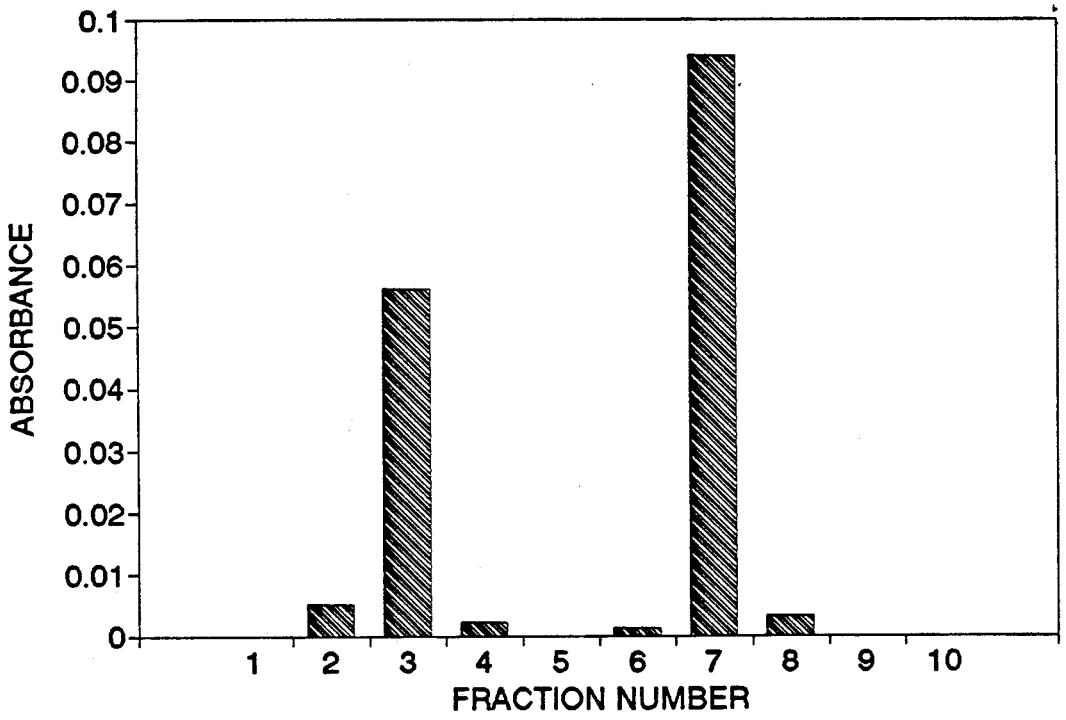

Figure 3.1 The cation exchange chromatograms for the standards of MMA, DMA, and arsenobetaine.

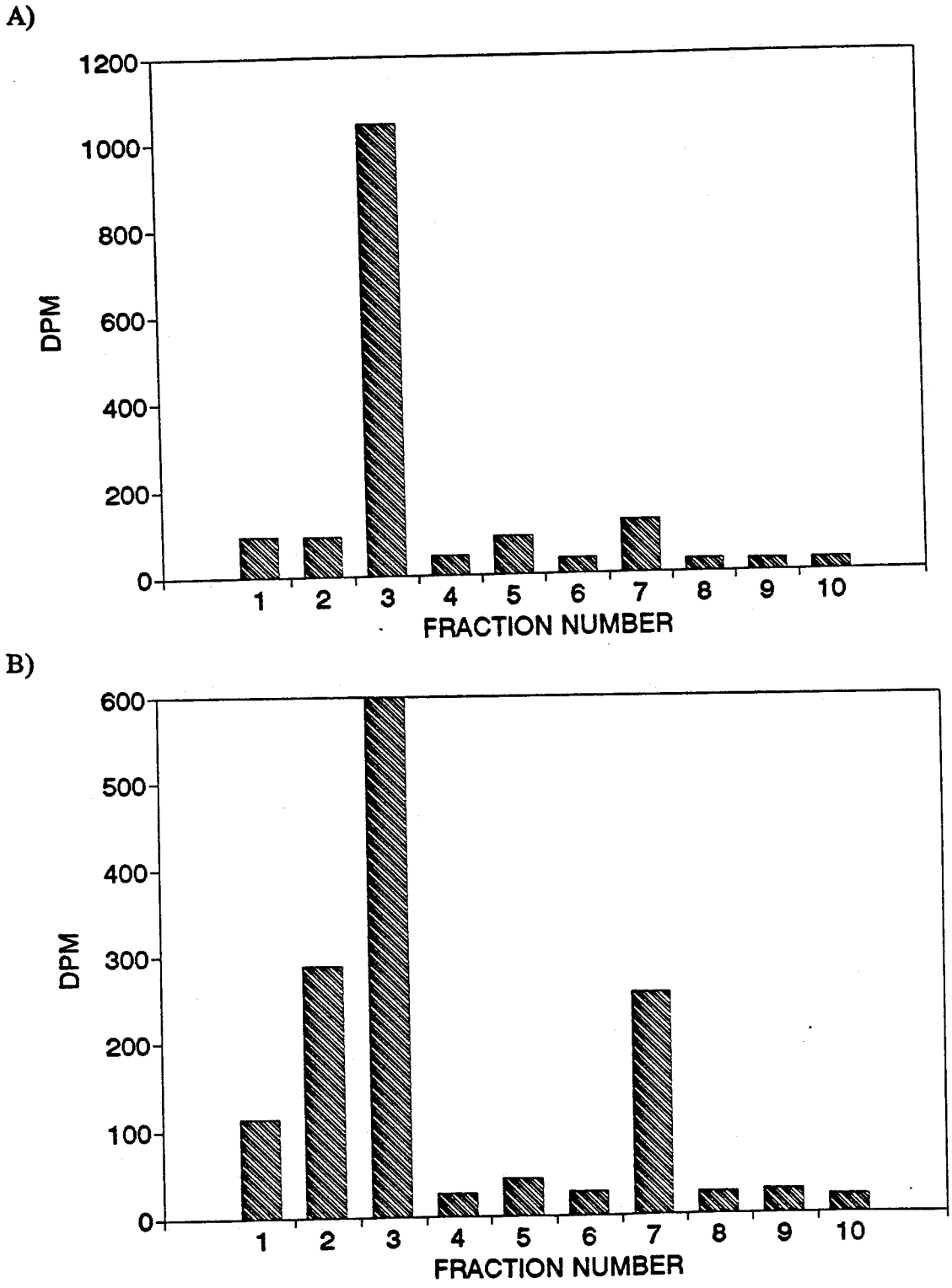

Figure 3.2 The cation exchange chromatograms of the phenol extract from the "experimental seawater" on days 4 (A) and 7 (B) after [^{3}H]-MMA exposure.

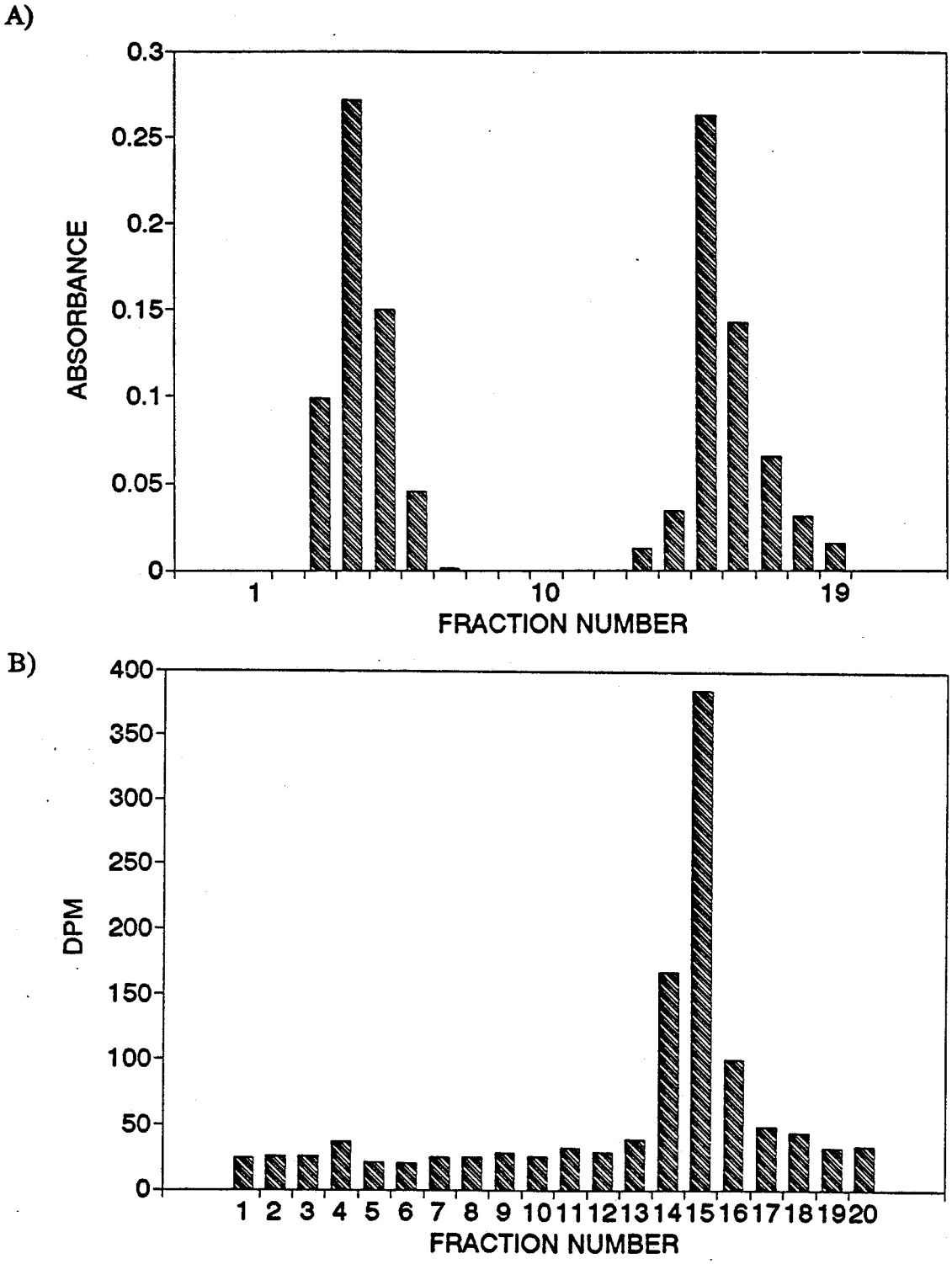

Figure 3.3 HPLC chromatograms; (A) arsenobetaine, MMA, and DMA on the anion exchange column at pH 4, (B) the compound eluting in fraction 3 (Figure 3.2 (B)) on the anion exchange column at pH 4.

A)

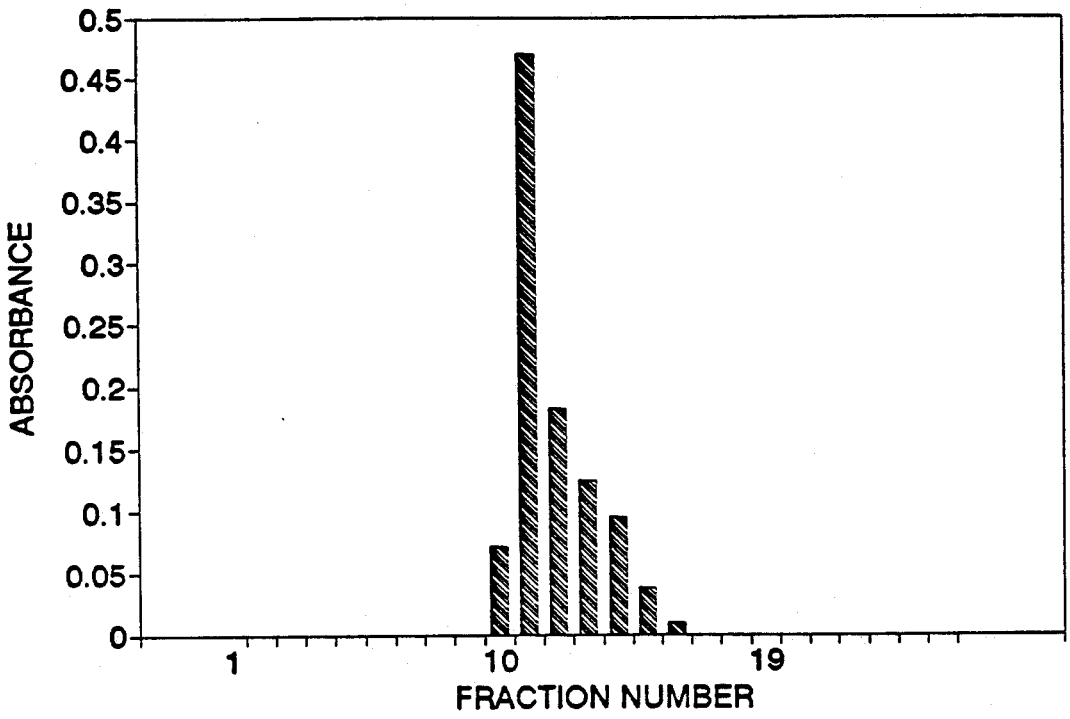

B)

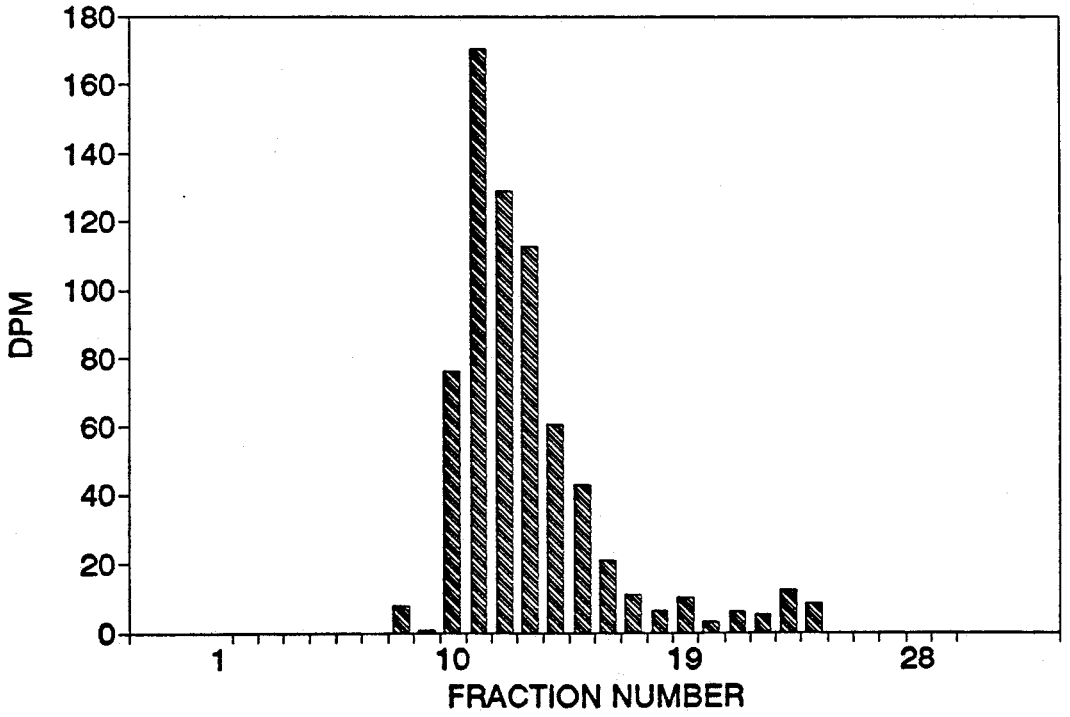

Figure 3.4 HPLC chromatograms; (A) MMA on the size exclusion column and (B) of the compound eluting in fraction 3 (Figure 3.2 (B)) on the size exclusion column.

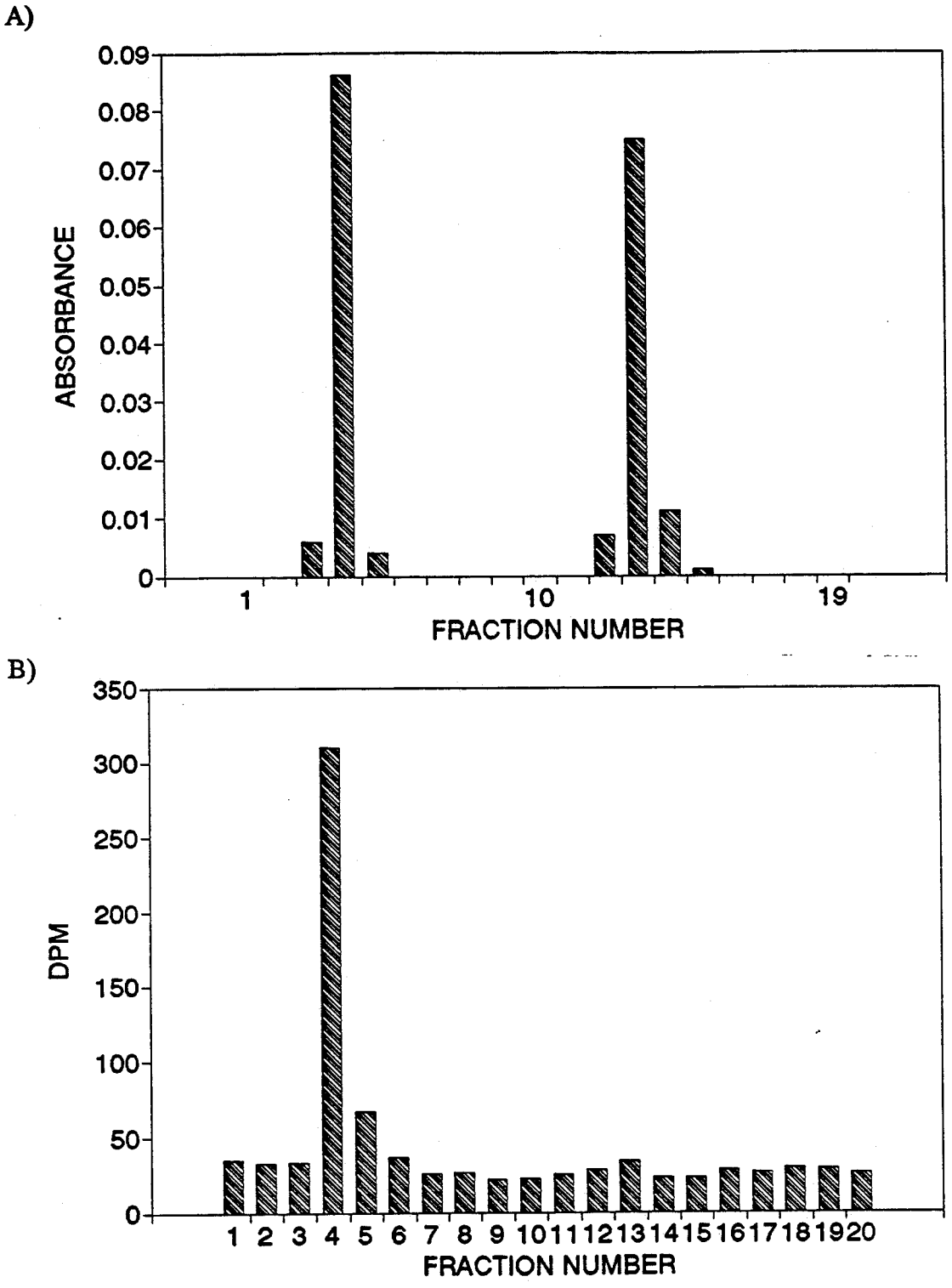

Figure 3.5 HPLC chromatograms; (A) arsenobetaine and DMA on the anion exchange column at pH 6.67, (B) the compound eluting in fraction 7 (Figure 3.2 (B)) on the anion exchange column at pH 6.67.

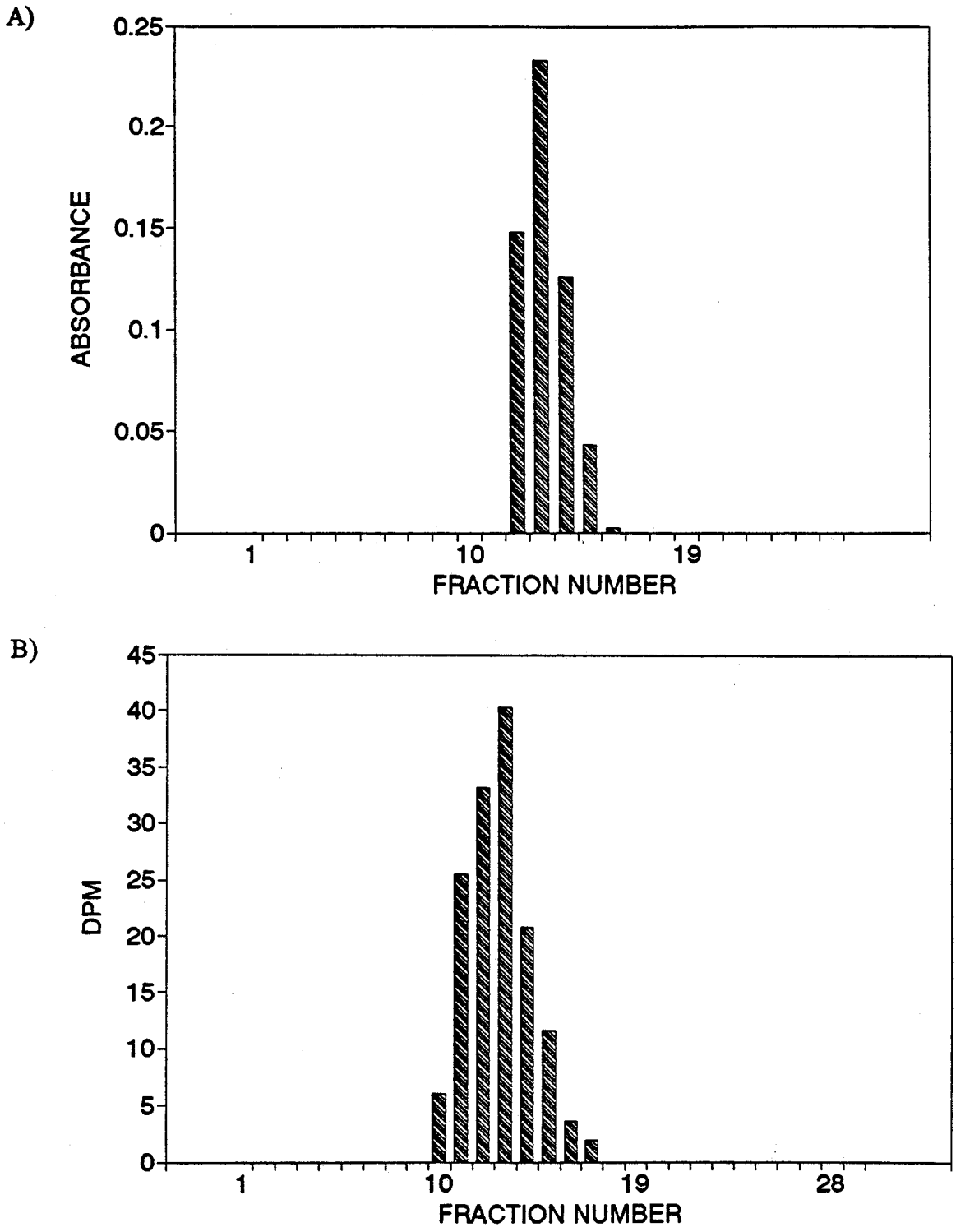

Figure 3.6 HPLC chromatograms; (A) arsenobetaine on the size exclusion column, and (B) of the compound eluting in fraction 7 (Figure 3.2 (B)) on the size exclusion column.

These results describe for the first time the isolation of arsenobetaine from seawater. The isolation of arsenobetaine from the present experiments may have been facilitated by the use of elevated arsenic concentrations and by the use of a radioactive label to allow easier detection.

The chromatograms in Figure 3.2 show a change in the relative amounts of arsenobetaine and MMA on days 4 and 7. The amount of arsenobetaine increased in the absence of mussels which indicates that it is being bio-synthesized, at least in part, by microscopic organisms which are present in seawater.

b) [^{3}H]-DMA:

The cation exchange chromatograms of the [^{3}H]-containing compounds extracted from the "experimental seawater" are displayed in Figure 3.7. The most notable feature of these chromatograms is the low level of activity, which is barely above the background. Arsenobetaine is tentatively identified in fraction 7 (Figure 3.7) by the chromatographic technique described above. The elution profile from the anion exchange (pH 6.67) HPLC column for the compound(s) eluting in fraction 7 (Figure 3.7 (B)) from the cation exchange column is displayed in Figure 3.8.

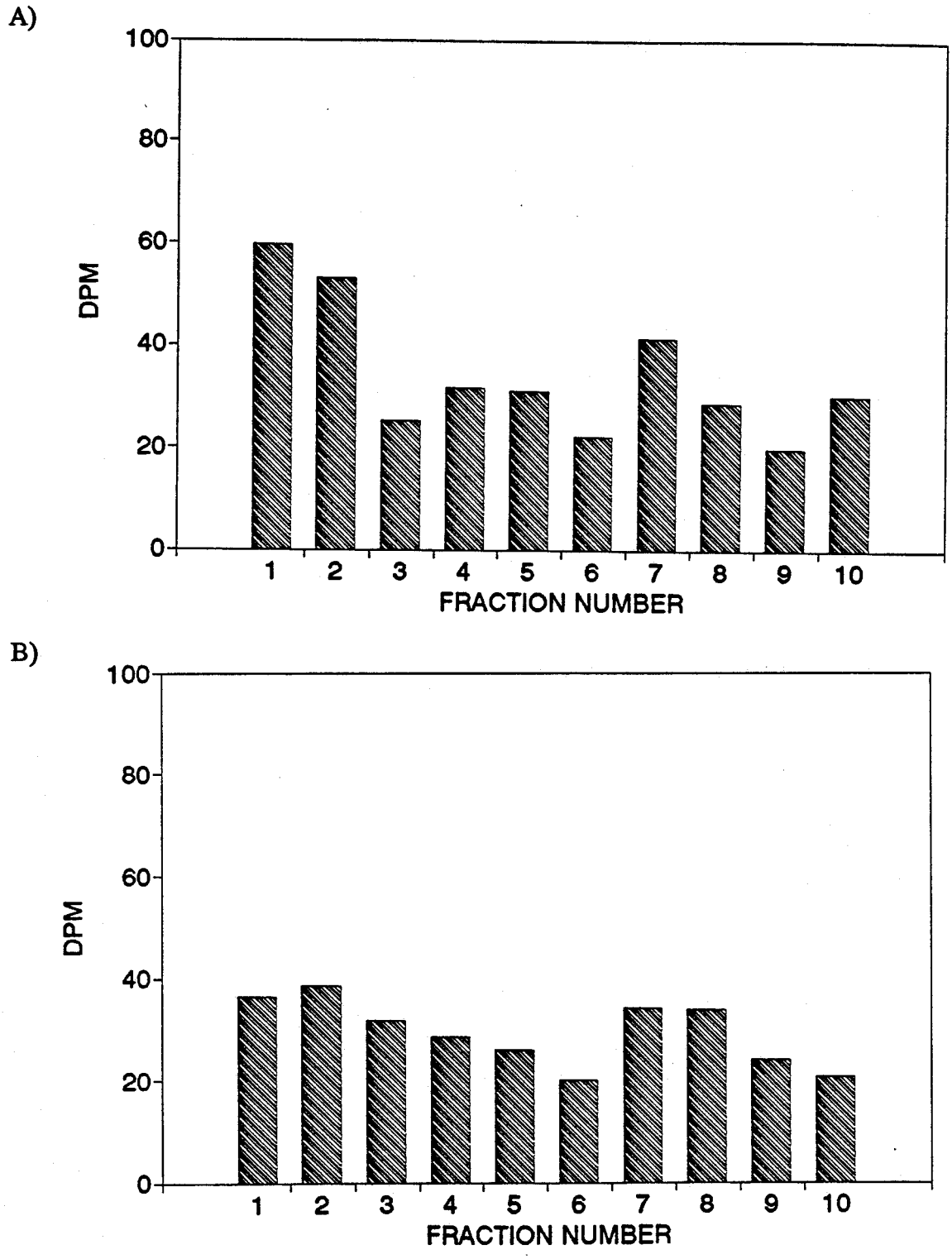

Figure 3.7 The cation exchange chromatograms for the experimental seawater on days 4 (A) and 7 (B) after [^{3}H]-DMA exposure.

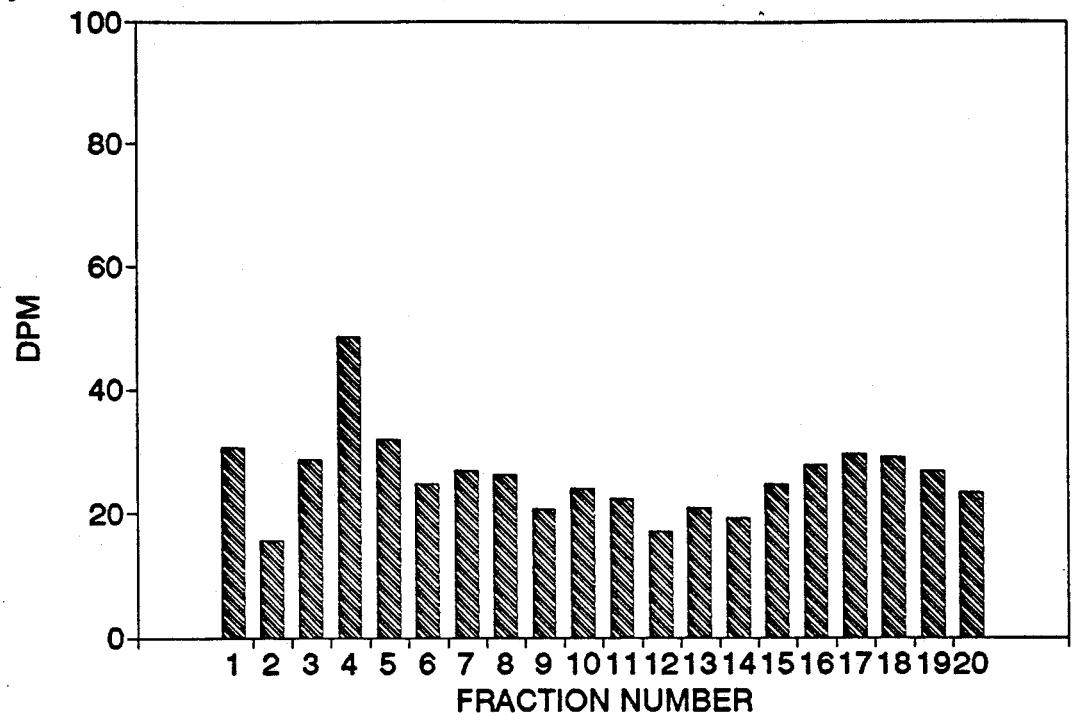

Figure 3.8 The HPLC chromatogram for the compound eluting in fraction 7 (Figure 3.7 (A)) on the anion exchange column at pH 6.67.

3.3.2 Control seawater after exposure to [^{3}H]-MMA and [^{3}H]-DMA

The seawater from the control 15 liter tank was filtered, counted, extracted with phenol, back extracted with deionized water, and then counted again as described above. The chromatographic results and identification of the [^{3}H]-labeled compounds extracted from the seawater are described below. Either [^{3}H]-MMA or [^{3}H]-DMA was added to the seawater at the beginning of the experiment.

a) [^{3}H]-MMA:

The cation and anion exchange chromatograms of the [^{3}H]-containing compounds extracted from the "control seawater" are displayed in Figures 3.9 and 3.10.

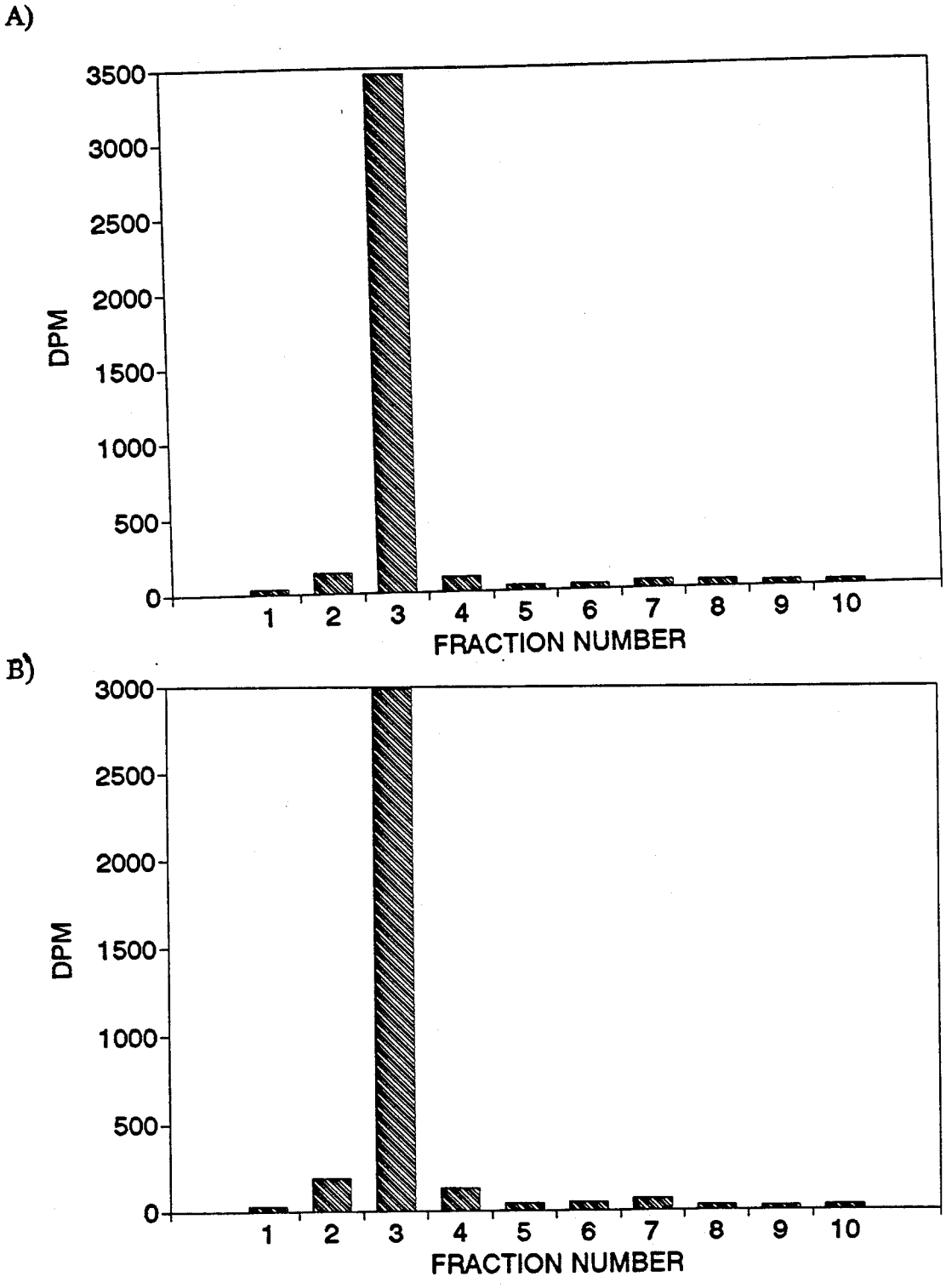

Figure 3.9 The cation exchange chromatograms for the phenol extract from the "control seawater" on days 4 (A) and 7 (B) after [^{3}H]-MMA exposure.

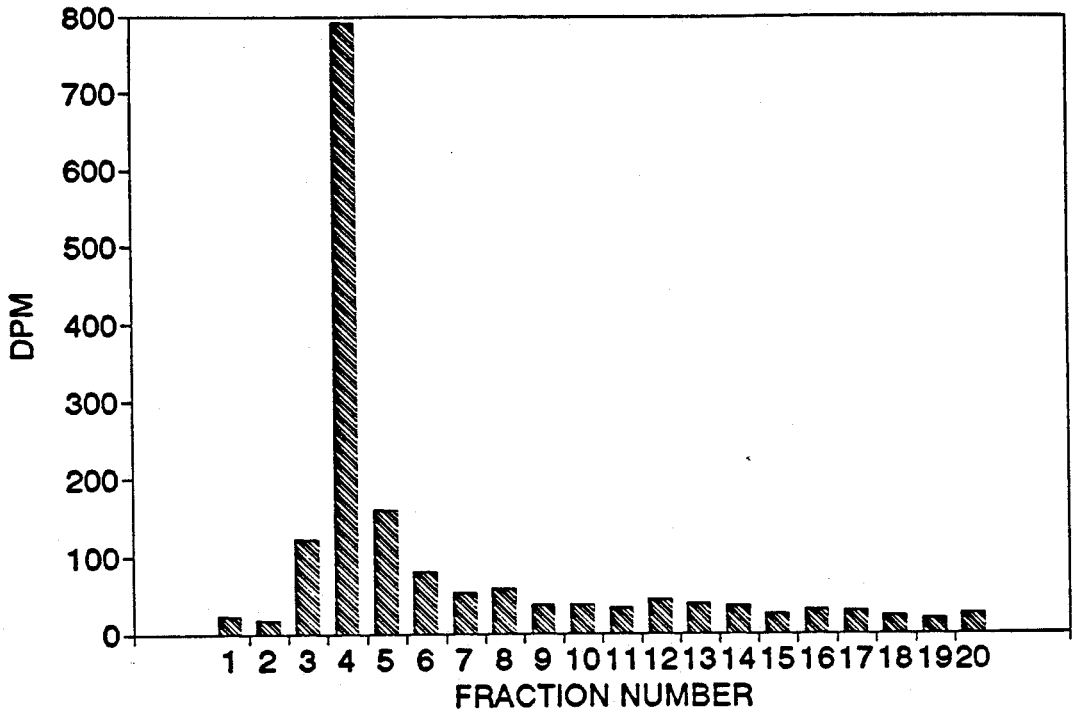

Figure 3.10 The HPLC chromatogram for the compound eluting in fraction 7 (Figure 3.9 (B)) on the anion exchange column at pH 6.67.

The compounds eluting in fractions 3 and 7 from the cation exchange column (Figure 3.9) were identified as MMA and arsenobetaine by using the chromatographic techniques described above. Arsenobetaine is confirmed by the chromatogram in Figure 3.10 for the elution profile from the anion exchange HPLC column at pH 6.67.

These results confirm that MMA can be converted to arsenobetaine in natural seawater. Mussels were never present in the tank so the transformation must be accomplished by organisms at lower trophic levels. The ratio of arsenobetaine to MMA present in the control (Figure 3.9) is much less than that found in the "experimental seawater" (Figure 3.2). This could mean that arsenobetaine is being synthesized by

mussels and/or other microscopic organisms that are symbiotic or otherwise present in seawater with the mussels. It is impossible to distinguish between the contributions of the organisms associated with the mussels and those of the mussels in the current set of experiments.

b) [^{3}H]-DMA:

The cation and anion exchange chromatograms of the [^{3}H]-containing compounds extracted from the "control seawater" are displayed in Figures 3.11 and 3.12.

The compound eluting in fraction 7 from the cation exchange column (Figure 3.11) is identified as arsenobetaine by using the chromatographic techniques described above. Arsenobetaine is confirmed by the chromatogram in Figure 3.12 for the elution profile from the anion exchange HPLC column at pH 6.67.

It seems that DMA is more easily biotransformed to arsenobetaine than MMA. This conclusion is supported by the work in Chapters 4 and 5 which indicates that DMA passes more freely through model cell membranes than MMA. Thus, it would be more readily available for biotransformation.

A)

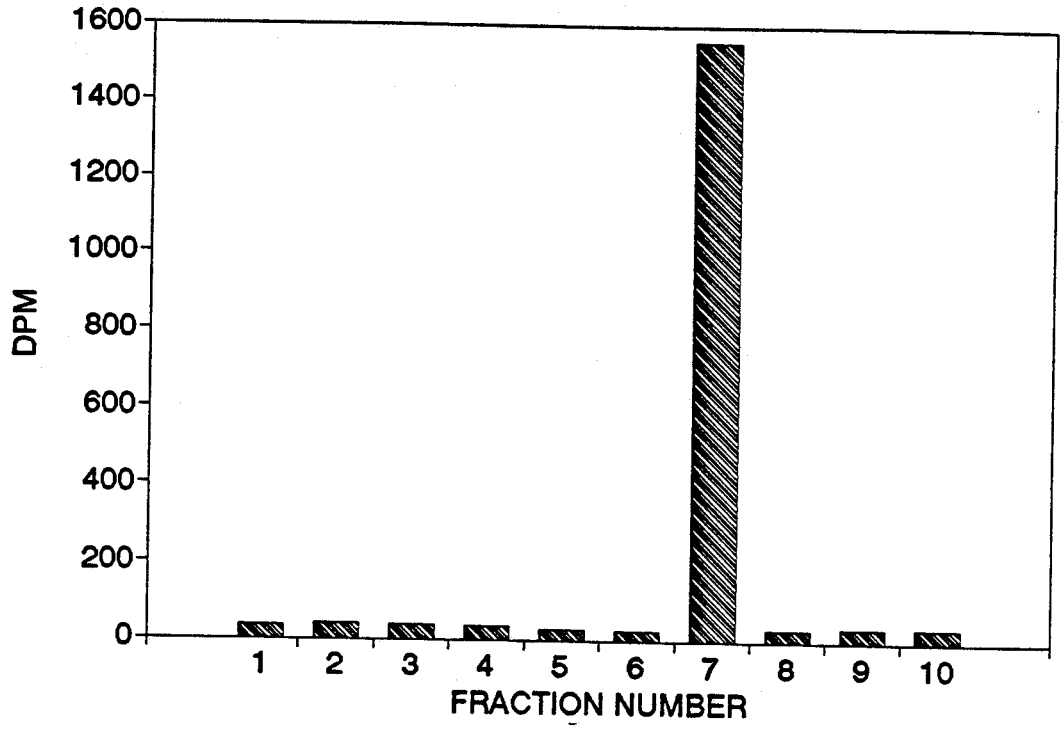

B)

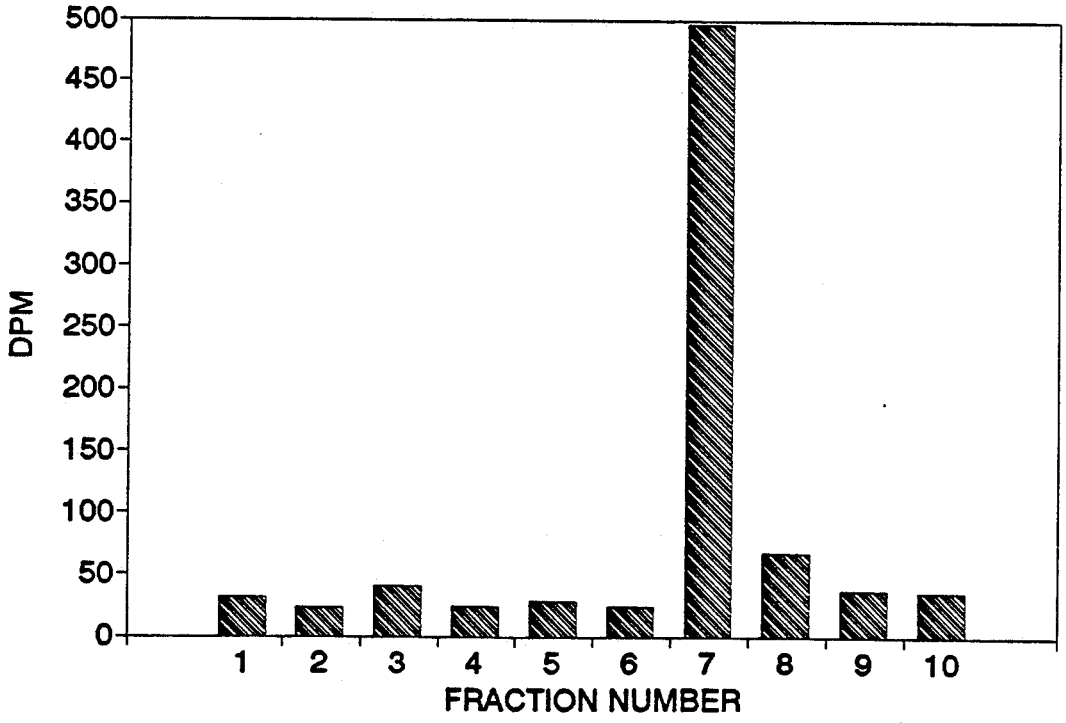

Figure 3.11 The cation exchange chromatograms for the phenol extract from the "control seawater" on days 4 (A) and 7 (B) after [^{3}H]-DMA exposure.

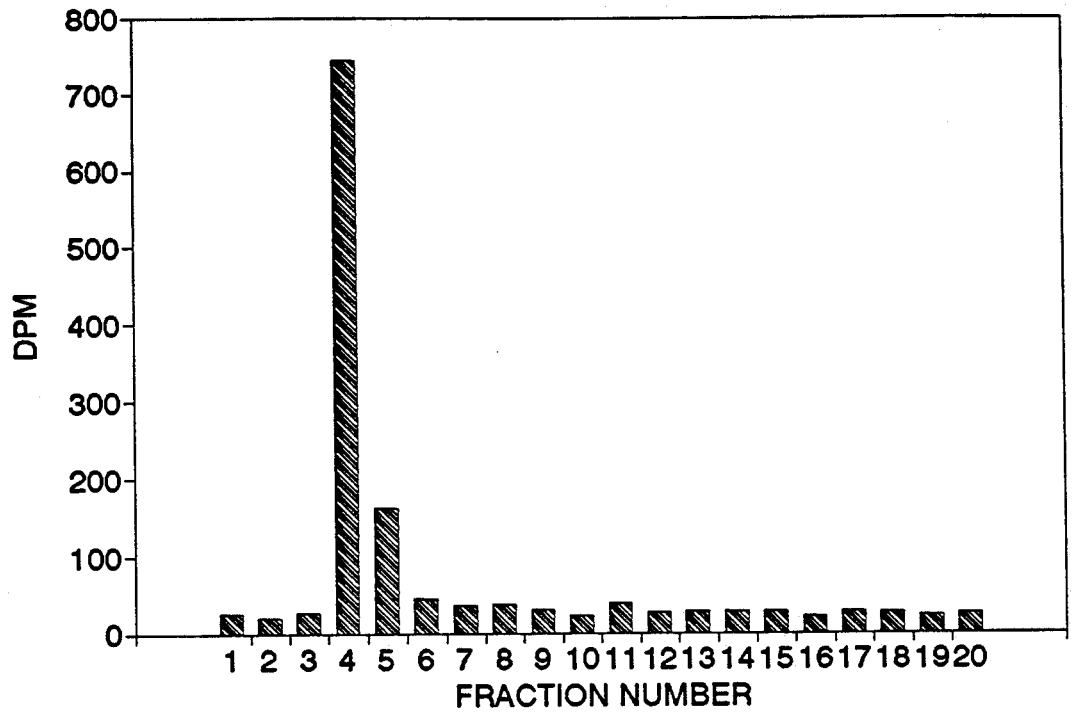

Figure 3.12 The HPLC chromatogram for the compound eluting in fraction 7 (Figure 3.12 (B)) on the anion exchange column at pH 6.67.

3.3.3 Mussel Flesh after exposure to [^{3}H]-MMA and [^{3}H]-DMA

After exposure of the mussels to the labeled arsenicals the flesh was homogenized, the [^{3}H]-containing compounds were extracted from the flesh with phenol and then back extracted into water.

a) [^{3}H]-MMA:

The cation exchange and anion exchange chromatograms of the [^{3}H]-containing compounds phenol extracted from the mussel flesh after 4 days exposure to the label and

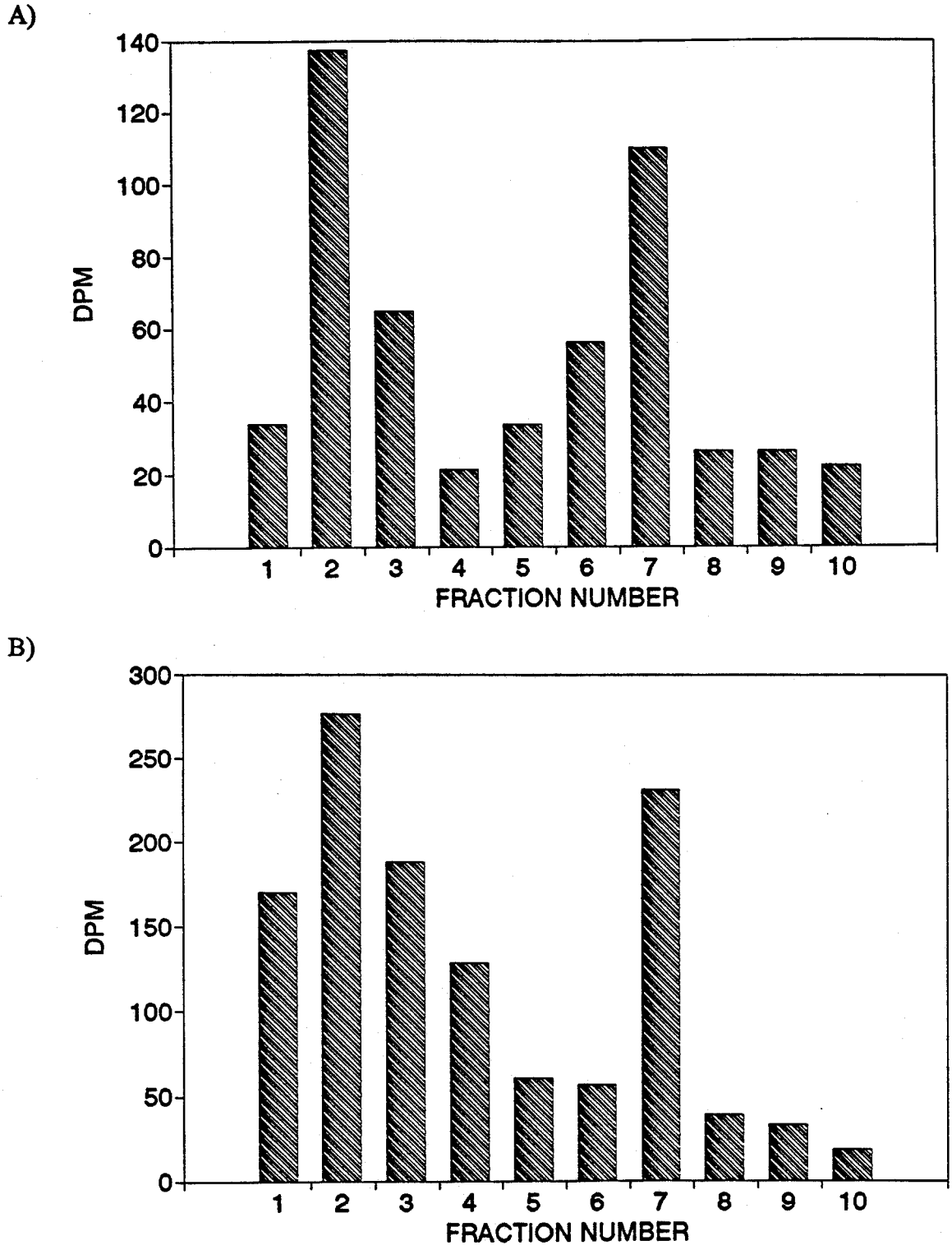

Figure 3.13 The cation exchange chromatograms for the phenol extracted compounds from the mussel flesh on days 4 (A) and 7 (B) after [^{3}H]-MMA exposure.

after the full 7 day cycle (4 days exposure, 3 days wash) are displayed in Figures 3.13 and 3.14.

The compound eluting in fraction 7 from the cation exchange column (Figure 3.13) is identified as arsenobetaine by using the chromatographic techniques described above.

The chromatographic behaviour of the compound in fraction 2 of Figure 3.13 does not match that of any of the available standards. Also, the elution profile for this compound from the anion exchange HPLC column shown in Figure 3.14, does not compare with that of MMA standard shown in Figure 3.3. Its chromatographic behaviour indicates that it is neutral, as it elutes in the void volume from both the cation and anion exchange columns. Arsenic is present in the fraction (by using GFAA) and its possible that the arsenical is a neutral arsenosugar such as 2',3'-dihydroxypropyl 5-deoxy-5-dimethylarsinylriboside **6a**.

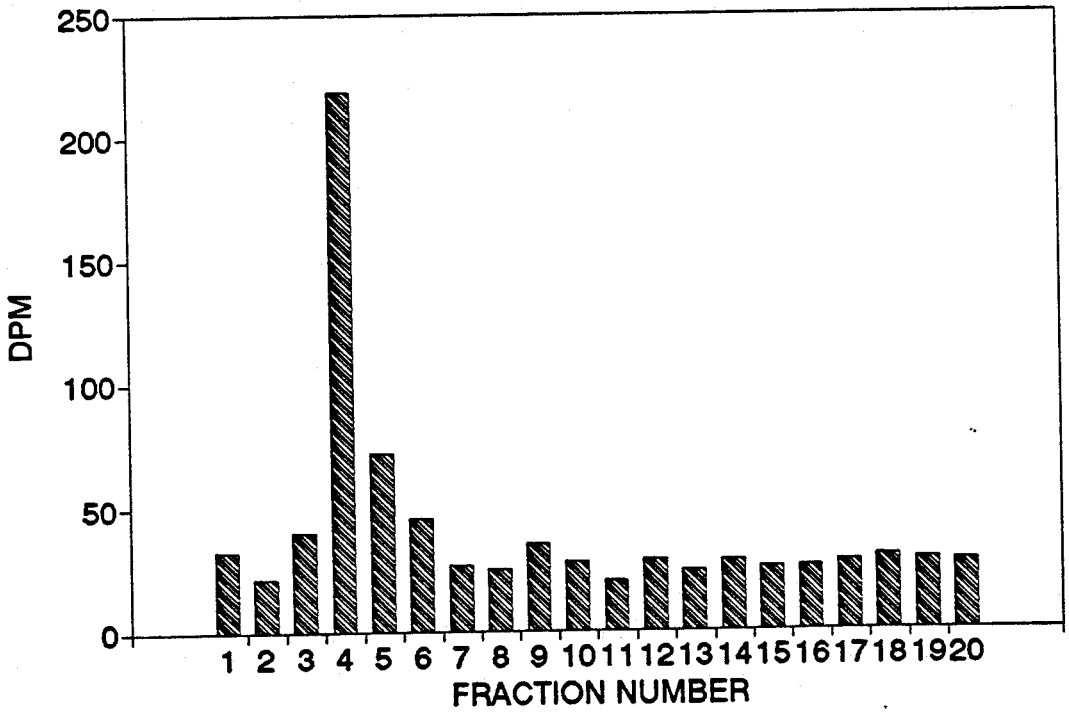

Figure 3.14 The HPLC chromatogram for the compound eluting in fractions 2 and 3 (Figure 3.13 (B)) on the anion exchange column at pH 4.

The two chromatograms in Figure 3.13 are quite similar in that the ratio of arsenobetaine to the unknown is almost the same. Between days 4 and 7 the mussels were exposed to continuously circulating seawater (from the ocean) and any [^{3}H]-labeled compounds that were not bound to the mussels would be quickly washed away. Thus, the chromatograms indicate that within the experimental uncertainty the mussels are not bio-synthesizing arsenobetaine from any of the compounds they have accumulated while being exposed to labeled MMA. This finding supports the hypothesis that arsenobetaine in mussels is accumulated from the surroundings.

b) [^{3}H]-DMA:

The flesh of the mussels exposed to labeled DMA was examined in a similar manner. The compound eluting in fraction 7 from the cation exchange column (Figure 3.15) is identified as arsenobetaine by means of the chromatographic techniques described above.

The compound in fraction 2 appeared to be the same unidentified arsenical isolated from the MMA exposure experiment. Again, as in Figure 3.13 the two cation exchange chromatograms (Figure 3.15) are quite similar. This supports the idea that mussels selectively accumulate arsenicals, as was shown by Francesconi in controlled uptake experiments where mussels readily bio-accumulated arsenobetaine and arsenocholine, but do not bio-accumulate trimethylarsine oxide or 2-dimethylarsinylethanol.[99]

These results indicate that either MMA or DMA can act as a precursor to arsenobetaine and are part of the same bio-synthetic pathway.

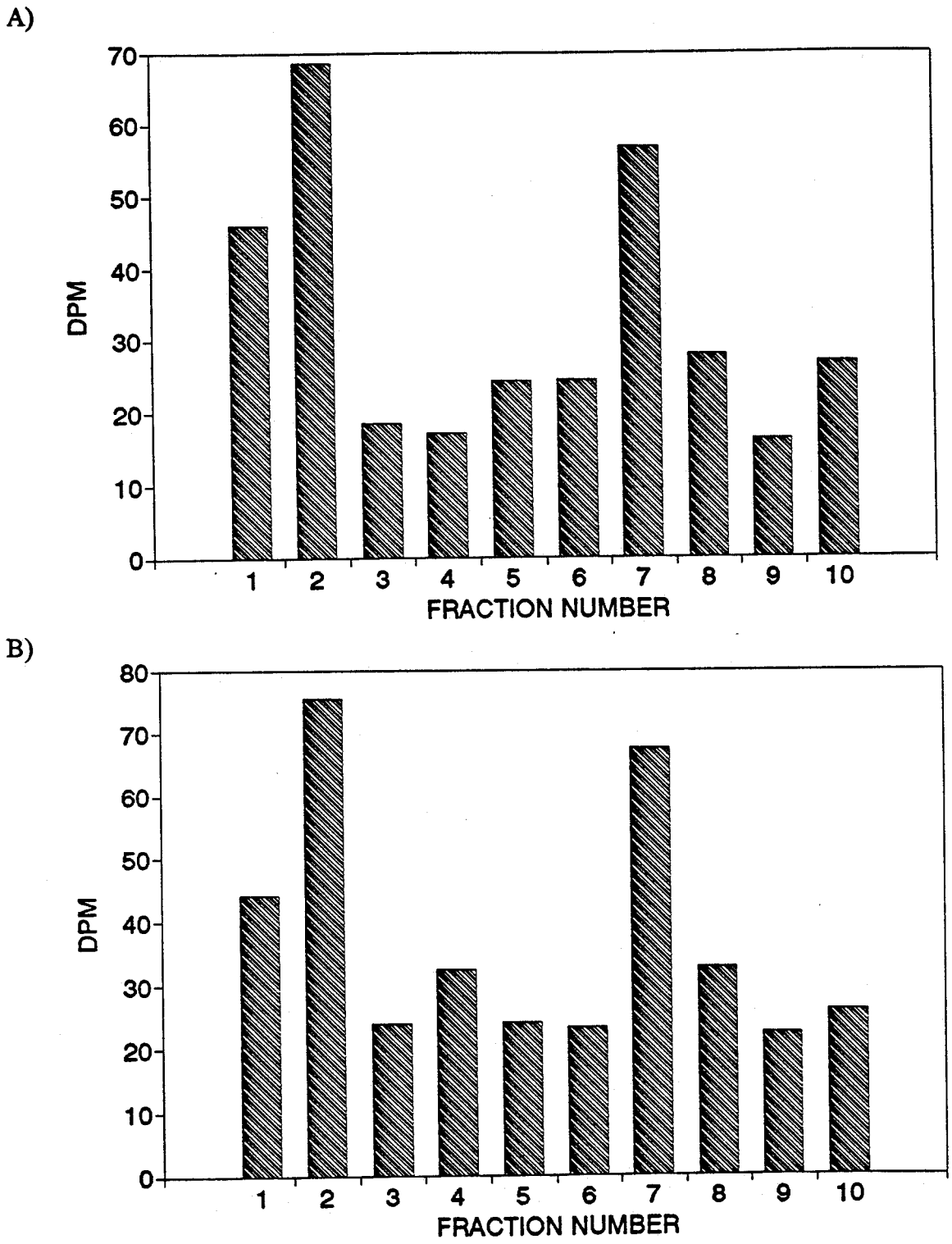

Figure 3.15 The cation exchange chromatograms for the phenol extracted compounds from the mussel flesh on days 4 (A) and 7 (B) after [^{3}H]-DMA exposure.

3.3.4 The extraction efficiency of [^{3}H]-labeled compounds which were extracted from seawater and mussel samples

Each of the samples was counted prior to and after the phenol extractions in order to determine the percentage of [^{3}H]-labeled compounds which were extracted from the matrix by the phenol. These results are summarized in Table 3.1.

Table 3.1 Percentage of [^{3}H]-labeled compounds which were extracted from the seawater and mussel samples.

	"experimental seawater"	"control seawater"	mussels
MMA starting	10%	10%	80%
DMA starting	5%	40%	85%

The extraction efficiency of the phenol extraction procedure (Section 3.2.4) for both MMA and DMA was experimentally determined to be about 10%. The phenol extractions were designed by Cannon *et al* to extract arsenobetaine from a complex sample matrix.[42] The extraction efficiency of the phenol extraction proceedure for arsenobetaine was experimentally determined to be close to 100%. The results from Table 3.1 show that there is a much higher percentage of [^{3}H]-labeled compounds extracted from the mussels than from the seawater. This indicates that the composition of [^{3}H]-labeled arsenicals in the mussels is different than in the water. This difference supports the notion that mussels selectively accumulate organoarsenic compounds from seawater, rather than randomly accumulating compounds at the percentages at which they are found

in the seawater (as was discussed in Section 3.3.3). When DMA, rather than MMA was used as the starting substrate in the "control seawater" there is a greater percentage of [^{3}H]-labeled compounds extracted from the seawater. This greater percentage indicates that more biotransformations to arsenobetaine and compounds similar in structure to arsenobetaine have occured. Such a finding supports the earlier results which suggest that DMA is more readily biotransformed into arsenobetaine than is MMA (discussed in Section 3.3.2). The low percentage of [^{3}H]-labeled compounds extracted from the "experimental seawater" when [^{3}H]-DMA was the starting substrate agrees with the earlier results (Section 3.3.1b) which showed that level of radioactivity in the extracts from the seawater was quite low. This tends to suggest that the rate of conversion of the [^{3}H]-DMA to [^{3}H]-arsenobetaine by the microscopic organisms in the seawater followed by the uptake of the [^{3}H]-arsenobetaine by the mussels must occur rapidly within the time scale of the experiment. This is consistent with the observed depletion of the [^{3}H]-label in the seawater.

3.3.5 Examination of the [^{3}H]-labeled compounds in the seawater after the experiment described in Section 3.2.5

The seawater collected on days 4, 7 and 10 was filtered and the filtrate was subjected to the phenol extraction proceedure (outlined in Section 3.2.6). Approximately 10% of the [^{3}H]-labeled compounds in the seawater were extracted by the phenol extractions. The extracted compounds were back extracted into deionized water and evaporated (rotary) to dryness. This was redissolved in 1 ml of deionized water and applied to a size exclusion HPLC column. The compounds were eluted by using 5 mM ammonium acetate and the resulting chromatograms are displayed in Figures 3.16 A, B

and C for days 4, 7 and 10, respectively. The chromatogram in Figure 3.16 A from day 4 shows that the majority of the extracted [^{3}H]-labeled compounds are eluted between fractions #12 and #16. This indicates that the [^{3}H]-label is distributed in the seawater among compounds of a similar size. The size exclusion chromatograms for the standards MMA, DMA, and arsenobetaine are shown in Figures 3.4 A, 3.17 and 3.6 A, respectively. Each of these three standards elute with approximately the same retention volume. The chromatogram in Figure 3.16 B from day 7 is quite different than the chromatogram produced on day 4 because most of the extracted [^{3}H]-labeled compounds are eluted between fractions #11 and #30 showing that the extracted [^{3}H]-label has been redistributed amongst compounds of different sizes. This redistribution of the label occurred during the time when mussels were not present in the seawater. Therefore, as was shown in the previous experiments involving the "control seawater", the small, non-circulating tank contains a wide variety of microscopic organisms which are capable of the biotransformation of arsenic. The mussels were placed back into the seawater between days 7 and 10 and the resulting chromatogram for day 10 is shown in Figure 3.16 C. This chromatogram resembles the chromatogram from day 4 more closely than it resembles the chromatogram from day 7. The amount of extracted [^{3}H]-labeled compounds eluting between fractions #19 and #30 has decreased in the chromatogram for day 10 when compared to the chromatogram for day 7. This suggests that the mussels may be bioaccumulating or biosynthesizing the compounds found in the latter chromatographic fractions.

This particular study is inconclusive, but it does accentuate the fact that the arsenic cycling in the ocean is based upon complex interactions between microscopic and macroscopic organisms.

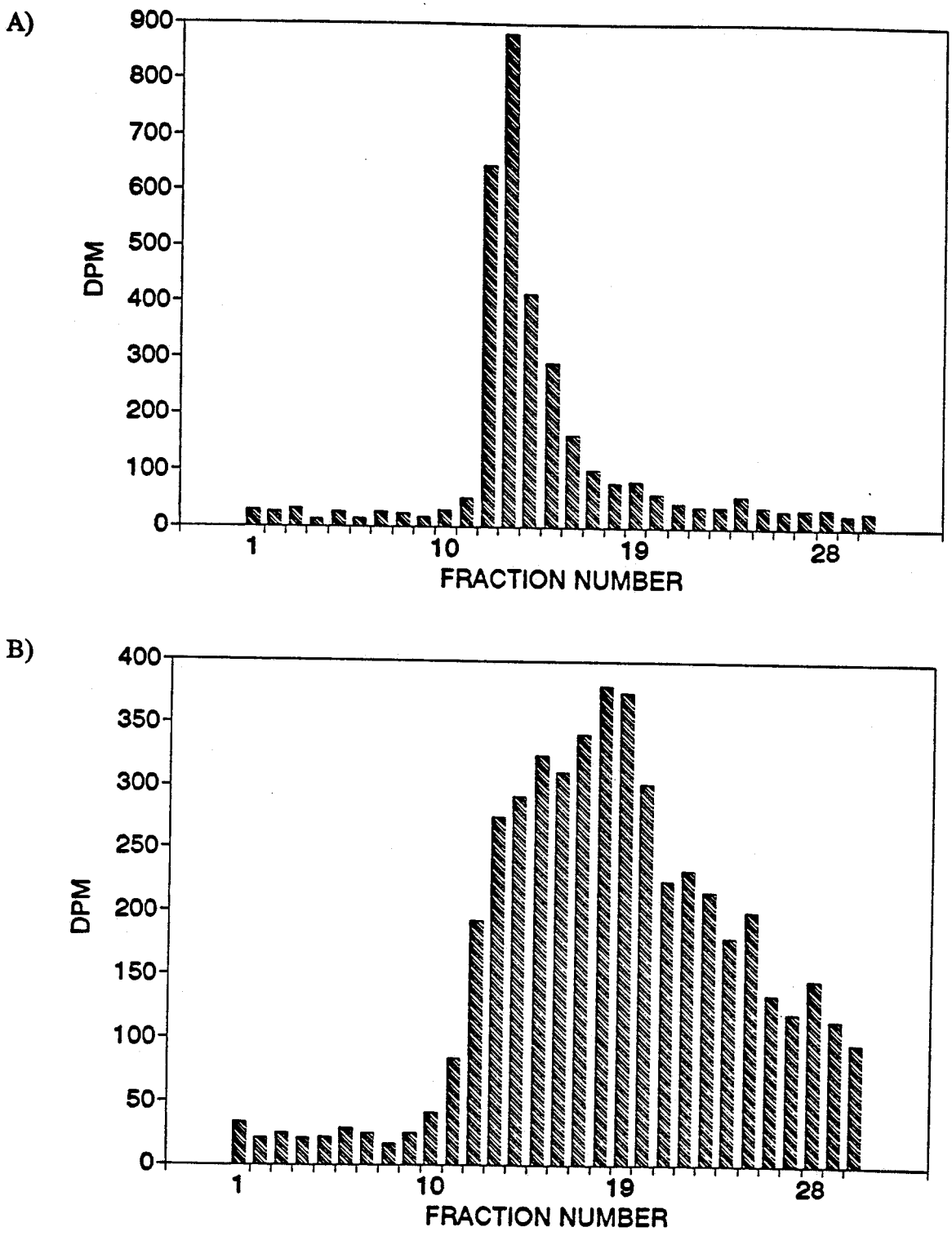

Figure 3.16 (please see complete caption below.)

C)

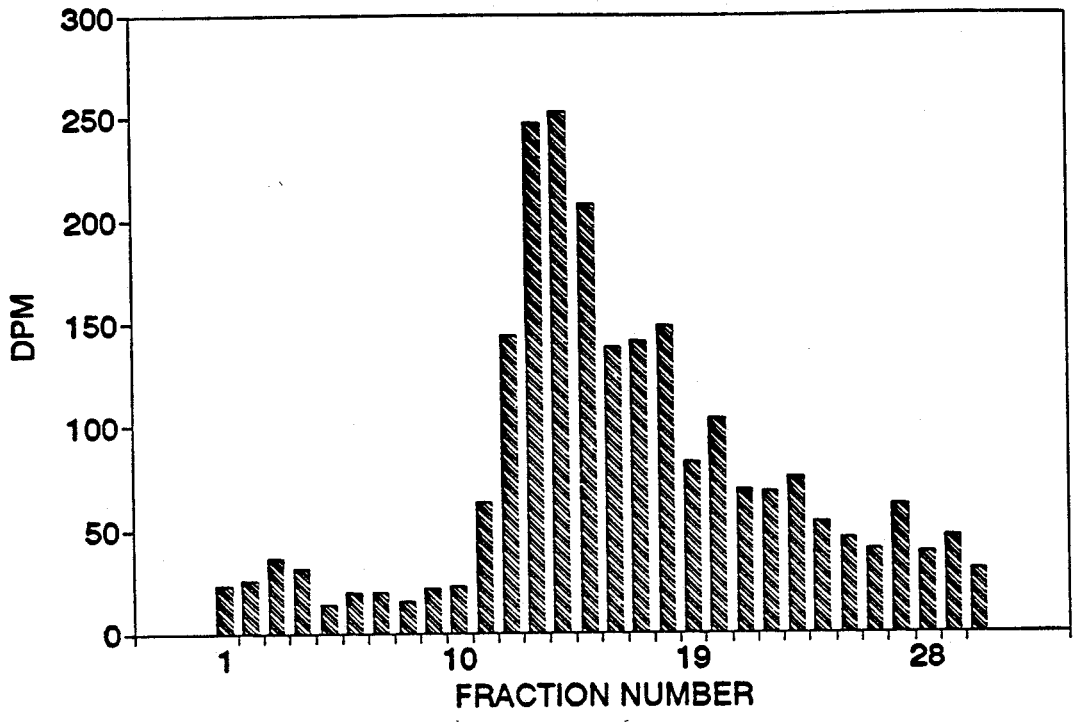

Figure 3.16 The size exclusion HPLC chromatogram for the "experimental seawater" on days 4 (A), 7 (B), and 10 (C).

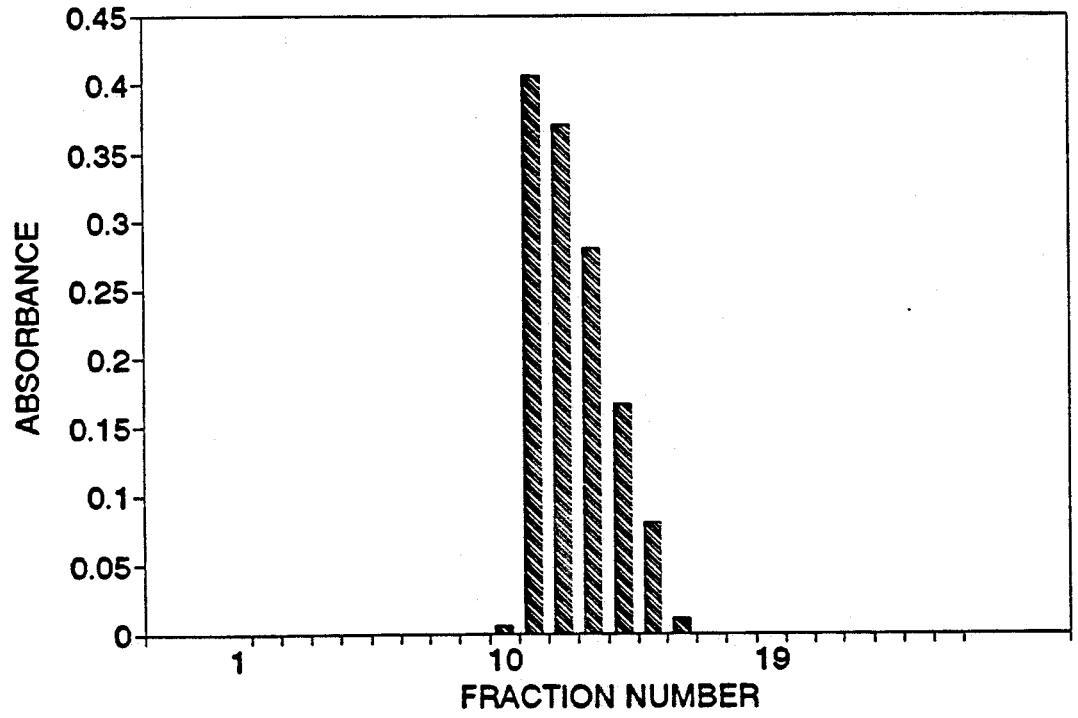

Figure 3.17 The size exclusion HPLC chromatograms for the DMA standard.

3.3.6 Summary

The results from this chapter indicate that both MMA and DMA may be biotransformed to arsenobetaine in the marine environment. In particular, it was shown that naturally occuring microscopic organisms are capable of performing this biotransformation. Within the uncertainty of the experiments described in this chapter it does not appear that the mussels are capable of biosynthesizing arsenobetaine. Thus, mussels appear to accumulate their arsenobetaine content via uptake from the water column. The results also show that mussels accumulate compounds selectively, as they bioaccumulate both arsenobetaine and an unknown compound, while the starting substrates are not bioaccumulated by the mussels within the detection limits of the experiments.

DMA is biotransformed more readily to arsenobetaine than is MMA. This result indicates that DMA is either more direct link to arsenobetaine in the biochemical pathway, or that DMA is more rapidly bioaccumulated by the microscopic organisms in seawater than is MMA. The results of work described in Chapters 4 and 5 predict that DMA will be more rapidly bioaccumulated by microscopic organisms than MMA.

Future work may involve trying to isolate the microscopic organisms in seawater which perform the biotransformations described in this chapter and the previous chapter.

CHAPTER 4

THE USE OF LIPOSOMES IN PREDICTING THE BIOMOBILITY AND BIOACCUMULATION OF MMA AND DMA

4.1 INTRODUCTION

4.1.1 How do molecules get across membranes?

The translocation of matter across biological membranes is a fundamental physico-chemical processes in living systems. The two major components of biological membranes are phospholipids and proteins (Figure 4.1). The proteins are inserted into phospholipids which are orientated in a bilayer.[145] These bilayers form a continuous sheet around cells and cellular organelles. For a molecule to enter or leave the cell or organelle it must cross this barrier.

Molecules may cross this barrier either by active transport or by passive diffusion. Active transport typically requires metabolic energy and is defined as the movement of a metabolite or an inorganic ion across a membrane usually in the direction that is against the concentration gradient. Passive (simple) diffusion occurs when molecules and ions cross either the lipid region of the barrier or flow through the aqueous channels formed by the proteins, in a nonspecific way. This movement is driven solely by the difference in the chemical or electrochemical potential of the species on the two sides of the membrane.

The lipid region is a hydrophobic environment. Thus, if the permeant is to diffuse through this region of the membrane all of the bonds that the permeant has made with the aqueous medium surrounding the membrane must be broken. It is not thermodynamically favorable for a charged molecule to enter into the hydrophobic environment of the inner bilayer.[144] If a molecule does succeed in entering the hydrophobic region of the

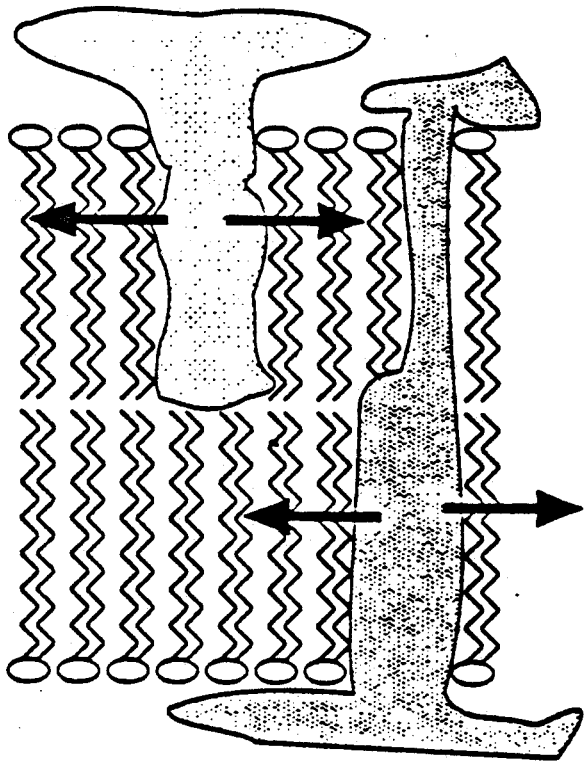

Figure 4.1 The Fluid-Mosaic model of the cell membrane. The arrows represent the directions of the lateral diffusion of the proteins.

membrane by passing through the tightly packed head groups which present a significant barrier to diffusion, then it will pass through the flexible hydrocarbon tails relatively easily as this region has a much lower barrier to intramembrane movement.[146]

There are two possible mechanisms for the diffusion of molecules across the cell membrane in which the permeant does not have to enter the hydrophobic core of the bilayer. Membranes are typically in a fluid state which allows small molecules to diffuse into and out of the vacancies (defects) in the outer bilayer (Figure 4.2a), thus moving from an aqueous environment into the apolar interior of the membrane. If a vacancy in the

lattice of the inner leaflet becomes available the permeant can then diffuse across the membrane. Membrane pores could also be formed by either the micellar arrangement of the phospholipid bilayers (Figure 4.2b) or by protein channels (Figure 4.2c) within the membrane. Thus, the permeant could pass through the bilayer without being impeded by the hydrophobic region.

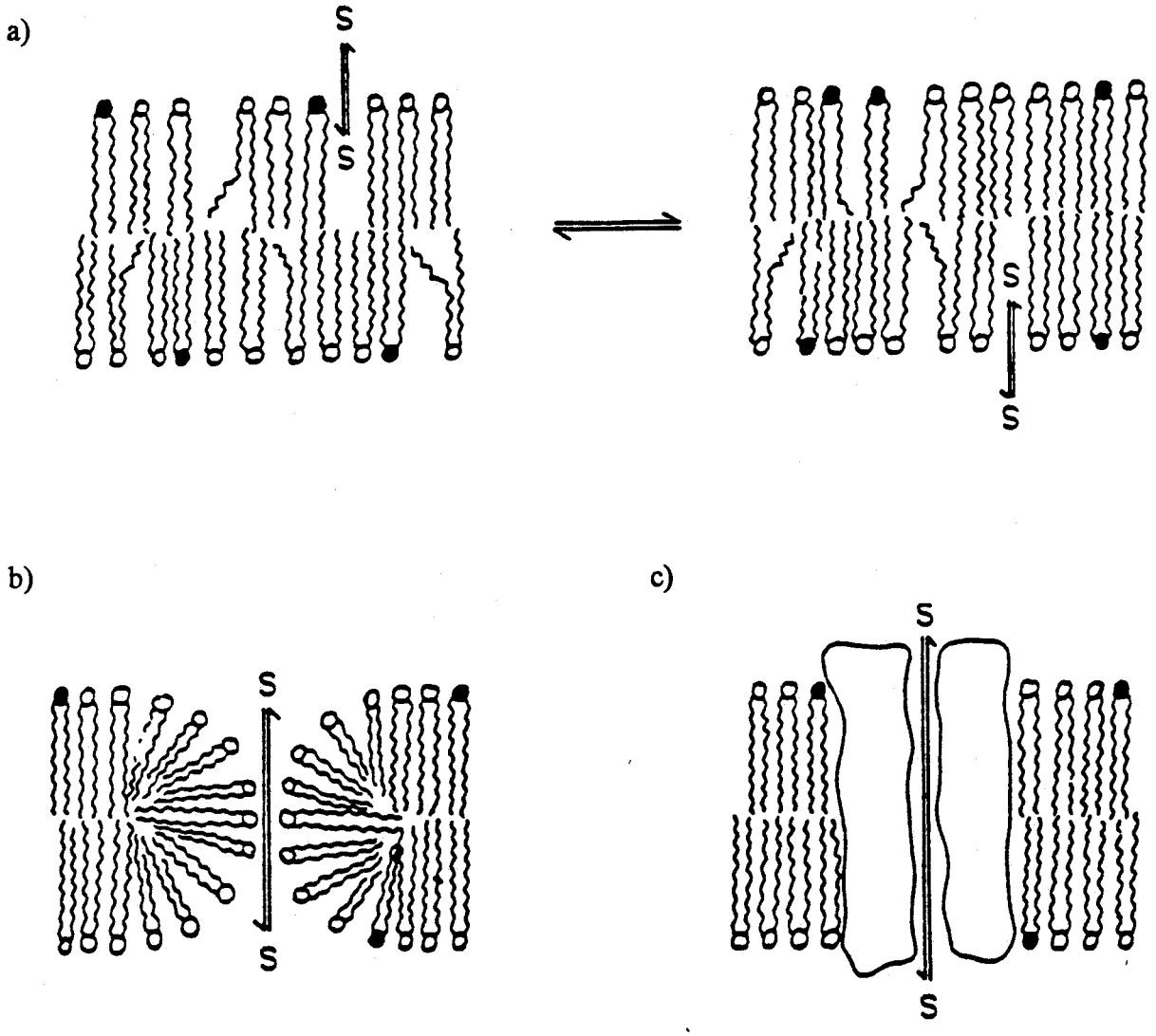

Figure 4.2 Mechanisms of permeation through the bilayer without entry into the hydrophobic region.

4.1.2 Structures of main phospholipids found in cell membranes

The structures of the six major phospholipids found in cell membranes are displayed in Figure 4.3. For the purposes of this thesis, phosphatidylcholine was the only phospholipid used. Phosphatidylcholine is the most common lipid found in eukaryotic plasma membranes and is a zwitterion composed of a glycerol-phosphate ester with a

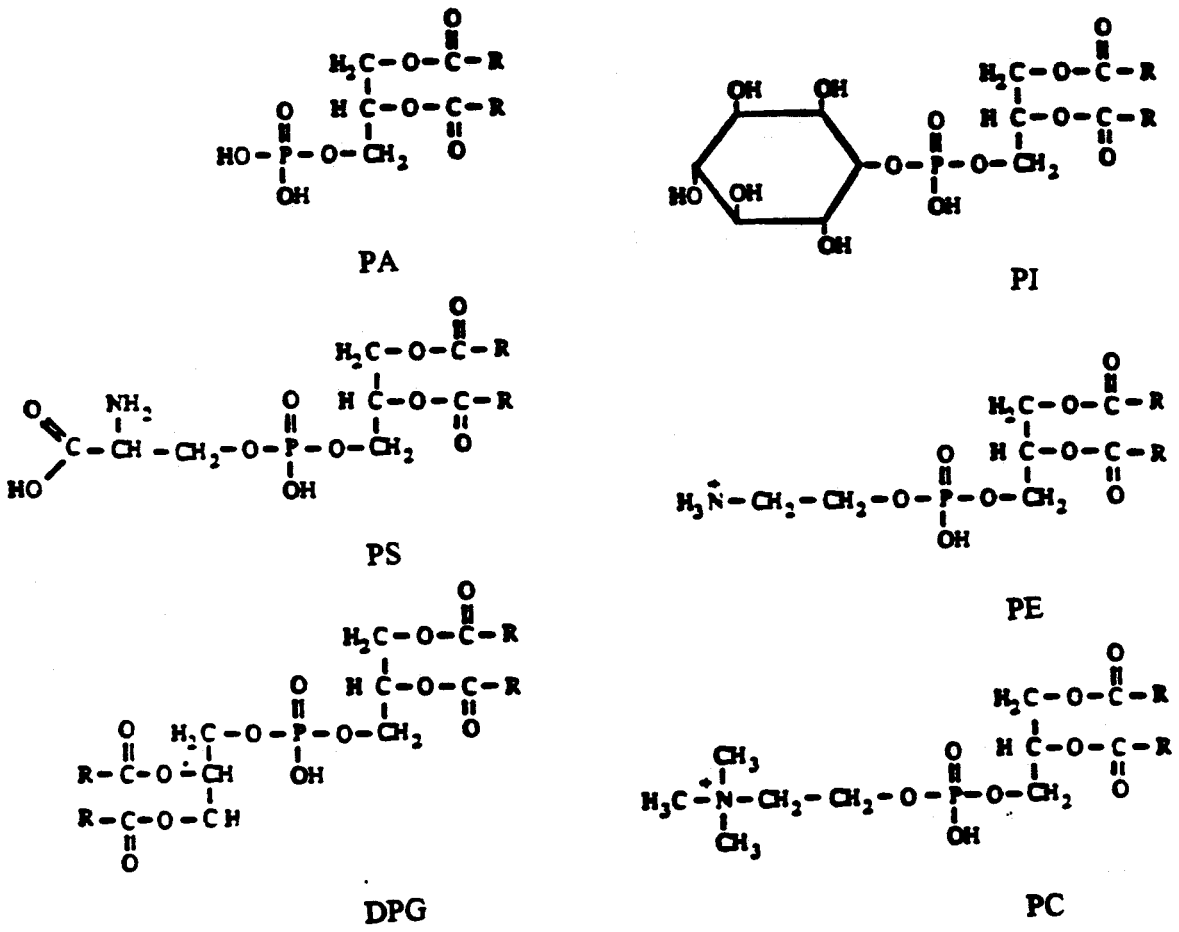

Figure 4.3 Structures of the major phospholipids found in cell membranes; PA, phosphatidic acid; PS, phosphatidyl serine; PC, phosphatidyl choline; PE phosphatidylethanolamine; PI, phosphatidylinositol; DPG, diphosphatidylglycerol. R is the side chain (Figure 4.4).

choline head group and two acyl chains.[131] The fatty acid side chains (Figure 4.4) of egg derived phosphatidylcholine are palmitic acid (32%), stearic acid (15%), oleic acid (31%), and linoleic acid (16%).[132] In addition, there are other fatty acids present in trace amounts in egg phosphatidylcholine.

a) $CH_3(CH_2)_{14}CO_2H$
b) $CH_3(CH_2)_{16}CO_2H$
c) $CH_3(CH_2)_7CH{=}CH(CH_2)_7CO_2H$
d) $CH_3(CH_2)_4(CH{=}CHCH_2)_2(CH_2)_6CO_2H$

Figure 4.4 The structure of the side chains of egg phosphatidyl choline; (a) palmitic acid, (b) stearic acid, (c) oleic acid, and (d) linoleic acid.

4.1.3 Structures of hydrated phospholipids

When the dry phospholipids are hydrated a variety of lipid structures are formed. These structures are displayed in Figure 4.5. The structure most important to this thesis is the liposome. Liposomes are single walled (unilamellar) or multiwalled (multilamellar) concentric shells in a spherical structure. A small volume of water is separated by the bilayer from the bulk aqueous solution (as shown in Figure 4.5c). The head groups are immersed in the water; the hydrocarbon chains, being hydrophobic, point away from the water to the center of the bilayer. This is energetically the most favorable arrangement, as the water molecules are at a far lower energy when they are surrounded by other water

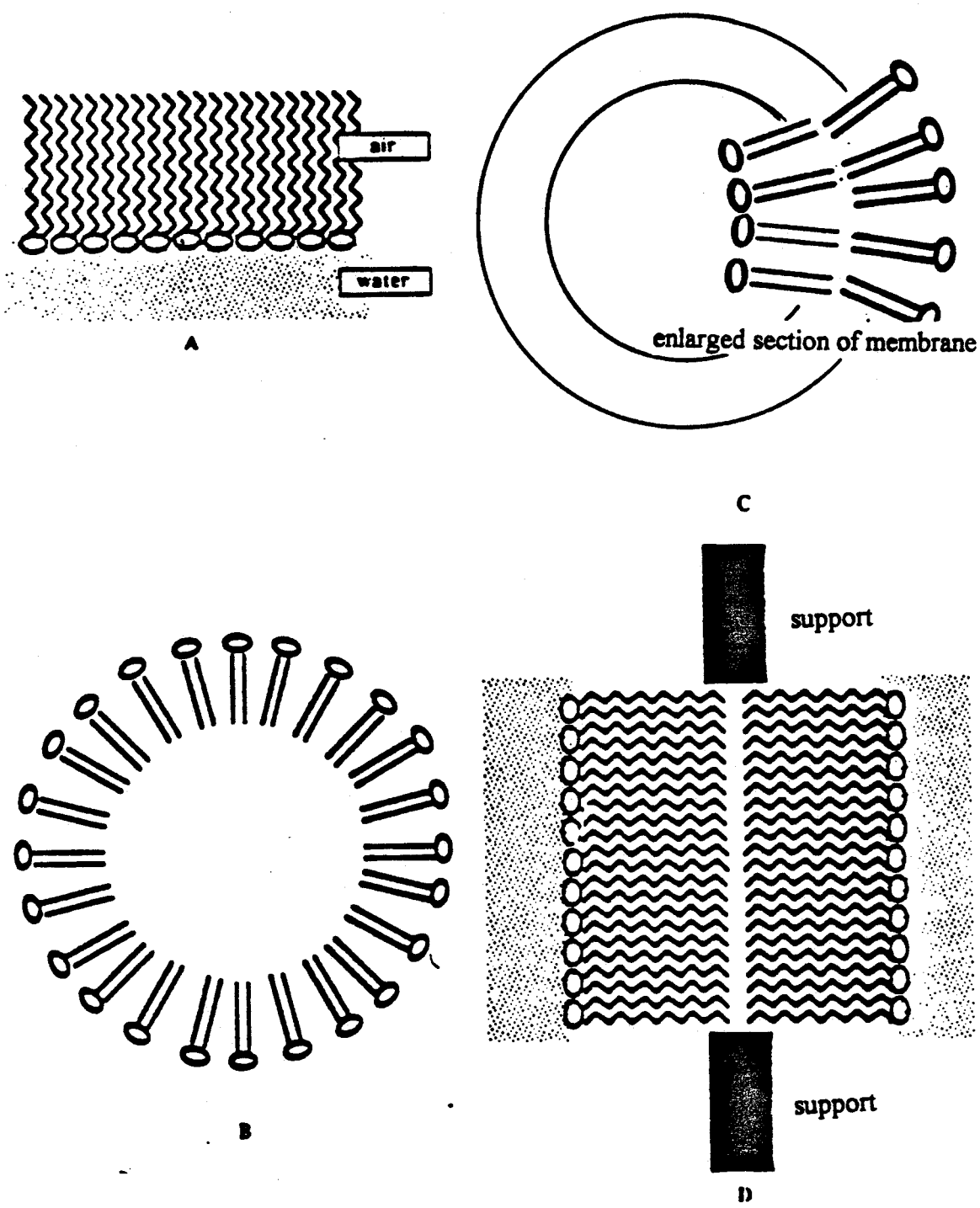

Figure 4.5 Structures of phospholipids which are formed upon hydration; A) a monolayer formed at an air-liquid interface; B) a micelle; C) an example of a liposome, (see Section 4.1.6); D) a black membrane, a planar bilayer, that separates two aqueous phases.

molecules with which they can hydrogen-bond, than when this bonding is interupted by hydrocarbon chains. Thus, water will be excluded from the region of the hydrophobic, hydrocarbon chains. Likewise, the hydrocarbon chains will line up with one another to form bilayers, which is the most thermodynamically favorable configuration.

4.1.4 The mobility of the lipid components within the bilayer

The phospholipid molecules within the bilayer are in constant motion. The possible modes of mobility are displayed in Figure 4.6.

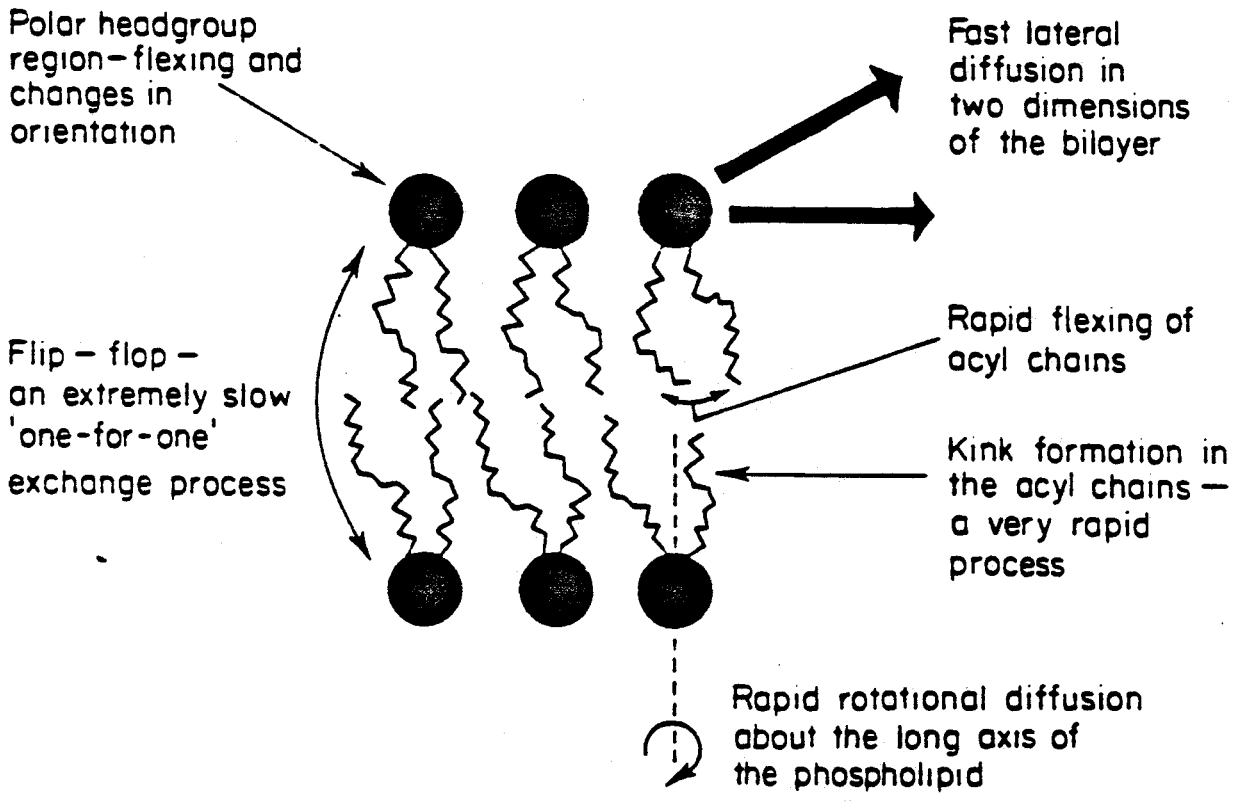

Figure 4.6 Modes of mobility of the lipid components of the bilayer.

The freedom of rotation around the carbon-carbon bonds in a saturated fatty acid leads to an extended configuration that allows maximum intermolecular interactions to stabilize the structure. When cis double bonds are present, the chain becomes fixed preventing efficient packing of the molecules, leading to less favorable interactional energy. The insertion of cholesterol into the bilayer restricts the motion within the bilayer (Figure 4.7).

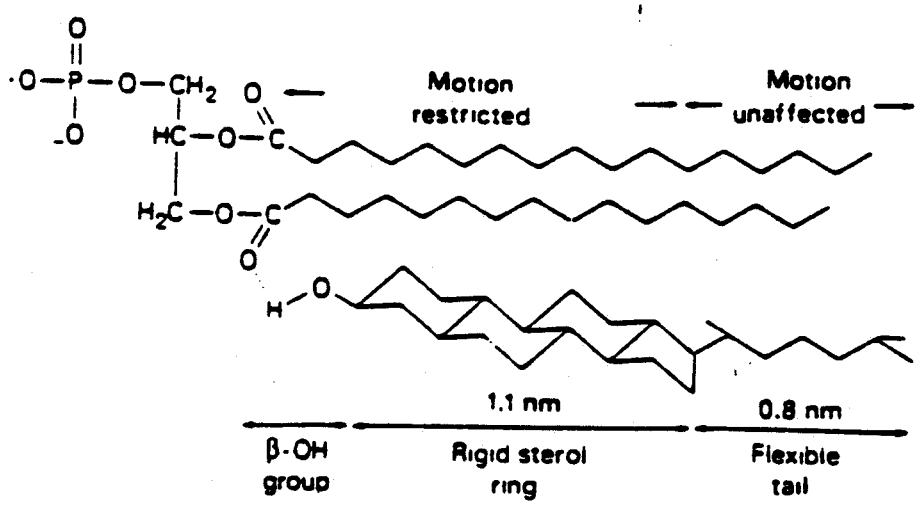

Figure 4.7 Insertion of cholesterol into a phospholipid bilayer. A schematic representation of the alignment of a cholesterol molecule with a phospholipid in a lipid bilayer.

4.1.5 Liposomes as models for biological membranes

The liposome was developed by Bangham *et al.* as a model for biological membranes.[127] They were the first to discover that the hydration of lipids results in the formation of sealed vesicles.[128] In 1972, Cohen and Bangham made an extensive study of the capacity of a large number of non-electrolytes to cross the membrane of such vesicles.[129] They found that the permeability of a molecule across the liposomal membrane is highly dependent upon its size and its solubility in an organic solvent. Thus, they showed that the basic permeability properties of biological membranes are mimicked by these artificial lipid bilayers. In addition, because the composition of the bilayer can be precisely controlled which allows liposomes to be formed with a similar membrane composition to actual cells, studies have shown that liposomes are excellent models for transport studies; they behave as useful models of biological membranes.[130]

4.1.6 Types of liposomes

There are three types of liposomes: multilamellar vesicles (MLVs) which form spontaneously upon the hydration of lipid and contain multiple bilayers, small unilamellar vesicles (SUVs), which are less than 50 nm in diameter and contain a single bilayer and large unilamellar vesicles (LUVs), which are between 100 and 400 nm in diameter and also contain only one bilayer.[133] MLVs are unsuitable as models for membranes because of difficulties in reproducible production and variations in size. SUVs are also unsuitable as models for membranes because of the high degree of membrane curvature and miniscule trapped volumes. However, LUVs may be made reproducibly to specific sizes and are quite stable which makes them the ideal choice for a model membrane system.[130]

4.1.7 Large Unilamellar Vesicles (LUVs)

LUVs may be produced through solvent evaporation/vaporization,[134] sonication,[135] and extrusion techniques.[126] The extrusion technique is the most reproducible and was employed in this thesis. In the extrusion technique, the LUVs are produced by passing MLVs through polycarbonate filters of defined pore size under moderate pressure (≤ 500 psi). This is achieved by using a device known as, "The Extruder" (Figure 4.8).[126,136] The relatively high pressures allow homogeneously sized LUVs to be produced ranging in size between 50 and 200 nm in diameter depending upon the filter size.[137] Electron micrographs of vesicles produced after extrusion through

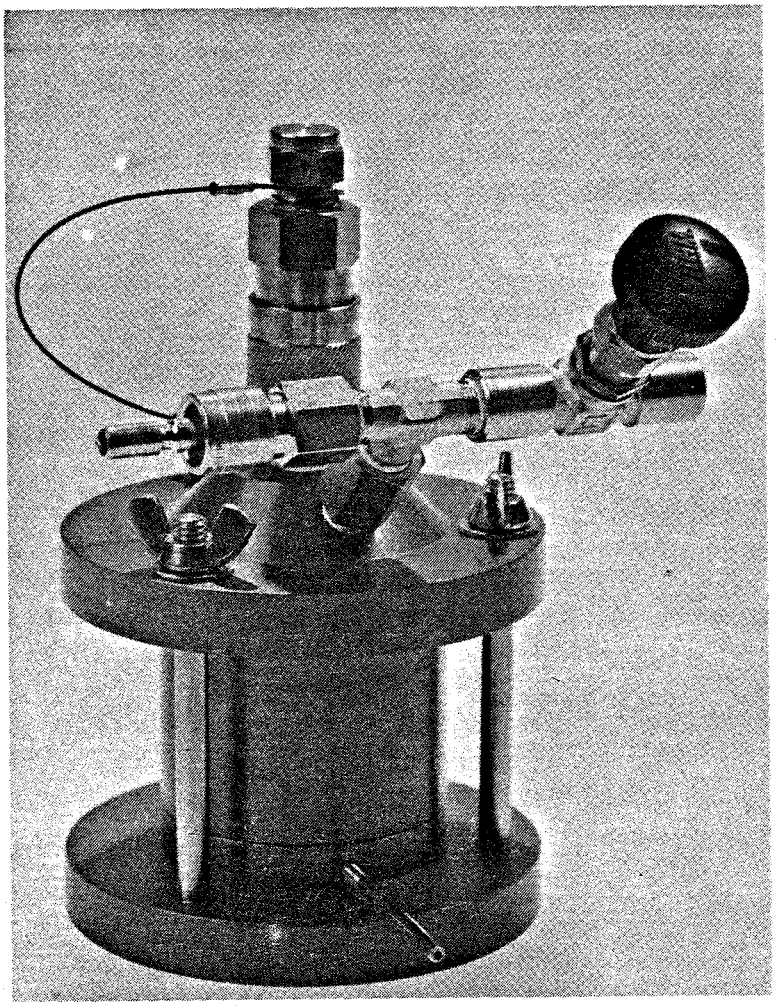

Figure 4.8 The Extruder.

different sized filters are displayed in Figure 4.9. The mean diameter and standard deviation (S.D.) of the extruded LUVs is displayed in Table 4.1.[137]

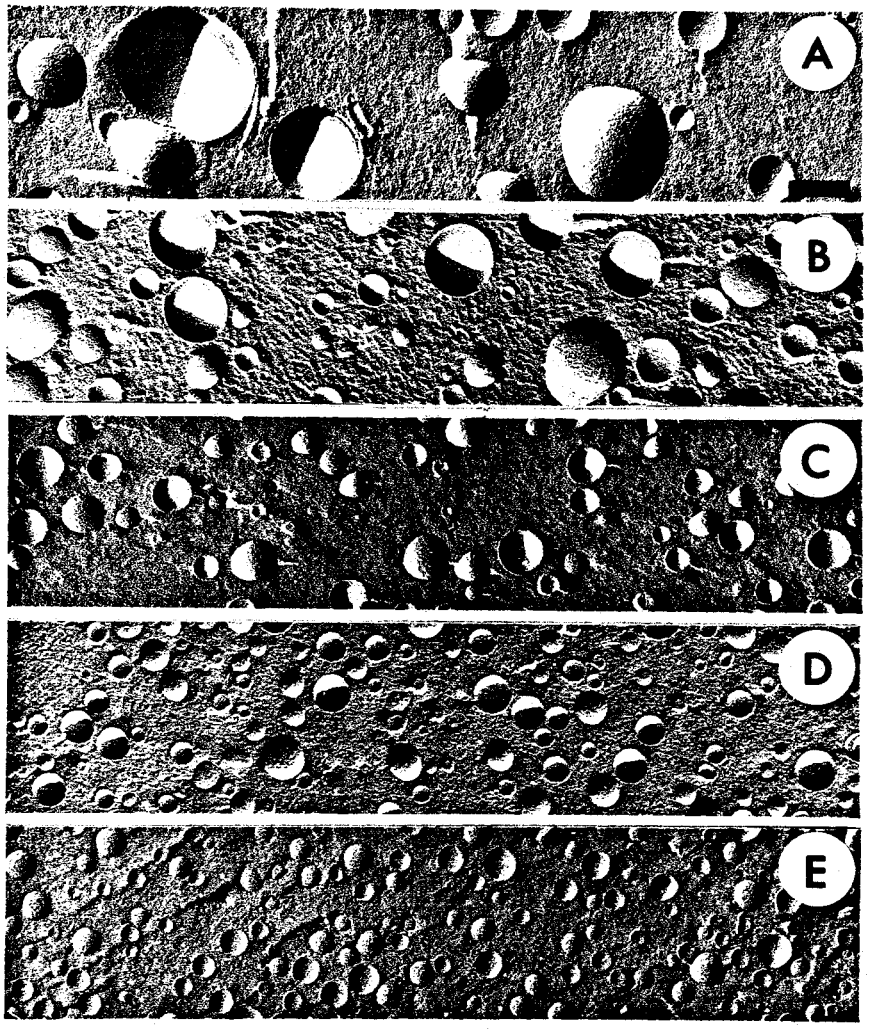

Figure 4.9 Electron micrographs of vesicles prepared by extrusion through; A) 400; B) 200; C) 100; D) 50; and E) 30 nm pore size polycarbonate filters. (from reference 137).

Table 4.1 Mean diameter of LUVs produced via the extrusion technique.

Filter pore size (nm)	Mean diameter±S.D. (nm) Electron microscopy	Mean diameter±S.D. (nm) Light scattering
400	243 ± 91	not determined
200	151 ± 36	180 ± 55
100	103 ± 20	139 ± 36
50	68 ± 19	74 ± 18

The degree of unilamellarity of the extruded LUVs was tested by Mayer *et al.*[137] They measured the intensity of the signal from the phosphorus molecules, on the phospholipids of LUVs produced by the extrusion technique, before and after the addition

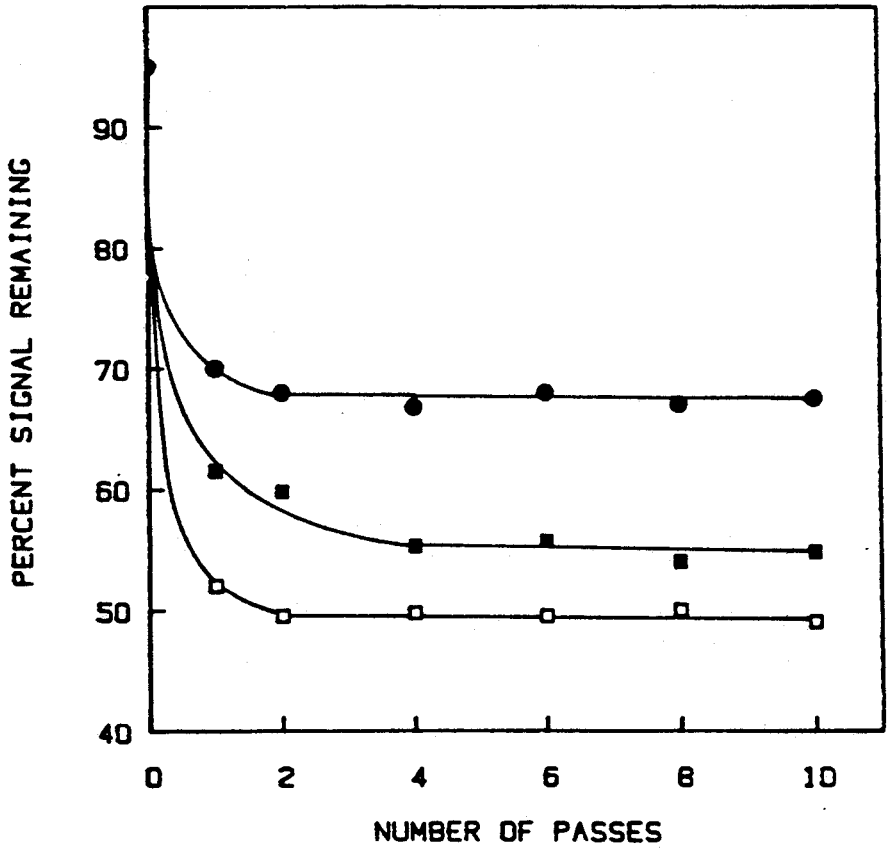

Figure 4.10 Test of the unilamellarity of vesicles extruded the indicated number of times through 400 (•), 200 (■), and 100 (□) nm pore size filters.

of Mn^{+2} by using ^{31}P-NMR. The Mn^{+2} broadens the spectroscopic signals of the phospholipids on the outside of the bilayer so that only the spectroscopic signals from the phospholipids on the inside of the bilayer remain. The results from this experiment are displayed in Figure 4.10. If the phospholipid bilayer were completely unilamellar, only 50% of the initial signal would remain after the addition of the Mn^{+2}.

4.1.8 How is biomobility of environmentally sensitive compounds traditionally modelled?

In order to assess the environmental impact of a compound it is desirable to have some measure of its ability to pass through biological membranes. When estimations of this type are needed octanol/water partition coefficients are often quoted.[108] For example, the octanol/water partition coefficients for chlorobenzenes and chlorophenols correlates linearly with the uptake of chlorobenzenes and chlorophenols by trout, as shown by Neely *et al.*[109] This correlation is generally useful because many of the organic compounds which are either known to or suspected to constitute a hazard to the environment are highly lipid soluble[110] and, therefore, have relatively large o/w partition coefficients ($>10^2$). These compounds usually exist as a single molecular species in the environment and do not possess ionizable groups. This is fortunate because a partition coefficient is defined as the distribution of a **single** molecular species between two phases.[111]

4.1.9 Difficulties in using partition coefficients to predict the biomobility of weak acids

Weak acids such as MMA and DMA dissociate in solution producing two or three molecular species. This makes partition coefficients difficult to determine because the

exact identity of the molecular species in each phase is rarely known. For example, in the partitioning of an aliphatic carboxylic acid with a pKa of 4.5 and the aqueous phase buffered at pH 8.5, only 1/10000th of the acid will be in the neutral form in the aqueous phase, and yet almost one-half of that present in the octanol phase will be the un-ionized species.[111] Further difficulties arise because these hydrophilic compounds partition very poorly into octanol and therefore, would have very small partition coefficients ($<10^{-2}$). Thus, there are many difficulties in accurately determining the partition coefficients for weak acids. This uncertainty makes it quite difficult to correlate partition coefficients with the bioaccumulation of weak acids.

In general, an additional drawback to using partition coefficients to predict biomobility and bioaccumulation for any molecule is that a partition coefficient is derived from a system at equilibrium and, therefore, does not contain any kinetic information which is necessary if the rate of uptake is to be predicted.

4.1.10 The bioaccumulation of arsenicals by *Candida humicola*

The uptake of arsenate by *Candida humicola* cells was investigated by Cullen *et al.*[112] At arsenate concentrations lower than 0.02 mM there seems to be a linear relationship between the rate of uptake by the cells and the external arsenate concentration. If phosphate is added to the external solution at an equimolar amount to the arsenate, the rate of arsenate uptake by the cells was reduced to about twenty percent of the rate in the absence of phosphate. If the cells were incubated with electron transport inhibitors, the rate of arsenate uptake by the *C. humicola* was decreased. Thus, it was concluded that the the uptake of arsenate by the cells required an active transport mechanism. Arsenate uptake has also been monitored for several other organisms, usually

with the objective of studying its effect on phosphate uptake[113-124] and to establish its role as a metabolic precursor to more complex organoarsenicals.[5]

The uptake of arsenite, MMA, and DMA by *C. humicola* cells was also measured by Cullen *et al*,[112] and there was no detectable uptake of these arsenicals within the first 30 minutes of adding them to the *C. humicola* cells. Culturing the cells in the presence of MMA and DMA did not affect their ability to uptake arsenite, MMA and DMA. Thus, it was concluded that the uptake of arsenite, MMA, and DMA by the cells was via slow passive diffusion.

4.1.11 The bioaccumulation of DMA and MMA by unicellular organisms

There are considerable differences in the uptake of DMA and MMA by unicellular algae. When grown for 10 days in a medium containing 2 ppm DMA *Isochrisis galbana* accumulated ~76% of the available arsenic.[19] From media containing 1 ppm and 5 ppm MMA, the same cellular concentration of *I. galbana* over the same time period accumulated ~25% of the available arsenic. In a similar experiment, *Dunaliella tertiolecta* accumulated ~50% of DMA and ~19% of MMA from media containing 0.5 ppm of the appropriate arsenical.

Recent work by Hao Li[125] with the marine algae *Acetabularia cliftonii* has shown that when grown in 10 ppm DMA for 7 days the algae accumulate 28.08 ppm DMA, while the same cellular concentration of algae over the same time period, grown in 10 ppm MMA, the algae accumulate only 6.48 ppm MMA. Hao Li observed similiar results from the same types of accumulation experiments with *A. cliftonii* from a medium which contained 0.9 ppm of either DMA or MMA. In these experiments, algae accumulated 20.39 ppm of DMA and 1.56 ppm of MMA.

4.1.12 Scope of work

As discussed in Section 4.1.9 partition coefficients are a poor model to use to predict the bioaccumulation and biomobility of DMA and MMA, because of the inherent difficulties associated with the measurement of partition coefficients for weak acids. Clearly, an alternate model is desirable and this new model would preferably contain a kinetic component so that phrases such as "slow passive diffusion" which was used to describe the entry of DMA and MMA into the *C. humicola* cells[112] can be quantified. The diffusion coefficients across liposomal membranes should model the environmental biomobility and bioaccumulation of weak acids more closely than partition coefficients In this chapter, this hypothesis will be tested by measuring both the diffusion coefficients across the liposomal membrane and the o/w partition coefficients for MMA and DMA.

4.2 THEORY

The following equations are used to describe the one directional efflux of [^{3}H] labeled MMA and DMA from LUVs which were labeled with [^{14}C]. The permeant was trapped inside the LUVs, a concentration gradient was established so that the permeant diffused from the inside to the outside of the LUVs, and the amount of radiolabeled permeant remaining inside of the LUVs was measured at specific time intervals.

4.2.1 The rate constant, permeability coefficient and activation energy

The results in this chapter were obtained by means of efflux measurements where the rate of diffusion out of the LUVs in response to the concentration gradient is monitored. Efflux studies require less radioactivity and it has been established that the results obtained are essentially the same as from influx (where the rate of diffusion into the LUVs is monitored) measurements.[138] Assuming that the permeation of arsenicals across the liposomal membrane follows first order kinetics and that the influx of molecules is negligable, the following equation can be written for efflux;

$$-\partial X/\partial t = \underline{k}(X) \qquad [4.1]$$

where X is the concentrations (mols/L) of the radiolabeled compound inside the LUVs at time t and $\underline{k}$ is the first order rate constant (s^{-1}). Integration gives;

$$\ln((X_0)/(X)) = \underline{k}t \qquad [4.2]$$

where X_0 is the concentration of the radiolabeled compound inside the LUVs at t = 0

$$-\ln X_0 + \ln X = -\underline{k}t \qquad [4.3]$$

X and X_0 are concentrations and are proportional to the amount of permeant trapped in the LUVs where, the permeant and the liposome concentrations are represented by the ^{3}H and the ^{14}C labels, respectively; thus

$$X = \alpha\,(^3H/^{14}C)_t \qquad \text{and} \qquad X_0 = \alpha\,(^3H/^{14}C)_0 \qquad [4.4]$$

It is now possible to write:

$$-\ln \alpha\,(^3H/^{14}C)_0 + \ln \alpha\,(^3H/^{14}C)_t = -\underline{k}t \qquad [4.5]$$

which leads to;

$$\ln\,(^3H/^{14}C)_t = -\underline{k}t + C \qquad [4.6]$$

A plot of $\ln\,(^3H/^{14}C)_t$ versus t will yield a slope equal to $-\underline{k}$ and an intercept equal to $(^3H/^{14}C)_0$.

From the first-order rate constant $\underline{k}$; the permeability coefficient P (cm s^{-1}) can be calculated if the area and the trapped volume of the LUVs are known.[138]

$$P = \underline{k} \times \text{Volume/Area} \qquad [4.7]$$

Assuming that the average size of an EPC head group is 60 Angstroms^2 and that a single bilayer is formed, the area is calculated to be 1.81×10^3 cm^2 (μmol lipid)$^{-1}$. Finally the activation energy for the diffusion can be calculated with the aid of an Arrhenius plot according to equation [4.8]:

$$P = A \exp(-Ea/RT) \qquad [4.8]$$

where; P = permeability, A = constant, Ea = activation energy and R and T have their usual meanings.

4.3 EXPERIMENTAL

4.3.1 Scintillation Counting

The [^{3}H]- and [^{14}C]- activity was measured by using a Packard 2000 CA liquid scintillation counter. Packard software was used for a simultaneous determination of both labels. Typically, 100 µl of sample was added to a 20 ml glass scintillation vial which contained 800 µl of deionized water and 9 ml of scintillation cocktail. The samples were counted for two minutes.

4.3.2 Chemicals and Reagents

Egg phosphatidyl choline (EPC) and [^{14}C]-dipalmitoylphosphatidyl choline (DPPC) were purchased from Avanti Polar Lipids, Birmingham, AL, USA, and Du Pont Canada, respectively. The synthesis of the [^{3}H]-MMA and [^{3}H]-DMA used in this chapter is described in chapter 6.

4.3.3 Preparation of LUVs and Sampling Technique.

Dry EPC (75 mg) with [^{14}C]-DPPC as the label was hydrated with buffer [1 cm^{3}, 20 mmol dm^{-3} Hepes ($C_8H_{18}N_2O_4S$) and 150 mmol dm^{-3} NaCl adjusted to pH 7.4] containing either 17 mg of [^{3}H]-MMA or [^{3}H]-DMA. The resulting multilamellar liposomes were subjected to five freeze-thaw cycles employing liquid nitrogen to enhance solute distribution.[139] The solution was then transferred to a device, Figure 4.8, (Sciema Technical Services Ltd, Richmond, B.C., Canada) that was used to extrude multilamellar liposomes through 100 nm pore size filters (Nucleopore Inc.) under 300 psi (2000 kPa). After ten such extrusions LUVs were produced.[126] The untrapped compound was removed from the LUVs by passing the solution through a Sephadex G-50 column (1.5

cm × 15 cm) that had been pre-equilibrated with the buffer. The LUVs (1.5 ml) were collected, diluted to 4.5 ml, divided into three equal portions and placed in a constant temperature bath. This point in the experiment was designated as time zero. The sampling proceedure is summarized in Figure 4.11. At appropriate intervals of time 100 μl was withdrawn and loaded onto a dry Sephadex G-50 column packed into a 1 cm^3 disposable syringe, and the LUVs were eluted by centrifugation at 2000 rpm for 2 minutes. Deionized water (800 μl) was added to the eluant along with Aqueous Counting Scintillant (ACS) (9 ml) from Amersham and the $^3H/^{14}C$ ratio was determined by scintillation counting.

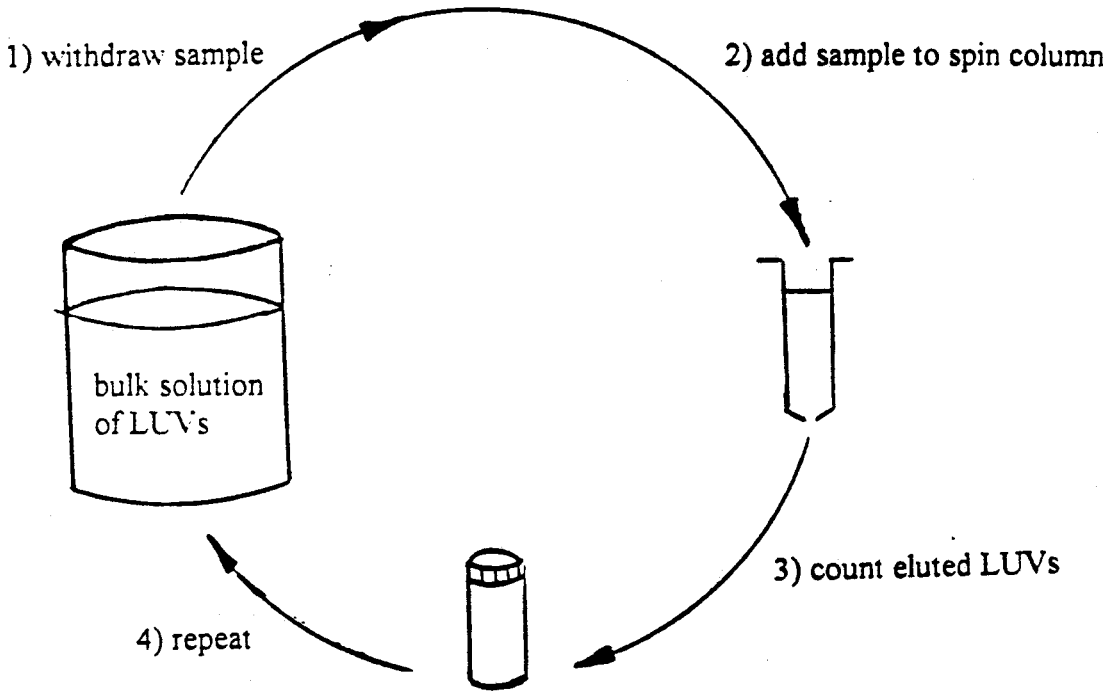

Figure 4.11 Radiolabeled sampling procedure.

4.3.4 Determination of Octanol/Water Partition Coefficients

Either [^{3}H]-MMA or [^{3}H]-DMA (4 mg) was added to buffer pH 7.4 (50 ml) and octanol (50 ml) in a volumetric flask. The flask was stoppered and submersed up to its neck in a thermostated bath set at 25 °C. Each flask was vigorously shaken every 5 minutes. After 30 minutes the two phases were separated by using a separatory funnel and 1 ml from each phase was withdrawn to be counted. The ratio of the counts was used to determine the partition coefficient.

4.4 RESULTS AND DISCUSSION

4.4.1 Rate constants and permeabilities for the diffusion of MMA and DMA across liposomal membranes (100 nm LUVs at pH 7.4)

Buffered solutions of MMA and DMA (pH 7.4) were used to hydrate dried lipid which was then extruded through 100 nm sized filters to form LUVs. A concentration gradient was established and the efflux of both molecules across the liposomal membrane was measured and plotted according to equation 4.6. The rate constants were determined from a linear regression of these plots which are shown in Figure 4.12.

The permeability coefficients were calculated from the rate constants and the phosphorus concentrations according to equation 4.7. The rate constants and permeability coefficients for MMA and DMA at three different temperatures are displayed in Table 4.2.

Table 4.2 Rate constants and permeability coefficients for MMA and DMA at pH 7.4 across the liposomal membrane (100 nm filter size).

Compound	Temperature (°C)	Rate constant (s^{-1})	Permeability (cm/s)
MMA	22	$1.4 (\pm 0.2) \times 10^{-7}$	$1.2 (\pm 0.3) \times 10^{-13}$
MMA	31	$6.3 (\pm 0.9) \times 10^{-7}$	$5.5 (\pm 1.1) \times 10^{-13}$
MMA	39	$2.1 (\pm 0.3) \times 10^{-6}$	$1.8 (\pm 0.4) \times 10^{-12}$
DMA	24	$4.3 (\pm 1.1) \times 10^{-5}$	$3.7 (\pm 1.1) \times 10^{-11}$
DMA	32	$2.3 (\pm 0.6) \times 10^{-4}$	$2.0 (\pm 0.6) \times 10^{-10}$
DMA	36	$2.8 (\pm 0.7) \times 10^{-4}$	$2.5 (\pm 0.8) \times 10^{-10}$

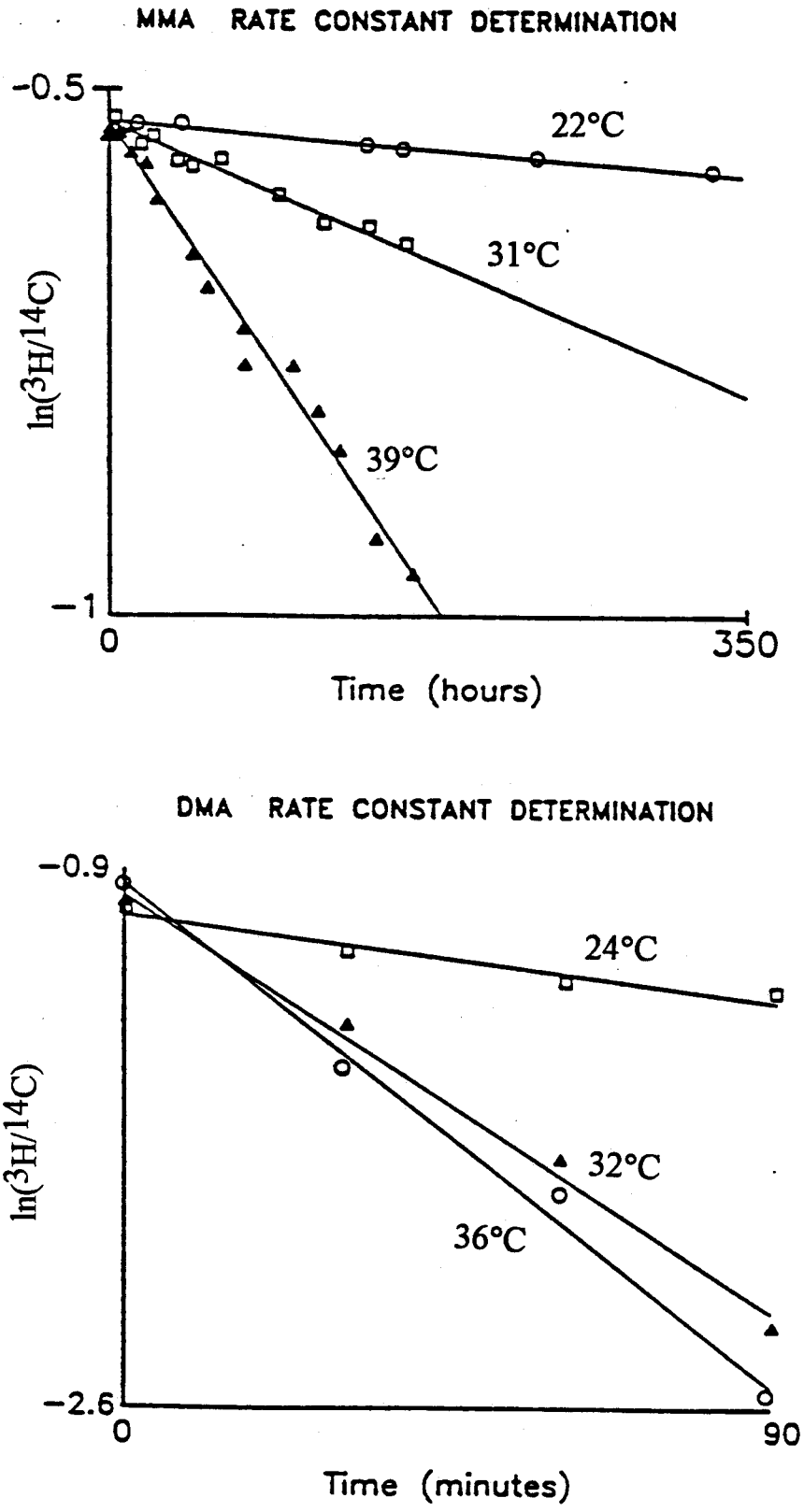

Figure 4.12 Efflux measurements of MMA and DMA. Data are plotted according to equation 4.6.

The results which are displayed in Table 4.2 show that the rate constants and the permeability coefficients for DMA are much greater than for MMA. At 25°C the interpolated values of the permeability coefficients across the liposomal membrane for DMA and MMA are 4.5×10^{-11} cm s^{-1} and 1.4×10^{-13} cm s^{-1}, respectively. The only structural difference between the permeants is the substitution of a $-CH_3$ group for an -OH group. The data support the notion that a hydroxyl group added to a molecule will decrease the permeability 100-1000 fold, while adding a methyl group will increase the permeability 5 fold.[140] Also, MMA has $pK_1 = 4.58$ and $pK_2 = 7.82$, whereas DMA has $pK = 6.19$.[5] At a pH of 7.4, which is the pH of the uptake studies described in Section 4.1.3, ~95% of the DMA is present as an anion with a single negative charge; the remaining 5% is neutral. At pH 7.4 approximately 75% of the MMA is present as an anion with a single negative charge and the remaining 25% is doubly negatively charged.

4.4.2 Activation energy for the diffusion MMA and DMA across liposomal membranes (100 nm LUVs at pH 7.4)

The natural logarithms of the permeability coefficients were plotted versus the reciprocal temperature (Figure 4.13). The activation energies for the diffusion of MMA and DMA across the liposomal membranes were determined from a linear regressions of the plots according to equation 4.8. The results are displayed in Table 4.3.

Table 4.3 The activation energy required for diffusion of MMA and DMA through the liposomal membrane at pH 7.4.

Compound	Activation Energy (KJ mol^{-1})
MMA	220 ± 35
DMA	130 ± 30

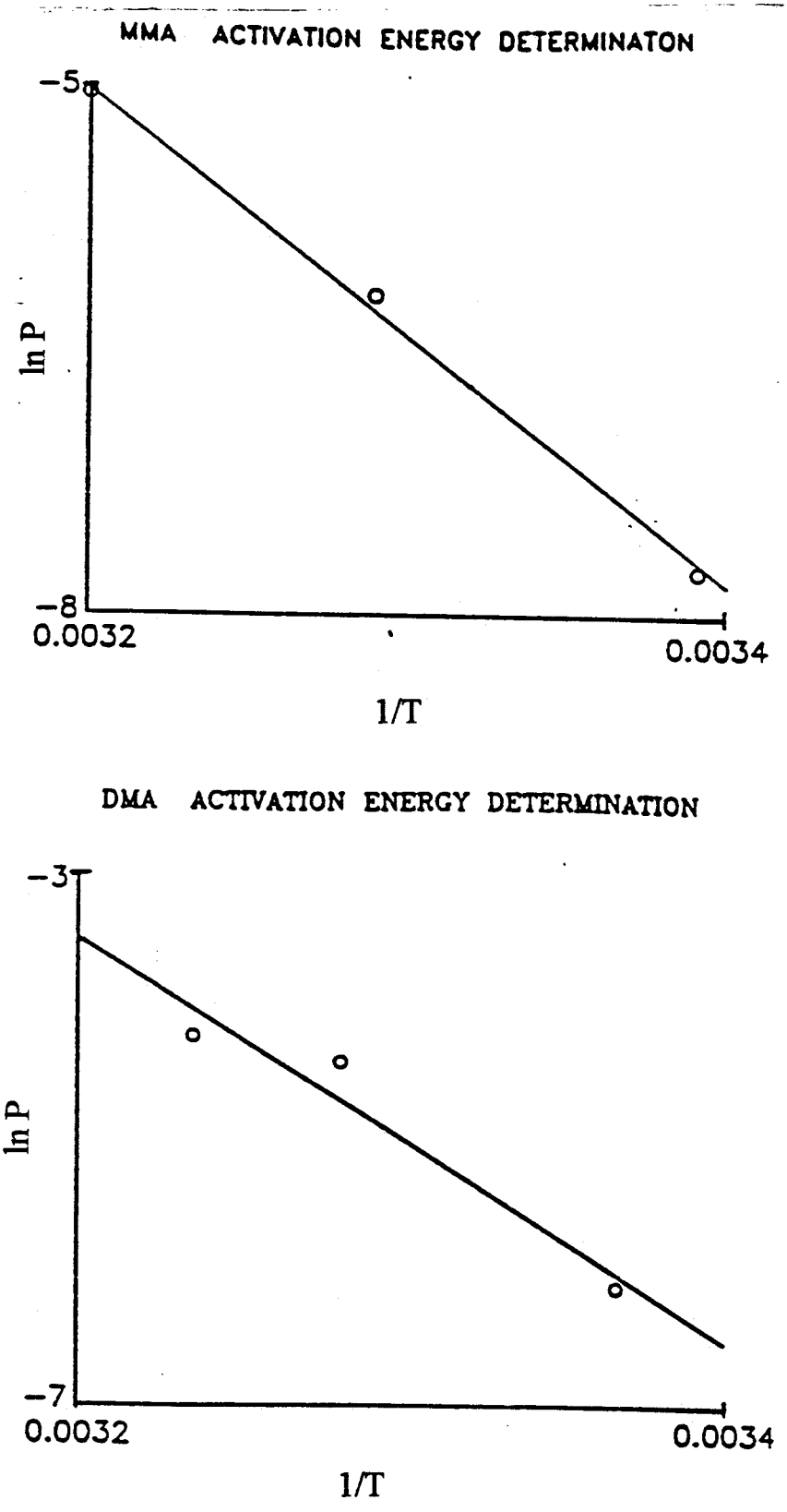

Figure 4.13 Activation energy determinations for MMA and DMA. Data are plotted according to equation 4.8.

The activation energy for the diffusion of a molecule through a membrane is the energy required for the molecule to enter into the phospholipid bilayer from the aqueous phase. The differences in the activation energy for MMA and DMA could partially be explained by the fact that MMA has a greater hydrogen bonding capability with the surrounding water molecules than does DMA. Indeed, it has been shown in previous studies with erythritol, glycerol and glycol, that the activation energy for permeation through artificial membranes corresponds directly with the number of hydrogen bonds that need to be broken in order for the permeant to undergo complete dehydration.[141]

4.4.3 Octanol/Water partition coefficients

Either [^{3}H]-MMA or [^{3}H]-DMA was added to buffer and octanol and the ratio of counts in the two phases was determined giving the octanol/water partition coefficients for both compounds. The results are displayed in Table 4.4.

Table 4.4 The octanol/water partition coefficients for MMA and DMA.

Compound	Octanol/water partition coefficients
MMA	$7.4 (\pm 1.5) \times 10^{-3}$
DMA	$8.4 (\pm 1.7) \times 10^{-3}$

The two partition coefficients are essentially the same, whereas the permeability coefficients vary by a factor of 330. To a first approximation permeability coefficients and partition coefficients are related by Overton's rule which states that one is proportional to the other.[142] However, in practice the situation is more complex as factors such as permeant size, shape, charge and hydrogen bonding capability, all affect the relationship.

Charged species do not significantly partition into organic solvents which is why the partition coefficients for both molecules are quite small. For comparison purposes glucose has permeability and octanol/water partition coefficients of 3.0×10^{-11} cm s^{-1} and 1.0×10^{-3}, respectively. The permeability[138] of water is 4.4×10^{-3} cm s^{-1} with an activation energy of 33-38 kJ mol^{-1} and an octanol/water partition coefficient[143] of 0.041.

4.4.4 Summary

The permeability coefficients through the liposomal membrane (1.4×10^{-13} cm s^{-1} and 4.5×10^{-11} cm s^{-1} for MMA and DMA, respectively) provides a better indication of the environmental mobility for DMA and MMA than do octanol/water partition coefficients (7.4×10^{-3} and 8.4×10^{-3} for MMA and DMA, respectively). Based upon partition coefficients one would expect a similiar biomobility for both DMA and MMA. This is clearly not the case, as shown by the results in Section 3.3.2, (where DMA is taken up by microscopic organisms and biotransformed much more rapidly into arsenobetaine than is MMA) if the rate determining step is assumed to be the entry of the either DMA or MMA into the microscopic organisms. The results of the permeability coefficient would lead to the prediction that a cell would be more likely to accumulate DMA than MMA, if the only mechanism of entry into the cell is via passive diffusion (Section 4.1.4). This supposition is in agreement with the results described above for *I.galbana* and *D.tertiolecta* (Section 4.1.5). In addition, the use of liposomes has enabled a quantification of the phrase "slow passive diffusion". The permeability coefficients also contain a kinetic component which gives an indication of the rate of uptake which is lacking from partition coefficients. These ideas are further investigated in the next chapter.

CHAPTER 5

THE DEVELOPMENT OF AN NMR TECHNIQUE TO MEASURE THE RATE OF DIFFUSION THROUGH LUVs AND ITS APPLICATION TO MMA AND DMA

5.1 INTRODUCTION

5.1.1 Traditional techniques used to measure the diffusion coefficients across the membranes of LUVs

The permeability coefficients for various molecules (neutral and charged) across lipid bilayers such as those found in LUVs and other types of membranes can be measured by using several different techniques.[146] These techniques require measurements of the change of concentration of the permeant on either side of the membrane as a function of time. The sampling proceedure typically involves withdrawing small aliquots from the bulk solution of LUVs (as in Chapter 4) and separating the permeant molecules on the outside of the LUVs from those on the inside of the LUVs. The separation can be achieved by using chromatography,[154] millipore filters,[155] extraction and various washing techniques. Usually the permeant is labeled with radioactivity or is fluorescent so that the concentration after separation can be measured.

LUVs and cells also shrink or swell in response to changes in the osmotic pressure across the membrane.[146] This change of volume can be measured by using light scattering techniques which allows the rate of the flow of water across the membrane to be measured.[156] Also, since the rate of flow of permeants across the membrane alters the osmotic pressure, the rate of permeation of substances other than water can be determined.

5.1.2 Spectroscopic techniques used to measure the diffusion coefficients across the membranes of LUVs

Spectroscopy may be used to measure the diffusion of molecules across membranes if the spectroscopic signals of the permeant can be differentiated on either side of the membrane. In NMR spectroscopy, this can be accomplished through the use of shift or broadening agents.[157] The area of a spectroscopic signal is directly proportional to the number of molecules which generate the signal. As the permeant molecules diffuse across the membrane, the corresponding spectroscopic signals on either side of the membrane will change in intensity and the rate constant for the diffusion process can be determined by measuring the rate at which these spectroscopic signals change. The rate constant can then be correlated to the permeability coefficient for the diffusing molecule.

For example, the permeability coefficient for Na^+ crossing the membrane of LUVs was determined by using ^{23}Na-NMR spectroscopy[158] and the shift agent $Dy(PPPi)_2^{7-}$. In addition, Prestegard et al. used NMR spectroscopy in conjunction with Pr^{+3} to measure the permeability coefficients for maleic acid[159] crossing the membranes of LUVs produced by sonication.

The osmotic permeability has also been measured by using the NMR transverse relaxation times (T_2) of the extra-vesicular water and the intra-vesicular water.[160] If Mn^{+2} was added to the outside of the LUVs the transverses relaxation times of the water on the inside and the outside would be different. Cafisio and Hubbel have used ESR spectroscopy to follow the transmembrane movement of the spin-labeled phosphonium ion.[161] Thus, the use of using magnetic resonance spectroscopic techniques to measure the diffusion coefficients across membranes is not a new one, however, work in the field is limited to a few select molecules.

5.1.3 Advantages of using spectroscopy over traditional techniques to measure the diffusion of molecules across membranes

Spectroscopic techniques, such as NMR and ESR permit the diffusion of molecules across membranes to be monitored without a physical separation thus eliminating the sampling procedure. Instead of the labour intensive procedure used in Chapter 4 (see Figure 4.11) the sample simply remains in the magnet and spectra are recorded and stored automatically. In addition, the system is closed and nothing is added to or withdrawn from the media during the diffusion of the permeant. This is unlike the procedure in Chapter 4 where samples were continuously withdrawn from the bulk media. Also, because the system is closed, the experiments can be monitored until equilibrium is reached enabling the trapped volume to be determined (see Section 5.3.7). The absence of radioactivity decreases the costs of the permeant and eliminates the scintillation vials and fluid and improves the safety of the working environment. Also, the elimination of the disposable spin columns which were composed of a syringe and some Sephadex (as used in Chapter 4) reduces the costs substantially.

5.1.4 Difficulties in using NMR spectroscopy to measure the diffusion of molecules across membranes

The most difficult part of using NMR spectroscopy to measure the diffusion of molecules across membranes is in finding a suitable shift agent. The shift agent must be able to shift the spectroscopic signal while not reacting with the permeant molecules or with any other molecules in the system. The shift agent must also be impermeable to the membrane and, in addition the spectroscopic signals from the permeant should not resonate at the same position as any of the other molecules in the system. The best permeant molecules for this technique have fairly simple NMR spectra with a singlet that

can be shifted, because it is difficult to shift doublets and triplets so that they are properly resolved. The other important limiting factor is the rate at which the permeant molecules diffuse across the membrane. If the permeant diffuses with a permeability coefficient greater than 10^{-8} cm s^{-1}, then it becomes difficult to measure the coefficients accurately without using T_2 measurements. There are also solubility limitations on the permeant. There must be enough permeant in solution so that the spectroscopic signal can be clearly detected.

5.1.5 Scope of the work

In this chapter, a NMR spectroscopic technique was developed to measure the diffusion coefficients for molecules across liposomal bilayers. The NMR spectroscopic technique employed ^{1}H-NMR with Mn^{+2} as a shift and broadening agent, LUVs produced by the extrusion technique and both MMA and DMA as the permeant molecules. The development of this technique allowed further investigation of the permeation of MMA and DMA across the liposomal membrane. The effects of changes to the pH, temperature, liposome size and membrane composition on the rate constants were studied. In addition, the theory to properly describe the diffusion across the spherical liposomal membranes was developed and equations to describe the processes were derived.

5.2 THEORY

5.2.1 What causes molecules to diffuse across membranes?

There will be a net diffusion (transport) of molecules across a membrane if there is a chemical potential difference across the membrane.

$$\text{ie} \quad \Delta\tilde{\mu} = \tilde{\mu}^{out} - \tilde{\mu}^{in} \neq 0 \qquad [5.1]$$

where $\tilde{\mu}$ is the chemical potential and is defined as;

$$\tilde{\mu} = \tilde{\mu}^{*} + RT\ln a + zF\varepsilon + Vp \qquad [5.2]$$

where a is the activity, ε is the membrane potential and p is the osmotic pressure.

If the osmotic pressure and membrane potential are equivalent on both sides of the membrane and there is a difference in chemical potential ($\Delta\tilde{\mu} \neq 0$), then this difference is caused by an unequal activity across the membrane. Activity is related to concentration by the following formula;

$$a = \gamma_{\pm} C \qquad [5.3]$$

where $\gamma_{\pm}$ is the activity coefficient and C (mol ml^{-1}) is the concentration.

The net flux across a membrane is defined as;[146]

$$JA = DA\partial C/\partial x \cong DA\Delta C/\Delta x = DA(C^{out}-C^{in})/\Delta x \qquad [5.4]$$

where J (mol cm^{-2} s^{-1}) is the flux, A (cm^2) is the surface area, D (cm^2 s^{-1}) is the diffusivity coefficient and x (cm) is the membrane thickness.

A schematic diagram of the net flux across a membrane in response to a chemical potential difference is displayed in Figure 5.1.

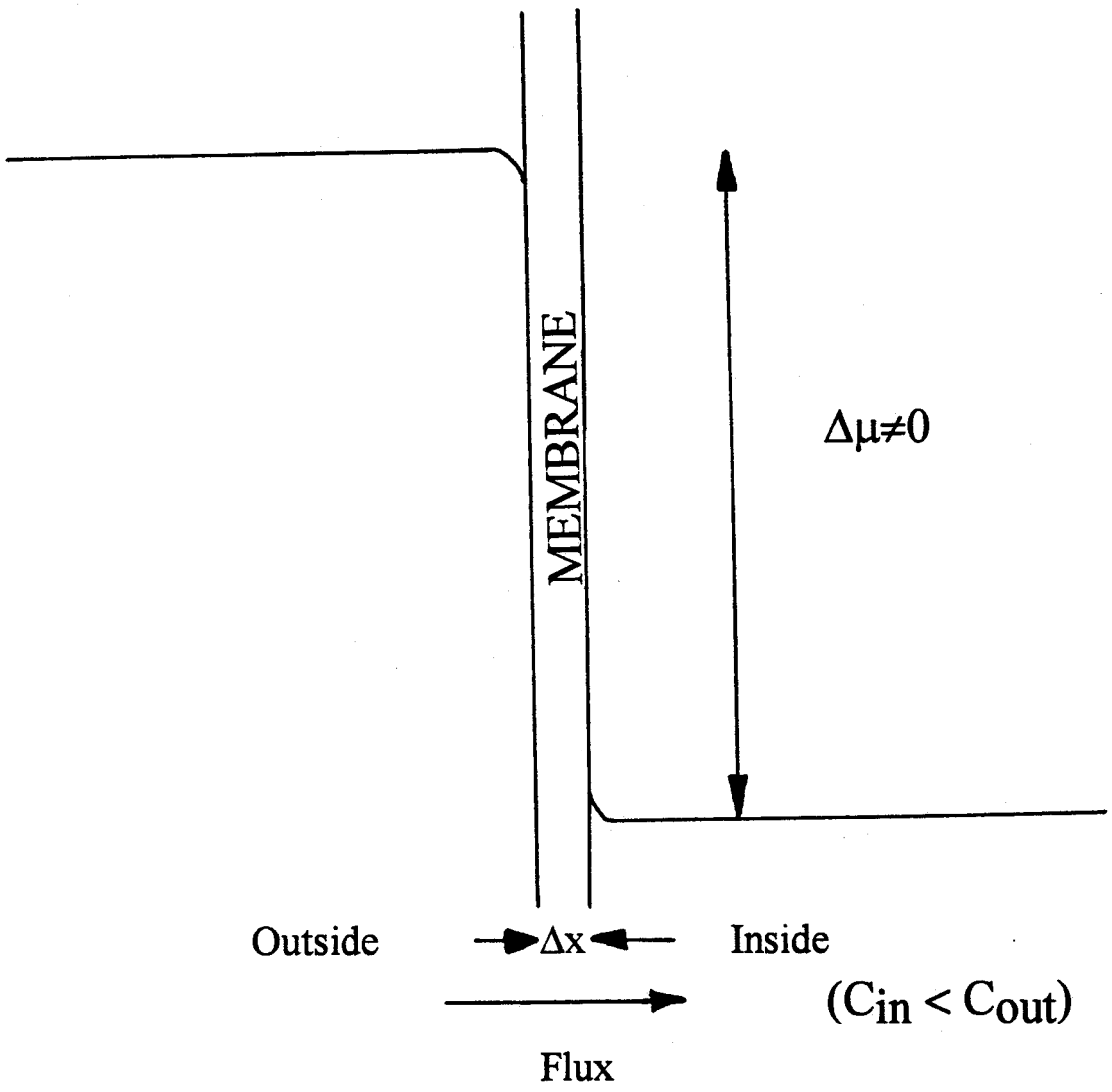

Figure 5.1 Flux across a membrane in response to a difference in chemical potential.

5.2.2 Diffusion from a spherical vesicle.

The net flux of molecules across a sphere may be described by Ficks 1st Law as:

$$JA = DA\partial C/\partial r = D4\pi r^2\partial C/\partial r = \partial n_{out}/\partial t \qquad [5.5]$$

where A (cm^2) is the area, r (cm) is the radius, D is the diffusivity coefficient ($cm^2\ s^{-1}$) and V_{in} (ml) is the trapped volume of the sphere, while C (mol ml^{-1}) is the concentration, and n is the number of moles or molecules.

The net flux may also be written as;

$$JA = \partial n_{out}/\partial t = -\partial n_{in}/\partial t = k'(n^m_{in}/V^m_{in} - n^m_{out}/V^m_{out})$$
$$= k'K(n^{aq}_{in}/V^{aq}_{in} - n^{aq}_{out}/V_{out}) = k(n^{aq}_{in}/V^{aq}_{in} - n^{aq}_{out}/V_{out}) \qquad [5.6]$$

where n^m_{in} and n^m_{out} are the number of molecules or moles of permeant on the surface of the inside and outside of the sphere, respectively, n^{aq}_{in} and n^{aq}_{out} are the number of molecules in solution on the inside and outside of the sphere, respectively, K is the partition coefficient ($K = C^m/C^{aq}$), k' ($cm^3\ s^{-1}$) is the rate constant within the membrane, k ($cm^3\ s^{-1}$) is the rate constant across the membrane and equals k'K and V is the volume (cm^3). The equation is written in terms of number of molecules or moles instead of the more traditional concentrations because NMR spectroscopy provides a direct measure of the number of particles rather than a concentration measurement. The above terms are displayed schematically in Figure 5.2.

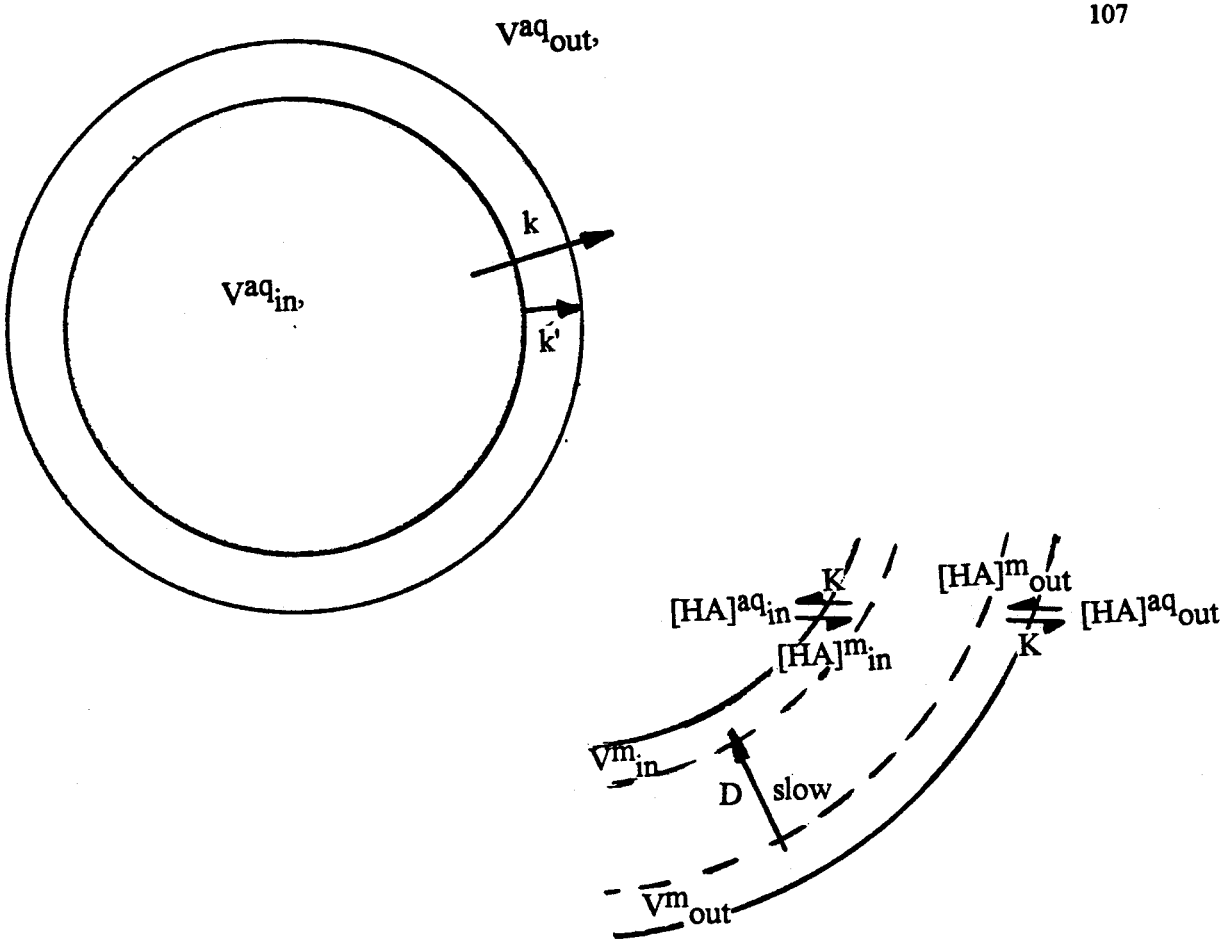

Figure 5.2 Schematic depiction of V^{aq}_{in}, V^{aq}_{out}, V^{m}_{in}, V^{m}_{out}, D, K, k', k, $[HA]^{m}_{out}$ $[HA]^{m}_{in}$ $[HA]^{aq}_{out}$ $[HA]^{aq}_{in}$.

Ficks 2nd Law states that:

$$\partial C/\partial t = (D/r^2)\partial/\partial r(r^2\partial C/\partial r) \qquad [5.7]$$

At equilibrium ($\partial C/\partial t = 0$):

$$\partial/\partial r(r^2\partial C/\partial r) = 0 \qquad [5.8]$$

$$r^2\partial C/\partial r = e \qquad [5.9]$$

where e is a constant, therefore,

$$\partial C/\partial r = e/r^2 \qquad [5.10]$$

Integrating 5.10 gives;

$$C = -e/r+b \quad [5.11]$$

$$C^m_{in} = -e/r_{in}+b \quad [5.12]$$

$$C^m_{out} = -e/r_{out}+b \quad [5.13]$$

$$C^m_{in} - C^m_{out} = -e(1/r_{in} - 1/r_{out}) = -a((r_{in} - r_{out})/r_{in}r_{out}) \quad [5.14]$$

$$e = -([C^m_{in} - C^m_{out}]r_{in}r_{out}/[r_{in} - r_{out}]) \quad [5.15]$$

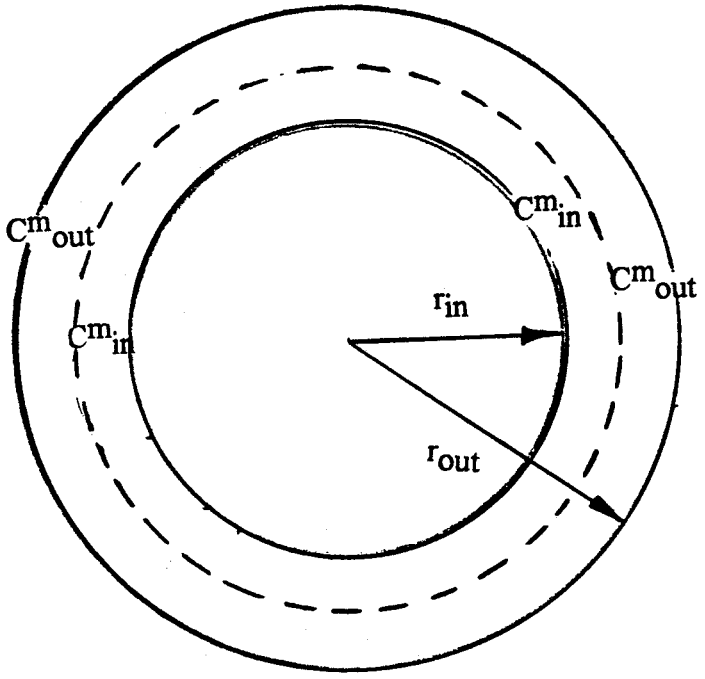

Figure 5.3 Schematic depiction of C^m_{in}, C^m_{out}, r_{in} and r_{out}.

Substituting equation [5.10] into equation [5.5] gives:

$$JA = AD\partial C/\partial r = 4\pi r^2 De/r^2 = 4\pi De \quad [5.16]$$

Substituting equation [5.15] into equation [5.16] gives:

$$JA = 4\pi D r_{in}r_{out}[C^m_{in}-C^m_{out}]/(r_{in}-r_{out}) \quad [5.17]$$

$$JA = 4\pi D r_{in} r_{out}[n^m_{in}/V_{in} - n^m_{out}/V_{out}]/(r_{in} - r_{out}) \quad [5.18]$$

From equation [5.6]

$$JA = k'[n^m_{in}/V_{in} - n^m_{out}/V_{out}]$$

Therefore, rearranging equations [5.6] and [5.18] to solve for k' gives:

$$k' = 4\pi r_{in} r_{out} D/(r_{in} - r_{out}) = AD/\Delta x \quad [5.19]$$

Thus, the rate constant is dependent upon the diffusivity coefficient within the membrane and upon the area and the thickness of the sphere. Large Unilamellar Vesicles (LUVs) are spherical.

5.2.3 The Permeability Coefficient and Activation Energy

The permeability coefficient contains three terms that are very difficult to measure in biological membranes: Δx the thickness of the membrane; D the diffusivity coefficient within the membrane and K the partition coefficient of the permeant between the membrane and the aqueous solution. The combination of these three terms given in equation 5.20, is defined as the permeability coefficient (P in units of cm s^{-1}). P is relatively easy to measure.

$$P = DK/\Delta x \quad [5.20]$$

Rearranging equations [5.19] and [5.21] and solving for P gives:

$$P = k'K/A = k/A \quad [5.21]$$

The activation energy for diffusion may be calculated by using equation [4.8] from Section 4.2.1 of the previous chapter.

5.2.4 Derivation of the Equations used to describe the number of particles on either side of the membrane

The equations used to describe the number of particles on both the inside and the ouside of the LUVs at any time during the experiment are derived after the following assumptions are made. The rate of diffusion into the LUVs (influx) will equal the rate of diffusion out of the LUVs (efflux). The LUVs are of uniform size and the volume does not change during the course of the experiment (i.e., the conditions on both sides of the membrane are isotonic). The activity coefficients have values of 1 and, therefore, the activities of the acids are equal to the concentrations. The dissociation of the acid is rapid with respect to the time of diffusion so that the acid dissociation can always be considered an equilibrium process. Assuming that the permeant does not decompose or react with any of the molecules which are present.

The net flux of molecules may be written as:

$$-\partial n_{in}/\partial t = \partial n_{out}/\partial t = k(n_{in}/V_{in}-n_{out}/V_{out}) \qquad [5.22a]$$

$$\partial C/\partial t = \underline{k}(C_{in}-C_{out}) \qquad [5.22b]$$

where n is either the number of mols or the number of particles and C is the concentration of the permeant in the aqueous solution on either the inside or the outside of the membrane, respectively. k (ml s^{-1}) and $\underline{k}$ (s^{-1}) are both rate constants to describe the diffusion of the permeant.

Let:

$$N = n^{o}_{in}+n^{o}_{out} = n^{eq}_{in}+n^{eq}_{out} = n^{t}_{in}+n^{t}_{out} \qquad [5.23]$$

where N is the total number of molecules and n^{o}, n^{eq} and n^{t} are the number of molecules initially, at equilibrium and at any time during the experiment. N is a constant because the number of molecules in the NMR tube does not change.

Also let:

$$V' = (1/V_{in}+1/V_{out}) \quad [5.24]$$

Substituting equation [5.23] into equation [5.22a] gives:

$$\partial n_{out}/\partial t = k((N-n_{out})/V_{in}-n_{out}/V_{out}) \quad [5.25]$$

$$= k(N/V_{in}-n_{out}(1/V_{in}+1/V_{out})) \quad [5.26]$$

Substituting equation [5.24] into equation [5.26] gives:

$$\partial n_{out}/\partial t = k(N/V_{in} - n_{out}V') \quad [5.27]$$

Rearranging and integrating equation [5.27] gives;

$$\partial n_{out}/(N/V_{in} - n_{out}V') = k\partial t \quad [5.28]$$

$$\ln(N/V_{in} - n_{out}V') \,|\, {}^{nt}_{no} = -V'kt \quad [5.29]$$

There will be some permeant molecules outside of the LUVs at time zero in the experiments (ie. $n^{o}_{out} \neq 0$) therefore:

$$\ln((N/V_{in}-n^{t}_{out}V')/(N/V_{in}-n^{0}_{out}V')) = -V'kt \quad [5.30]$$

$$\ln((N-n^{t}_{out}V'V_{in})/(N-n^{0}_{out}V'V_{in})) = -V'kt \quad [5.31]$$

Let:

$$f = V_{in}/V_{out} \quad [5.32]$$

where f is the ratio of the volumes inside and outside the LUVs.

Substituting equation [5.32] into equation [5.31] gives:

$$\ln(1-(n^{t}_{out}-n^{t}_{out}f)/N)-\ln(1-(n^{0}_{out}-n^{0}_{out}f)/N) = -V'kt \qquad [5.33]$$

Let the number of particles inside and outside of the LUVs at equilibrium be written as:

$$n^{eq}_{out} = N/(1+f) \qquad [5.34]$$

and $$n^{eq}_{in} = N/(1+(1/f)) \qquad [5.35]$$

Substituting equation [5.34] into equation [5.33] gives:

$$\ln(1-(n^{t}_{out}-n^{t}_{out}f)/n^{eq}_{out}(1+f))-\ln(1-(n^{0}_{out}-n^{0}_{out}f)/n^{eq}(1+f)) = -V'kt \qquad [5.36]$$

$$\ln(1-n^{t}_{out}/n^{eq}_{out})-\ln(1-n^{0}_{out}/n^{eq}_{out}) = -(1+f)kt/V_{in} \qquad [5.37]$$

$$\ln(n^{eq}_{out}-n^{t}_{out})-\ln(n^{eq}_{out}-n^{0}_{out}) = -(1+f)kt/V_{in} \qquad [5.38]$$

Equation [5.38] may be rearranged to yield equation [5.39] which gives the number of particles **outside** the LUVs at any time t:

$$n^{t}_{out} = n^{eq}_{out}+(n^{0}_{out}-n^{eq}_{out})e^{-(1+f)kt/V_{in}} \qquad [5.39a]$$

or $$n^{t}_{out} = n^{eq}_{out}+(n^{0}_{out}-n^{eq}_{out})e^{-(1+f)\underline{k}t} \qquad [5.39b]$$

where $\underline{k} = k/V_{in}$

Substituting equations [5.23] and [5.35] into equation [5.38] and rearranging gives equation [5.40] which gives the number of particles **inside** the LUVs at any time t:

$$n^{t}_{in} = n^{eq}_{in}+(n^{0}_{in}-n^{eq}_{in})e^{-(1+f)kt/V_{in}} \qquad [5.40a]$$

or $$n^{t}_{in} = n^{eq}_{in}+(n^{0}_{in}-n^{eq}_{in})e^{-(1+f)\underline{k}t} \qquad [5.40b]$$

5.2.5 Permeation of a Weak Acid

For a molecule such as DMA, which is comprised of two molecular species in solution (as shown in Figure 5.4), the overall flux of molecules from the LUVs will be a combination of the two species. This combination may be written as;

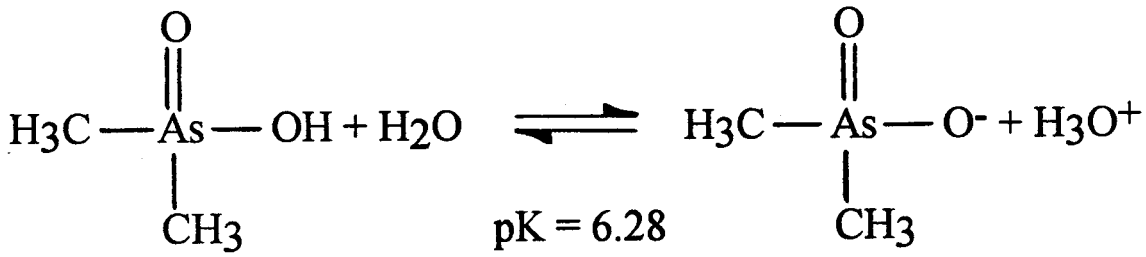

Figure 5.4 The two chemical species of DMA in aqueous solution.

$$\partial n_{in}/\partial t = \partial n_{AHin}/\partial t + \partial n_{A^-in}/\partial t \qquad [5.41a]$$

or $$\partial n_{in}/\partial t = k_{AH}(n_{AHin}/V_{in} - n_{AHout}/V_{out}) + k_{A^-}(n_{A^-in}/V_{in} - n_{A^-out}/V_{out}) \qquad [5.41b]$$

where the subscripts AH and A^- refer to the neutral and anionic forms of the weak acid.

Let:

$$n_{AH} = \alpha n \text{ and } n_{A^-} = (1-\alpha)n \qquad [5.42]$$

where n is the total number of particles and α is the degree of dissociation of the weak acid and equals $Ka/(Ka+[H^+])$ for a monoprotic weak acid and $Ka/([H^+]^2+K_1K_2+K_1[H^+])$ for a diprotic weak acid.

Substituting equation [5.42] into equation [5.41] gives:

$$-\partial n_{in}/\partial t = k_{AH}(\alpha n_{in}/V_{in}-\alpha n_{out}/V_{out}) + k_{A^-}((1-\alpha)n_{in}/V_{in}-(1-\alpha)n_{out}/V_{out}) \quad [5.43]$$

$$-\partial n_{in}/\partial t = \alpha k_{AH}(n_{in}/V_{in}-n_{out}/V_{out}) + (1-\alpha)k_{A^-}(n_{in}/V_{in}-n_{out}/V_{out}) \quad [5.44]$$

If αk_{AH} is equal to $(1-\alpha)k_{A^-}$ the rate of overall flux of molecules will be independent of pH, however, if αk_{AH} is greater than $(1-\alpha)k_{A^-}$ the rate of overall flux of molecules will be pH dependent.

The methyl resonance of DMA, a weak acid, is composed of both the neutral and the anionic molecules. The position of the combined methyl resonance for the neutral and the anionic forms of DMA varies slightly depending upon the percentage of each chemical species. The integral of the combined methyl resonance is related to the number of particles of each chemical species by constant scaling factors such that:

$$I_{total} = I_{DMAH}n_{DMAH} + I_{DMA^-}n_{DMA^-} \quad [5.45]$$

where I_{total} is the total integral and $I_{DMAH} \cong I_{DMA^-}$ are the scaling factors.

The rate of change of the total integral may be written as:

$$\partial I/\partial t = I_{DMAH}\partial n_{DMAH}/\partial t + I_{DMA^-}\partial n_{DMA^-}/\partial t \quad [5.46]$$

If the anionic form of the molecule does not significantly permeate the membrane then $k_{AH} >>> k_{A^-}$. For this sitation, $\partial n_{AHin}/\partial t >>> \partial n_{A^-in}/\partial t$, and $(1-\alpha)k_{A^-}(n_{in}/V_{in}-n_{out}/V_{out})$ (equation [5.44]) will be approximately equal to 0. Thus, $I_{DMA^-}\partial n_{DMA^-}/\partial t$ (equation [5.46]) will also be equal to 0. Therefore, the equations used to describe the

rate of change of the total integral may be written as;

$$I^t_{out} = I^{eq}_{out} + (I^0_{out} - I^{eq}_{out})e^{-(1+f)\alpha k_{AH} t/V_{in}} \quad [5.47a]$$

or $$I^t_{out} = I^{eq}_{out} + (I^0_{out} - I^{eq}_{out})e^{-(1+f)\alpha \underline{k}_{AH} t} \quad [5.47b]$$

and $$I^t_{in} = I^{eq}_{in} + (I^0_{in} - I^{eq}_{in})e^{-(1+f)\alpha k_{AH} t/V_{in}} \quad [5.48a]$$

or $$I^t_{in} = I^{eq}_{in} + (I^0_{in} - I^{eq}_{in})e^{-(1+f)\alpha \underline{k}_{AH} t} \quad [5.48b]$$

Thus, the rate constant will vary linearily with the $[H^+]$ since:

$$[DMAH] = [DMA^-][H^+]/K_A \quad [5.49]$$

Thus,

$$k = \alpha k_{AH} \quad [5.50a]$$

$$\underline{k} = \alpha \underline{k}_{AH} \quad [5.50b]$$

and $$P = \alpha P_{AH} \quad [5.50c]$$

where k, $\underline{k}$ and P are the pH dependent diffusion coefficients; while k_{AH}, $\underline{k}_{AH}$, and P_{AH} are the diffusion coefficients for the neutral species of the weak acid.

5.2.6 Comment on D, P, k', k, $\underline{k}$, k_{AH}, $\underline{k}_{AH}$, and P_{AH}

To avoid confusion later the diffusivity coefficient (D in $cm^2\ s^{-1}$) and the permeability coefficient (P in $cm\ s^{-1}$) are properties of the membrane and the permeant and are independent of liposomal size, trapped volume and surface area. They are related by the following formula;

$$P = DK/\Delta x \quad [5.52]$$

where Δx is the thickness of the membrane and K is the partition coefficient.

The rate constant for the permeant within the membrane (k' in $cm^3\ s^{-1}$) is defined in Section 5.2.2 as:

$$k' = DA/\Delta x \qquad [5.53]$$

The rate constant across the membrane (k in $cm^3\ s^{-1}$) is related to the rate constant within the membrane by the partition coefficient such that:

$$k = k'K = DAK/\Delta x = PA \qquad [5.54]$$

Since the trapped volume is incorporated into k, it will scale only with the surface area of the LUVs. If unilamellarity is assumed, and the same amount of lipid is present in each experiment, k will be independent of the size of the LUVs.

The traditional first order rate constant ($\underline{k}$ in s^{-1}) is dependent upon the size of the LUVs and is proportional to 1/r. It is defined as:

$$\underline{k} = k/V = PA/V = DAK/V\Delta x = 3DK/r\Delta x \qquad [5.55]$$

where r is the radius of the LUVs.

Weak acids or bases are present in aqueous solution as neutral and as charged molecules whose ratio will vary with pH. The pH apparent rate constant will be a combination of the rate constants for both the neutral and charged molecules. The rate constant for the neutral form of the molecules is designated as k_{AH} ($cm^3\ s^{-1}$) or $\underline{k}_{AH}$ (s^{-1}) and is independent of the pH. The permeability coefficient follows the same pattern and P_{AH} is the permeability coefficient for the neutral form of the molecule.

5.3 EXPERIMENTAL

5.3.1 Instrumentation

A Bruker AM 400 NMR spectrometer was used to acquire the spectra. The samples (0.6 ml) were placed in high precision NMR sample tubes (178 mm × 5 mm (outer diameter)) from Norell, Inc., Landisville, New Jersey USA. The water signal was suppressed by using a presaturation pulse as shown in Figure 5.5. The first pulse is at the frequency of the water signal which becomes saturated. The second pulse is over a much wider range of frequencies and is implemented while the water signal is still saturated.

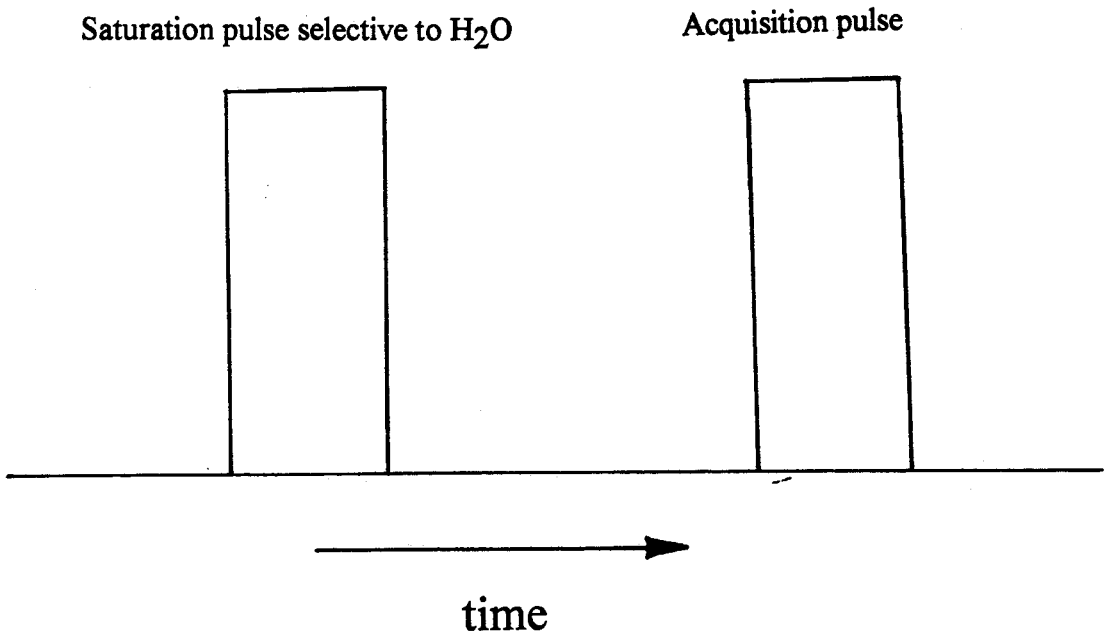

Figure 5.5 The pulse sequence used for water suppression.

The program which operates the spectrometer in the water suppression and the various delay modes is displayed in Figure 5.6. This program was designed to automatically aquire spectra at specific time intervals during the diffusion experiments.

```
JOHN FILE:JOHN
; JOHN:AU PROGRAM FOR DIFFUSION EXPERIMENTS
 II
2 ZE
 VD
1 D1 HG
 GO=1 DO
 WR #1
 IF #1
 IN=2
 EXIT
VD VDLIST.001
1-25 = APPROPRIATE DELAYS
```

Figure 5.6 The microprogram designed to operate the spectrometer.

The delays between sample acquisition were varied depending upon temperature, pH, membrane composition, and permeant molecule. To establish the best set of delays it

is necessary to have some idea about to the length of the experiment until equilibrium is reached. The delay may be calculated according to the following formula:

$$VD(1)+(D1+AQ)+(NS+DS)+\sim 30ms = delay \qquad [5.56]$$

where VD is the variable delay, D1 is the duration of the presaturation pulse (0.5 seconds), AQ is the acquisition time (1.016 seconds), NS is the number of scans (100), and DS is the number of dummy scans (2). The easiest way to determine the delay was to time the spectrometer with a stopwatch as it pulsed the required number of times.

The spectra were acquired by using a pulse width of 6 milliseconds. A line broadening term of 10 Hz was used during the Fourier Transformation. The resonance position of TSP which was added to the external solution was used to reference the spectra to 0 ppm.

5.3.2 Chemicals and Reagents

Egg phosphatidyl choline (EPC) was purchased from Avanti Polar Lipids, in Birmingham, Alabama, USA, while the sodium salts·6 H_2O of both DMA and MMA were purchased from the Fisher Scientific Company, Fair Lawn, New Jersey, U.S.A.

5.3.3 Determination of the pK_A's for DMA and MMA

The pKa's for both DMA and MMA were determined by using the following procedure. Either MMA or DMA (3.5 g) was dissolved in deionized water (100 ml). An aliquot of this solution (25 ml) was withdrawn and placed into an Erlenmeyer flask (250 ml) which was stirred. HCl (0.1 M) was slowly added to this solution and the resulting pH was monitored by using an Orion pH Meter with a Fisher electrode which had been calibrated with standard sloutions at pHs 4, 7, and 11. These titrations were performed in triplicate.

The ^{1}H-NMR resonance position of the methyl group on both DMA and MMA was also measured as the pH was varied from 2 to 11 in increments of 1 and the data was tabulated and plotted.

5.3.4 Preparation of LUVs and Sampling Technique

The following experimental conditions were employed for the diffusion experiments that used NMR spectroscopy to measure the rate of efflux of both DMA and MMA across the liposomal membrane. DMA or MMA (50 mg) was dissolved in 2 ml Hepes (300 mmolar in D_2O) and the pH of the resultant solution was adjusted by using either NaOH or HCl. This solution was added to dry egg phosphatidyl-choline (0.4 g) and vortexed to produce a milky white solution. The egg phosphatidyl-choline (1 g) was dissolved in chloroform (10 ml) and stored in a freezer. The chloroform solution (2 ml) was withdrawn and pipetted into a glass test-tube and most of the chloroform was removed by blowing a gentle stream of nitrogen gas over top of the solution. The remaining chloroform was removed by placing the test-tube in a vacuum apparatus for at least 4 hours. The milky white solution was transferred to a plastic test-tube that was sealed with a screw on cap. This test-tube was submerged in liquid nitrogen until frozen (10 s) and was then submerged in water bath (50°C) until it had thawed (4 minutes). This process (freeze-thawing) was repeated 5 times to increase the unilamellarity of the phospholipid bilayer. The freeze-thawed lipid was added to an extrusion device (Figure 4.8) which contained 2 polycarbonate filters. The filters had pore diameters ranging from 50 to 200 nm depending upon the size of LUVs which were being used in the experiment. A nitrogen tank was attached to the extrusion device and the lipid was forced through the filters with a pressure of between 200 to 500 psi. The extrusion proceedure was repeated 10 times to ensure that all of the Large Unilamellar Vesicles (LUVs) which were produced by this technique were approximately the same size. The 2 ml of LUVs were divided into 2 equal aliquots so that the experiments could be performed in duplicate. The LUVs (1

ml) were added to a Sephadex G50 column (1.5 cm × 4 cm) and were eluted by using Hepes buffer (40 mmolar in H_2O at the appropriate pH). This proceedure removes most of the DMA that was not encapsulated and establishes the desired concentration gradient for diffusion studies. Approximately 1 ml of the diluted vesicles were collected and a timer was started, as this was designated as time 0 in the experiments. The eluted LUVs (400 μl) were added to a NMR tube which already contained Mn^{2+} (40 μl of 30 mmolar in D_2O), Hepes (135 μl of 40 mmolar in D_2O), TSP (25 μl of 40 mmolar in D_2O) and either glucose (28 mg) or NaCl (4.6 mg). The water supressed ^1H-NMR spectra (25) were obtained at the appropriate time intervals by using a Bruker AM 400 spectrometer which had been programmed with the micro-program listed in Figure 5.6.

5.3.5 Concepts to consider when designing these experiments

These experiments require careful setting up because there are a number of parameters which can be varied to produce optimum results. The initial permeant concentration and buffer concentration inside of the LUVs must be set up so that the ΔpH inside of the vesicles after the permeant has diffused out is relatively small (≤0.3 units of pH). If the buffer concentration is too high with respect to the permeant concentration the spectroscopic signal from the buffer will overwhelm the signal from the permeant. A really high buffer concentration also causes the spectrometer to select a low receiver gain which decreases the sensitivity as well. One way to avoid some of these difficulties is to make the buffer concentration on the outside of the LUVs about 10% of the concentration of the inside. The buffering capacity on both sides will still be the same because of the volume difference. The buffer should also be relatively impermeable to the membrane over the time scale of the experiments.

It is important to have a large trapped volume (≈10% of the total volume) so that

the initial permeant concentration produces the maximum signal on the spectrometer and that the equilibrium position is easily measurable. To ensure a large trapped volume the maximum amount of lipid (0.2g per ml) which is easily extruded is generally used and the length of the Sephadex column is kept fairly short (1.5×5cm), to avoid a significant dilution of the LUVs.

The osmotic pressure on both the inside and outside of the LUVs should be fairly constant so that the LUVs do not burst or shrivel up. To prevent this from happening a relatively impermeable substance (compared to the permeant) needs to be added to the outside of the LUVs.

The spectroscopic shift of the permeant is dependent upon the ratio of the concentration of the shift agent to the permeant and upon the pH of the surrounding solution. Finding the appropriate shift agent requires patience as different shift agents tend to shift different types of compounds.[147] Success cannot be guaranteed.

3-(Trimethylsilyl) proprionic-2,2,3,3-d_4 acid, sodium salt (TSP) which is often used to reference the spectra sometimes reacts with the buffer or the permeant and should be eliminated or replaced in this situation with another spectral reference material. The signal to noise ratio increases with number of scans and, therefore, the number of scans shoud be maximized depending upon the time the permeant takes to reach equilibrium.

5.3.6 Bligh-Dyer Extraction

The phospholipid concentration of the post-column LUVs was determined so that the permeability coefficient could be calculated (see Section 5.3.9). Because of interference the sample must be free from arsenic when UV-visible spectrometry is used for phosphorus determinations. Therefore, the arsenic and the phospholipids must be

separated and this separation is achieved by using the Bligh-Dyer extraction proceedure. In this proceedure, the LUVs (0.5 ml) were diluted to 1 ml by adding deionized water. Methanol (2.2 ml) and chloroform (1 ml) were added to the diluted vesicles and the solution was vortexed to produce a single phase mixture. Deionized water (1 ml) and chloroform (1 ml) were added to the solution causing it to separate into two phases. The top phase contained methanol, water, and the arsenicals while the bottom phase contained chloroform and the phospholipids.

5.3.7 Phosphorus assay

An aliquot of the chloroform (15 μl) from the Bligh-Dyer extraction was pipetted into a 20 ml test-tube. Standards of 2×10^{-3} M Na_2HPO_4 (0, 50, 100 and 200 μl) were also pipetted into separate 20 ml test-tubes. Perchloric acid (0.65 ml) was added to each of the test-tubes which were then covered with a marble and placed in a metal test-tube rack which was sitting on a heating mantle which was turned to maximum heat. After about 90 minutes the samples were allowed to cool and FISKE (0.75 ml) and ammonium molybdate (7.0 ml) were added. The samples were vortexed and then placed into a steam bath for 15 minutes. The standards were placed into a UV160U Shimadzu spectrometer and a calibration curve was plotted. The unknown was placed into the spectrometer and the phosphorus concentration was determined from the calibration curve.

5.3.8 Processing the spectra

A ^{1}H-NMR spectrum of DMA both on the inside and the outside of LUVs is displayed in Figure 5.7. The presaturated water suppression technique is effective in reducing/removing the water signal while not interferring with the interesting region of the spectra. The large series of 4 peaks beween 3.3 and 2.6 ppm is from the Hepes buffer.

The broad peak centered at 1.78 ppm is the shifted and broadened (by Mn^{+2}) spectroscopic signal of the methyl-group of the DMA molecules which are on the outside of the LUVs. Likewise, the narrow peak at 1.65 ppm is the spectroscopic signal of the DMA on the inside of the LUVs. The DMA and Hepes peaks were integrated as shown in Figure 5.7. The data were tabulated and the process was repeated for each of the 25 spectra which constituted a diffusion experiment. An example of the raw data obtained from one run is displayed in Table 5.1.

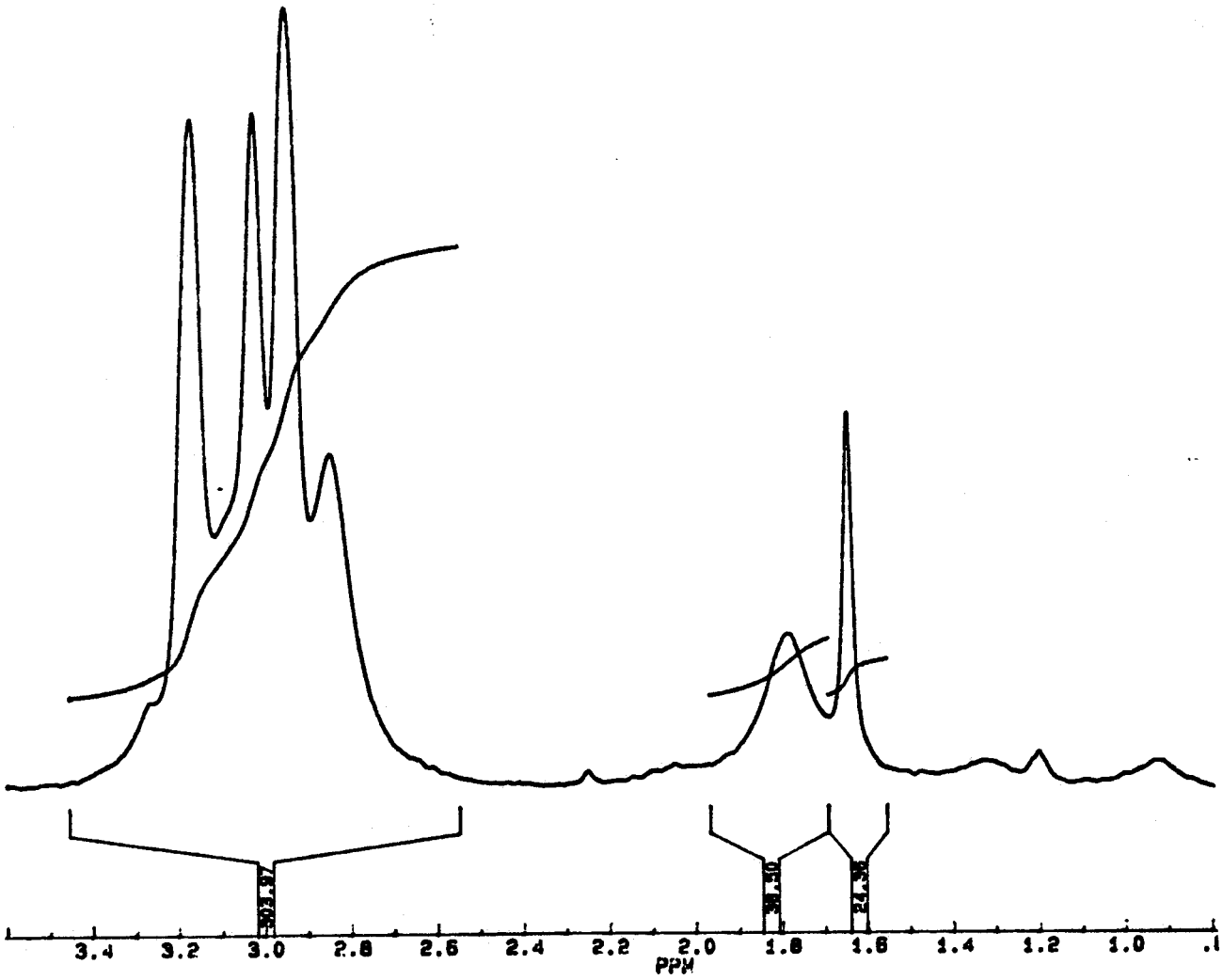

Figure 5.7 The ^{1}H-NMR spectrum of DMA and LUVs.

Table 5.1 Raw data from a diffusion experiment

Experimental time (s)	Hepes Integral	DMA_{in} Integral	DMA_{out} Integral
0	304.09	45.22	29.10
300	319.97	39.27	41.11
600	310.79	35.63	45.35
900	313.93	30.65	49.61
1200	309.56	27.70	50.77
1500	298.39	22.49	52.82
1800	304.34	22.67	54.24
2100	318.07	21.75	62.78
2400	294.20	17.89	57.15
2700	298.70	17.88	59.38
3000	302.97	17.26	61.81
3300	297.33	15.46	61.19
3900	301.98	14.65	62.83
4500	307.91	12.78	67.24
5100	303.49	12.22	65.29
5700	320.08	11.62	71.13
6900	316.10	12.28	70.66
8100	316.11	10.80	69.30
9300	293.88	7.00	66.17
10500	300.51	7.24	68.12
12300	313.33	9.24	71.55
14100	300.45	7.23	66.87
15900	305.51	6.88	70.31
19500	323.43	9.21	72.99
19800	319.66	7.81	72.40

The integrals measured from the spectra at the various time intervals of the DMA molecules on both the inside and the outside of the LUVs were divided by the Hepes integral for calibration purposes. This process helped to minimize instrumental variability and the results of this process are displayed in Table 5.2 and in Figure 5.8. Instrumental variability is caused by changes to the shimming parameters and may be observed by the changes to the Hepes integral during the experiment (Table 5.1).

Table 5.2 Integral ratios and time for a diffusion experiment

Experimental time (s)	Integral ratio DMA_{in}/Hepes	Integral ratio DMA_{out}/Hepes
0	0.1487	0.0957
300	0.1227	0.1285
600	0.1146	0.1459
900	0.0976	0.1580
1200	0.0895	0.1640
1500	0.0754	0.1770
1800	0.0745	0.1782
2100	0.0684	0.1974
2400	0.0608	0.1942
2700	0.0599	0.1986
3000	0.0570	0.2040
3300	0.0520	0.2058
3900	0.0485	0.2080
4500	0.0415	0.2184
5100	0.0403	0.2151
5700	0.0363	0.2222
6900	0.0388	0.2235
8100	0.0342	0.2192
9300	0.0238	0.2251
10500	0.0241	0.2267
12300	0.0295	0.2283
14100	0.0241	0.2226
15900	0.0225	0.2301
19500	0.0285	0.2257
19800	0.0244	0.2265

The internal to external volume ratio was determined from the spectra that were obtained when the system had reached equilibrium (ie. the spectroscopic signals were neither increasing nor decreasing). The equilibrium position will be different for experiments where glucose was used to balance the osmotic pressure than for the experiments where NaCl was used to balance the osmotic pressure because of the salt-effect (see page 128).

For the data in Table 5.2 the integral ratio for the outside and the inside DMA molecules at equilibrium were determined to be 0.225 and 0.026, respectively. The equilibrium concentrations of DMA is assumed to be equal on both sides of the membrane if glucose was used to balance the osmotic pressure, therefore, the value for f is written as:

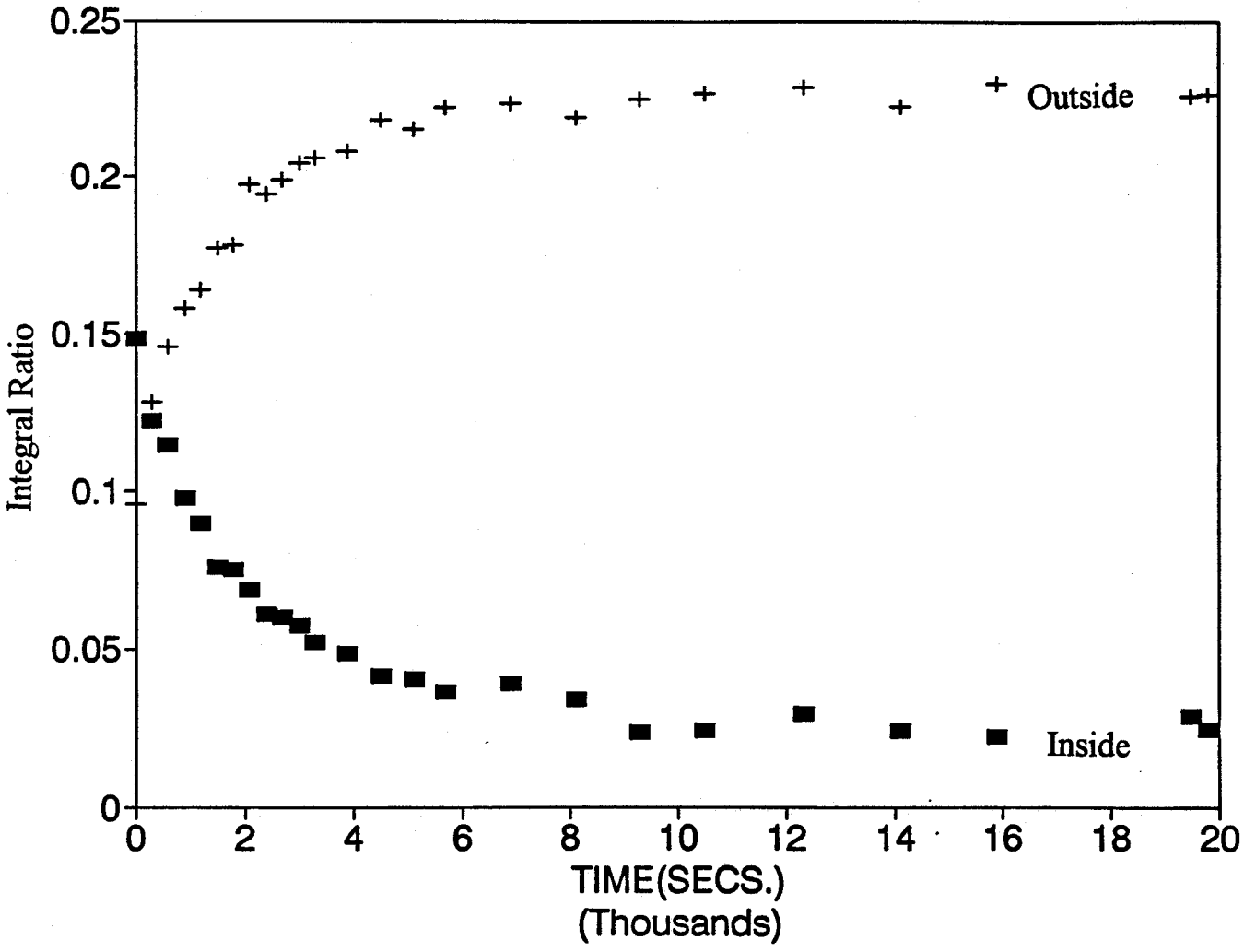

Figure 5.8 An example of a plot of the inside (■) and outside (+) integral ratios versus time for the diffusion of DMA through a liposomal membrane.

$$f = I^{eq}_{in}/I^{eq}_{out} = V_{in}/V_{out} \qquad [5.56a]$$

For the data in Table 5.2; f = 0.026/0.225 = 0.116.

Since the total volume (V_{total}) in the NMR tube is known:

$$V_{in} + V_{out} = V_{total} = 0.6 \text{ ml} \qquad [5.56b]$$

Equations [5.56a] and [5.56b] may be combined which allows V_{in} and V_{out} to be calculated.

Thus, V_{in} = 0.062 ml and V_{out} = 0.538 ml

When NaCl is used to minimize the osmotic pressure, it is necessary to correct the equilibrium concentrations of DMA to account for the "salt-effect," which is observed whenever a large amount of inert electrolyte is added to a weak acid. The degree of dissociation of the weak acid varies under these conditions. The "salt-effect" is increased in magnitude as the concentration of the electrolyte is increased. The true value of f, for the concentration of NaCl used in some of the diffusion experiments is calculated as follows:

$$f = f_{apparent}/(\gamma_{\pm})^2 = 1.78 f_{apparent} \qquad [5.57]$$

where $f_{apparent}$ is the integral ratio of the DMA_{in}/DMA_{out} at equilibrium in the presence of NaCl and ($\gamma_{\pm}$) is the activity coefficient of the media in the presence of the NaCl.

Equation [5.57] is derived as follows:

The NaCl establishes a Gibbs-Donnan potential where;

$$\text{inside} \quad \Delta G_{in} = \Delta G^{o}_{in} + RT\ln(Q)_{in} \qquad [5.58]$$

outside $\Delta G_{out} = \Delta G^{o}_{out} + RT\ln(Q)_{out}$ [5.59]

where G (Joules or Calories) is the Gibbs free energy.

At equilibrium, the chemical potential difference will be 0, therefore:

$$\Delta G_{in} = \Delta G_{out} = 0 \quad [5.60]$$

also, $$\Delta G^{o}_{in} = \Delta G^{o}_{out} \quad [5.61]$$

therefore, $$Q_{in} = Q_{out} \quad [5.62]$$

and $$[DMA^-]_{in}[H^+]_{in}(\gamma_\pm)^2_{in}/[DMAH]_{in}(\gamma_\pm) = [DMA^-]_{out}[H^+]_{out}(\gamma_\pm)^2_{out}/[DMAH]_{out}(\gamma_\pm) \quad [5.63]$$

however, $(\gamma_\pm)_{in} \cong 1$ in the absence of any salt, $\gamma_\pm$ for the [DMAH] both inside and outside is also $\cong 1$, and $(\gamma_\pm)_{out} \neq 1$ because of the NaCl on the outside of the LUVs. Therefore, in the presence of a salt:

$$f = V_{in}/V_{out} = I^{eq}_{in}/(\gamma_\pm)^2 I^{eq}_{out} = C^{eq}_{in}/(\gamma_\pm)^2 C^{eq}_{out} \quad [5.64]$$

Equation [5.57] is derived for these experiments by substituting $(\gamma_\pm) = 0.75$ (the activity coefficient for the concentration of NaCl used) into equation [5.60].

The data in Table 5.2 is now plotted according to the linear equations:

$$\ln(I^{eq}_{out} - I^{t}_{out}) = -(1+f)kt/V_{in} + \ln(I^{eq}_{out} - I^{o}_{out}) \quad [5.67a]$$

and $$\ln(I^{t}_{in} - I^{eq}_{in}) = -(1+f)kt/V_{in} + \ln(I^{o}_{in} - I^{eq}_{out}) \quad [5.67b]$$

or $$\ln(I^{eq}_{out} - I^{t}_{out}) = -(1+f)\underline{k}t + \ln(I^{eq}_{out} - I^{o}_{out}) \quad [5.68a]$$

and $$\ln(I^{t}_{in} - I^{eq}_{in}) = -(1+f)\underline{k} + \ln(I^{o}_{in} - I^{eq}_{out}) \quad [5.68b]$$

and these plots are displayed in Figure 5.9:

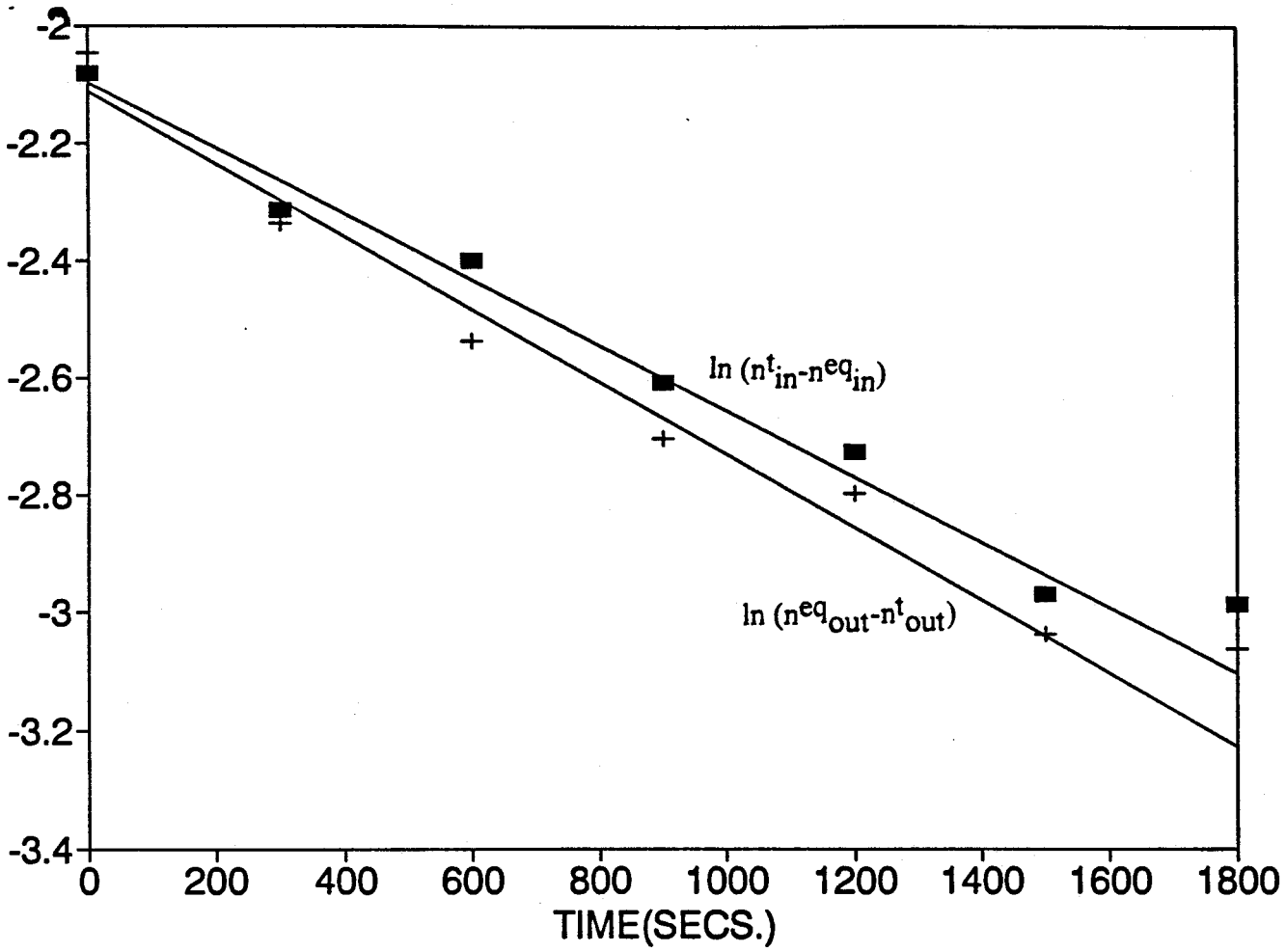

Figure 5.9 An example of a plot of ln (n^t_{in}-n^{eq}_{in}) (■) and ln (n^{eq}_{out}-n^t_{out}) (+) versus time for the diffusion of DMA through a liposomal membrane.

The pH dependent rate constants (k's) for the diffusion of the molecules, as monitored by changes to the inside and the outside peak were determined from the slopes ($-(1+f)k/V_{in}$) or ($-(1+f)\underline{k}$) of the lines.

The slope of the line for the inside peaks was -0.00056 ± 0.00003

therefore, $k = 0.000032 (\pm 0.000004)$ cm^3 s^{-1} and $\underline{k} = 0.00051 (\pm 0.00003)$ s^{-1}

The slope of the line for the outside peak was -0.00062 ± 0.00005

therefore, $k = 0.000035 (\pm 0.000005)$ cm^3 s^{-1} and $\underline{k} = 0.00056 (\pm 0.00005)$ s^{-1}

The rate constants for the inside and the outside sets of data which tended to agree within about 10% were averaged. Thus, $k = 0.000034 (\pm 0.000009)$ cm^3 s^{-1} and $\underline{k} = 0.00059 (\pm 0.00010)$ s^{-1} for the data from the experiment in Tables 5.1 and 5.2.

The time (t) in the equations [5.47] and [5.48] will contains an τ term which is the time from the collection of the LUVs from the column to the time when the first FID was aquired. This term varied from 120 to 600 seconds and was timed by using a stopwatch. This time was added to each of the experimental times, therefore:

$$t = t_{exp} + \tau \qquad [5.69]$$

where t is the total time of diffusion from when the LUVs exited the column and t_{exp} is the time from when the first spectra was recorded. Thus equations [5.67a and b] may be rewritten as:

$$\ln(I^{eq}_{out} - I^{t}_{out}) = -(1+f)kt_{exp}/V_{in} + -(1+f)k\tau/V_{in} + \ln(I^{eq}_{out} - I^{o}_{out}) \qquad [5.70a]$$

and

$$\ln(I^{t}_{in} - I^{eq}_{in}) = -(1+f)kt_{exp}/V_{in} + -(1+f)k\tau/V_{in} + \ln(I^{o}_{in} - I^{eq}_{out}) \qquad [5.70b]$$

The intercepts from the plots in Figure 5.9 should be equal and are written as:

$$\text{Intercept} = -(1+f)k\tau/V_{in} + \ln(I^{eq}_{out} - I^{o}_{out}) \quad [5.71a]$$

$$= -(1+f)k\tau/V_{in} + \ln(I^{o}_{in} - I^{eq}_{out}) \quad [5.71b]$$

The values for the intercepts in Figure 5.9 were -2.09 ± 0.04 and -2.11 ± 0.06 for the inside and the outside DMA integral ratios, respectively. τ was measured to be 450 seconds for the experiment in Figures 5.8 and 5.9. I^{o}_{in} and I^{o}_{out} were then calculated to be 0.189 ± 0.004 and 0.064 ± 0.002, respectively.

The values for the terms were substituted into equations 5.47 and 5.48 and the calculated values for the inside and outside DMA ratios were determined. The results are displayed in Table 5.3 and are plotted in addition to the experimental data (Table 5.2) in Figure 5.10.

Table 5.3 Calculated integral ratios for the diffusion experiment in Table 5.2.

Total time (s)	Calculated Integral ratio DMA_{in}/Hepes	Calculated Integral ratio DMA_{out}/Hepes
450	0.1510	0.1015
750	0.1307	0.1216
1050	0.1137	0.1383
1350	0.0995	0.1524
1650	0.0876	0.1642
1950	0.0776	0.1740
2250	0.0692	0.1823
2550	0.0622	0.1892
2850	0.0563	0.1950
3150	0.0514	0.1999
3450	0.0473	0.2040
3750	0.0438	0.2074
4350	0.0385	0.2126
4950	0.0348	0.2163
5550	0.0322	0.2189
6150	0.0303	0.2207
7350	0.0281	0.2229
8550	0.0271	0.2240
9750	0.0265	0.2245
10950	0.0263	0.2248
12750	0.0261	0.2249
14550	0.0260	0.2250
16350	0.0260	0.2250
19950	0.0260	0.2250
20250	0.0260	0.2250

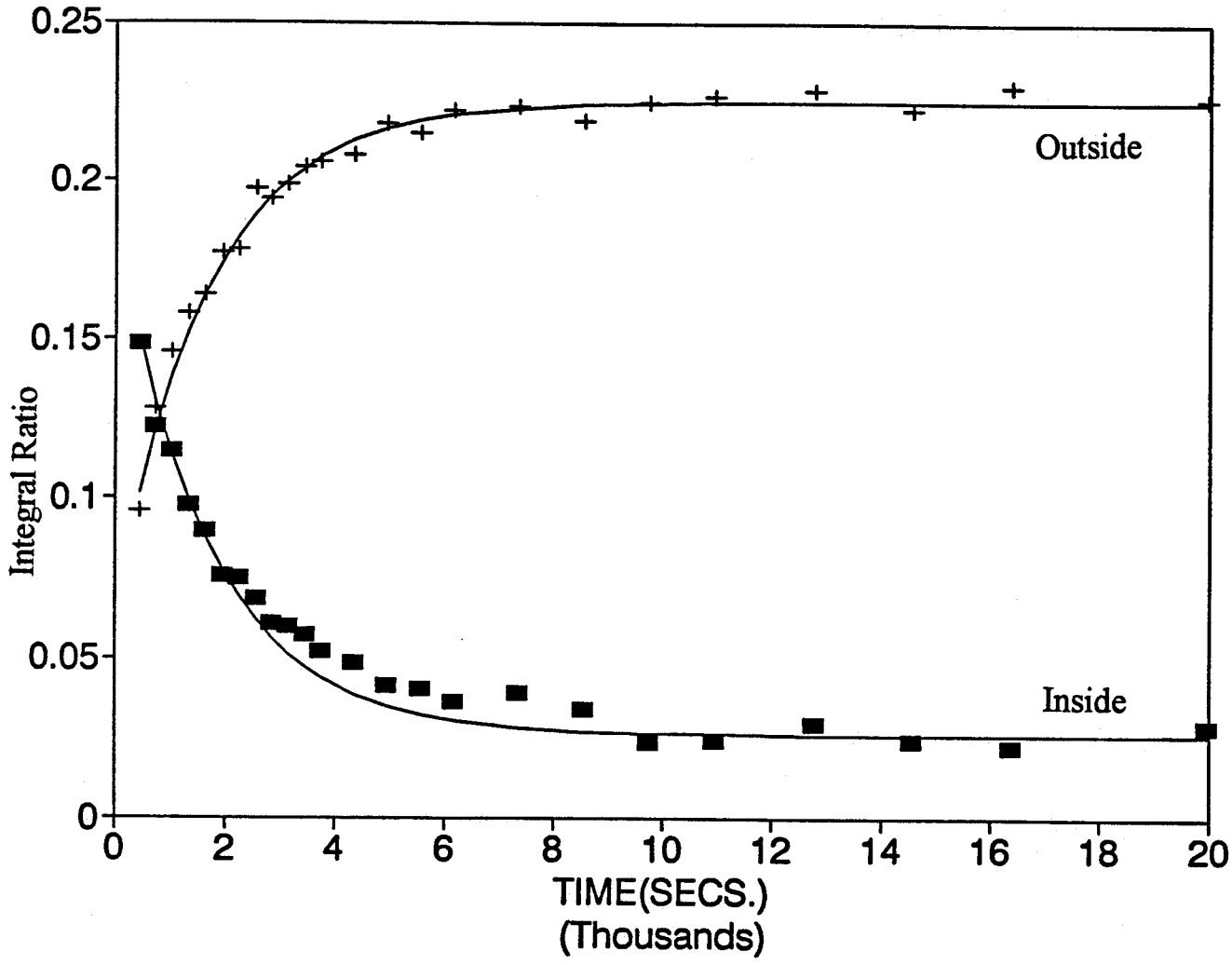

Figure 5.10 An example of the inside (■) and outside (+) integral ratios versus time for the diffusion of DMA through liposomal membranes. The solid lines are the experimental fits for the data which were generated by using equations [5.47] and [5.48].

5.3.9 Permeability Coefficient Determination

The permeability coefficients were determined from the rate constants and the phosphorus assay results. The trapped volume (V_{in}) per mol of phospholipid ($cm^3\mu mol^{-1}$) was determined. The area of an EPC head group is estimated to be 60 $Angstroms^2$, therefore, the area per μmol of phospholipid equals:

$= (6.023\times10^{23}molecules/mol \times 10^{-6}\mu mol/mol \times 60A^2/lipid\ molecule\times$

$10^{-16}cm^2/A^2)/2$

$=1.81\times10^3\ cm^2/\mu mol\ phospholipid$ [5.72]

The permeability is determined according to the following:

$P = k(cm^3s^{-1})V(cm^3\mu mol^{-1})/V_{in}(cm^3)A(cm^2/\mu mol)$ [5.73a]

$= \underline{k}(s^{-1})V(cm^3\mu mol^{-1})/A(cm^2/\mu mol)$ [5.73b]

By using the phosphorus assaying technique, the total amount of lipid in the above experiment was determined to be 0.0088 ± 0.0010 mmols. Since the internal volume was 0.062 cm^3, the ratio of internal volume to lipid was $7.1 \pm 0.9\ cm^3\ mmol^{-1}$. Therefore, the permeability for the above experiment may be written as:

$P = (0.00059\pm0.00010\ s^{-1} \times 7.1 \pm 0.9cm^3s^{-1}) / (1.81 \times 10^3cm^2/\mu mol \times 10^3\ \mu mol/mmol)$

$= 2.3\ (\pm\ 0.7) \times 10^{-9}\ cm\ s^{-1}$

5.4 RESULTS AND DISCUSSION

5.4.1 pK determinations for MMA and DMA

Either MMA or DMA was dissolved in deionized water and HCl was added to the solution in small aliquots and the resulting changes in pH were monitored. The results were plotted and the pK's were determined from the inflection points. The average results for the pK's from three potentiometric titrations are displayed in Table 5.3.

Table 5.3 pK's for MMA and DMA

	pK_1	pK_2
MMA	4.11 (3.6)[a]	8.77 (8.2)[a]
DMA	6.28 (6.2)[a]	-

a) Literature values[148] are given in brackets.

The experimental value for DMA agrees with the literature values, however, the experimental values for MMA seem to vary by 0.5 units of pK. (The MMA was submitted for micro-analysis and these results confirmed its purity.) The pH electrode was standardized with fresh buffer at pH's 4 and 7, therefore, the experimentally obtained values were used in the calculations.

In addition to the potentiometric titrations, the effects of pH upon the spectroscopic shift of the protons in the methyl group attached to the arsenic was investigated (see top of page 120). Solutions of both MMA and DMA were made up at different pH's at the ionic strength of the diffusion experiments and the resonance

Table 5.5 The ^{1}H-NMR methyl resonance positions for MMA and DMA with variations in pH.

pH	MMA resonance position (ppm)	pH	DMA resonance position (ppm)
1.88	2.1577	2.45	2.0396
3.49	2.0519	3.10	1.9721
4.19	1.9215	4.08	1.9647
5.16	1.8132	5.28	1.9561
5.39	1.8083	6.06	1.8572
5.65	1.8034	7.22	1.6334
7.43	1.7911	7.50	1.6216
8.16	1.7665	8.50	1.6053
8.56	1.7296	9.90	1.6000
9.02	1.6484	10.60	1.5977
9.83	1.5352	11.74	1.5977
10.22	1.5057		
11.04	1.4885		

The variation in the methyl resonance position with pH allows the ΔpH inside of the LUVs to be monitored during an experiment. The buffering capacity on both the inside and the ouside of the LUVs was designed so that the ΔpH on both sides was ≤ 0.3 pH units. The data in Table 5.6 and Figure 5.13 for the inside methyl resonance position during the diffusion experiments of DMA out of the LUVs at a pH 7.4 and a temperature of 24°C shows that the pH on the inside of the LUVs is fairly constant and the ΔpH is ≤ 0.3 pH units. The outside methyl resonance was more difficult to monitor because of the broadening effects of the Mn^{+2}.

Table 5.6 The ^{1}H-NMR methyl resonance positions for DMA during a diffusion experiment.

Experimental Time (s)	Methyl resonance position ppm	Experimental Time (s)	Methyl resonance position ppm
0	1.6287	4800	1.6189
300	1.6262	5400	1.6213
600	1.6189	6600	1.6164
900	1.6213	7800	1.6139
1200	1.6139	9000	1.6164
1500	1.6164	10200	1.6164
1800	1.6213	11400	1.6164
2100	1.6189	13200	1.6140
2400	1.6189	15000	1.6164
2700	1.6213	16800	1.6164
3000	1.6213	20400	1.6164
3600	1.6164	24000	1.6238

positions of the methyl group(s) at were plotted versus the pH. The tabulated data are displayed in Table 5.5 and the plots are displayed in Figures 5.11 and 5.12.

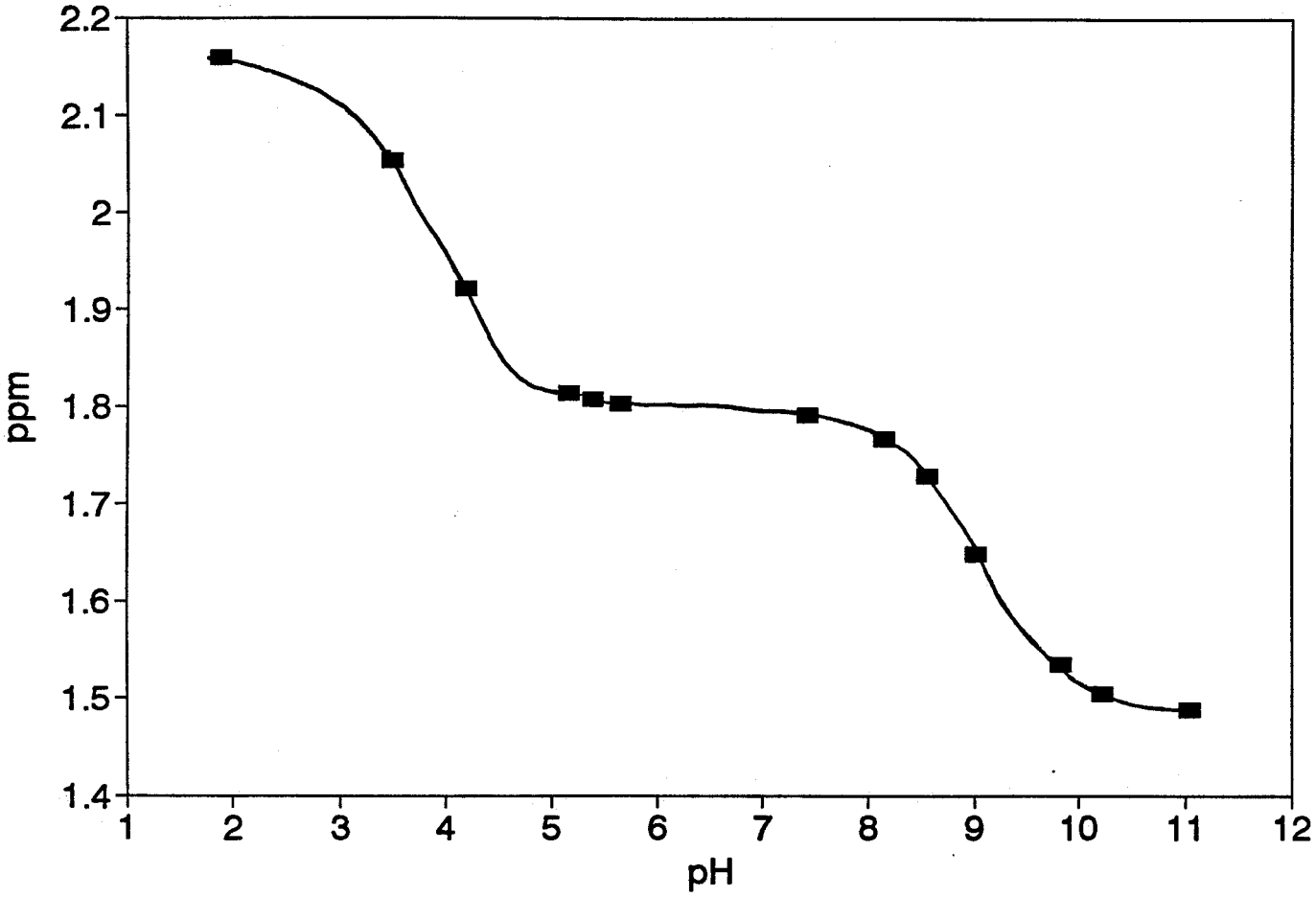

Figure 5.11 A plot of the ^{1}H-NMR methyl resonance positions for MMA versus pH.

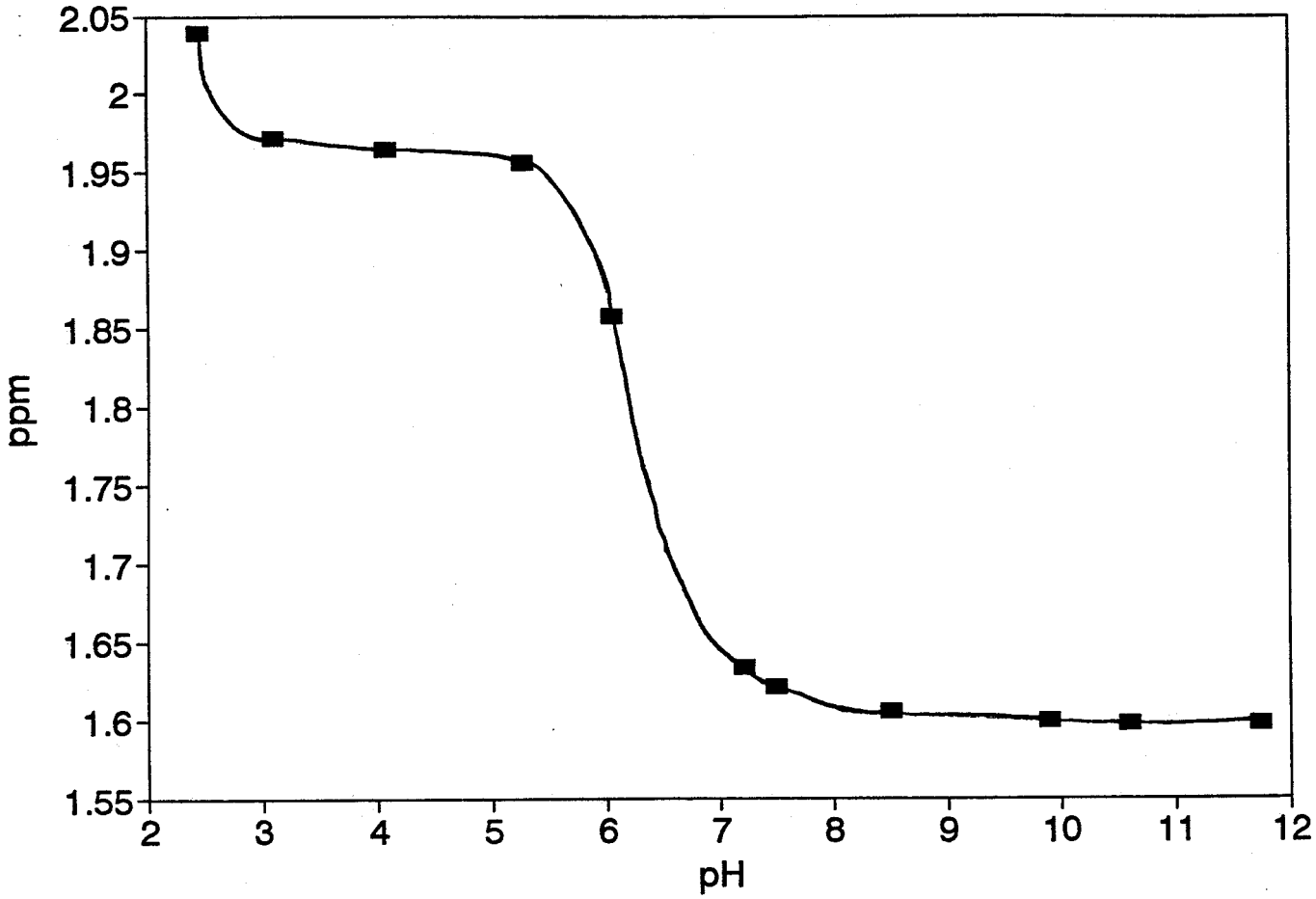

Figure 5.12 A plot of the ^{1}H-NMR methyl resonance positions for DMA versus pH.

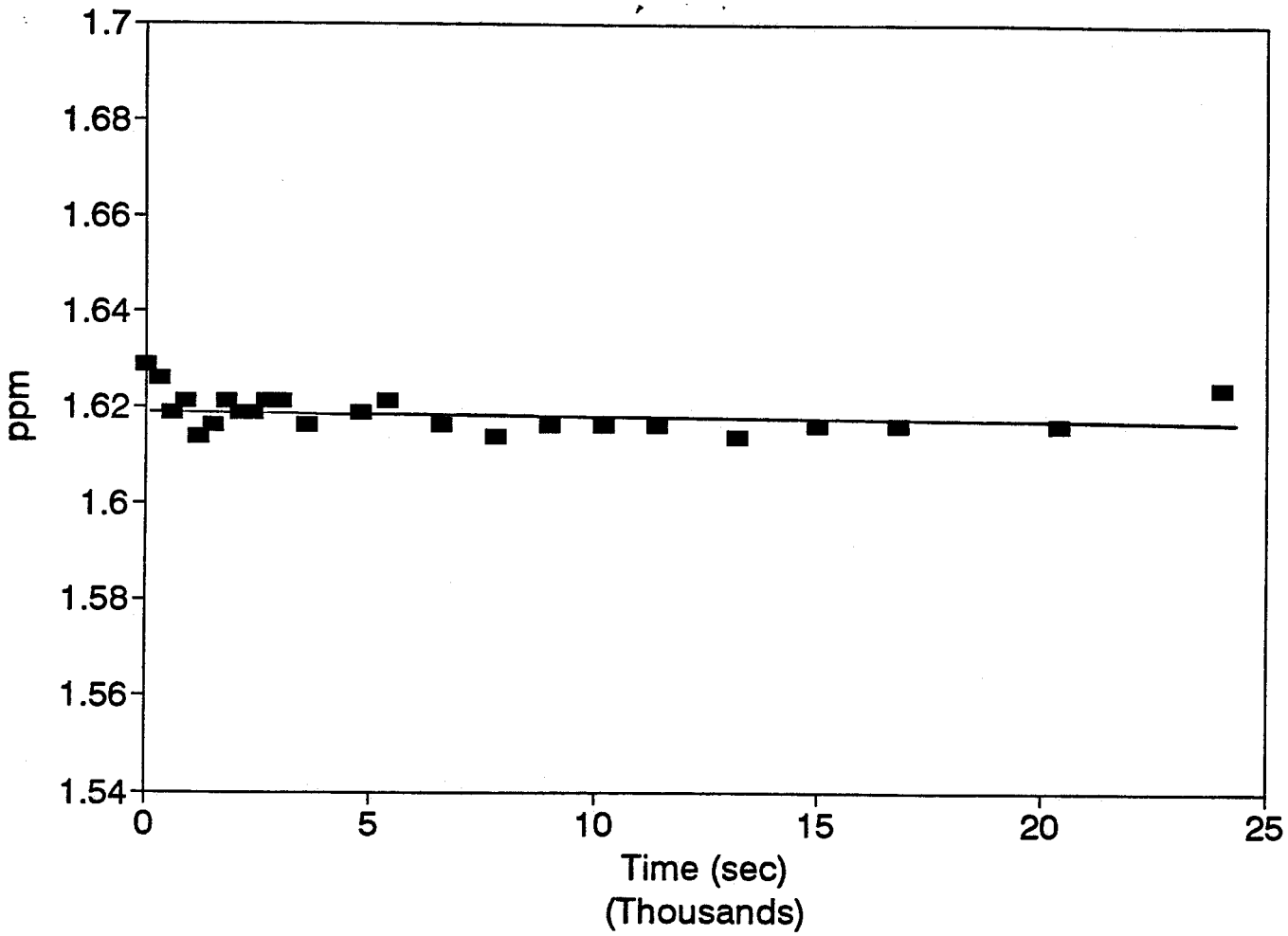

Figure 5.13 A plot of the ^{1}H-NMR methyl resonance positions for DMA versus time for a diffusion experiment.

5.4.2 The diffusion of DMA through LUVs of various sizes

DMA was encapsulated by EPC and the mixture was freeze-thawed, extruded through filters and passed down a Sephadex column as described in Section 5.3.4. The pore sizes of the filters (50, 100, 200, and 400nm) were varied to produce the desired size of LUVs. Glucose was used to balance the osmotic pressure and each of the experiments was performed at a pH of 7.4 and a temperature of 24°C. The values listed in Table 5.7 for $\underline{k}$, k, and P are the pH dependent rate constants and permeability coefficients.

Table 5.7 DMA diffusion through various sized LUVs (Temp = 24°C and pH = 7.4).

filter pore size (nm)	average size of LUVs (nm)[149]	$\underline{k}$ (s^{-1}) × 10^{-4}	k (cm^3s^{-1}) × 10^{-5}	P ($cm\ s^{-1}$) × 10^{-9}
50	68 ± 19	3.8 ± 0.6	2.7 ± 0.7	1.6 ± 0.5
100	103 ± 20	3.4 ± 0.5	2.9 ± 0.7	1.6 ± 0.5
200	151 ± 36	2.9 ± 0.4	2.7 ± 0.7	1.5 ± 0.5
400	243 ± 91	1.4 ± 0.2	1.3 ± 0.3	0.6 ± 0.2

The values for the rate constant $\underline{k}$ decrease as the size of the LUVs increase. This is expected as its magnitude should vary with 1/r, where r is the radius of the vesicle (see Section 5.2.6). Incorporating the internal volume into the rate constant to obtain the values for k produces rate constants which are more independent of vesicle size. Indeed, this is certainly the case for LUVs produced by extrusion through filters of 50, 100, and 200 nm pore sizes. These values are expected to vary with the area of the vesicles (see

Section 5.2.6), however, the total surface area of the vesicles in the first three experiments will be approximately the same. This is because the same amount of lipid was used in each case and the phospholipids arrange themselves into a single bilayer. When filters of 400nm pore size are used the phospholipids assemble in multiple bilayers. It has been shown that only 30% of the phospholipid is on the outside, while 70% remains on the inside of the vesicles[149]. This leads to decreased total surface area which is why k is smallest for the LUVs produced by extrusion through the largest pore size filters. The permeability coefficients are theoretically independent of vesicle size (see Section 5.2.6); however, as it is defined as $DK/\Delta x$, the permeability coefficient should decrease as the thickness of the bilayer Δx increases. The LUVs produced which have a single bilayer all have similiar permeability coefficients, while the LUVs produced which contain some multiple bilayers have a decreased permeability relative to the others.

5.4.3 DMA pH study

DMA was encapsulated by EPC and the mixture was freeze-thawed, extruded through 200 nm filters, and passed down a Sephadex column as described in Section 5.3.4. Both Glucose and NaCl were used to balance the osmotic pressure and the experiments were performed at 5 different pHs at a temperature of 24°C. The values listed in Tables 5.8 and 5.9 for $\underline{k}$, k, and P are the pH dependent rate constants and permeability coefficients, respectively, and are the average values obtained after performing the experiments in duplicate. The data for the rate constants was plotted vs the $[H^+]$ (Figures 5.14 and 5.15).

Table 5.8 DMA pH Study (Temp = 24°C with NaCl outside)

pH	$\underline{k}$ (s^{-1}) $\times 10^{-4}$	k ($cm^3 s^{-1}$) $\times 10^{-5}$	P ($cm\ s^{-1}$) $\times 10^{-9}$
7.00	11.4 ± 1.7	14.5 ± 3.6	11.0 ± 3.3
7.15	8.5 ± 1.3	8.9 ± 2.2	3.9 ± 1.2
7.40	6.0 ± 0.9	5.7 ± 1.4	3.0 ± 0.9
7.73	2.3 ± 0.3	2.4 ± 0.6	1.5 ± 0.5
7.97	1.9 ± 0.3	1.6 ± 0.4	1.4 ± 0.4

Table 5.9 DMA pH Study (Temp = 24°C with glucose outside)

pH	$\underline{k}$ (s^{-1}) $\times 10^{-4}$	k ($cm^3 s^{-1}$) $\times 10^{-5}$	P ($cm\ s^{-1}$) $\times 10^{-9}$
7.00	18.5 ± 2.8	12.8 ± 3.2	8.5 ± 2.5
7.15	6.8 ± 1.0	8.1 ± 2.0	4.4 ± 1.3
7.40	5.8 ± 0.8	5.2 ± 1.3	2.8 ± 0.8
7.73	2.9 ± 0.4	3.0 ± 0.8	1.5 ± 0.5
7.97	1.50 ± 0.2	1.6 ± 0.4	1.2 ± 0.4

The slope and the intercept for the plot in Figure 5.14 are 1300 ± 68 and $(1.27 \pm 7.18) \times 10^{-6}$, respectively, while the slope and intercept for the plot in Figure 5.15 are 1400 ± 200 and $(-7.13 \pm 220) \times 10^{-6}$, respectively. These results for the efflux of DMA provide conclusive evidence that the neutral form of the molecule is dominating the diffusion. As the $[H^+]$ approaches 0 the percentage of DMA^- approaches 100. This hypothetical situation is

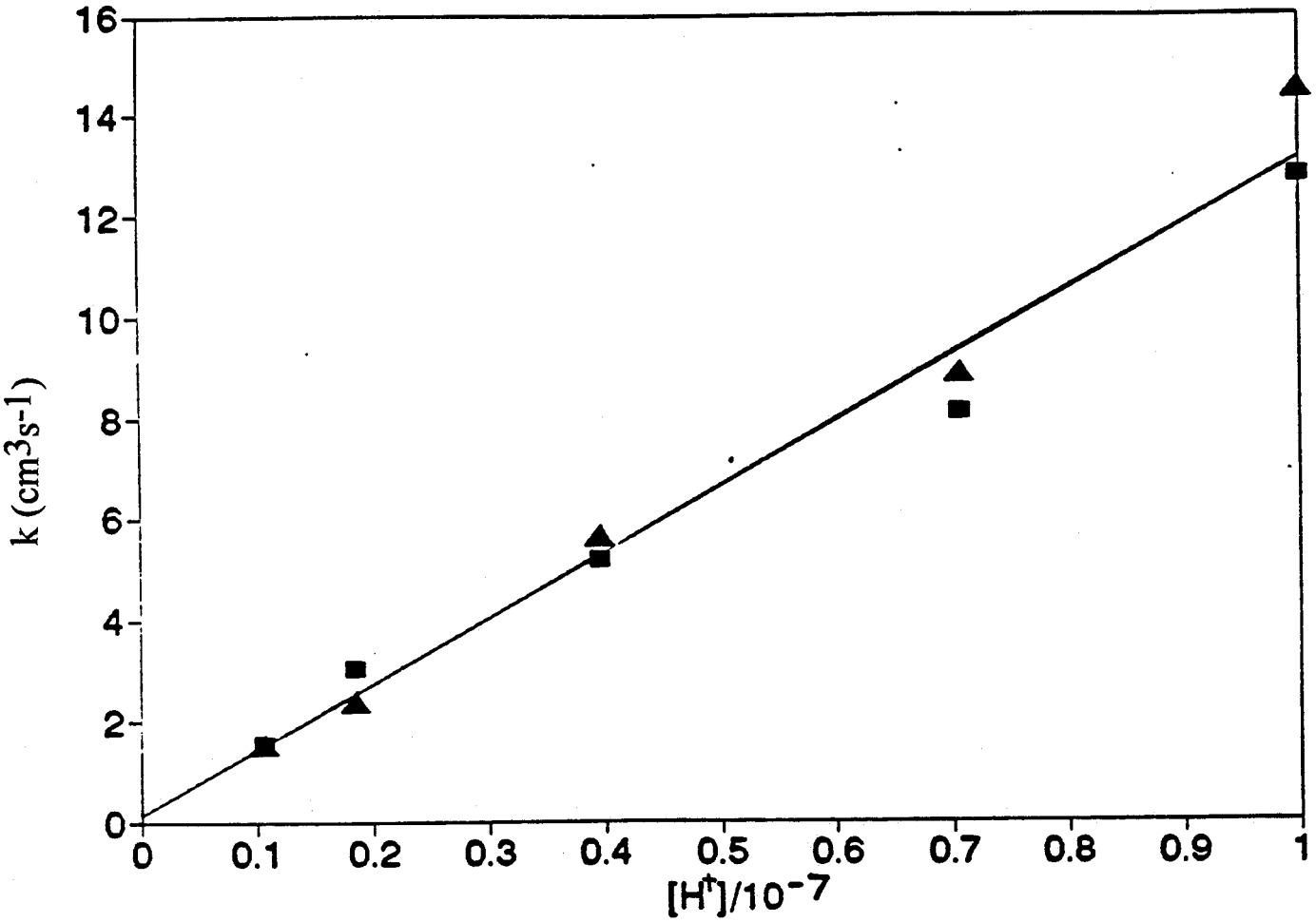

Figure 5.14 A plot of the pH dependant rate constants (k in cm^3s^{-1}) vs the $[H^+]$ for the efflux of DMA at 24°C. Either glucose (▲) or NaCl (■) was added to the outside of the 200 nm LUVs to balance the osmotic pressure.

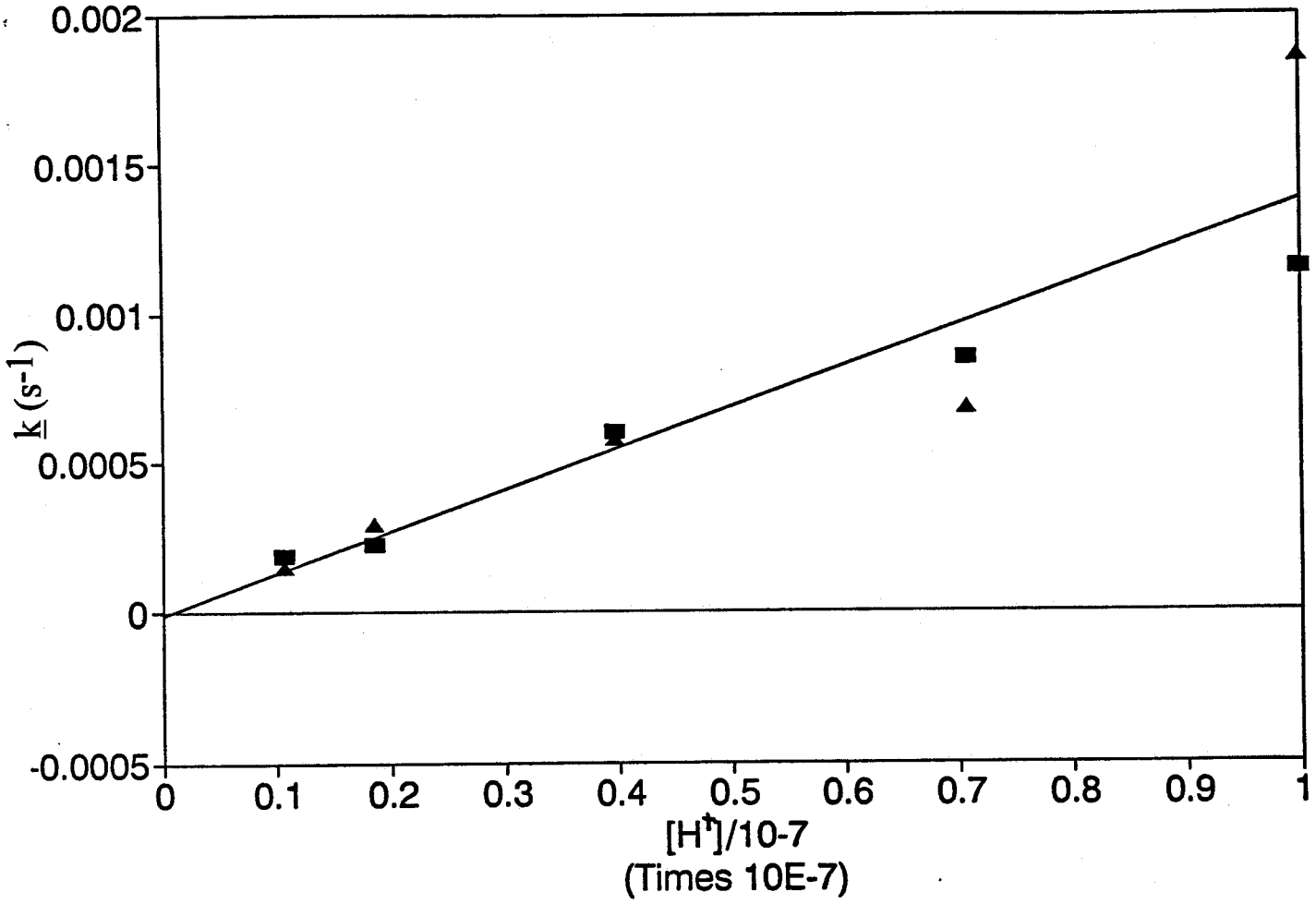

Figure 5.15 A plot of the pH dependant rate constants ($\underline{k}$ in s^{-1}) vs the $[H^+]$ for the efflux of DMA at 24°C. Either glucose (▲) or NaCl (■) was added to the outside of the 200 nm LUVs to balance the osmotic pressure.

represented by the y-intercepts on the graphs in Figures 5.14 and 5.15 which are both 0 within the uncertainty of the line. Therefore, the rate constants for DMA^- are not measurable by these experiments and are at least 10^3 to 10^4 times slower than the rate constants for DMAH. This is a conservative estimate based upon equation [5.43] because the overall rate constant is a combination of the individual rate constants times the concentration of each molecular species. The concentration of the anion is 10 to 100 times that of the neutral species at the pH's investigated and it still does not make a contribution to the overall rate constant, hence the rate constant for the anionic species must be very small.

By using equations 5.50a, b, and c the values for k_{AH}, $\underline{k}_{AH}$, and P_{AH} at 24°C through 200 nm LUVs were determined to be 9.28 ($\pm$ 0.56) $\times$ 10^{-4} cm^3s^{-1}, 10.1 ($\pm$ 1.4) $\times$ 10^{-3} s^{-1}, and 5.8 ($\pm$ 1.0) $\times$ 10^{-8} cm s^{-1}, respectively. These values are independent of pH.

There is a much higher percentage of error on the slopes and the intercepts for the graph in Figure 5.15 than the graph in Figure 5.14. This indicates that incorporating the trapped volume into the rate constants decreases the variability between experiments and produces results which are more reproducible.

These experiments also demonstrate that either NaCl or glucose may be used on the outside of the LUVs to balance the osmotic pressure because when the equilibrium position is corrected for the salt effect by using equation 5.57 the results displayed in Tables 5.8 and 5.9 are approximately equal.

5.4.4 MMA pH and temperature study

MMA was encapsulated by EPC and the mixture was freeze-thawed, extruded through 200 nm filters, and passed down a Sephadex column as described in Section 5.3.4. NaCl was used to balance the osmotic pressure and the experiments were

performed at 5 different temperatures and 2 different pHs. The MMA diffused out of the LUVs very slowly and NMR spectra were taken 3 times a day for about a week. The samples were placed in water baths at the appropriate temperatures when spectra were not being recorded. The results for these experiments are displayed in Tables 5.10 and 5.11.

Table 5.10 MMA Diffusion Coefficients (pH = 6.98) through 200 nm LUVs.

Temp (°C)	k (cm^3s^{-1}) × 10^{-6}	$\underline{k}$ (s^{-1}) × 10^{-5}	P (cm s^{-1}) × 10^{-11}
24.0	0.53 ± 0.13	0.27 ± 0.04	0.69 ± 0.21
29.4	0.69 ± 0.17	0.36 ± 0.05	0.88 ± 0.26
31.0	1.37 ± 0.34	1.02 ± 0.15	1.31 ± 0.39
38.5	2.06 ± 0.52	1.06 ± 0.15	2.63 ± 0.79
47.8	12.5 ± 3.1	9.3 ± 1.4	11.9 ± 3.6

Table 5.11 MMA Diffusion Coefficients (pH = 7.40) through 200 nm LUVs.

Temp (°C)	k (cm^3s^{-1}) × 10^{-6}	$\underline{k}$ (s^{-1}) × 10^{-5}	P (cm s^{-1}) × 10^{-11}
24.0	0.20 ± 0.05	0.11 ± 0.02	0.28 ± 0.08
29.4	0.46 ± 0.12	0.26 ± 0.04	0.63 ± 0.19
31.0	0.38 ± 0.09	0.33 ± 0.05	0.70 ± 0.21
38.5	1.46 ± 0.37	0.81 ± 0.12	2.01 ± 0.60
47.8	5.3 ± 1.3	4.6 ± 0.7	9.8 ± 2.9

At a pH of 6.98 the species and percentages of each are; MMAH (0.133%), MMA^- (98.3%) and MMA^{-2} (1.59%) while at a pH of 7.40 the species and percentages of each are; MMAH (0.049%), MMA^- (95.8%) and MMA^{-2} (4.08%). The pH independent rate constants and permeability coefficients are calculated according to equations 5.50a, b, and c and the results are displayed in Tables 5.12 and 5.13. The diffusion coefficients in Table 5.12 are from the experiments at pH 6.98; while the diffusion coefficients in Table 5.13 are from the experiments at pH 7.4.

Table 5.12 MMAH Diffusion Coefficients through 200 nm LUVs (from Table 5.10).

Temp (°C)	k_{AH} (cm^3s^{-1}) $\times 10^{-6}$	$\underline{k}_{AH}$ (s^{-1}) $\times 10^{-5}$	P_{AH} ($cm\ s^{-1}$) $\times 10^{-11}$
24.0	400 ± 120	205 ± 50	780 ± 270
29.4	520 ± 160	270 ± 70	1020 ± 360
31.0	1040 ± 310	770 ± 190	2580 ± 900
38.5	1550 ± 470	800 ± 200	3030 ± 1060
47.8	9400 ± 2800	7000 ± 1700	23500 ± 8300

Table 5.13 MMAH Diffusion Coefficients through 200 nm LUVs (from Table 5.11).

Temp (°C)	k_{AH} (cm^3s^{-1}) $\times 10^{-6}$	$\underline{k}_{AH}$ (s^{-1}) $\times 10^{-5}$	P_{AH} ($cm\ s^{-1}$) $\times 10^{-11}$
24.0	410 ± 120	230 ± 60	880 ± 310
29.4	930 ± 280	520 ± 130	1980 ± 690
31.0	760 ± 230	670 ± 170	2310 ± 690
38.5	2960 ± 890	1660 ± 420	6320 ± 2200
47.8	10700 ± 3200	9390 ± 2300	32500 ± 11000

These results indicate that the neutral form of the molecule is dominating the diffusion, because the pH independent diffusion coefficients calculated from the pH dependent diffusion coefficients at pHs 6.98 and 7.40 are relatively close.

Arrhenius plots of the pH independent permeabilities for MMA (from the diffusion data obtained at pHs 6.98 and 7.4) versus the inverse temperature are plotted according to equation 4.8 and are shown in Figure 5.16. The slopes of these lines equal -14300 ± 700 and -13200 ± 2400 from the diffusion experiments at 6.98 and 7.4, respectively. The

Figure 5.16 A plot of the $\ln(P_{AH})$ from the diffusion experiments at pHs 6.98 ( ) and 7.4 ( ) versus 1/T.

average activation energy for the permeation of the MMAH through the phospholipid bilayer was calculated by using equation 4.8 and is displayed in Table 5.14.

Table 5.14 The activation energy for the permeation of MMAH through the phospholipid bilayer of LUVs.

Compound	Activation Energy
MMAH	114 ± 10 KJ mol^{-1}

These experiments were performed at pHs where the percentage of the anionic species was approximately 1000 times greater than that of the neutral species and, therefore, an **attempt** was made to determine the diffusion coefficients for the anionic species.

At pH 6.98, $P_{AH}(0.00133) + P_{A^-}(0.983) = P_{6.98}$

likewise at pH 7.4 $P_{AH}(0.00049) + P_{A^-}(0.958) = P_{7.4}$

Thus, at each temperature there are two unknowns and two equations. When the equations are solved the results which are presented in Table 5.15 are obtained. The errors on the values for P_{A^-} are estimated to be at least 200% and, therefore, are not tabulated.

Table 5.15 Permeability coefficient determination for MMA^-.

Temp (°C)	P_{AH} (cm s^{-1}) $\times 10^{-13}$	P_{A^-}(cm s^{-1}) $\times 10^{-13}$
24.0	47400	4.87
29.4	28600	51.1
31.0	72100	36.0
38.5	69200	174
47.8	225000	908

If a similar type of reasoning is applied to the rate constants the results displayed in Table 5.16 are obtained. The errors on the values for P_{A^-} are estimated to be at least 200% and, therefore, are not tabulated.

Table 5.16 Rate constant determination for MMA^-.

Temp (°C)	k_{AH} ($cm^3\ s^{-1}$) $\times 10^{-8}$	k_{A^-} ($cm^3\ s^{-1}$) $\times 10^{-8}$	$\underline{k}_{AH}$ (s^{-1}) $\times 10^{-7}$	$\underline{k}_{A^-}$ (s^{-1}) $\times 10^{-7}$
24.0	39000	1.14	19000	2.08
29.4	26800	33.9	11300	20.8
31.0	119500	-22.0	82500	-7.90
38.5	68300	117	27200	71.1
47.8	854000	113	546000	203

The scatter of these results and a few negative numbers indicates that the **error** in these numbers is very high. However, these results show that the diffusion coefficients for the anionic form of the molecule seem to be approximately 1000 to 10000 times smaller than those for the neutral form of the molecule.

5.4.5 DMA temperature study

DMA was encapsulated by EPC and the mixture was freeze-thawed, extruded through 200 nm filters, and passed down a Sephadex column as described in Section 5.3.4. These experiments were performed at 4 different temperatures all at a pH of 7.4. Glucose was used to balance the osmotic pressure. The results from these experiments are displayed in Table 5.17.

Table 5.17 DMA Diffusion Coefficients (pH 7.4) through 200 nm LUVs.

Temp (°C)	k (cm^3s^{-1}) $\times 10^{-5}$	$\underline{k}$ (s^{-1}) $\times 10^{-4}$	P ($cm\ s^{-1}$) $\times 10^{-9}$
24.0	5.2 ± 1.3	5.8 ± 0.9	2.8 ± 0.8
28.0	6.3 ± 1.6	9.9 ± 1.5	3.8 ± 1.1
30.0	8.0 ± 2.0	7.0 ± 1.0	4.1 ± 1.2
33.0	10.3 ± 2.6	15.6 ± 2.3	8.3 ± 2.5

The pH independent values for these experiments are calculated according to equations 5.50a, b, and c and the results of these calculations are displayed in Table 5.18.

Table 5.18 DMAH Diffusion Coefficients through 200 nm LUVs.

Temp (°C)	k_{AH} (cm^3s^{-1}) $\times 10^{-5}$	$\underline{k}_{AH}$ (s^{-1}) $\times 10^{-4}$	P_{AH} ($cm\ s^{-1}$) $\times 10^{-9}$
24.0	87 ± 22	97 ± 15	46 ± 14
28.0	107 ± 26	166 ± 25	63 ± 19
30.0	135 ± 34	118 ± 18	68 ± 20
33.0	173 ± 43	263 ± 40	139 ± 41

An Arrhenius plot of the pH independent permeabilities versus the inverse temperature according to equation 4.8 is displayed in Figure 5.17. The slope of this line equals -10400 ± 2800, while the intercept equals 18.0 ± 0.2. The activation energy for the

permeation of the DMAH through the phospholipid bilayer was calculated by using equation 4.8 and is displayed in Table 5.19.

Table 5.19 The activation energy for the permeation of DMAH through the phospholipid bilayer of LUVs.

Compound	Activation Energy
DMAH	86 ± 20 KJmol^{-1}

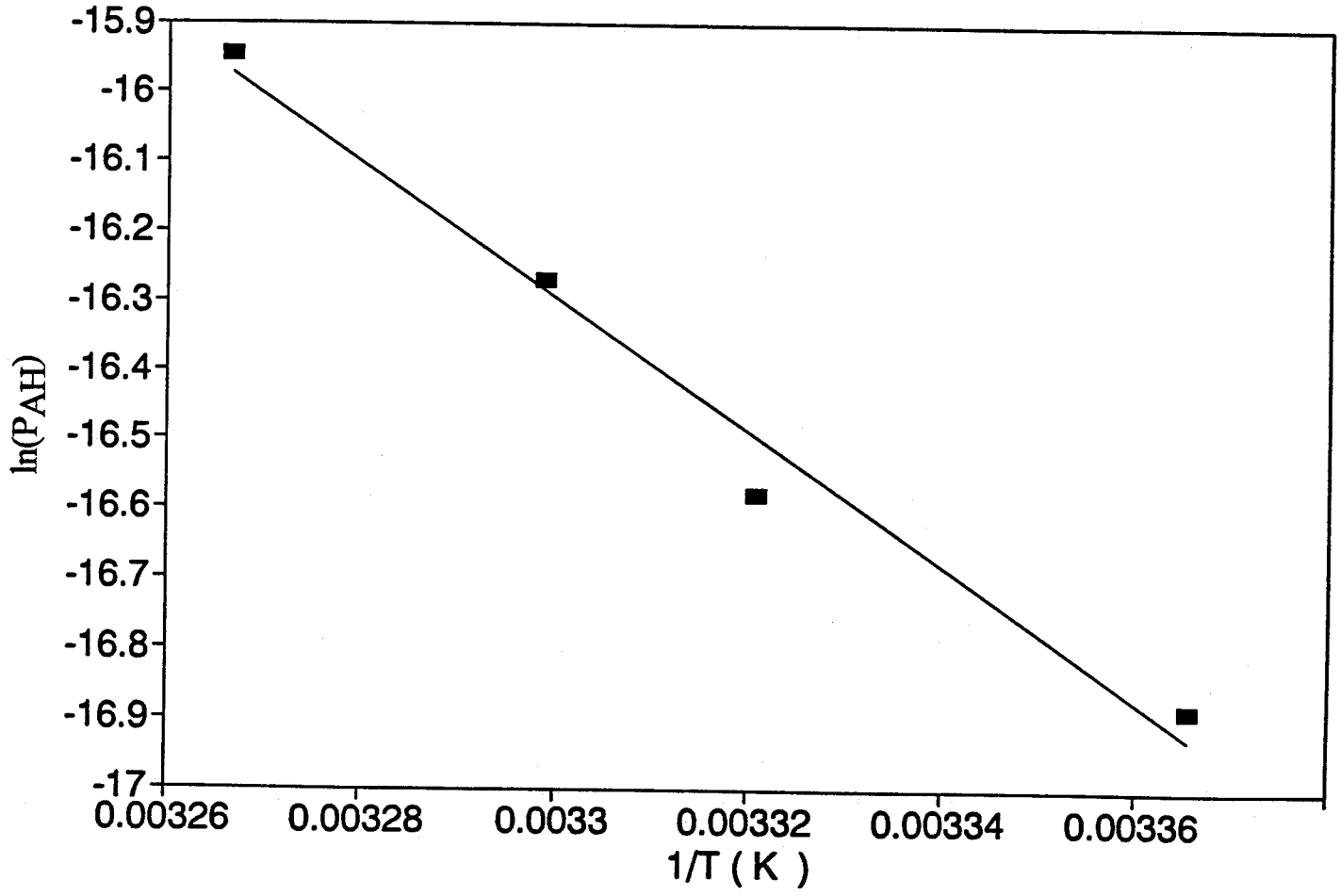

Figure 5.17 A plot of the $\ln(P_{AH})$ versus 1/T for the activation energy determination for DMAH diffusion through a phospholipid bilayer.

The activation energy for the diffusion of MMAH across the liposomal membranes (114 KJ mol^{-1}) is greater than the activation energy for DMAH (86 KJ mol^{-1}), as determined by using the NMR technique. A similar result was observed earlier in Section 4.4.2, although the difference in the activation energies for MMA and DMA is less (MMA was found to have an activation energy of 220 KJ mol^{-1} and DMA was found to have an activation energy of 130 KJ mol^{-1} by using the radioactive method and 100 nm LUVs). MMA has a greater hydrogen bonding capability with the surrounding water molecules than does DMA and, therefore, would be expected to have a greater activation energy. Indeed, it has been shown in previous studies with erythritol, glycerol, and glycol[150] that the activation energy for permeation through artificial membranes corresponds directly to the number of hydrogen bonds that need to be broken in order for the permeant to undergo complete dehydration.

5.4.6 DMA temperature study with cholesterol in the membrane

DMA was encapsulated by EPC and the mixture was freeze-thawed, extruded through 200 nm filters, and passed down a Sephadex column as described in Section 5.3.4. These experiments were performed at a pH of 7.0 with 5 different temperatures. Glucose was used to balance the osmotic pressure. The results from these experiments are displayed in Table 5.20.

The pH independent values for these experiments are calculated according to equations 5.50a, b, and c, and the results of these calculations are displayed in Table 5.21.

Table 5.20 DMA Diffusion Coefficients (pH 7.0) through 200 nm LUVs (55:45, EPC:Cholesterol).

Temp (°C)	k ($cm^3 s^{-1}$) $\times 10^{-5}$	$\underline{k}$ (s^{-1}) $\times 10^{-4}$	P ($cm\ s^{-1}$) $\times 10^{-10}$
22.0	1.6 ± 0.4	1.3 ± 0.2	3.8 ± 1.1
27.0	2.8 ± 0.7	3.1 ± 0.5	7.8 ± 2.3
32.0	4.5 ± 1.1	4.8 ± 0.7	10.9 ± 3.3
37.0	11.2 ± 2.8	11.1 ± 1.7	20.7 ± 6.2
42.0	14.2 ± 3.6	14.8 ± 2.2	29.6 ± 8.9

Table 5.21 DMAH Diffusion Coefficients through 200 nm LUVs (55:45, EPC:Cholesterol).

Temp (°C)	k_{AH} ($cm^3 s^{-1}$) $\times 10^{-5}$	$\underline{k}_{AH}$ (s^{-1}) $\times 10^{-4}$	P_{AH} ($cm\ s^{-1}$) $\times 10^{-10}$
22.0	11.7 ± 3.0	9.1 ± 1.4	28 ± 8
27.0	20.3 ± 5.1	22.7 ± 3.4	57 ± 17
32.0	33.0 ± 8.3	35.0 ± 5.3	80 ± 24
37.0	82 ± 21	80 ± 12	151 ± 45
42.0	104 ± 26	107 ± 16	216 ± 65

An Arrhenius plot is constructed, Figure 5.18, of the pH independent permeabilities versus the inverse temperature according to equation 4.8. The slope of this line equals -9440 ± 580, while the intercept equals 12.3 ± 0.1. The activation energy for

the permeation of the DMAH through the phospholipid bilayer containing 45 mol % cholesterol was calculated by using equation 4.8 and is displayed in Table 5.22.

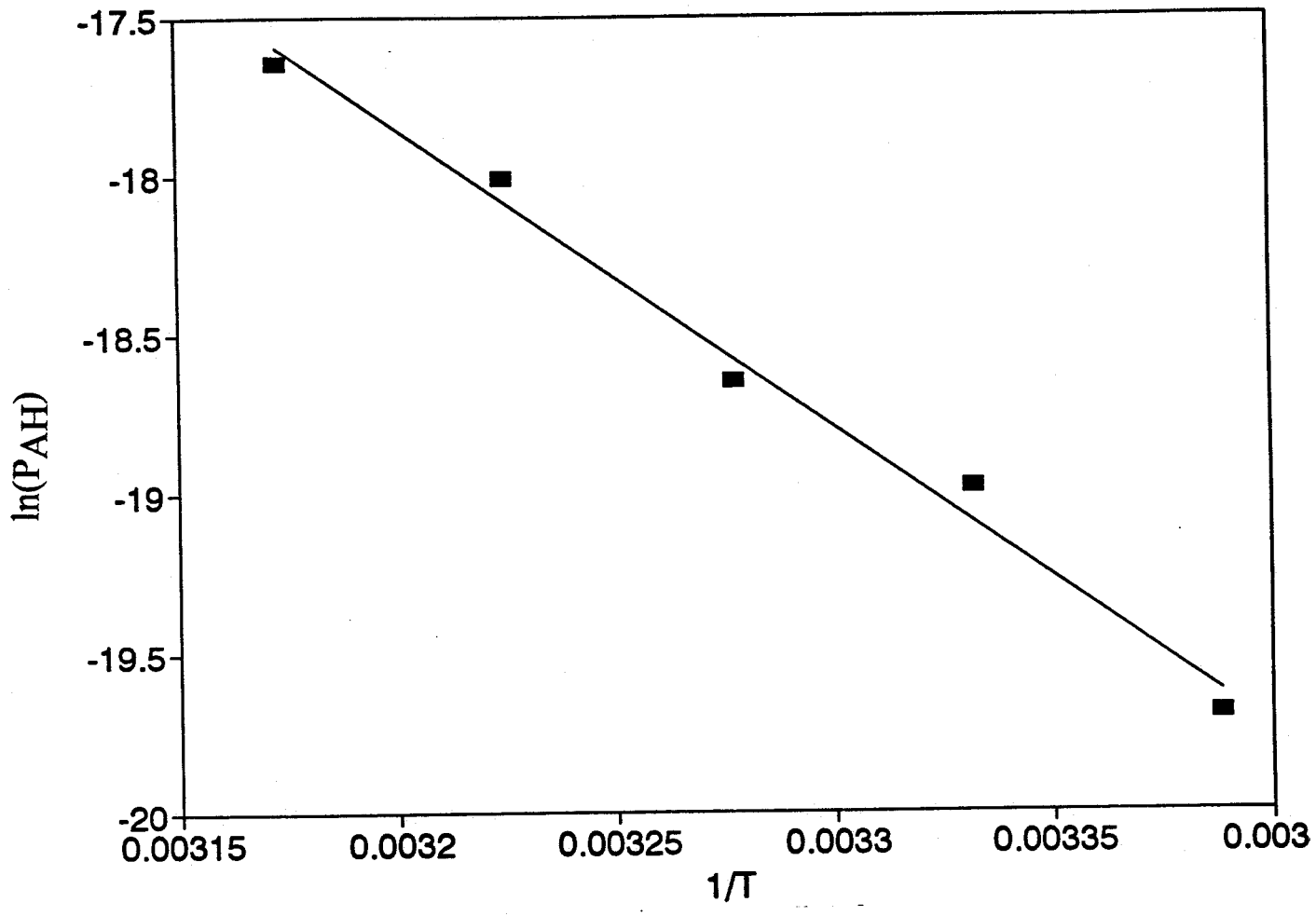

Figure 5.18 A plot of the $\ln(P_{AH})$ versus 1/T for the activation energy determination for DMAH diffusion through a phospholipid bilayer which contains cholesterol.

Table 5.22 The activation energy for the permeation of DMAH through a phospholipid bilayer which contains cholesterol.

Compound	Activation Energy
DMAH	78 ± 5 KJ mol^{-1}

The addition of cholesterol to the membrane decreases both the rate constants and the permeability coefficients for DMA (see Tables 5.17, 5.18, 5.20, and 5.21). This is expected as the addition of cholesterol to the phospholipids will decrease the viscosity of the hydrocarbon region of the membrane,[151] which will result in the decrease of the diffusion coefficients for DMA. Addition evidence which supports a decrease in the entropy of the LUVs following the addition of cholesterol is provided by the Arrhenius plot in Figure (5.18). The activation energy (78 KJ mol^{-1}) for when cholesterol is incorporated into the membrane is approximately the same (within experimental uncertainty) as the activation energy (86 KJ mol^{-1}) when the membrane is composed only of phospholipid. However, the Arrhenius constants which relate to the entropy of the membrane are 6.6×10^7 and 2.2×10^5 for the phospholipid and the phospholipid/cholesterol membranes, respectively. This result is consistant with the findings of De Gier et al. which showed that although the permeability coefficients may change as the composition of the bilayer changes, the activation energy for a permeant will be independent of the bilayer composition.[150]

5.4.6 Comments on how the results obtained in this chapter apply to biological samples and possible uses for the technique in the future.

The results in this chapter show that DMA will pass through biological membranes much more rapidly than MMA, if the only mechanism for transport through the membranes is via slow passive diffusion. The neutral species of each of these weak acids is the major species which permeates through the membrane and the rate constant and permeability coefficients at 24°C for the neutral DMA are 1.08 ($\pm$ 0.08) $\times$ 10^{-3} cm^3s^{-1} and 3.3 ($\pm$ 0.08) $\times$ 10^{-8} cm s^{-1}. The rate constant and permeability coefficient at 24°C for the neutral MMA are 3.93 ($\pm$ 0.05) $\times$ 10^{-4} cm^3s^{-1} and 5.44 ($\pm$ 0.05) $\times$ 10^{-9} cm s^{-1}, respectively. Thus, there is a pH dependence on the diffusion coefficients and as the pH decreases the corresponding diffusion coefficients increase in magnitude. A culture of *C.humicola* was innoculated with DMA and produced 87 nmoles of trimethylarsine at pH 5 while only 41 and 2 nmoles of trimethylarsine were produced at pHs 6 and 7, respectively.[152,153] Under identical conditions, a culture inoculated with MMA produced 9, 6, and 0 nmols of trimethylarsine at pHs 5, 6 and 7, respectively. Assuming that the rate limiting step is the diffusion of the DMA or MMA into the cell, then these results may be explained by higher diffusion coefficients with decreased pH. Also, there is much more trimethylarsine produced for the experiments when DMA is the starting substrate rather than MMA. This is similiar to the results reported in Chapter 3 which showed that arsenobetaine is produced more readily when DMA is the precursor rather than MMA. It may be argued that the differences in the diffusion coefficients of DMA and MMA are the main reasons for the differences in these two experiments. The composition of the membrane effects the diffusion coefficients of DMA and MMA as it was shown that the addition of cholesterol to the membranes decreases the diffusion coefficients.

Ideally, the NMR techniques to determine diffusion and permeability described in this chapter would be applicable to a wide range of molecules. However, it is limited to

molecules which have pH dependent permeability coefficients of $\leq 1\times10^{-8}$ cm s^{-1}, otherwise the molecule permeates too quickly to be measured. The technique could be used to investigate the permeation of other environmentally sensitive compounds and the effects of these compounds on membranes. Perhaps the most useful application will involve the use of DMA as a probe molecule to study the effects of altering the membrane properties upon the diffusion coefficients. The composition of the membrane could be altered by using different combinations of phospholipids, by adding various amounts of cholesterol and perhaps even some ionophores such as valinomycin.

5.5 SUMMARY

The work presented in this thesis provides information about the biotransformations and biomobility of MMA and DMA in the marine environment. This work shows that both MMA and DMA are metabolic precursors to arsenobetaine and that microscopic organisms in the water column are responsible for these biotransformations. Mussels do not appear to be capable of synthesizing arsenobetaine which is bioaccumulated by mussels from seawater. DMA is more readily biotransformed to arsenobetaine than is MMA. This difference is postulated to be the result of different rates of diffusion of these compounds into cells and this notion is supported by the results from diffusion experiments. Initially, these experiments were carried out with radiolabeled permeants and model cells (liposomes) and were later modified by using ^{1}H-NMR methodology in conjunction with shift agents which enabled the spectroscopic signal of the permeant on both the inside and the outside of the liposomes.

CHAPTER 6

THE SYNTHESIS OF ORGANOARSENICALS RELEVANT TO THIS THESIS

6.1 INTRODUCTION

Much of the work in the preceeding chapters involved arsenic compounds which were not readily available. The synthesis of the [^{3}H]-MMA and [^{3}H]-DMA was essential for the studies on the biotransformations in chapters 2 and 3, and on the biomobility in chapter. The synthesis of arsenobetaine was very important because its identification in seawater and mussels was based upon chromatographic comparisons with the synthetic standard. In addition, trimethylarsine, trimethylarsine oxide, and tetramethylarsonium ion were synthesized. The details of these syntheses are contained in this chapter.

6.2 EXPERIMENTAL AND RESULTS

6.2.1 Synthesis of [^{3}H]-MMA from arsenite

The following procedure is based upon a method outlined in reference 162, but changes were made in order to incorporate the [^{3}H]-label. Arsenite (2.8 g) was dissolved in 10 M NaOH (8 ml) and the solution was added to a Carius tube (25 ml). The [^{3}H]-methyl iodide (10 mCi) in 1 ml of toluene was obtained from Amersham, USA in a small cylindrical, sealed glass vial fitted with a break seal. The break seal was smashed with a spatula and the contents of the vial were poured into the reaction tube along with the deionized water (1 ml) which was used to rinse out the vial. Unlabelled methyl iodide (2 ml) was also added to the reaction tube which was sealed and heated at 120°C with a sand bath. After 48 hours the reaction tube was removed from the sand bath and white crystals

were precipitating out of the solution. The reaction tube was cooled in an ice bath and additional crystals precipitated out of solution. The reaction tube was cracked open and the solution was poured out leaving the crystals in the tube. Ethanol (2 × 10 ml) was added to the solution to precipitate the remaining crystals (5.898 g) which were removed by filtration. The crystals were identified as the Na salt of [^{3}H]-MMA and the purity was examined by using ^{1}H NMR spectroscopy. The ^{1}H-NMR (200 MHz in D_2O) spectrum, Figure 6.1, shows a singlet at 1.48 ppm. This corresponds with the resonance position for the singlet found in the literature for the ^{1}H-NMR spectrum for MMA (at pH 12.6 in D_2O).[163]

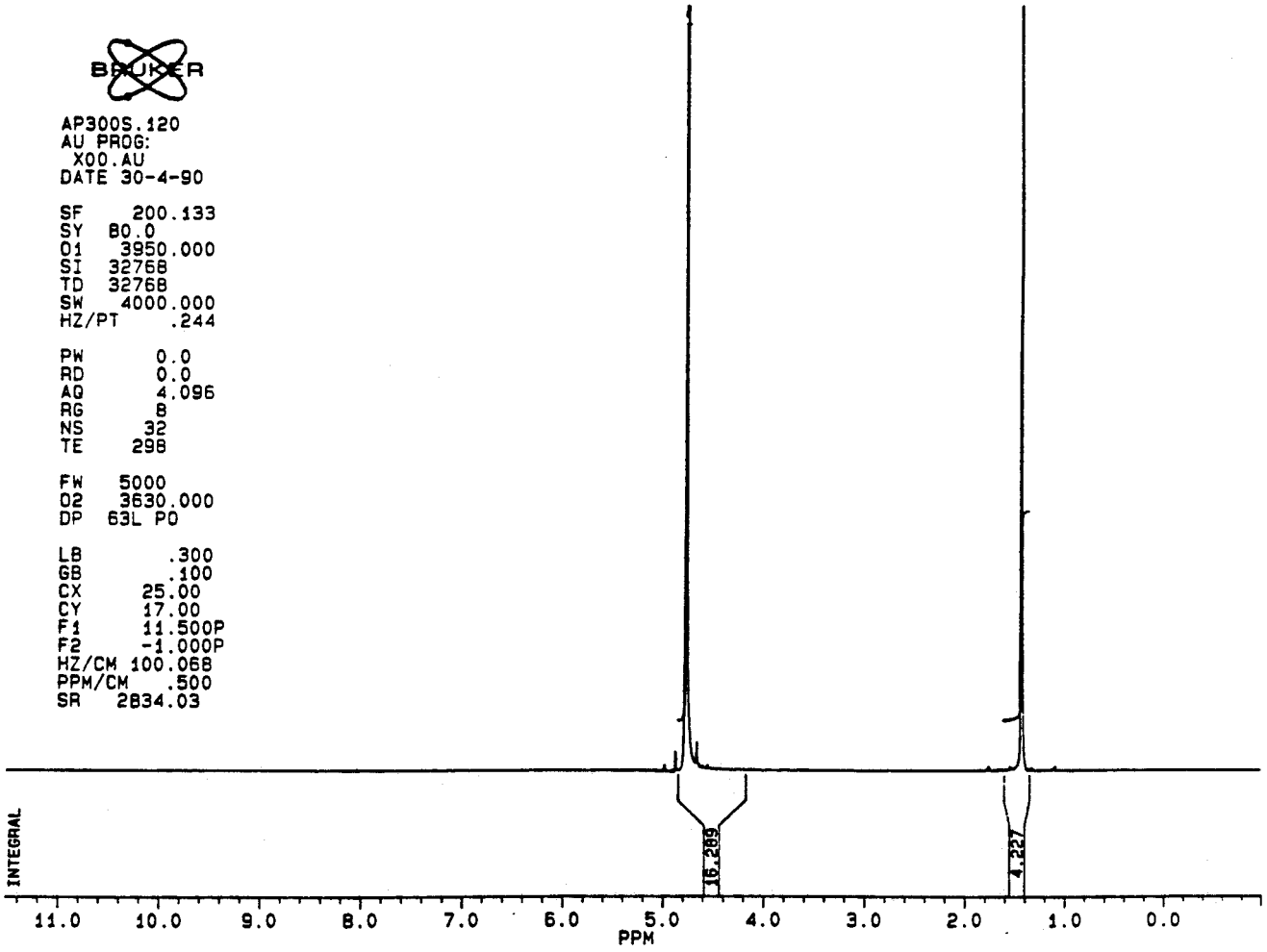

Figure 6.1 ^{1}H-NMR (200 MHz in D_2O) spectrum of [^{3}H]-MMA.

6.2.2 Synthesis of [^{3}H]-DMA from [^{3}H]-MMA

[^{3}H]-MMA (2.0 g) was dissolved in the minimum amount of warm deionized water (≈ 10 cm^3), then sulphur dioxide was bubbled through the solution until saturation occured. The solution was boiled for 2 minutes, quickly cooled to 4°C, and neutralized with sodium carbonate. The solution was evaporated to dryness and the methylarsine oxide was extracted from the residue by using benzene. Removal of the benzene left a foul-smelling solid. This was dissolved in the minimum amount of methanol (≈ 15 cm^3), and placed in a Carius tube. Methyl iodide and sodium hydroxide slightly in excess of stoichiometric amounts were added and the reaction tube was sealed and heated at 45°C for three days. The methanol was then evaporated and the residue was redissolved in a minimum amount of deionized water. Hydrogen peroxide (0.6 cm^3, 30%) was slowly added and the excess was boiled off. The reaction mixture was then added to a Sephadex LH-20 column (1 cm × 30 cm) and eluted with water. The first 60 cm^3 was collected and the water was evaporated. The sample was then added to an Amberlite IRA-410 anion-exchange column (1.5 × 70 cm) and eluted with water. The arsenic compound (0.56 g) eluting between 60 and 190 cm^3 was isolated as the Na salt of [^{3}H]-DMA. This was confirmed by using ^{1}H NMR spectroscopy. The ^{1}H-NMR (200 MHz in D_2O) spectrum, Figure 6.2, shows a singlet at 1.60 ppm. This corresponds with the resonance position for the singlet found in the literature for the ^{1}H-NMR spectrum for DMA (at pH 12.6 in D_2O).[163]

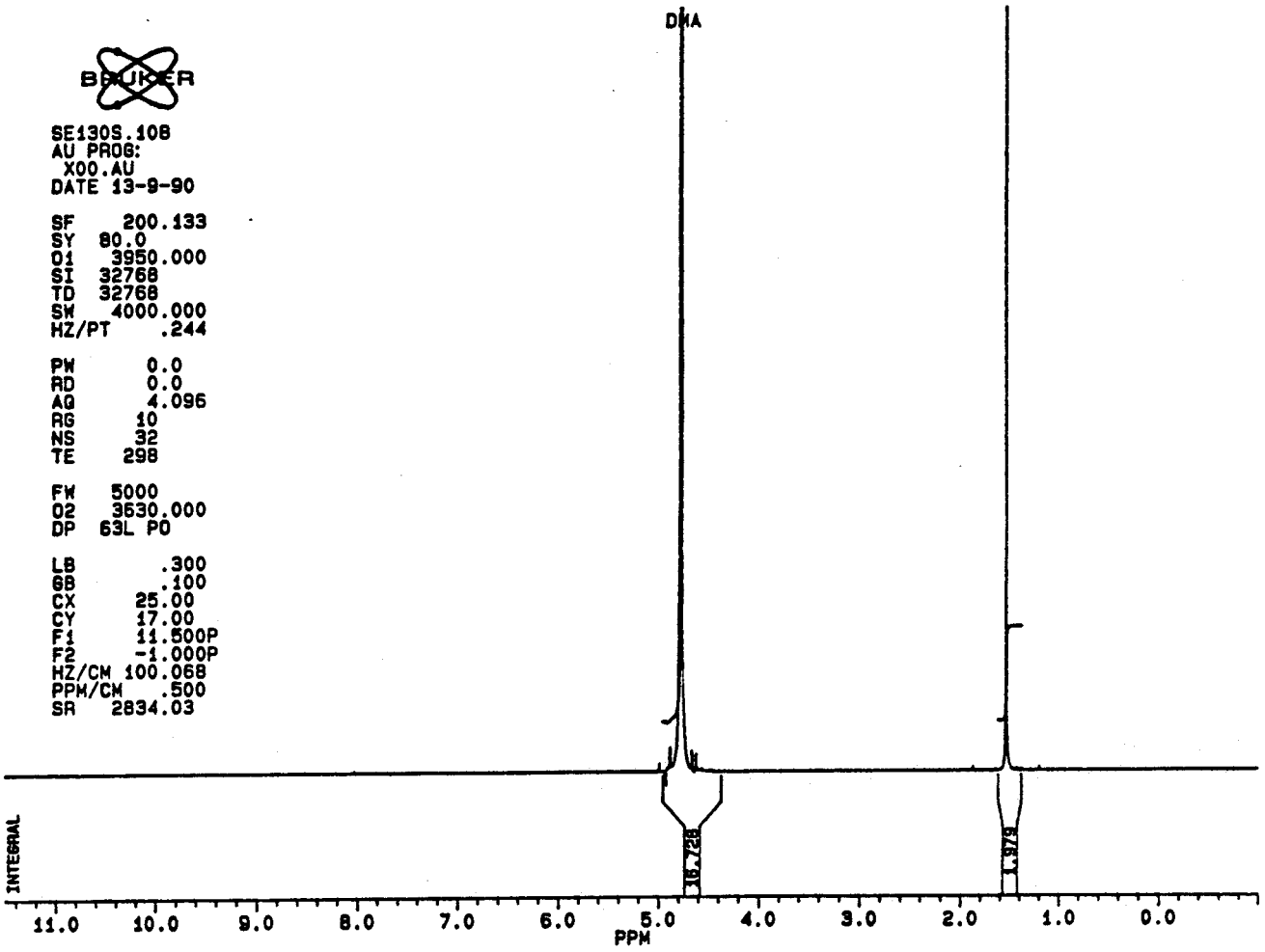

Figure 6.2 ^{1}H-NMR (200 MHz in D_2O) spectrum of [^{3}H]-DMA.

6.2.3 Synthesis of trimethylarsine from arsenic trichloride

The following proceedure is based upon a synthesis outlined in reference 164. A two necked (250 ml) round bottomed flask was equipped with a reflux condensor, a stirrer, a separatory funnel (which contained methyl iodide (10 ml) in dry di-n-butyl ether (10 ml)) and a T joint so that a positive pressure of argon could be maintained through out

the reaction. Magnesium turnings (4.02 g), dry di-n-butyl ether (20 ml) and a few crystals of I_2 were added to the flask. The Grignard reaction was initiated by adding a few drops of the contents of the separatory funnel to the stirred magnesium/dibutyl ether mixture. After the reaction had started the remaining methyl iodide solution was added dropwise over the period of 1 hour. The flask was cooled with an ice/water bath during the addition. After all the methyl iodide had been added, the cloudy mixture was gently heated for approximately 30 minutes and then recooled by using the ice/water bath. A small amount of the magnesium remained unreacted. Arsenic trichloride (10 g in 25 ml of dry di-n-butyl ether) was added dropwise through the addition funnel to the cooled reaction mixture (ice/water bath). After the addition of the arsenic trichloride solution (which took about 20 minutes) the reaction mixture was stirred for approximately 2 hours at room temperature. The condenser was then replaced with a distillation apparatus. The mixture was heated to decompose the $(CH_3)_3As{\cdot}MgX_2$ adduct. Trimethylarsine and some di-n-butyl ether distilled under these conditions and were collected and stored in a tube that was sealed with a Teflon screw type apparatus. The mixture was redistilled to isolate trimethylarsine which was divided up and stored in sealed glass tubes. Trimethylarsine is a clear liquid and is very poisonous and flammable upon contact with air. Its synthesis was confirmed by its use in subsequent reactions (Sections 6.2.4, 6.2.5 and 6.2.6).

6.2.4 Synthesis of tetramethylarsonium iodide from trimethylarsine

A reaction tube containing methyl iodide (1.42 g) in dry diethyl ether (4 ml) was connected to a vacuum line and cooled in liquid nitrogen. A tube containing trimethylarsine (0.306 g) was also connected to the vacuum line and the contents were transferred under vacuum to the reaction tube. The reaction tube was sealed and then

warmed to room temperature. White crystals started to form almost immediately and the reaction was allowed to proceed for approximately 4 hours. After the reaction had been completed the crystals which were identified as tetramethylarsonium iodide were filtered from the solution and air dried. The purity of the crystals (0.135 g) was checked by using ^{1}H NMR spectroscopy and DCI-MS. The ^{1}H-NMR (200 MHz in D_2O) spectrum, Figure 6.3, shows a singlet at 1.95 ppm. This corresponds with the resonance position for the singlet found in the literature for the ^{1}H-NMR spectrum for tetramethylarsonium iodide.[99] The DCI mass spectrum is displayed in Figure 6.4. The base peak corresponds to the tetramethylarsonium ion.

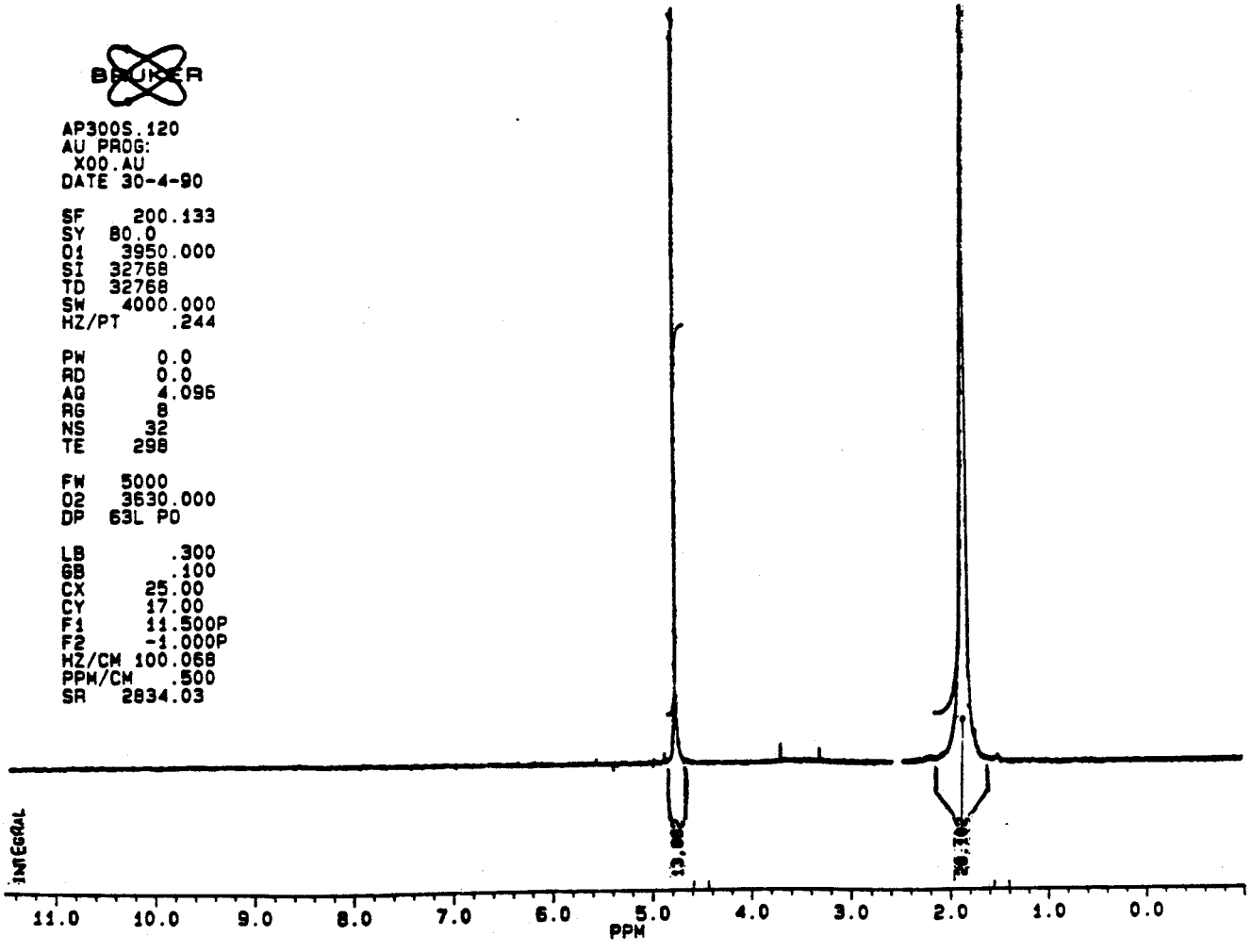

Figure 6.3 ^{1}H-NMR (200 MHz in D_2O) spectrum of tetramethylarsonium iodide.

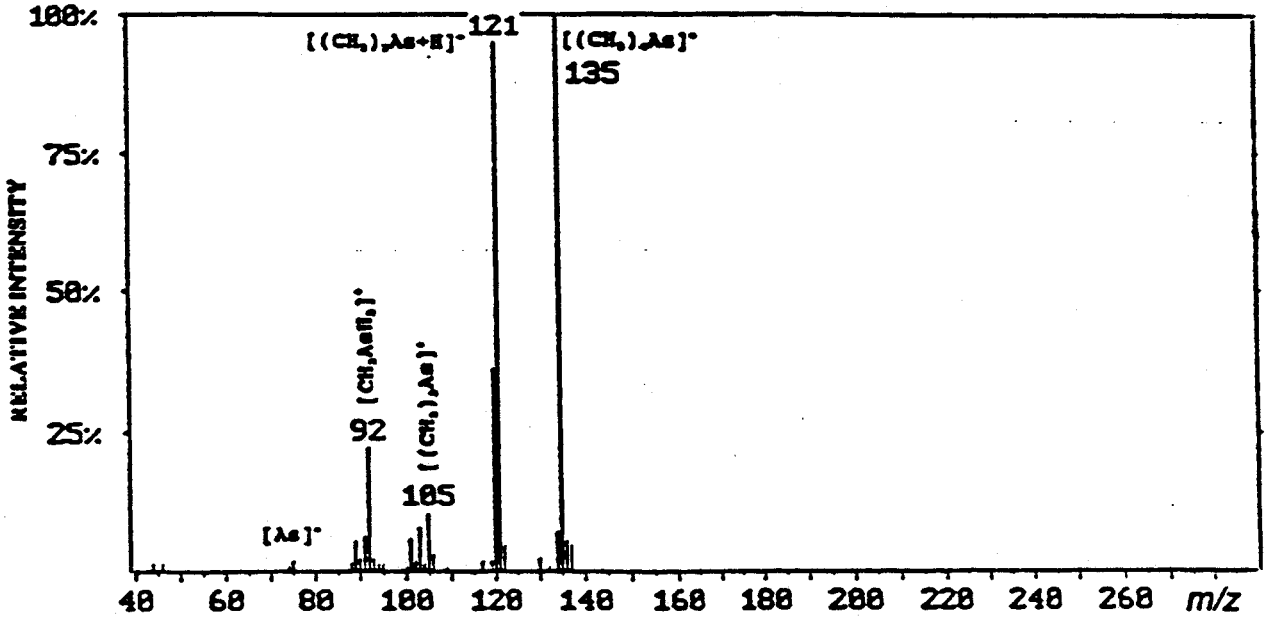

Figure 6.4 DCI mass spectrum of tetramethylarsonium iodide.

6.2.5 Synthesis of trimethylarsine oxide from trimethylarsine

A reaction tube containing hydrogen peroxide (1.5 ml) in dry diethyl ether (7 ml) was connected to a vacuum line and cooled in liquid nitrogen. A tube containing trimethylarsine (0.642 g) was also connected to the vacuum line and the contents were transferred under vacuum to the reaction tube. The reaction tube was sealed and then warmed to room temperature. The ether layer was initially cloudy, but became clearer as the reaction proceeded. There was a continual stream of bubbles from the aqueous to the ether layer. After 24 hours the contents of the reaction tube were transferred to a round bottom flask and the ether and water was rotary evaporated off leaving a white lava-like solid. This solid was quickly sublimed at one atmosphere and stored in a sealed vial which

was placed into a dessicator. The purity of the crystals (0.198 g) was checked by using ^1H NMR spectroscopy and DCI-MS. The ^1H-NMR (200 MHz in D_2O) spectrum, Figure 6.5, shows a singlet at 1.7 ppm. This corresponds with the resonance position for the singlet found in the literature for the ^1H-NMR spectrum for trimethylarsine oxide.[165] The DCI mass spectrum is displayed in Figure 6.6. The base peak of the spectrum of trimethylarsine oxide corresponds to $[M + H^+]$ ions.

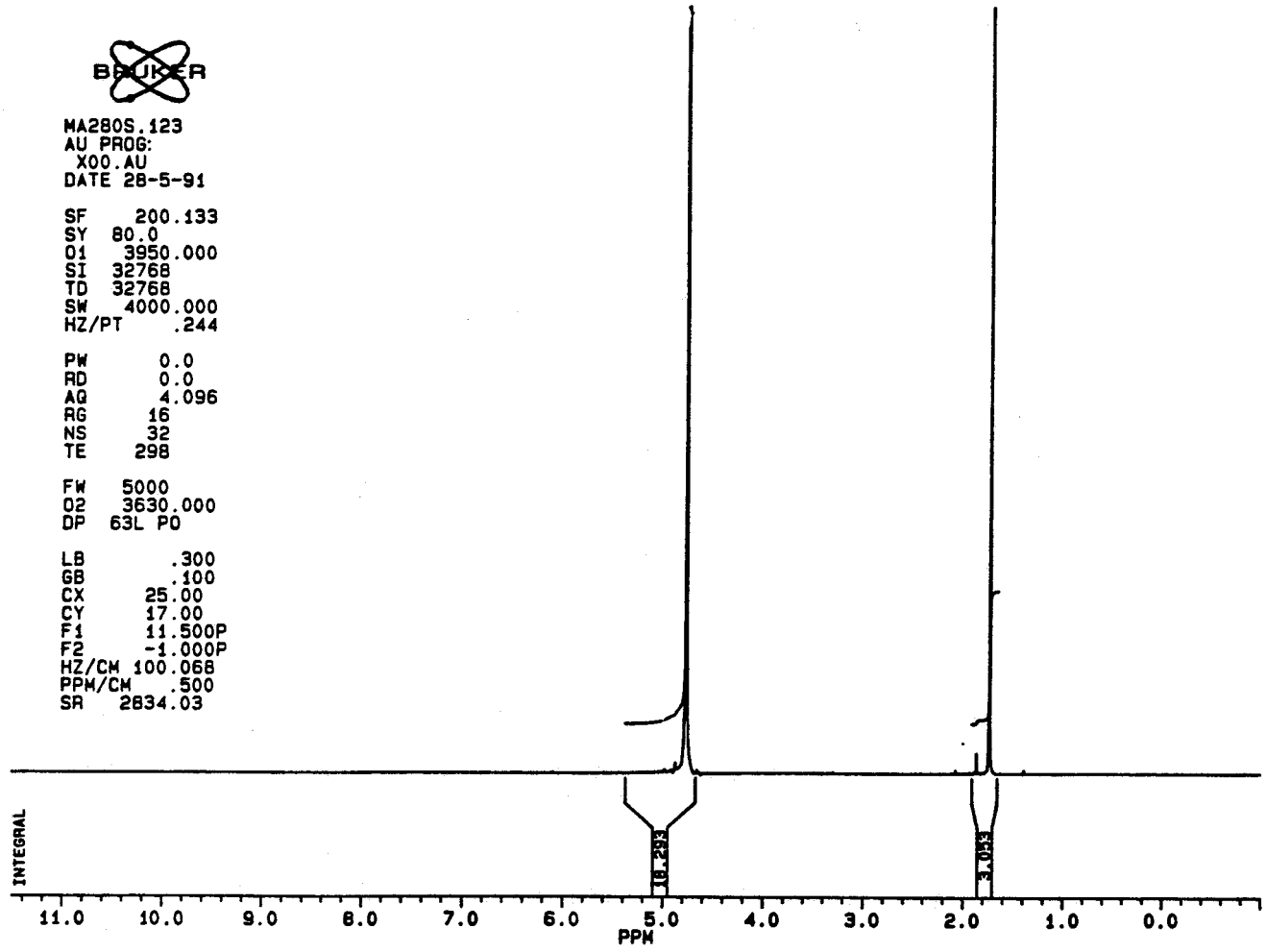

Figure 6.5 ^1H-NMR (200 MHz in D_2O) spectrum of trimethylarsine oxide.

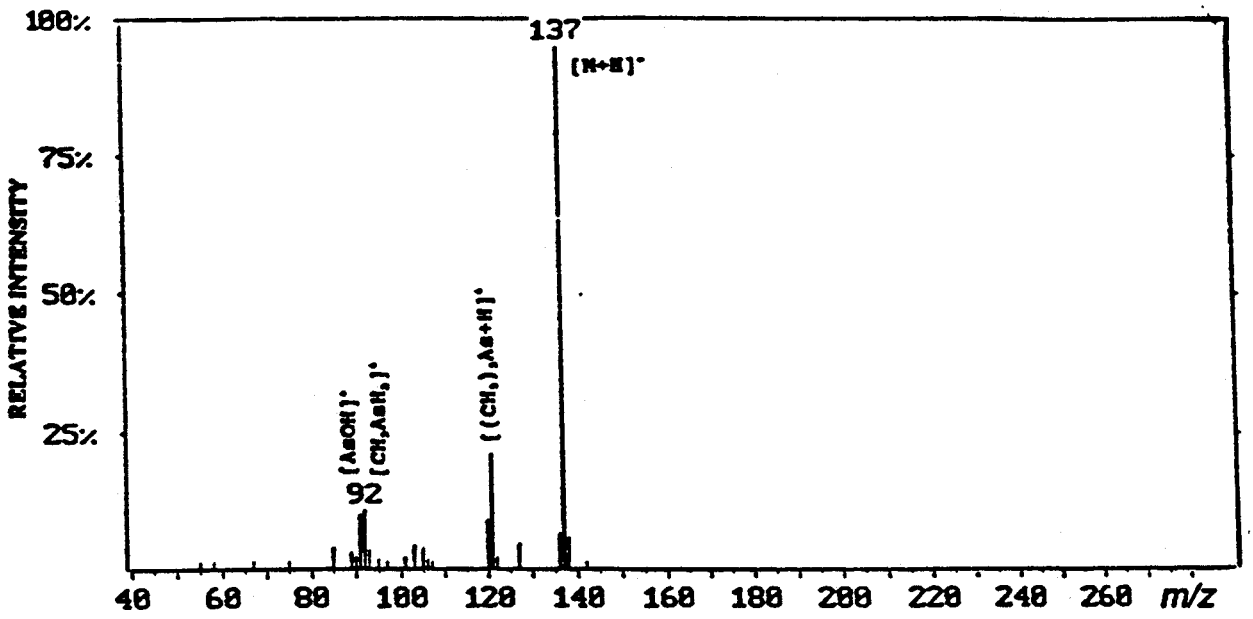

Figure 6.6 DCI mass spectrum of trimethylarsine oxide.

6.2.6 Synthesis of arsenobetaine from trimethylarsine

The following proceedure is based upon a synthesis outlined in reference 164. A reaction tube containing ethyl-bromoacetate (1.5 g) in dry dibutyl ether (4 ml) was connected to a vacuum line and cooled in liquid nitrogen. A tube containing trimethylarsine (0.45 g) was also connected to the vacuum line and the contents were transferred under vacuum to the reaction tube. The reaction tube was sealed and then warmed to room temperature. The clear reaction became cloudy and white crystals started to precipitate out of solution. After 24 hours the solvent was decanted and the white crystals were dissolved in a minimum amount of deionized water. This was applied to an Amberlite IRA-410 column (70 × 1.5 cm in the OH^- form) and was eluted by using

water. Aqueous eluant (150 ml) was collected and rotary evaporated to dryness leaving white crystals which were identified as arsenobetaine and were dried on the vacuum line. The purity of the crystals (0.353g) was checked by using ^{1}H NMR spectroscopy and DCI-MS. The ^{1}H-NMR (200 MHz in D_2O) spectrum, Figure 6.7, shows a singlet at 2 ppm from the 9 identical protons attached to the methyl groups and a singlet at 3.5 ppm from the 2 identical protons in the methylene group. This corresponds to the ^{1}H-NMR spectrum found in the literature for arsenobetaine.[43] The ratios of the areas is 4.52 which corresponds to the expected value of 4.5. The DCI mass spectrum is displayed in Figure 6.8. This spectrum indicates a protonated molecule as well as a fragmentation pattern that allows for positive identification of the compound.

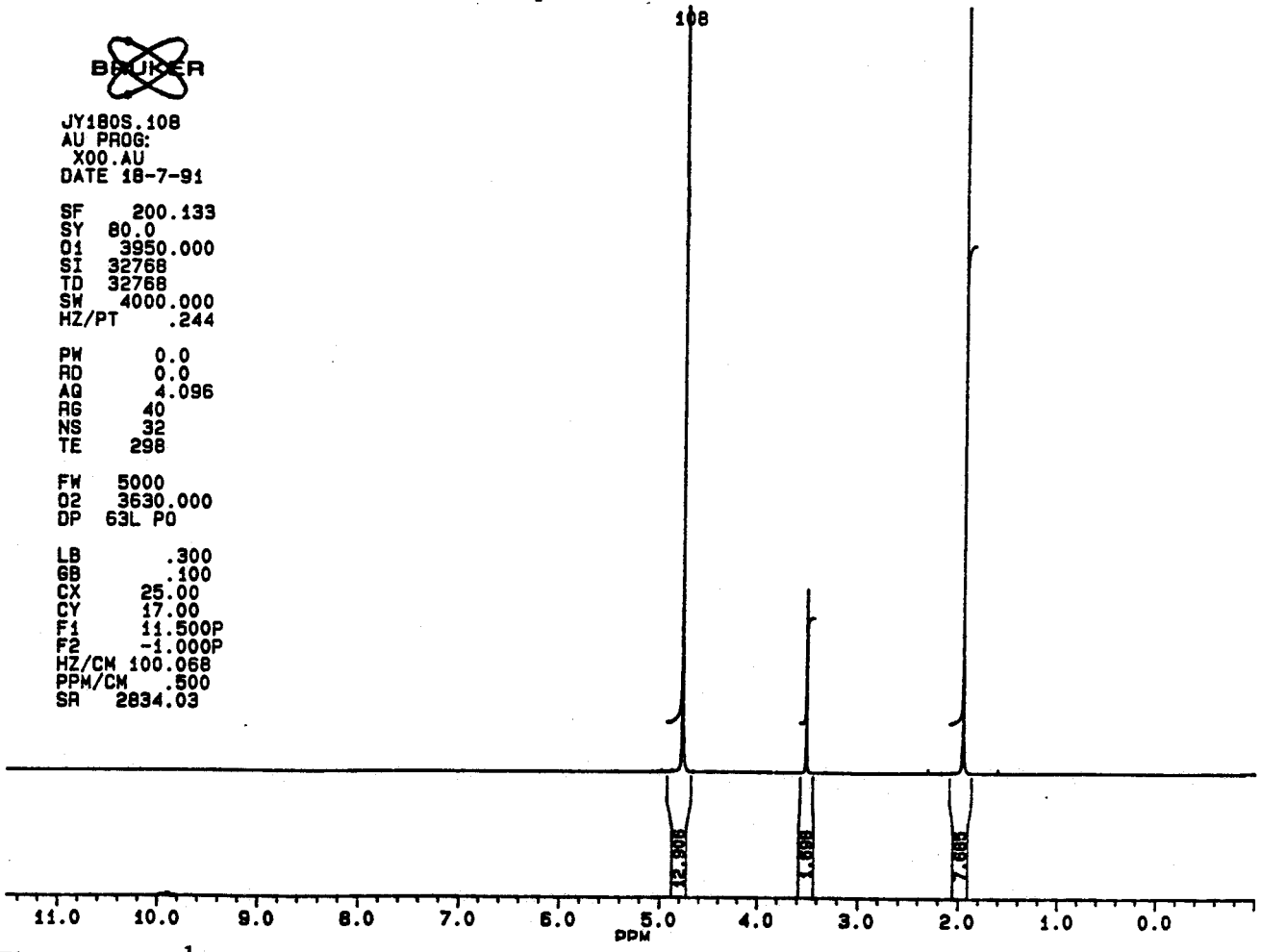

Figure 6.7 ^{1}H-NMR (200 MHz in D_2O) spectrum of arsenobetaine.

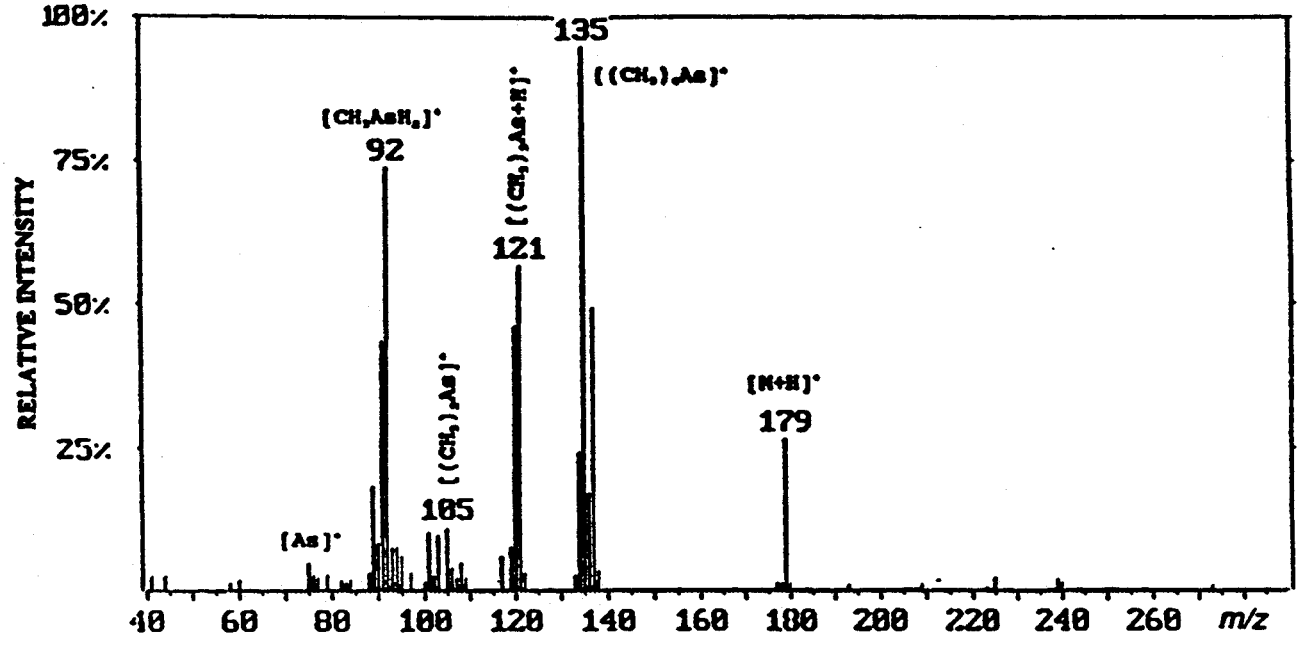

Figure 6.8 DCI mass spectrum of arsenobetaine.

BIBLIOGRAPHY

1. National Research Council, *Arsenic*; National Academy of Sciences: Washington DC, 1977, p16.
2. Sanders, J.G. *Marine Env. Res.*, 1980, 3, 257.
3. Faust, S.D.; Aly, O.M. *Chemistry of Natural Waters*, Ann Arbor Science Publishers, 1981, p257.
4. Boyle, R.W.; Jonasson, I.R. *J. Geochem. Explor.*, 1973, 2, 251.
5. Cullen, W.R.; Reimer, K.J. *Chem Rev.*, 1989, 89, 713.
6. National Research Council of Canada, *The Effects of Arsenic in the Canadian Environment*; Ottawa, 1978.
7. Shibata, Y.; Morita, M.; Fuwa, K. *Adv. Biophys.*, 1992, 28, 31.
8. Betrand, G. Comptes Rend. Hebd. *Sceances*, 1902, 134, 1434.
9. Betrand, G. Comptes Rend. Hebd. *Sceances*, 1903, 137, 232.
10. Tassilly, E.; Leroide, *J. Bull. Soc. Chim. (France)*, 1911, 9, 63.
11. Cox, H.E. *Analyst*, 1925, 50, 3.
12. Chapman, A.C. *Analyst*, 1926, 51, 548.
13. Edmonds, J.S.; Francesconi, K.A.; Cannon, J.R.; Raston C.L.; Skelton, B.W.; White, *A.H. Tetrahedron Lett.*, 1977, 18, 1543.
14. Peoples, S.A. *Arsenic Pesticides; ACS Symposium Series 7*, American Chemical Society, Washington, DC, 1974.
15. Penrose, W.R. *CRC. Crit. Rev. Environ. Control*, 1974, 4, 465.
16. Andreae, M.O. *Deep Sea Res.*, 1978, 25, 391.
17. Sanders, J.G. *Marine Chem.*, 1985, 17, 329.
18. Andreae, M.O. *Arsenic; Industrial, Biomedical, Environmental Perspectives. Proceedings of the Arsenic Symposium*, Van Nostrand, New York, 1983.
19. Tsang, A., *Masters Thesis*, The University of British Columbia, 1990.
20. Johnson, D.L.; Braman, R.S. *Deep Sea Research*, 1975, 22, 503.

21. Andreae, M.O. *Anal. Chem.*, 1977, 49, 820.

22. Andreae, M.O.; Klumpp, D. *Environ. Sci. Technol.*, 1979, 13, 738.

23. Whyte, J.N.C.; Engar, J.R. *Bot. Mar.*, 1983, 26, 159.

24. Sanders, J.G.; Windom, H.L. *Estuarine Coastal Mar. Sci.*, 1980, 10, 555.

25. Sanders, J.G. *J. Phycol.*, 1979, 15, 424.

26. Tamaki, S.; Frankenberger, W.T., *Rev. Environ. Contam. Tox.*, 1992, 124, 79.

27. Sanders, J.G. *Estuar. Coast. Mar. Sci.*, 1979, 9, 95.

28. Edmonds, J.S.; Francesconi, K.A. *J. Chem. Soc., Perkin Trans. I*, 1983, 2375.

29. Edmonds, J.S., Francesconi, K.A. *Nature*, 1977, 265, 436.

30. Edmonds, J.S.; Francesconi, K.A.; Healy, P.C.; White, A.H. *J. Chem. Soc., Perkin Trans. I*, 1982, 2989.

31. Benson, A.A.; Summons, R.E. *Science (Washington, DC)*, 1981, 211,482.

32. Edmonds, J.S.; Francesconi, K.A.; Hansen, J.A. *Experientia*, 1982, 38, 643.

33. Jin, K.; Hayashi, T.; Shibata, Y.; Morita, M. *Appl. Organomet. Chem.*, 1988, 2, 365.

34. Morita, M.; Shibata, Y. *Chemosphere*, 1988, 17, 1147.

35. Whyte, J.N.C.; Englar, J.R. *Botanica Marina,* 1983, 26, 159.

36. Cooney, R.V.; Mumma, R.O.; Benson, A.A. *Proc. Natl. Acad. Sci.*, 1978, 75, 4262.

37. Shibata, Y.; Morita, M. *Agric. Biol. Chem.*, 1988, 52, 1087.

38. Klumpp, D.W.; Peterson, P.J. *Mar. Biol.*, 1981, 62, 297.

39. Edmonds, J.S.; Morita, M.; Shibata Y. *J Chem. Soc. Perkin (I)*, 1987,

40. Bottino, N.R.; Cox, E.R.; Irgolic, K.J.; Aeda, S.; McShane, W.J.; Stockton, R.A.; Zingaro, R.A. *Organometetals and Organometalloids Occurence and Fate in the Environment. Am. Chem. Soc. Symp. Ser.*, 1978, 82, 116.

41. Maher, W.; Butler, E. *Appl. Organomet. Chem.*, 1988, 2, 191.

42. Cannon, J.R.; Saunders, J.B.; Toia, R.F. *Sci. Tot. Environ.*, 1983, 31, 181.

43. Cannon, J.R.; Edmonds, J.S.; Francesconi, K.A.; Raston, C.L.; Saunders, J.B.; Skelton, B.W.; White, A.H., *Aust. J. Chem.*, 1981, 34, 787.

44. Luten, J.B.; Riekwel-Booy, G.; Rauchbarr, A. *Environ. Health Perspect.*, 1982, 45, 165.

45. Shiomi, K.; Kakehashi, Y.; Yamanaka, H.; Kikuchi, T. *Appl Organomet. Chem.*, 1987, 1, 177.

46. Dodd, K. *Ph.D. Thesis*, The University of British Columbia, 1988.

47. Shiomi, K.; Kakehasi, Y.; Yamanaka, H.; Kikuchi, T. *Appl. Organomet. Chem.*, 1988, 2, 1.

48. Lawrence, J.F.; Michalik, P.; Tam, G.; Conacher, H.B.S. *J. Agric. Food Chem.*, 1986, 34, 315.

49. Norin, H.; Christakopoulos, A. *Chemosphere*, 1982, 11, 287.

50. Norin, H.; Ryhagr, R.; Christakopoulos, A.; Sandstrom, M. *Chemosphere*, 1983, 12, 299.

51. Shiomi, K.; Shinagawa, A.; Igarashi, T.; Yamanaka, H.; Kikuchi, T. *Experientia*, 1984, 40, 1247.

52. Francesconi, K.A.; Stick, R.V.; Edmonds, J.S. *Experientia*, 1990, 46, 464.

53. Edmonds, J.S.; Francesconi, K.A. *Sci. Tot. Environ.*, 1987, 64, 317.

54. Penrose, W.R. *J.Fish. Res. Board Can.*, 1975, 32, 2385.

55. Norin, H.; Ryhage, R.; Christakopoulos, A.; Sandstrom, M. *Chemosphere*, 1985, 14, 313.

56. Shibata, Y.; Morita, M. *Appl. Organomet. Chem.*, 1992, 6, 343.

57. Yancey, P.H.; Clark, M.E.; Hand, C.; Bowlus, R.D.; Somero, G.N. *Science*, 1982, 217, 1214.

58. Stauffer, R.E.; Thompson, J.M. *Geochim. Cosmochim. Acta.*, 1984, 48, 2547.

59. Braman, R.S.; Foreback, C.C. *Science (Washington, DC)*, 1973, 182, 1247.

60. Andreae, M.O.; *Deep Sea Res.*, 1978, 25, 391.

61. Baker, M.D.; Wong, P.T.S.; Chau, Y.K.; Mayfield, C.I.; Inniss, W.E. *Can J. Fish Aquat. Sci.*, 1983, 40, 1245.

62. Woolson, E.D., *ACS Symposium Series 7; American Chemical Society*; Washington, DC, 1975.

63. Anake, M.; Schneider, H.J.; Bruechner, C. *Spurenelem Symoposium, Arsenic, 3rd*, Friedrich-Shiller-University, Jena, 1980.

64. Lederer, W.H.; Fensterheim, R.J. *Arsenic: Industrial, Biomedical, Environmental Perspectives (Proc. Arsenic Symp. 1981)*, Van Nostrand, New York, 1983.

65. Woolson, E.A. *Topics in Environmental Health; Biological and Environmental Effects of Arsenic*, Elsevier, Amsterdam, 1983, 6, 51.

66. Walsh, L.M.; Sumner, M.E.; Keeney, D.R. *Environ. Health Perspect.*, 1977, 19, 67.

67. Sachs, R.M.; Michael, J.L. *Weed Sci.*, 1971, 19, 558.

68. Andreae, M.O. *Limnol. Oceanogr.*, 1979, 24, 440.

69. Howard, A.G.; Arbab-Zavar, M.H.; Apte, S. *Estuarine Coastal Shelf Sci.*, 1984, 19, 493.

70. Howard, A.G.; Arbab-Zavar, M.H.; Apte, S. *Mar. Chem.*, 1982, 11, 493.

71. Unlu, M.Y. *Chemosphere*, 1979, 8, 269.

72. Wrench, J.; Fowler, S.W.; Unlu, M.Y. *Mar. Pollut. Bull.*, 1979, 10, 18.

73. Unlu, M.Y.; Fowler, S.W. *Mar. Biol. (Berlin)*, 1979, 51, 209.

74. Cooney, R.V.; Benson, A.A. *Chemosphere*, 1980, 9, 335.

75. Klumpp, D.W., Peterson, P.J. *Mar. Biol.*, 1981, 62, 297.

76. Klumpp, D.W. *Mar. Biol.*, 1980, 58, 257.

77. Klumpp, D.W. *Mar. Biol.*, 1980, 58, 265.

78. Shiomi, K.; Orii, M.; Yamanaka, H.; Kikuchi, T. *Nippon Suisan Sukkaishi*, 1987, 53, 103.

79. Cullen, W.R.; Dodd, M. *Appl. Organomet. Chem.*, 1989, 3, 79.

80. Cullen, W.R.; Dodd, M., *unpublished results.*

81. Thayer, J.S. *Organometallic Compounds and Living Organisms*; Academic, New York, 1984, p189.

82. Challenger, F. *Chem. Rev.*, 1945, 36, 315.

83. Challenger, F.; Higginbottom, C.; Ellis, L. *J. Chem. Soc.*, 1933, 95.

84. Challenger, F. *Chem. Soc. Q. Rev.*, 1955, 9, 255.

85. Cantoni, G.L. *J. Biol. Chem.*, 1953, 204, 403.

86. Challenger, F.; Lisle, D.B.; Dransfield, P.B. *J. Chem. Soc.*, 1954, 1760.

87. Cantoni, G.L. *J. Biol. Chem.*, 1953, 204, 403.

88. Cantoni, G.L. *J. Am. Chem. Soc.*, 1952, 74, 2942.

89. Cullen, W.R.; Frose, C.L.; Lui, A.; McBride, B.C.; Patmore, D.J.; Reimer, K.J. *J Organomet. Chem.*, 1977, 139, 61.

90. Cullen, W.R.; McBride, B.C.; Reimer, M. *Bull. Environ. Contam. Toxicol.*, 1979, 21, 157.

91. Cullen, W.R.; Erdman, A.E.; McBride, B.C.; Pickett, A.W. *J. Microbiol. Methods*, 1983, 1, 297.

92. Cullen W.R.; McBride, B.R.; Reglinski, J. *J. Inorg. Biochem.*, 1984, 21, 45.

93. Cullen W.R.; McBride, B.R.; Reglinski, J. *J. Inorg. Biochem.*, 1984, 21, 179.

94. McBride, B.C.; Wolfe, R.S. *Biochem.*, 1971, 10, 4312.

95. Cullen W.R., Kent, D.; McBride, B.C., *unpublished results.*

96. Shariatpanahi, M.; Anderson, A.C.; Abdelghani, A.A. *J. Environ. Sci. Health*, Part B, 1981, B16, 35.

97. Shariatapanahi, M.; Anderson, A.C.; Abdelghani, A.A.; Englande, A.J. *Biodeteriation 5*; Wiley New York, 1983.

98. Shariatapanahi, M.; Anderson, A.C.; Abdelghani, A.A. *Trace Subst. Environ. Health*, 1982, 16, 170.

99. Francesconi, K.A., *Ph.D. Thesis*, The University of Western Australia, 1991.

100. Edmonds, J.S.; Francesconi, K.A. *Experientia,* 1987, 43, 553.

101. Francesconi, K.A.; Stick, R.V.; Edmonds, J.S. *J. Chem. Soc. Chem. Comm.*, 1991, 928

102. Lawrence, J.F.; Michalik, P.; Tam, G.; Conacher, H.B.S. *J. Agric. Fd. Chem.*, 1986, 34, 315.

103. Francesconi, K.A.; Stick, R.V.; Edmonds, J.S. *Sci. Tot. Environ.*, 1989, 79, 59.

104. Borchardt, T. *Mar. Biol.*, 1983, 76, 67.

105. Borchardt, T., Burchert, 5.; Hablizel, H.; Karbe, L.; Zeitner, R. *Mar. Ecol. Prog. Ser.*, 1988, 42, 17.

106. Cullen, W.R.; Dodd, M.; Nwata, B.U.; Reimer, D.A.; Reimer, K.J. *Appl. Organomet. Chem.*, 1989, 3, 351.

107. Francesconi, K.A.; Edmonds, J.S. *Heavy Metals in the Environment, vol. 2*, 1987, p71.

108. Renberg, L.O.; Sundstrom, S.G. *Toxicol. Environ. Chem.*, 1985, 10, 333.

109. Neely, W.B.; Branson, D.R.; Blau, G.E. *Environ. Sci. Technol.*, 1974, 8, 1113.

110. Tulip, M.T.; Huntzinger, O. *Chemosphere*, 1978, 7, 849.

111. Hansch, L.A.; Leo, A.; Elkins, D. *Chem. Rev.*, 1971, 71, 525.

112. Cullen, W.R.; McBride, B.C.; Pickett, A.W. *Appl. Organomet. Chem.*, 1990, 4, 119.

113. Friedberg, I. *Biochim. Biophy. Acta.*, 1977, 466, 451.

114. Jung, C.; Rothstein, A. *Biochem. Pharmacol.*, 1965, 14, 1093.

115. Rothstein, A.; Donovan, K. *J. Gen. Physiol.*, 1963, 46, 1075.

116. Jennings, D.H.; Hooper, D.C.; Rothstein, A. *J. Gen. Physiol.*, 1958, 41, 1019.

117. Vidal, F.V.; Vidal, V.M.V. *Mar. Biol.*, 1980, 60, 1.

118. Da Costa, E.W.B. *Appl. Microbiol.*, 1972, 23, 46.

119. Button, D.K.; Dunker, S.S.; Morse, M.L. *J. Bacteriol.*, 1973, 113, 599.

120. Borst-Pauwels, G.W.F.H.; Peter, J.K.; Jager, S.; Wijffels, C.C.B.M. *Biochim.*

Biophys. Acta, 1965, 94, 312.

121. Beppa, M.; Arima, K. *J. Bacteriol.*, 1964, 88, 151.

122. Rosenberg, H.; Gerdes, R.J.; Chegwidden, K. *J. Bacteriol.*, 1977, 131, 505.

123. Harold, F.M.; Baarda, J.R. *J. Bacteriol.*, 1966, 91, 2257.

124. Harold, F.M.; Spitz, E. *J. Bacteriol.*, 1975, 122, 266.

125. Cullen, W.R.; Li, H., *unpublished results.*

126. Hope, M.J.; Bally, M.B.; Webb, G.; Cullis, P.R. *Biochim. Biophys. Acta.*, 1985, 812, 55.

127. Bangham, A.D.; Hill, M.W.; Miller, N.G.A. *Methods in Membr. Biol.*, 1974, 1, 1.

128. Bangham, A.D.; Standish, M.M.; Watkins, J.C. *J. Mol. Biol.*, 1965, 13, 238.

129. Cohen, B.E.; Bangham, A.D. *Nature (London)*, 1972, 236, 173.

130. Harrigan, P.R., *Ph.D. Thesis*, The University of British Columbia, 1991.

131. Small, D.M. *The Physical Chemistry of Lipids from Alkanes to Phospholipids*, Plenum Press, New York, 1986.

132. Blok, M.C.; de Gier, J; Van Deenen, L.L.M. *Biochim. Biophys. Acta.*, 1974, 367, 202.

133. Hope, M.J.; Bally, M.B.; Mayer, L.D.; Janoff, A.S.; Cullis, P.R. *Chem. Phys. Lipids*, 1986, 40, 89.

134. Mayer, L.D.; Bally, M.B.; Hope, M.J.; Cullis, P.R. *Chem. Phys. Lipids.*, 1986, 40, 333.

135. Szoka, F.; Papahadjopolous, D. *Annu. Rev. Biophys. Bioeng.*, 1980, 9, 467.

136. Olson, F.; Hunt, T.; Szoka, F.C.; Vail, W.J.; Papahadjopolous, D. *Biochim. Biophys. Acta.*, 1979, 557, 9.

137. Mayer, L.D.; Hope, M.J.; Cullis, P.R. *Biochim. Biophys. Acta*, 1986, 858, 161.

138. Brunner, J.; Graham, D.E.; Hauser, H.; Semenanza, G.; *J. Membr. Biol.*, 1980, 57, 133.

139. Mayer, L.D.; Hope, M.J.; Cullis, P.R.; Janoff, A.S. *Biochim. Biophys. Acta.*, 1986, 817, 193.

140. Stein. W.C. *Channels Carriers and Pumps,* Academic Press, New York, 1990.

141. De Gier, J.; Mandersloot, J.G.; Hupes, J.V.; McElhaney, R.N.; VanBeek, W.P. *Biochim. Biophys. Acta.*, 1971, 233, 610.

142. Orbach, L.A.; Finkelstein, A. *J. Gen. Physiol.*, 1980, 66, 251.

143. Hansch, L.A.; Elkins, C, *Chem Rev.*, 1971, 71, 525.

144. Parsegian, V.A. *Nature (London)*, 1969, 221, 944.

145. Lehninger, *Biochemistry,* Second Edition, 1975.

146. Stein, W.D. *Transport and Diffusion Across Cell Membranes*, Academic Press, New York, 1986.

147. Williams, R.J.P. *Q.Rev. (London)*, 1970, 24, 331.

148. Baes, C.F.; Mesmer, R.E. *The Hydrolysis of Cations*, Wiley, New York, 1976.

149. Mayer, L.D.; Hope, M.J.; Cullis, P.R. *Biochim. Biophys. Acta.*, 1986, 858, 161.

150. De Gier, J.; Mandersloot, J.G.; Hupkes, J.V.; McElhaney, R.N.; Van Beek, W.P. *Biochim. Biophys. Acta*, 1971, 233, 610.

151. McElhaney, R.N.; DeGier, *J. Biochim. Biophys. Acta.*, 1973, 298, 500.

152. Cox, D.P.; Alexander, M. *Appl. Microbiol.*, 1973, 25, 408.

153. Cox, D.P.; Alexander, M. *Bull. Environ. Contam. Toxicol.*, 1973, 9, 84.

154. Brunner, J.; Graham, D.E.; Hauser, H.; Semenza, G. *J. Memb. Biol.*, 1980, 57, 133.

155. Brahm, J. *J. Gen. Physiol.*, !983, 81, 283.

156. Carruthers, A.; Melchoir, D.L. *Biochem.*, 1983, 22, 5797.

157. Bergelson, L.D.; Bystrov, V.F. *Proc. 9th Fed. Em. Biochem. Soc. Meet.*, 1974, 35, 33.

158. King, G.F.; Deegan, J.; Smith, R.; Matouschek, A.; Campbell, A.P. *Biochem. Soc. Trans. 625th meeting,* 1987, 594.

159. Prestegard, J.H.; Cramer, J.A.; Viscio, D.B. *Biophys. J.*, 1979, 26, 575.

160. Conlon, T.; Outhred, R. Biochim. *Biophys. Acta.*,1972, 288, 354.

161. Caficio, D.S.; Hubbell, W.L. *Biophys. J.*, 1982, 39, 263.

162. Cullen, W.R.; McBride, B.C.; Pickett, A.W.; Hansseini, M. *Appl. Organomet. Chem.*, 1988, 3, 71.

163. Antonio, T.; Chopra, A.K.; Cullen, W.R.; Dolphin, D. *J Inorg. Nucl. Chem.*, 1979, 41, 1220

164. Claeys, E.G. *J. Organomet. Chem.*, 1966, 5, 446.

165. Merijanian, A.; Zingaro, R.A. *Inorg. Chem.*, 1966, 5, 187.